Answers in a flash; optical analysis of exocytosis in Human Cultured Endothelial Cells

ATHINOULA MELI

A thesis submitted to UCL for the degree of Doctor of Philosophy

Division of Molecular Neuroendocrinology

National Institute for Medical Research
Mill Hill London NW7 1 AA

2009

I, Athinoula Meli confirm that the work presented in this thesis is my own. Where information has been derived from other sources, I confirm that this has been indicated in the thesis.

ABSTRACT

Endothelial cells line all of our blood vessels. They monitor and respond to signals generated during injury, infection and disease by releasing a wide range of molecules that regulate blood flow, coagulation, inflammatory responses and vessel growth. Protein mediators are released by exocytosis of intracellular organelles, and a major trigger for this type of secretion is an increase in intracellular free calcium ion concentration ($[Ca^{2+}]_i$). Mitochondria are thought to influence Ca^{2+} homeostasis through local Ca^{2+} buffering. Due to a lack of sensitive and time-resolved assays for endothelial exocytosis little is known about the precise relationship between Ca^{2+}-signalling and exocytosis, and the influence of Ca^{2+} buffering by mitochondria.

Using fluorescence and biochemical techniques I have investigated the relationship between secretagogue-evoked Ca^{2+}-signalling and the influence of mitochondrial function on the exocytosis of two distinct organelle populations in cultures of Human Umbilical Vein Endothelial Cells (HUVEC); 1) the Weibel-Palade body (WPB) the main storage organelle for pro-coaguland and inflammatory mediators, and 2) the non-WPB, a non-stored and morphologically distinct organelle that can contain a range of inflammatory and anti-coagulant molecules.

These two distinct organelle populations were labeled for fluorescence microscopy by targeted expression of chimeras of green (EGFP) or red (mRFP) fluorescent proteins in living HUVEC. Exocytosis was evoked by both physiological and pharmacological secretogogues that increase $[Ca^{2+}]_i$. The times of exocytosis of individual organelles were monitored by flashes of light from granule EGFP, produced by pH changes within the organelle upon fusion. In the same experiments, $[Ca^{2+}]_i$ and intra-mitochondrial Ca^{2+} concentration ($[Ca^{2+}]_m$) were monitored using fluorescent Ca^{2+}-indicators.

The data obtained has defined more precisely the relationship between agonist-evoked changes in $[Ca^{2+}]_i$ and secretory vesicle exocytosis in HUVEC. These studies will contribute to a better understanding of the processes that regulate secretion of biomolecules from the endothelium.

CONTENTS

1 INTRODUCTION 13

1.1 Outline 14
1.2 The Endothelium 14
1.2.1 Historic background 14
1.2.2 The endothelium as a secretory organ 15
1.3 Secretory Organelles of ECs 16
1.3.1 The Weibel Palade Body and its cargo 16
1.3.2 The non-WPB- secretory organelle for t-PA 19
1.4 Signalling pathways leading to WPB release 22
1.5 WPB Secretagogues used in this thesis 23
1.5.1 Histamine 24
1.5.2 Thrombin 27
1.5.3 Ionomycin 29
1.6 Regulation of intracellular Ca^{2+} homeostasis 31
1.6.1 The initial phase of the $[Ca^{2+}]_i$ response and Capacitative Ca^{2+} entry 31
1.6.2 The prolonged phase of the $[Ca^{2+}]_i$ response and $[Ca^{2+}]_i$ oscillations 34
1.6.3 The decay phase of the $[Ca^{2+}]_i$ response; cytoplasmic $[Ca^{2+}]_i$ removal mechanisms 37
1.7 The secretory pathway: From ER to fusion 41
1.7.1 Secretory vesicle formation in EC 41
1.7.2 Constitutive and regulated secretion 45
1.7.3 The role of the cytoskeleton in exocytosis 47
1.7.4 Pools of granules 47
1.8 Molecular fusion machinery 48
1.8.1 Regulated exocytosis 48
1.8.2 Constitutive exocytosis 52
1.8.3 Modes of fusion 54
1.9 Haemostatic and inflammatory responses of the endothelium 54
1.9.1 Involvement of WPB protein Von Willebrand Factor (vWF) in Haemostasis 55
1.9.2 Tissue-Plasminogen Activator (t-PA)- Fibrinolysis 58
1.9.3 Inflammation 59
1.9.4 Defects in vWF or t-PA formation/ secretion lead to disease 62
1.10 Mitochondria 63
1.10.1 Mitochondria structure 63
1.10.2 Oxidative phosphorylation 66
1.10.3 Pathways of mitochondrial Ca^{2+} cycling 67
1.10.4 Mitochondrial Ca^{2+} homeostasis 68
1.10.5 Oscillatory $[Ca^{2+}]_m$ signals 71
1.10.6 Mitochondria and secretion 71
1.10.7 Mitochondria in disease 73
1.11 Thesis Aims 74

2 Experimental Methods 75

2.1 Protocols and Reagents 76
2.1.1 Tissue culture 76
2.1.2 Expression of fusion proteins by Nucleofection 76
2.1.3 Constructing mito-EGFP from mito-DsRed 79
2.1.4 Antibodies, Reagents and Immunocytochemistry..... 80
2.1.5 GFP ELISA 81
2.2 Imaging..... 85
2.2.1 Basic epifluorescence imaging apparatus 85
2.2.2 Total Internal Reflection Fluorescence Microscopy (TIRFM) 87
2.2.3 Agonist stimulation of a single HUVEC..... 89
2.2.4 Determining the time-point of agonist arrival at the cell 90
2.2.5 Ammonium Chloride (NH_4Cl) pulse technique..... 94
2.2.6 Data analysis and measurements..... 96
2.3 Description of Imaging..... 97
2.3.1 Imaging $[Ca^{2+}]_i$ changes with Fura-2 97
2.3.2 Establishing Fura-2/AM loading conditions 102
2.3.3 Imaging changes in $[Ca^{2+}]_m$ with X-Rhod-1 104
2.3.4 Establishing dual-loading conditions for X-Rhod-1/AM and Fura-2/AM 108
2.3.5 Imaging $\Delta\Psi_m$ Collapse with TMRE 110

3 GFP as a tool to probe changes in secretory granule pH and to determine the time of fusion pore formation during exocytosis of the non-WPB secretory organelle 116

3.1 Introduction 117
3.1.1 GFP Structure..... 117
3.1.2 The pH-sensitivity of GFP 120
3.1.3 pH in the secretory pathway..... 120
3.1.4 GFP as a pH indicator in the secretory pathway of HUVEC..... 121
3.1.5 GFP as a marker of fusion..... 125
3.1.6 Aim..... 125
3.2 Methods and Results 126
3.2.1 Targeted expression of EGFP or mEGFP to WPBs in living cultured HUVEC.....126
3.2.2 EGFP Labelling of the non-WPB Organelle in cultured HUVEC 128
3.2.3 Imaging 131
3.2.4 Determining the intra-granule pH of the non-WPB organelle..... 131
3.2.5 Determining the resting $pH_{non\text{-}WPB}$ from fluorescence changes during fusion 139
3.2.6 Determining the point of WPB and non-WPB fusion for kinetic studies 141
3.3 Discussion 145
3.3.1 EGFP as an indicator of exocytosis 145
3.3.2 WPB fusion pore formation 146
3.3.3 Granular pH..... 146

4 Concentration-dependence and kinetics of agonist-evoked WPB exocytosis 148

4.1 Introduction 149
4.2 Methodology 151
4.2.1 Epifluorescence imaging of $[Ca^{2+}]_i$ and EGFP 151
4.2.2 Defining the delays of agonist evoked- WPB exocytosis 151
4.3 Biochemical detection of agonist-evoked secretion of WPB targeted EGFP 154
4.3.1 Secretion of WPB targeted EGFP in proregion-EGFP expressing HUVEC 154
4.3.2 Dose-dependence of histamine or thrombin -evoked secretion of WPB targeted EGFP 156
4.4 Histamine-evoked WPB exocytosis. 156
4.4.1 Concentration-dependence of histamine-evoked WPB exocytosis 156
4.4.2 Delays, rates and extent of histamine-evoked WPB exocytosis ... 157
4.5 Thrombin-evoked WPB exocytosis 164
4.5.1 Concentration-dependence of thrombin-evoked WPB exocytosis. 164
4.5.2 Delays, rates and extent of thrombin-evoked WPB exocytosis 164
4.5.3 Comparison of histamine and thrombin evoked WPB fusion 167
4.6 Time-course and extent of ionomycin-evoked WPB exocytosis 171
4.7 Comparison of secretagogue-evoked WPB exocytosis 173
4.8 Discussion 175
4.8.1 Biochemical detection of secreted EGFP. 175
4.8.2 Evidence for a threshold for Ca^{2+}-driven WPB exocytosis 176
4.8.3 Kinetics of agonist evoked-elevations of $[Ca^{2+}]_i$ and WPB exocytosis 177
4.8.4 High concentrations of histamine and thrombin fail to release all WPBs 180

5 Optical analysis of exocytosis of the non-WPB secretory organelle 181

5.1 Introduction 182
5.2 TIRF live cell imaging of t-PA-EGFP and proregion-mRFP co-expressing HUVEC 183
5.3 Spontaneous fusion of the non-WPB organelles in unstimulated HUVEC 185
5.4 Histamine-evoked non-WPB organelle exocytosis. 185
5.4.1 Concentration-dependence of histamine-evoked non-WPB organelle exocytosis. 185
5.4.2 Delays and rates of histamine-evoked non-WPB exocytosis 186
5.5 Ionomycin-evoked non-WPB organelle exocytosis 191
5.6 Discussion 194
5.6.1 Kinetics of the histamine-evoked exocytosis of the non-WPB organelle 194
5.6.2 Extent of stimulated fusion of the non-WPB organelle 195
5.6.3 Comparison of WPB and non-WPB organelle exocytosis 199

6 Mitochondria and WPB exocytosis..... 203

6.1 Introduction 204
6.2 Epifluorescence imaging of WPB exocytosis and changes in $[Ca^{2+}]_i$ and $[Ca^{2+}]_m$..... 206
6.3 Simultaneous Measurements of $[Ca^{2+}]_i$ and $[Ca^{2+}]_m$ in single HUVEC206
6.3.1 Is X-Rhod-1 measuring changes in $[Ca^{2+}]_m$? 206
6.3.2 Stimulus-evoked $[Ca^{2+}]_m$ changes..... 210
6.4 Action of FCCP 214
6.4.1 FCCP collapses the mitochondrial $\Delta\Psi_m$ 214
6.4.2 FCCP causes an increase in proregion-mEGFP fluorescence..... 218
6.4.3 FCCP treatment blocks mitochondrial Ca^{2+} uptake 219
6.5 Measuring $[Ca^{2+}]_m$, $[Ca^{2+}]_i$ and secretion under conditions of mitochondrial Ca^{2+} uptake inhibition..... 224
6.5.1 Effect of Inhibition of mitochondrial Ca^{2+} uptake on histamine evoked increases in $[Ca^{2+}]_i$..... 224
6.5.2 Effect of Inhibition of mitochondrial Ca^{2+} uptake on histamine evoked WPB exocytosis..... 224
6.6 Discussion 226
6.6.1 Using X-Rhod-1 to measure mitochondrial Ca^{2+}..... 229
6.6.2 Mitochondrial Ca^{2+} uptake during histamine action in HUVEC .. 229
6.6.3 Possible effects of mitochondrial inhibitors on cellular ATP levels 230
6.6.4 FCCP and the fluorescence of WPB targeted EGFP 231
6.6.5 FCCP–induced $[Ca^{2+}]_i$ rises 231
6.6.6 FCCP effects on histamine-evoked Ca^{2+} signalling..... 232
6.6.7 FCCP decreases stimulated WPB exocytosis 234

7 Ca^{2+} Oscillations and WPB exocytosis in human endothelial cells..... 236

7.1 Introduction 237
7.2 Histamine evoked Ca^{2+}-oscillations in cultured HUVEC 239
7.3 Extracellular Ca^{2+}-dependence of the prolonged histamine-evoked $[Ca^{2+}]_i$ phase..... 242
7.4 Simulating Ca^{2+} spikes with well defined intervals by controlled puff application of histamine 246
7.5 Ca^{2+} oscillations and WPB exocytosis in proregion-mEGFP expressing HUVEC during continuous exposure to histamine..... 260
7.6 Ca^{2+} oscillations in Cycloheximide (CHX) treated proregion-mEGFP expressing HUVEC..... 268
7.7 Discussion 277
7.7.1 $[Ca^{2+}]_i$ oscillations in non-nucleofected HUVEC 277
7.7.2 Simulated Ca^{2+} spiking and WPB exocytosis 279
7.7.3 Ca^{2+} spiking in proregion-mEGFP expressing HUVEC..... 282

8 Summary and Conclusions..... 285

9 Acknowledgments 292

10 Supplementary material 293

11 ABBREVIATIONS 294

12 REFERENCES 296

LIST OF FIGURES AND TABLES

Figure 1.1 Immuno-labelled WPBs or non-WPBs in a single HUVEC.....21

Figure 1.2 Histamine, thrombin and ionomycin cell membrane action.....30

Figure 1.3 Endothelial cell $[Ca^{2+}]_i$ sequestration.....39

Figure 1.4 Possible secretory pathways of the WPB…….....…….….53

Figure 1.5 Inflammatory and haemostatic action of the endothelium…….…..61

Figure 1.6 The mitochondrial network in HUVEC…….…..65

Figure 1.7 Mitochondrial Metabolism…….…..70

Figure 2.1 GFP-tagged constructs…….……78

Figure 2.2 Constructing mito-EGFP from mito-DsRed…….…...82

Figure 2.3 GFP ELISA…….…….83

Figure 2.4 Basic configuration for imaging…….…….86

Figure 2.5 TIRFM…….……88

Figure 2.6 Agonist application setup……..…...91

Figure 2.7 Agonist application…….…….92

Figure 2.8 Effect of fluid shear due to puff application on resting $[Ca^{2+}]_i$ in HUVEC…….……92

Figure 2.9 Defining the delay in drug arrival…….……...93

Figure 2.10 NH_4Cl action on the secretory organelles…….…….95

Figure 2.11 Chemical and Spectral properties of Fura-2…….…….99

Figure 2.12 Transmission properties of Olympus UPLSAPO x100 1.40NA and U-Plan-APO x100 1.35NA objectives…….....100

Figure 2.13 Excitation spectral imaging of Fura-2 loaded HUVEC……..…101

Figure 2.14 Fura-2 loading conditions ……...103

Figure 2.15 Chemical and Spectral properties of X-Rhod-1……..106

Figure 2.16 X-Rhod-1 co-localizes with mito-tracker Green and mito-EGFP ..107

Figure 2.17 Establishing appropriate Fura-2 and X-Rhod-1 co-loading conditions…….…....109
Figure 2.18 Loading conditions for TMRE…….……113
Figure 2.19 TMRE titration…….114
Figure 3.1 The GFP molecule…….….119
Figure 3.2 *In vitro* and *in vivo* pH titration of EGFP fluorescence [1] …….....……...123
Figure 3.3 pH_{WPB} during maturation [1].....125
Figure 3.4 Expression of proregion-mEGFP and proregion-EGFP fluorescently labels WPB in cultured HUVEC……..127
Figure 3.5 Co-expression of t-PA-EGFP and proregion-mRFP in single HUVEC stained with an antibody for vWF……130
Figure 3.6 Optical arrangements for single granule fluorescent measurements..135
Figure 3.7 Measuring the pHWPB using the NH_4Cl technique……...137
Figure 3.8 pH distributions of the WPB compared to the non-WPB organelle...138
Figure 3.9 The t-PA-EGFP population of non-WPBs undergoing exocytosis differs from the mature WPB population in pHg…….....140
Figure 3.10 Determining the time-point of WPB or non-WPB fusion ……...143
Figure 3.11 Comparison of the EGFP fluorescence between a single WPB and non-WPB organelle upon fusion……..144
Figure 4.1 Setup schematic for simultaneous imaging of Fura-2 and EGFP…...154
Figure 4.2 Defining the delays in drug arrival, Ca^{2+} rise and exocytosis……153
Figure 4.3 ELISA detection of secreted EGFP with maximal agonist concentration stimulation……155
Figure 4.4 Dose response relations for histamine and thrombin evoked secretion of soluble EGFP……...158
Figure 4.5 Concentration-dependence of histamine-evoked WPB exocytosis...160
Figure 4.6 Delays of histamine-evoked WPB exocytosis……...161
Figure 4.7 Rates of histamine-evoked WPB exocytosis…….163
Figure 4.8 Extent of histamine-evoked WPB degranulation……...163
Figure 4.9 Concentration-dependence of thrombin-evoked WPB exocytosis…165
Figure 4.10 Delays of thrombin-evoked WPB exocytosis…….166
Figure 4.11 Rates of thrombin-evoked WPB exocytosis……168
Figure 4.12 Extent of thrombin-evoked WPB degranulation…….168

Figure 4.13 Comparison of *D1* and *D2* in representative single cell examples stimulated with 100μM histamine and 1U/ml thrombin……170
Figure 4.14 Time-course and extent of ionomycin-evoked WPB exocytosis.....172
Figure 4.15 Rates, delays and magnitude of WPB release evoked by histamine, thrombin and ionomycin…….173
Figure 5.1 TIRF/EPI setup schematic……..184
Figure 5.2 There is no unstimulated release of WPBs in contrast to the non-WPB organelle ……..187
Figure 5.3 Time-course of individual experiments recorded during unstimulated conditions……..…188
Figure 5.4 Concentration-dependence of histamine-evoked non-WPB exocytosis……189
Figure 5.5 Delays (*D2*) and maximal rates of histamine-evoked non-WPB exocytosis…….190
Figure 5.6 Ionomycin-evoked non-WPB exocytosis……...192
Figure 5.7 Comparison of the kinetics of non-WPB exocytosis stimulated with 100μM histamine and 1μM ionomycin……..193
Figure 5.8 Delays (*D2*) and maximal rates of the non-WPB and WPB histamine-stimulated exocytosis……...196
Figure 5.9 Comparison of histamine stimulated secretion frequencies between WPBs and non-WPB organelles……..197
Figure 6.1 Setup schematic for imaging Fura-2, EGFP and X-Rhod-1……...208
Figure 6.2 Mito-EGFP signal is independent of histamine stimulation……..209
Figure 6.3 Simultaneous monitoring of $[Ca^{2+}]_i$, $[Ca^{2+}]_m$ and exocytosis…….212
Figure 6.4 $[Ca^{2+}]_m$ increases are significant above 0.3μM histamine stimulation……213
Figure 6.5 FCCP collapses $\Delta\Psi_m$ and increases mito- EGFP fluorescence……..217
Figure 6.6 WPBs undergo pH changes due to FCCP action……221
Figure 6.7 FCCP inhibits mitochondrial Ca^{2+} uptake……..222
Figure 6.8 The inhibitors prevent mitochondrial Ca2+ uptake throughout the cell network of mitochondria……..223
Figure 6.9 Presence of inhibitors decreases the histamine induced $[Ca^{2+}]_i$ changes…….225

Figure 6.10 Summaries kinetics of stimulated WPB exocytosis during mitochondrial Ca^{2+} uptake inhibition……...227
Figure 6.11 Perfusion of inhibitors alone induced exocytosis which correlated to $[Ca^{2+}]_i$ rises……...235
Figure 7.1 $[Ca^{2+}]_i$ patterns generated by continuous stimulation with increasing histamine concentrations within individual HUVEC……...241
Figure 7.2 The sustained phase of the histamine-evoked $[Ca^{2+}]_i$ response depends on extracellular Ca^{2+}…….244
Figure 7.3 Extracellular Ca^{2+}-dependence of histamine-evoked WPB exocytosis…….245
Figure 7.4 The time-course of Ca^{2+} spikes produced by continuous or puff application of ionomycin or histamine……249
Figure 7.5 Simulating $[Ca^{2+}]_i$ spiking patterns by puff application of hormone..251
Figure 7.6 Controlled puff application on un-transfected HUVEC is also subjected to desensitization …….252
Figure 7.7 Controlled puff application causes a larger drop in the Ca^{2+} spike amplitude between the initial and subsequent spikes than seen during perfusion with histamine…….253
Figure 7.8 Pooled secretory responses to controlled puff application of 3μM histamine onto proregion-mEGFP nucleofected HUVEC…….……..257
Figure 7.9 Individual single cell examples that responded to controlled puff application of histamine with a larger exocytotic response during the second Ca2+ spike than the first……259
Figure 7.10 Nucleofected HUVEC respond with perturbed $[Ca^{2+}]_i$ oscillations when perfused with increasing histamine concentrations……...261
Figure 7.11 $[Ca^{2+}]_i$ spikes of proregion-mEGFP nucleofected cells were of longer duration and have a slower rate of rise than non-nucleofected cells……...262
Figure 7.12 Sham nucleofection and pEGFP-N1 nucleofection do not perturb the shape of the Ca^{2+} spikes ……..266
Figure 7.13 HUVEC expressing pEGFP-N1 construct……267
Figure 7.14 Treatment of t-PA-EGFP expressing HUVEC with 10μM CHX for 4hours inhibited t-PA-EGFP protein synthesis……..……..270

Figure 7.15 $[Ca^{2+}]_i$ responses between non-nucleofected untreated and CHX treated cells were similar …….272
Figure 7.16 $[Ca^{2+}]_i$ spike duration in CHX treated cells is similar to control…..273
Figure 7.17 Kinetics of WPB exocytosis in control and CHX treated HUVEC……...274
Figure 7.18 Examples of Ca^{2+} oscillations and WPB exocytosis from CHX treated single HUVEC…….276
Figure I. Single HUVEC co-expressing EGFP-GRO-α and proregion-mRFP……293
Table 1: Differences between WPB and non-WPB…….202

1 INTRODUCTION

1.1 Outline

This thesis focuses on the use of optical techniques to study exocytosis of secretory granules from cultured Human Umbilical Vein Endothelial Cells (HUVEC). Two granules were studied; the Weibel Palade Body (WPB), a true storage organelle of endothelial cells (EC), and a less well characterised granule called for the purposes of this thesis the non-WPB organelle. This chapter includes a brief introduction to the endothelium followed by a description of the two secretory organelles studied, the secretagogues used to study exocytosis and the pathways of intracellular Ca^{2+} release and sequestration that drive secretion. A detailed description of the secretory pathway and formation of the WPB follows including what is known about the regulation of WPB fusion. Then the role of the main WPB cargo protein von Willebrand Factor (vWF) and a non-WPB cargo protein the tissue plasminogen activator (t-PA) is summarised in regulating vascular homeostasis, injury and inflammation. Finally the role of mitochondria in endothelial cells and in other systems is reviewed.

1.2 The Endothelium

1.2.1 Historic background

The vascular endothelium forms the lining of blood vessels, a monolayer of cells that separates blood from vascular muscle (see review [2]). In 1628 the first observation of circulating blood took place by William Harvey and later on in 1660 Malphigi discovered the existence of a network of vessels separated from tissue [3]. The existence of cells lining blood vessels was discovered in the 1800s by von Recklingausen [2]. At that time the endothelium was characterized as an inert semi-permeable barrier that controls traffic of substances between plasma

and tissue by osmotic pressures [3]. It wasn't until the 1950s when George Palade performed electron microscopic studies of the endothelium [4], and James Gowans studied the interaction between lymphocytes and the endothelium [5] that the idea of the endothelium being a specialized organ emerged. Subsequent studies led to the characterization of the endothelium as a dynamic secretory organ [3, 6] with great heterogeneity arising from variations in local environment and vessel size [7]. Phenotypic endothelial differences across the vasculature include intracellular continuity, degree of fenestration [8], susceptibility to undergoing apoptosis [9] and differential protein expression such as of von Willebrand factor (vWF) [7] and tissue plasminogen activator (t-PA) [10]. Detailed study of the function of the endothelium first became feasible with the development of techniques to culture endothelial cells (EC) *in vitro* in the 1970s [11-13]. However, it has been established that the EC phenotype is altered under culture conditions [14]. Yet, EC in culture retain many properties of EC *in vivo*, making them a useful, practical model for the study of the endothelium and its properties (reviewed in [15]).

1.2.2 The endothelium as a secretory organ

The regulatory role of the endothelium on its two contact surfaces; the circulating blood and the smooth muscle layer is immense. This role is accomplished by secretion of factors responsible for mediating vessel growth, blood coagulation, regulation of blood flow, vessel permeability and nutrient and leukocyte traffic (reviewed in [16]). EC help control blood pressure and blood flow by the constitutive and regulated release of vasodilators such as nitric oxide (NO) and prostacyclin (PGI_2) [17] and vasoconstrictors such as endothelin (ET) and platelet-activating factor (PAF) [18, 19]. Moreover EC express or

constitutively release/secrete mediators to maintain normal blood fluidity under resting conditions [16]. The antithrombotic mediators of the endothelium can be divided into three groups; the mediators that prevent platelet aggregation and thus thrombus formation (primary haemostasis) such as PGI_2, NO and surface proteoglycans; the anticoagulants which act to suppress the activation of the coagulation pathway (secondary haemostasis), such as tissue factor pathway inhibitor (TFPI), protein C and annexin V; and those that act to dissolve the formed clot (fibrinolysis) such as tissue plasminogen activator (t-PA) and plasminogen activator inhibitor 1 (PAI-1) [16]. Some of these processes will be considered later in more detail. Furthermore the endothelium is responsible for promoting blood coagulation by regulated exocytosis during vascular injury, inflammation, hypoxia [20], ischemia, radiation or mechanical stimuli such as high shear stress [21, 22]. EC release pro- and anti-coagulant factors to promote and at the same time localise and limit blood coagulation under conditions of stimulation. Some of these factors are produced "on demand" for instance PGI_2, NO and PAF and others such as von Willebrand Factor (vWF) and tissue plasminogen activator (t-PA) reside in preformed secretory organelles such as the Weibel Palade Body (WPB) and the non-WPB respectively. In all, the endothelium can be described as a specialised secretory organ.

1.3 Secretory Organelles of ECs

1.3.1 The Weibel Palade Body and its cargo

The WPB is a secretory organelle made exclusively in EC, discovered in 1964 by Weibel and Palade from lung electron microscopy studies [23, 24]. The organelles were characterised as rod shaped of about 0.15μm in diameter and 2-

3μm in length consisting of tightly packaged fine tubules of approximately 15nm thick. Biochemical, immunofluorescence and structural studies suggested that the fine tubules in WPBs are von Willebrand factor (vWF) [25-27], the major protein of WPBs, comprising more than 95% of its cargo [28]. Figure 1.1A is a fluorescence image of a single HUVEC immune-labelled with an antibody against vWF illustrating the rod-shaped WPB organelles. The paracrystalline storage property of vWF [26] is thought to be necessary for the rapid release and simultaneous unravelling of the 100μm vWF filaments upon exocytosis [29], to efficiently capture platelets along their lengths [30, 31] in response to fluid shear [32, 33]. The role of vWF in haemostasis is considered later on in more detail. The nascent vWF protein consists of a pro-peptide (proregion) which is cleaved during maturation but remains non-covalently linked to the mature vWF protein in the WPBs [24, 34]. Upon exposure of the WPB lumen to physiological pH, proregion dissociates from mature vWF and rapidly disperses from the site of exocytosis [35]; whereas vWF adheres to the endothelial cell membrane or the exposed sub-endothelium [36-39]. Under conditions of low extracellular pH such as ischemia, proregion remains associated with secreted vWF [34]. The extracellular role of proregion is still under investigation. *In vitro* it can act as a ligand for the Very Late Antigen -4 integrin (VLA-4) present on monocytes [40], suggesting a potential role in chemotaxis. Other sources suggest proregion associates with IL-8 to promote neutrophil adhesion [41] and may play a role in platelet aggregation [42] as it contains a binding site for platelets [43].

Other core and membrane proteins in the WPB are co-packaged during the organelles' formation at the trans-Golgi-network (TGN) or are recruited during post-Golgi maturation of the organelle. The WPB membrane can contain the

leukocyte adhesion molecule P-selectin, also present in platelets [44, 45]. P-selectin translocates to the EC plasma membrane during WPB exocytosis and mediates neutrophil and monocyte rolling along activated endothelium by binding via the P-selectin glycoprotein ligand-1 (PSGL-1) in a Ca^{2+} dependent interaction [46]. P-selectin deficient mice exhibit an absence of leukocyte rolling on the endothelium [47]. About 20min after its secretion, P-selectin is thought to endocytose via a clathrin associated mechanism [48, 49] and recycle to the Golgi where it can be re-incorporated into newly forming WPB or sent to lysosomes for degradation [50]. P-selectin is not expressed in all endothelial cells and in those that do express it, it may not be found in all WPBs [51]. In addition, expression of P-selectin alone in an epithelial cell line does not lead to formation of pseudo-WPBs, but rather requires co-expression with vWF [52], suggesting no role for P-selectin in the formation of the WPB.

Small membrane GTP-binding proteins [53] that take part in transport or exocytosis, Rab27a [54], rab3D [55] and ralA [56] are thought to be recruited to the WPB membrane at some stage post-budding from the trans-Golgi network (TGN) and reflect maturation of the granule. Recently it has been suggested that Rab27a prevents exocytosis of mature WPBs in the absence of a stimulus, by anchoring the granules to the actin matrix in a complex with its effector molecule MyRIP [57]. Another component of the WPB membrane is the glycoprotein CD63 or lamp3 [58]. CD63 is also found in late endosomes and in lysosomes and is constitutively expressed at the cell surface of HUVEC. After internalization it can be delivered via endosomal structures to post-Golgi WPBs [59]. The function of CD63 on the WPB is unclear. The fact that the WPB contain Rab27a and CD63 on their membrane, both markers of secretory lysosomes in other cells [60-62],

has led to the suggestion that both organelles are somehow evolutionary related [63, 64].

In addition to the WPB membrane proteins, soluble core proteins include small chemokines such as IL-8 a neutrophil chemoattractant [41, 65, 66] and eotaxin-3 an eosinophil chemoattractant [67], which are up-regulated by tumour necrosis factor-α (TNF-α), Il-1 (IL-8) and Il-4 (eotaxin-3) [68]. In other cell types that do not form WPB, Il-8 is found in the Golgi [41].

Under certain conditions WPBs have been reported to contain the vasoconstrictor endothelin-1[69], anti-coagulant molecule tissue plasminogen activator (t-PA) [70], angiopoietins-1 and 2 [71, 72], osteoprotegerin [73, 74] and factor VIII [75].

1.3.2 The non-WPB- secretory organelle for t-PA

Tissue plasminogen activator (t-PA) is a serine protease important in fibrinolysis, discussed in more detail later. Although t-PA is continuously secreted by the endothelium under resting conditions, its rate of secretion increases during stimulation [76-78]. The secretory organelle for t-PA has long been under investigation, initially to understand whether spontaneously secreted t-PA was derived from a different population of secretory granules than that responsible for stimulated secretion of t-PA. It was found that t-PA was stored in WPBs from co-localization studies of t-PA and vWF in cultured EC [79]. Secretion studies further showed coordinated release of the two proteins in response to various secretagogues [70, 79, 80]. T-PA was targeted to pseudo-WPBs in co-expression studies of vWF and t-PA in ECV304, a cell line that does not endogenously express vWF, suggesting targeting of t-PA to the regulated pathway of secretion in the presence of

vWF [81]. Other biochemical studies however showed differential release of t-PA and vWF to Ca^{2+}-raising agonists such as thrombin [82], bradykinin [82], histamine [83] and ionomycin [84] possibly via a CaM/Ca^{2+}-dependent pathway [84] and to cAMP raising agents [85, 86], suggesting t-PA exists in a non-WPB type of granule. Using density gradient centrifugation Emeis (1997) identified a separate secretory granule for t-PA, small dense vesicles that underwent exocytosis when stimulated with high concentrations of thrombin [87]. Other reports also identified a population of granules morphologically distinct from WPBs, appearing as small punctuate structures of 0.1-0.2μm diameter [88, 89]. A controversy exists as to whether t-PA is packaged in WPBs or in a distinct small organelle called the "non-WPB organelle" for the purposes of this thesis. Work in our lab has shown that t-PA is found in both the WPB and the non-WPB organelle. Figure 1.1B shows a single HUVEC immuno-labelled with an antibody against t-PA demonstrating the punctate non-WPB organelles.

The non-WPB organelle lacks vWF, CD63 and P-selectin and does not recruit Rab27a (T Carter personal communication) or rab3D [55], but can contain a wide variety of molecules, depending on the status of the cell. Such cargo molecules may include protein S [90, 91], and t-PA [76]. The chemokines GRO-α and MCP-1 [92] have recently been identified in a population of secretory granules distinct from the WPB that can undergo stimulated exocytosis. That study did not show co-localisation of the GRO-α positive granules with t-PA positive granules; however evidence from unpublished work in our lab suggests that these organelles are indeed the same.

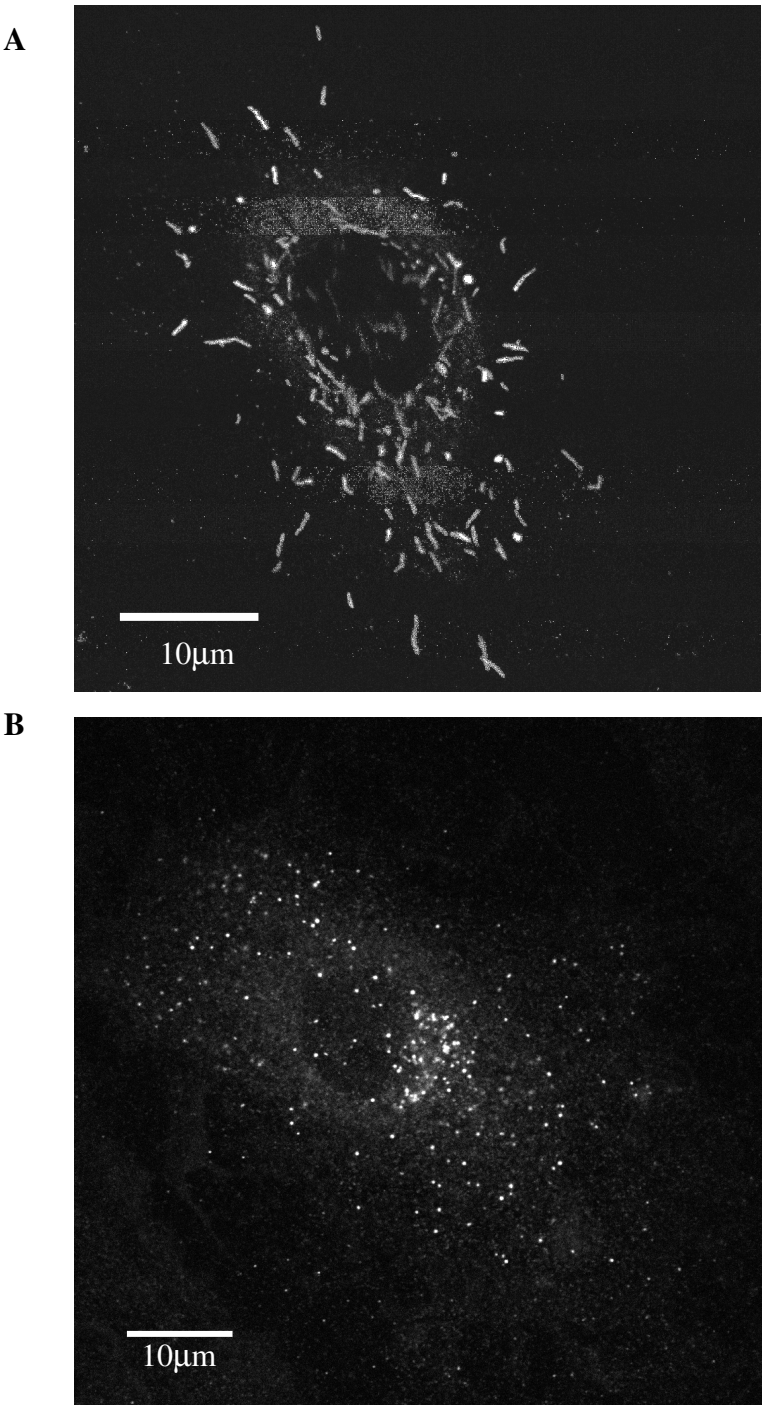

Figure 1.1 Immuno-labelled WPBs or non-WPBs in single HUVEC

*Immunofluorescence image showing a single HUVEC stained with an antibody specific for vWF (**A**), the major protein of the endothelial specific storage granules Weibel Palade Bodies, typically rod-shaped organelles and an antibody specific for endogenous t-PA (**B**), labelling the non-WPB organelles, appearing as small puncta.*

1.4 Signalling pathways leading to WPB release

WPB exocytosis can be triggered by mechanical and chemical stimuli, during physical exercise [93], by fluid shear stress [21, 94], and by physiological agonists [95, 96]. The physiological agonists can be crudely divided into secretagogues that increase intracellular free calcium ion concentration ($[Ca^{2+}]_i$), such as histamine [97-99], ATP [100, 101], vascular endothelial growth factor (VEGF) [102], PAR_2-activating peptide [51] and thrombin [103-105]; or intracellular cyclic adenosine monophosphate concentration (cAMP) [101] such as serotonin [106], vasopressin [107] and epinephrine [108].

Agonists such as histamine and thrombin, raise $[Ca^{2+}]_i$ by binding to G-protein coupled receptors (GPCRs) of the G_q-type on the EC membrane, leading to activation of phospholipase Cβ (PLCβ) [109]. PLC hydrolyzes phosphoinositide 4, 5 bisphosphate (PIP_2) to yield the soluble messenger inositol 1,4,5-trisphosphate (IP_3) and diacylglycerol (DAG) [110-113]. DAG activates protein kinase C (PKC) in the presence of Ca^{2+} [114] which may act as a feedback mechanism to regulate raised $[Ca^{2+}]_i$ but does not appear to be involved in vWF secretion [115-117]. IP_3 diffuses in the cytosol and acts on IP_3 Receptors (IP_3R) on the ER [118, 119] to trigger Ca^{2+} release. There are three IP_3R isoforms [120] and most cell types express more than 1 isoform of IP_3R [121, 122]. Endothelial cells have highest expression levels for type 1 IP_3R [123]. Intracellular Ca^{2+} rise is coupled to calmodulin activation (Ca^{2+}/CaM), which is thought to play a role in WPB exocytosis [84, 115], possibly via activation of molecules involved in the exocytotic machinery [124-126].

cAMP raising agonists bind to GPCRs of the G_s-type which results in the activation of adenylate cyclase (AC) and thus the formation of the second

messenger cAMP from ATP. cAMP is known to bind and activate protein kinase A (PKA) in ECs [108]. Inhibition of cAMP-activated PKA in HUVEC results in reduced vWF secretion [101, 107] suggesting a role for PKA in WPB exocytosis. cAMP is degraded by cyclic nucleotide phosphodiesterases (PDE).

cAMP- raising agents are slower and less efficient in triggering WPB exocytosis than Ca^{2+}-raising agents [127]. Moreover the two types of signaling pathways are also thought to have opposing effects on the cytoskeleton. While Ca^{2+} drives the recruitment of granules from the periphery and the center of the cell to the plasma membrane, intracellular cAMP rises drive only the recruitment of granules from the periphery and tend to trigger the formation of clusters of granules around the nucleus [127, 128]. Moreover Ca^{2+}-raising agents cause cell retraction and intercellular gap formation, whereas cAMP-raising agents strengthen the cortical actin network and preserve cell-cell contacts [127]. It is generally thought that cAMP-raising agents act in a more systemic manner, important in the physiological regulation of plasma vWF levels [93, 129], whereas Ca^{2+} elevating agents may evoke acute responses involved in inflammation or thrombosis.

1.5 WPB Secretagogues used in this thesis

In this thesis, WPB and non-WPB kinetics of exocytosis were determined for the physiological Ca^{2+}-elevating agonists, histamine and thrombin. The response to these agonists was compared to the receptor-independent pharmacological secretagogue ionomycin. Figure 1.2 shows a schematic of the action of the three secretagogues at the membrane receptor level.

1.5.1 Histamine

Histamine is a major mediator of acute inflammation and hypersensitivity responses. It is a hydrophilic vasoactive amine derived from the decarboxylation of the amino acid histidine, catalyzed by the enzyme L-histidine decarboxylase [130]. Histamine is broken down by histamine-N-methyltransferase and diamine oxidase [130].

Histamine has pleiotropic actions and is involved in smooth muscle cell proliferation [131], lymphocyte differentiation [132] and hematopoiesis [133]. The majority of histamine is stored in granules in mast cells [134] and basophils [135], leukocytes involved in allergic reactions. While basophils are only found in the circulation, mast cells migrate into the tissues. Mast cells and basophils are stimulated to secrete histamine when their IgE plasma membrane receptor is activated by the appropriate allergen cross-linked to IgE immunoglobulin [136]. Mast cell stimulation in tissue is thought to be involved in atherogenesis, while activation of mast cells in the human heart and coronary arteries are linked to coronary artery disease [137].

There are four subtypes of histamine receptors (HR), HR_1, HR_2, HR_3 and HR_4; all of which are aminergic G-protein coupled receptors (GPCRs), comprised of a heptahelical transmembrane protein that transduces extracellular signals via G proteins and intracellular second messenger systems [109]. HR_1 couples to G_q and leads to PIP_2 hydrolysis, HR_2 couples to G_s to activate adenylate cyclase and HR_3 and HR_4 couple to G_i to inhibit the adenylate cyclase pathway (reviewed [138]). Molecular properties, distribution and functional characteristics of histamine receptor subtypes differ in various species and tissues [139]. Across the endothelium HRs occur at high densities in venules whereas in arterioles, veins

and muscular arteries they have been found at lower densities with capillaries and the aorta showing the lowest levels [140]. The distribution and density of receptor subtypes is an important factor defining cellular responses [141]. Site-directed mutagenesis studies have identified the binding pocket of histamine on the human HR_1 receptor to be Asp^{107} in transmembrane domain 3, a conserved residue among all aminergic receptors, responsible for an ionic interaction with the amino group of histamine [142, 143]. The active and inactive states of HRs exist in equilibrium. HR agonists such as histamine, have a higher affinity for the active state of the receptor and antagonists for the inactive one. Specific binding to HR_1 by mepyramine, an HR_1 selective antagonist, has been used to study the binding characteristic of HR_1 agonists and antagonists. The association constant of mepyramine for the HR_1 is 1.6±0.4nM [144]. The affinity of histamine for the HR_1, measured as [^{3}H]mepyramine displacing ability (inhibition constant Ki), was determined by competition binding assays to be 16.9±0.1μM [143].

Receptor homologous desensitization is characterized by a loss of receptor responsiveness in the continuous presence of high concentrations of an agonist [145]. It was early established that the HR is prone to homologous desensitization [146] and PKC phosphorylation of HR_1 is thought to play a role in this mechanism [147]. Additional evidence of homologous desensitization of HR_1 came from studies in various cell lines including BC3H-1 cells, Hela cells and 1321N1 human astrocytoma cells [147-149] and smooth muscle preparations [150, 151]. These studies reported that prolonged or repetitive exposure of cell cultures to high histamine concentrations decreased the Ca^{2+} response, attributing this effect to the temporary inactivation of HR_1 leading to a reduced agonist affinity. On the contrary prolonged stimulation of human umbilical endothelial

cells with low concentrations of histamine induced $[Ca^{2+}]_i$ oscillations that were maintained unaffected by the duration of histamine stimulation [152]. Subsequent stimulations with higher histamine concentrations for a short period of time before returning back to low histamine concentrations did not affect the amplitude of the $[Ca^{2+}]_i$ spikes suggesting no apparent desensitization of the HR_1 in those studies [152].

Histamine released in the circulation results in transient, regional activation of endothelial cells. Endothelial cells express both HR_1 and HR_2 [153, 154]. *In vivo* HR_1 mRNA is found to be up-regulate during inflammatory conditions such as atherosclerosis and allergic rhinitis [155, 156]. *In vitro,* histamine HR_1 activation in human umbilical endothelial cells leads to $[Ca^{2+}]_i$ rises [152, 157] in a dose-dependent manner [97]. Downstream effects of histamine binding to EC include an increase in vascular permeability, first discovered by Dale and Laidlaw [158] and further characterised using electron microscopy by Majno and Palade in 1961 who demonstrated histamine creates junctional gaps between adjacent endothelial cells that could facilitate plasma to leak into the basement membrane [159]. Contraction in endothelial cells for the formation of junctional gaps is driven by the contractile proteins actin and myosin [160]. Moreover, histamine is a potent secretagogue stimulating PGI_2 [161] and vWF release [97], both in a dose dependent manner [97]. Histamine also stimulates secretion in a variety of other cell types including neurons [162] and adrenal gland cells [163].

1.5.2 Thrombin

Thrombin is a serine protease of the coagulation cascade [164] derived from the proteolytic cleavage of the zymogen pro-thrombin by the pro-thrombinase complex consisting of serine protease factor Xa and its cofactor Va, end products of the coagulation cascade [165]. Production of thrombin is regulated by thrombin itself in a positive feedback mechanism where thrombin activates factor V and factor VIII to propagate the coagulation cascade [166-168]. Thrombin also negatively regulates its production by activating protein C, via binding to thrombomodulin. Protein C acts to damp down the coagulation cascade, by inactivating many of the serine proteases involved in the cascade [169]. The ultimate role of thrombin is the conversion of the soluble plasma protein fibrinogen into insoluble fibrin. Thrombin also activates many cells including platelets, endothelial cells, epithelial cells, smooth muscle cells and hemopoietic cells to promote haemostasis [170-173]. Thrombin-activated platelets secrete many molecules that will act autologously to induce platelet shape change, aggregation and adhesion to the sub-endothelium to promote fibrin clot formation.

Thrombin acts through Proteinase Activated Receptors (PARs), which like the HR receptors, are G-protein coupled receptors [174, 175]. There are four PARs (PAR-1-4), of which thrombin activates PAR-1, 3 and 4 whereas PAR-2 is activated by trypsin or mast cell tryptase [176]. Thrombin activates PAR-1 and 3 with high potency and PAR-4 with low potency. Endothelial cells constitutively express PAR-1 and PAR-2 [177, 178] which play a functional role in the endothelium whereas PAR-3 and PAR-4 are limited to regulating platelet function [179]. The half maximal effective concentration (EC_{50}) of thrombin on PAR-1 activation was found to be 50 pM [180]. The interaction between thrombin and

PAR-1 on endothelial cells takes place between the anion binding site of Thrombin, a sequence of positively charged basic residues, and a sequence of negatively charged acidic residues on the amino-terminus of PAR-1 [176]. Thrombin cleaves the amino-terminus, an irreversible process, to expose a new amino-terminus and render the receptor active. Low concentrations of thrombin will eventually cleave and activate all the receptors on a cell; however the rate of receptor cleavage will depend on thrombin concentration. Studies in human pulmonary artery endothelial cells showed that both duration and concentration of thrombin stimulation regulate endothelial cell surface PAR-1 expression [181]. PAR-1 desensitization occurs by receptor inactivation and internalization during long exposures (>60min) to low doses (25nM) of thrombin [181]. The internalized receptors are sorted to lysosomes in endothelial cells and fibroblasts [182]. The recovery of the receptor responsiveness occurs by de novo synthesis and translocation of PAR-1 to the cell surface [181].

Following thrombin induced PAR-1 activation, PLC is activated through G_q to produce IP_3 which mobilises $[Ca^{2+}]_i$ and DAG which activates PKC [179]. Thrombin has been shown to produce a dose-dependent $[Ca^{2+}]_i$ rise and dose-dependent patterns of $[Ca^{2+}]_i$ signalling in endothelial cells [97, 183]. Thrombin-induced PAR-1 stimulation in endothelial cells leads to secretion of NO and PGI_2 [103] which may cause smooth muscle cell contraction [184]; reversible increase of microvascular permeability by formation of inter-endothelial gaps [185, 186] due to cadherins junction disassembly [187, 188] and vasoconstriction [189, 190] due to myosin light chain phosphorylation which results in mechanical contraction of the endothelium [191]. Histamine also induces endothelial gap formation but with less potency than thrombin [187]. Thrombin-induced secretion of von

Willebrand factor is thought to be due to $[Ca^{2+}]_i$ elevations instead of PKC-mediated signal transduction [115].

1.5.3 Ionomycin

Ca^{2+} ionophores such as ionomycin are often used as experimental tools to stimulate Ca^{2+}-dependent processes such as exocytosis [1, 83, 116] or to discharge intracellular Ca^{2+} stores [192, 193] independently of cell surface receptor activation. Ionomycin belongs to the family of polyether carboxylic acid antibiotics [194] isolated from the bacterium *Streptomyces conglobatus* [195]. Due to its dibasic acidic properties it selectively forms positively charged 1:1 lipid soluble complexes with divalent cations [196-201], with a high selectivity for Ca^{2+} over Mg^{2+} [201], to transport Ca^{2+} across membranes [202, 203]. Ionic or pH differences may induce variations in the affinity of ionomycin for Ca^{2+} [201, 204]. Ionomycin is a Ca^{2+} transporter in both directions between membranes such that Ca^{2+} equilibrates uniformly in all vesicles within a cell at all ionomycin concentrations used [205]. The ionomycin-induced Ca^{2+} transport across membranes can be influenced by plasma membrane depolarisation [204].

In EC ionomycin-induced emptying of the ER leads to a sustained $[Ca^{2+}]_i$ rise. This sustained rise is due to a store-regulated Ca^{2+} entry process, activated by ER Ca^{2+} depletion, which refills the intracellular Ca^{2+} store via the action of the Sarco-ER-Ca^{2+} ATPase (SERCA) pump on the ER [206]. Supporting evidence come from experiments where blocking the store-regulated Ca^{2+} entry pathway showed no change in the initial mobilization of Ca^{2+} observed but showed an inhibition of the plateau phase of ionomycin-evoked $[Ca^{2+}]_i$ responses [206].

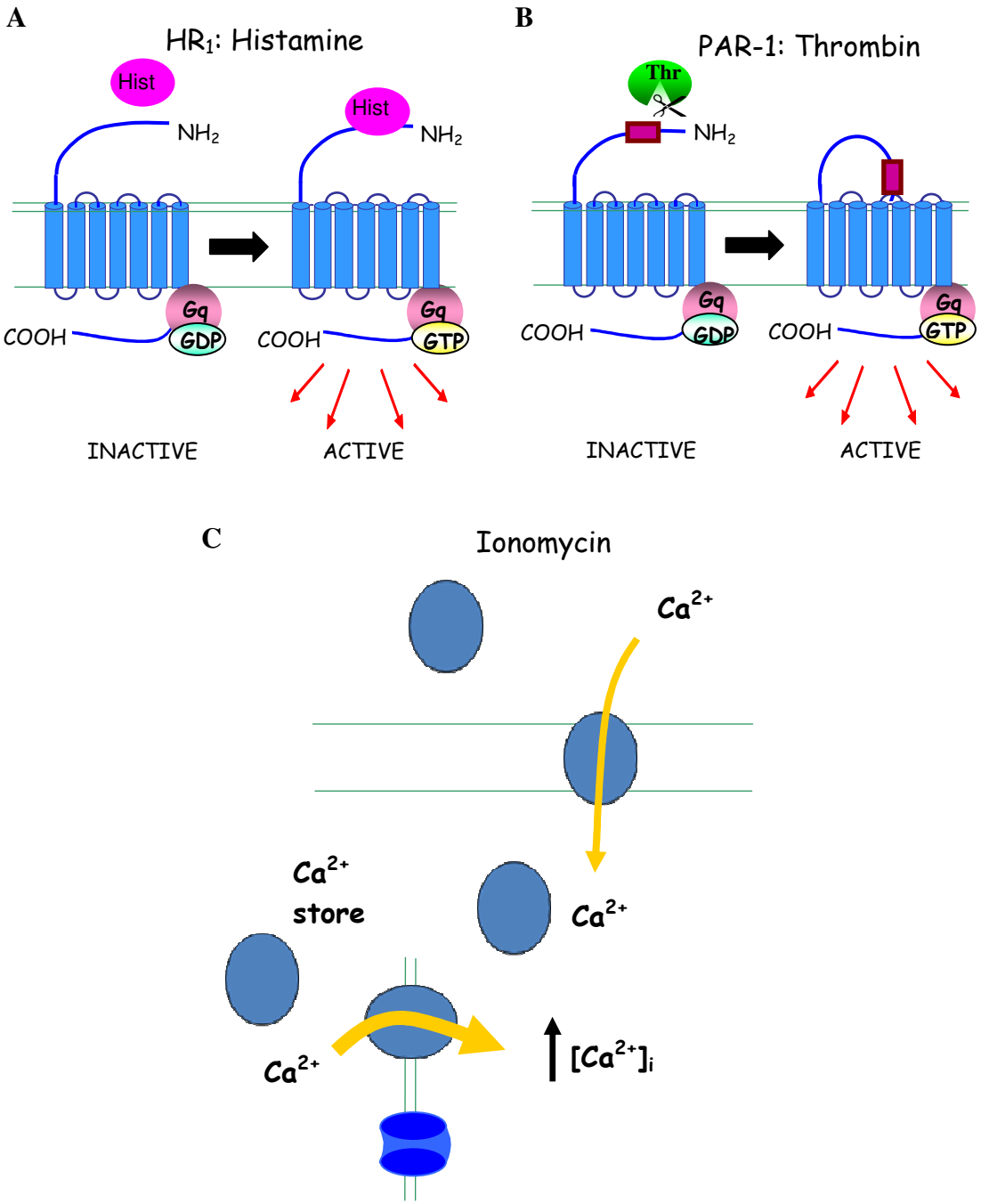

Figure 1.2 Histamine, thrombin and ionomycin cell membrane action

*Schematic of histamine (**A**), thrombin (**B**) and ionomycin (**C**) action at the cell membrane. Histamine in endothelial cells acts via the histamine receptor HR_1 and thrombin via the Proteinase-Activated Receptor 1 (PAR-1), both G-protein coupled receptors. Thrombin cleaves PAR-1 at the NH_2 terminus for the receptor to be activated. Ionomycin bypasses the receptor level and translocates Ca^{2+} ions into the cytosol mainly from the internal Ca^{2+} store.*

1.6 Regulation of intracellular Ca^{2+} homeostasis

Ca^{2+} is a major intracellular messenger in eukaryotic cells [207]. The regulation of Ca^{2+} levels is important for controlling cellular processes and to ensure that $[Ca^{2+}]_i$ does not reach cytotoxic levels [208]. The major Ca^{2+} store in the cell is the ER constituting approximately 75% of the total intracellular Ca^{2+} reserve in endothelial cells while the remaining 25% is handled by the mitochondria [209]. Both ER and mitochondria have high capacities for Ca^{2+} storage, reaching as high as 3mM in the ER most of which is bound to Ca^{2+} binding proteins (see review [210, 211]) such as calreticulin [212] or BiP [213]. The cytosolic Ca^{2+} response is biphasic; firstly an initial transient increase of $[Ca^{2+}]_i$ due to IP_3-evoked release from intracellular stores [214], followed by a prolonged phase, that can take the form of either a maintained $[Ca^{2+}]_i$ elevation, a decline to basal levels (~0.1μM) or periodic Ca^{2+} spikes (oscillations) [100, 105, 215-217]. The major pathways of intracellular Ca^{2+} sequestration are illustrated in Figure 1.3 and dissected below.

1.6.1 The initial phase of the $[Ca^{2+}]_i$ response and Capacitative Ca^{2+} entry

The initial phase of the $[Ca^{2+}]_i$ rise evoked by histamine or thrombin depends on the generation of IP_3 and the activation of the IP_3R on the ER membrane.

Early studies suggested that the agonist dependent depletion of the internal stores is a trigger for extracellular Ca^{2+} entry via plasma membrane channels. These studies used Mn^{2+} entry, monitored as quenching of cytosolic Fura-2 fluorescence in thrombin stimulated platelets [218] and endothelial cells [219]. This mechanism was described by Putney in 1986 as store-operated-Ca^{2+}-entry

(SOC) or capacitative Ca^{2+} entry (CCE) [220, 221] and is responsible for accomplishing long lasting Ca^{2+} influx in endothelial cells [222-224] and other non-excitable cell types [225-227]. Extensive studies have taken place to try and identify the Ca^{2+} entry channels. In 1992 Hoth et al discovered a non-voltage-gated Ca^{2+} selective current in mast cells activated by store depletion, which was called the I_{CRAC} (Ca^{2+}-release activated Ca^{2+}-current) [192, 228]. The I_{CRAC}, conducted by the CRAC channel, is a small inwardly rectifying current with a very positive reversal potential (>+60mV) suggesting a high selectivity for Ca^{2+} [229]. The CRAC channel is thought to be under negative feedback regulation by high local concentrations of Ca^{2+} and the extent of store depletion [230, 231]. I_{CRAC} currents activated by depleting intracellular Ca^{2+} stores by ionomycin or administrating the SERCA blocker thapsigargin have also been described in EC [232, 233].

Later on it was suggested that the CRAC channels are encoded by the Trp (transient receptor potential) genes [234], originally identified in a Drosophila photoreceptor mutant [235]. The sequence of Trp [236] was found to be homologous to mammalian voltage-dependent Ca^{2+} channels [237]. Heterologous expression of Trp in mammalian systems demonstrated enhanced CCE [238]. In vascular EC at least 19 Trp isoforms are expressed with diverse functions, including modulation of EC permeability, cytoskeleton rearrangement, oxidative stress induced responses and vascular tone activated by different stimuli (reviewed in [239]). TRP activation in EC is thought to fine-tune the membrane potential (PM) leading to altered driving force for Ca^{2+} entry (reviewed [240]). Due to the importance of TRP channels in controlling $[Ca^{2+}]_i$ signalling, their malfunction may lead to cardiovascular disorders [241]. TRP channels 1 (TRPC1)

[242, 243] or 4 (TRPC4) [244] have been proposed to mediate CCE in EC, however this is debatable due to their non-selectivity for Ca^{2+} [245].

Although research has led closer to the identity of CCE channels, the signalling pathways that couple intracellular store depletion to the plasma membrane to activate the Ca^{2+} entry channels remain unclear. Three mechanisms have been proposed by different groups (reviewed [246, 247]). Firstly a diffusible messenger pathway has been proposed [248] in which a small mobile factor is released from the stores upon their depletion, termed Ca^{2+}- influx factor (CIF) [249] which directly opens CRAC channels [250]. A likely proposed molecule to act as a diffusible messenger is microsomal P450 mono-oxygenase (P450MO) metabolites such as epoxyeicosatrienoic acid (EET). EET is synthesized from arachidonic acid which is produced by Ca^{2+} activation of Phospholipase A_2 (PLA_2) and acts as an endogenous ligand on CCE channels [251]. Ca^{2+} entry induced by EET has been reported previously in EC [252-255]. The second mechanism proposed for CCE signalling was the vesicle secretion model [256] in which CRAC channels are transported from the ER and inserted into the plasma membrane upon store depletion [257]. Finally the conformational coupling model was proposed which suggests the interaction between ER and plasma membrane for direct Ca^{2+} entry [258]. Originally IP_3Rs were thought to be physically attached to CRAC channels on the plasma membrane and function as messengers via direct protein-protein interactions [258, 259]. Recently two molecules have been identified as key players in the CCE mechanism in immune cells and HEK293 cells, Orai1 and STIM1 [260]. STIM1 is thought to reside on the ER membrane where it acts as a Ca^{2+} sensor and is activated upon ER Ca^{2+} depletion to redistribute into clusters that approach the plasma membrane [261]. These

aggregates were found to interact with Orai1 molecules on the plasma membrane and subunits of CRAC channels [262], leading to their activation and the direct entry of Ca^{2+} from the extracellular space into the ER (reviewed in [263]). Orai1 and STIM1 have recently been implicated to play a role in EC CCE mechanism [264].

1.6.2 The prolonged phase of the $[Ca^{2+}]_i$ response and $[Ca^{2+}]_i$ oscillations

In EC Ca^{2+} oscillations were first observed in cultured Human Umbilical Endothelial cells stimulated with histamine by Jacob et al [152] and later on with thrombin [183, 265], ATP [100, 215] and bradykinin [216, 266]. The mechanism underlying Ca^{2+} oscillations in non-excitable cells involves complex feedback behaviour by IP_3 and Ca^{2+} acting on the IP_3R [267, 268]. The open probability of the brain type I IP_3R Ca^{2+} channel, also found in endothelial cells [123], shows a bell shape relationship to local $[Ca^{2+}]_i$ [269]. Thus in the presence of IP_3, local $[Ca^{2+}]_i$ acts as a co-agonist to modify IP_3R activation in a biphasic manner; low concentrations increase the open probability of the channel whereas higher concentrations reach inhibitory levels terminating Ca^{2+} efflux into the cytosol [270, 271]. The interaction between Ca^{2+} and the IP_3R is thought to account for the abrupt up-stroke and rapid termination of the first period of Ca^{2+} release that gives rise to the spike-like appearance of the Ca^{2+} release profile [267]. Following IP_3R activation and Ca^{2+} release, cellular buffering mechanisms remove cytosolic Ca^{2+} [272] returning $[Ca^{2+}]_i$ levels back to resting levels (described in more detail below); allowing the slow recovery from Ca^{2+}-inhibition of the IP_3R by high Ca^{2+} [267]. After a period of time (that depends on the cell type and types of IP_3Rs expressed), a regenerative cycle of IP_3R receptor activation may occur, driven by the co-agonist effect of low Ca^{2+} in the continued presence of IP_3, leading to a

second round of Ca^{2+} release from the ER. Subsequent Ca^{2+} spikes arise in the same way and can be repeated as long as the cell is exposed to agonist that generates IP_3 [152]. The Ca^{2+}-dependency of the open probability of the IP_3-gated channels shifts according to the IP_3 concentration ($[IP_3]_i$), so that at low $[IP_3]_i$ the IP_3R is inhibited at lower local Ca^{2+}; whereas at high $[IP_3]_i$ the IP_3R activity persists in the face of high Ca^{2+} [273]. Thus following stimulation with very high agonist concentrations sustained rises in Ca^{2+} rather than Ca^{2+} spikes are often observed [152]. Refilling of the ER for maintaining the cytoplasmic $[Ca^{2+}]_i$ oscillations is achieved by capacitative entry of extracellular Ca^{2+} in endothelial cells [222-224] (1.6.1).

The Ca^{2+} released from a cluster of IP_3Rs propagates locally in the cytoplasm promoting nearby IP_3R clusters to release Ca^{2+} giving rise to a propagating wave of $[Ca^{2+}]_i$ within single cells. Such behaviour is observed in a wide variety of cells including pancreatic acinar cells [274], SMC [275], hepatocytes [276] and EC [277, 278].

Agonist-induced $[Ca^{2+}]_i$ oscillations may function to regulated cellular processes. In excitable cells $[Ca^{2+}]_i$ spikes coincide with exocytosis [279], for instance gonadotropin release in pituitary gonadotropes [280], catecholamine release from adrenal chromaffin cells [281, 282] and insulin secretion from pancreatic β-cells [283]. In non-excitable cell types $[Ca^{2+}]_i$ oscillations mediate cellular functions including fluid secretion and cell volume changes in salivary gland cells [284], fertilization of mouse oocytes [285], secretion from mast cells [286], cell migration in neutrophils [287], glycogenolysis in hepatocytes [227] and cell contraction in smooth muscle cells [288]. It is not clear what cellular functions are regulated by $[Ca^{2+}]_i$ oscillations in EC however the regulation of

secretion of vasoactive molecules such as NO, endothelin or PGI_2 has been suggested [289]. Interestingly it has been suggested that WPB exocytosis may not be regulated by $[Ca^{2+}]_i$ oscillations although a direct analysis was not carried out in that study [183].

Early work in hepatocytes showed that spike frequency during $[Ca^{2+}]_i$ oscillations is dependent on agonist concentration [227, 290]. A similar relationship between stimulus strength and Ca^{2+} oscillation frequency was also noted in endothelial cells [100, 152, 183, 215, 266]. These observations led to the idea that the frequency of Ca^{2+} oscillations might provide the means to regulate different cellular processes. Indeed the frequency of Ca^{2+} oscillations was found to elicit either long-term potentiation or depression in neurons [291], differential gene transcription and cell differentiation in T-cells [292], differential secretory patterns from exocrine pancreatic gland cells [293] and epithelial cells [294].

In addition to the sensitivity of the IP_3R to IP_3 and $[Ca^{2+}]_i$ levels, the frequency of Ca^{2+} oscillations is also regulated by several factors including the rate of cytoplasmic Ca^{2+} removal by Ca^{2+} pumps (see 1.6.3) and protein phosphorylation as initially suggested by Goldbeter et al [295]. Phosphorylation of the IP_3R by a series of kinases including protein kinase C (PKC) [296-298], Ca^{2+}/Calmodulin-dependent protein kinase II (CaMKII) [298], protein kinase A (PKA) [299-301] and cyclic GMP-dependent protein kinase [302] have been shown to regulate the potency of IP_3-evoked Ca^{2+} release in a feedback regulation. The activity of CaMKII [303] and PKC [266, 296] on the IP_3R is determined by the Ca^{2+} oscillation frequency and amplitude.

1.6.3 The decay phase of the $[Ca^{2+}]_i$ response; cytoplasmic $[Ca^{2+}]_i$ removal mechanisms

The decline in $[Ca^{2+}]_i$ following release from the stores is achieved by the action of membrane pumps responsible for intracellular Ca^{2+} homeostasis. These include the plasma membrane Ca^{2+}-ATPase (PMCA) [304] and the Na^+/Ca^{2+} exchanger (NCE) [272, 305, 306] on the plasma membrane; the Sarco-Endoplasmic Reticulum-Ca^{2+} ATPase (SERCA) on the ER [307] and the mitochondrial uniporter in endothelial cells (reviewed in [308]). The uniporter will be considered in more detail below (1.10). The PMCA and SERCA function at low transport rates, both with high affinities for Ca^{2+}, maintaining in this way resting $[Ca^{2+}]_i$ levels during the inter-spike period and are thought to play a role in determining the frequency of $[Ca^{2+}]_i$ oscillations in EC [304, 307]. The NCE however has low affinities for Ca^{2+} but can transport Ca^{2+} at much higher rates, able to extrude high concentrations of Ca^{2+} from the cytoplasm rapidly [309]. Different isoforms of pumps with specific rates of transport are thought to determine the time-course of Ca^{2+} transients in different cells [310].

The NCE is found on the plasma membrane but also on other intracellular organelles including mitochondria [311]. Its direction mode and rate of action depends on the Na^+ and Ca^{2+} gradient and the membrane potential across the plasma membrane [309]; thus reduction of the Na^+ gradient leads to an increase in $[Ca^{2+}]_i$ via NCE Ca^{2+} entry in EC [304, 306]. Inhibition of either the PMCA or NCE pump delays the decay phase of the agonist-stimulated $[Ca^{2+}]_i$ response suggesting both play a role in shaping Ca^{2+} transients in EC [193, 312].

The SERCA pump is responsible for clearing high cytosolic Ca^{2+} levels by pumping Ca^{2+} into the ER and maintaining ER Ca^{2+} levels constant during IP_3-

evoked Ca^{2+}-release [313]. The activity of the SERCA and PMCA Ca^{2+}-ATPases compete for the raised $[Ca^{2+}]_i$ and either pump accounts for the falling phase of Ca^{2+} spikes during Ca^{2+} oscillations in different cells. In HUVEC the SERCA pump is thought to be responsible for the decay phase of agonist-evoked Ca^{2+} release [307], whereas in rat microvascular EC the PMCA and NCE pumps play this role [314]. The SERCA is also suggested to contribute to the initial shape of the Ca^{2+} rise of individual spikes as it transports local Ca^{2+} into the ER suppressing the Ca^{2+} positive feedback mechanism on the IP_3Rs (1.6.2) [307].

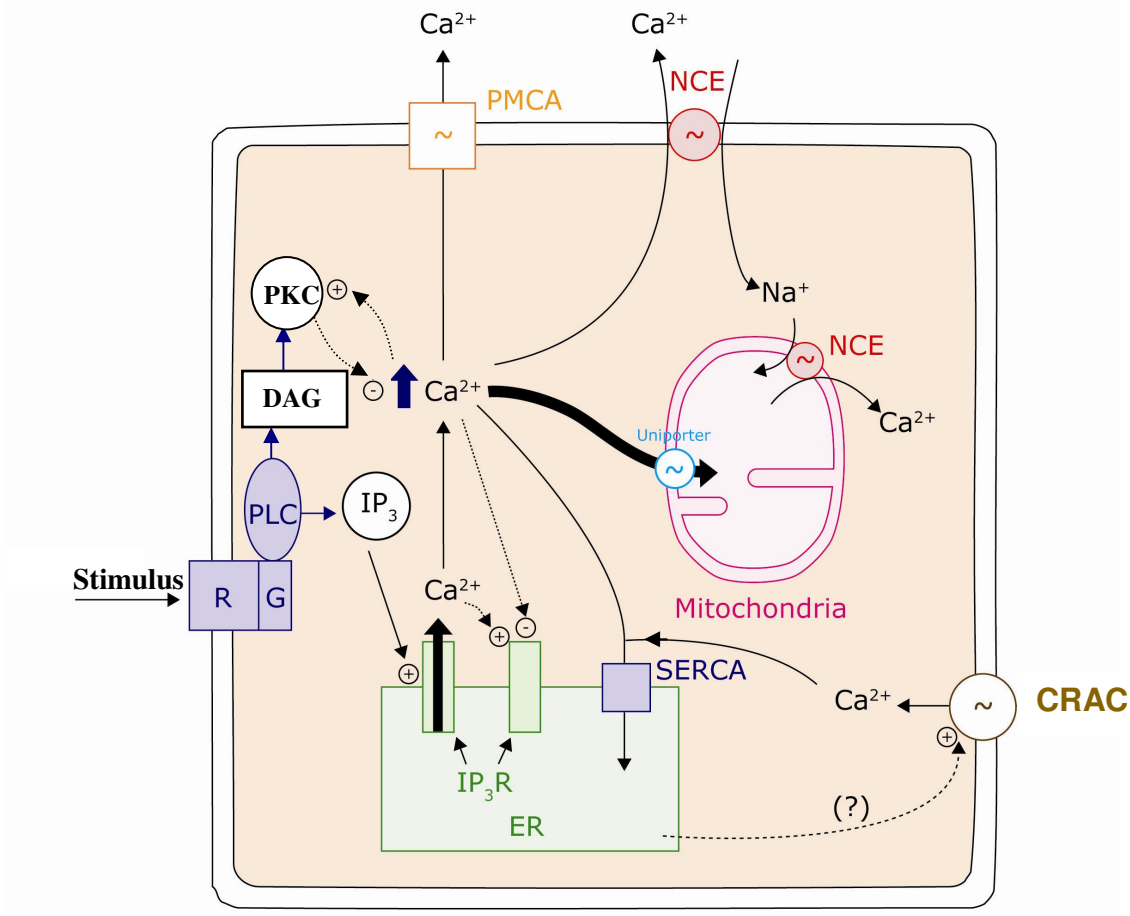

R=G-protein coupled Receptor	**ER=Endoplasmic Reticulum**
G= G-protein	**SERCA= Sarco/ER Ca^{2+} ATPase**
PLC= Phospholipase C	**PMCA=Plasma membrane Ca^{2+}**
IP_3= Inositol 1,4,5-trisphosphate	**ATPase**
PKC= Protein kinase C	**NCE= Na^+/Ca^{2+} exchanger**
IP_3R= IP_3 Receptor	**CRAC= Ca^{2+}-release activated Ca^{2+}**
DAG= Diacylglycerol	**channel**

Figure 1.3 Endothelial cell $[Ca^{2+}]_i$ sequestration

When a Ca^{2+}-raising agonist reaches the cell, it binds to and activates a G-protein coupled receptor (GPCR) which in turn interacts with a G-protein to activate PLC. In turn PLC catalyzes the formation of IP_3 and DAG. The later activates PKC which can regulate $[Ca^{2+}]_i$ via feedback mechanisms such as phosphorylation and inactivation of the GPCR. IP_3 diffuses to the ER to bind and activate IP_3R leading to an intracellular Ca^{2+} rise. Local Ca^{2+} regulates the IP_3R open probability. Increased $[Ca^{2+}]_i$ is sequestered from the cytoplasm via different pumps; the SERCA pump which drives Ca^{2+} into the ER, the PMCA and NCE which translocate Ca^{2+} outside the cell in parallel and the mitochondria uniporter. The NCE on the mitochondria functions to slowly discharge $[Ca^{2+}]_m$. Emptying of the ER triggers capacitative Ca^{2+} entry via CRAC channels, however their nature and signal for activation is under investigation.

1.7 The secretory pathway: From ER to fusion

Endothelial cells are complex secretory cells that function to control the processes of haemostasis, inflammation, vasoregulation and angiogenesis by secreting or releasing a wide range of molecules. Therefore it is important to understand the secretory pathways of EC and the route by which different mediators are trafficked and released. The two secretory granules that are the focus of this thesis have been described above. Here a brief overview of what is known about the formation and fusion of these endothelial organelles will be made.

1.7.1 Secretory vesicle formation in EC

1.7.1.1 VWF biosynthesis and WPB formation

The Weibel-Palade bodies (WPBs) are a population of rod-like storage granules, found in EC [23, 24, 315] (Figure 1.1A). The formation of the WPB is thought to be driven by its main cargo protein von-Willebrand factor (vWF) [28], as heterologous expression of vWF in other cell systems induced the formation of rod-like organelles that resembled the WPB [316, 317] and knock down of the protein inhibits WPB formation in EC [318]. The vWF gene is located on chromosome 12 [319, 320]. Direct amino acid sequence analysis of vWF [321] and cloning from EC cDNA libraries [319, 320] determined a 9kb mRNA coding for 2813 amino acid polypeptide [322] composed of a 22 amino acid signal peptide, 741 amino acid pro-peptide and 2050 amino acid mature vWF [323].

The cellular trafficking pathways for different secreted proteins all start with their synthesis by ribosomes attached to the membrane of the rough endoplasmic reticulum (rER) [324], an interconnected network of membrane tubules and

cisternae continuous with the nuclear envelope [325]. Ribosomes are attached to the ER membrane by their large subunit which holds the nascent peptide [326]. The newly synthesized polypeptides are transported through the translocon complex [327] on the ER membrane into the cisternal space of the ER, an irreversible step called segregation [328]. Various sugar modifications occur during translation and protein-protein interactions within the lumen of the ER that help facilitate protein folding, protein quality control and oligomerization [329].

During entry of vWF into the ER lumen, it is processed by removal of the signal peptide and addition of N-linked carbohydrates [330] before dimerizing by forming disulfide bonds between the C-terminus cysteine knot domains [331-333]. Dimerization allows the vWF protein to proceed from the cisternal space of the rough ER to the Golgi network [334, 335] in an energy dependent fashion via a carrier-mediated mechanism facilitated by COP-I in conjunction with ARF1 [336].

The Golgi complex is a series of membrane compartments consisting of three discrete groups of cisternae, the cis, medial and trans [337]. The cis-Golgi network (CGN) serves as a port of entry to the Golgi stack for secretory proteins excluding ER resident proteins. Proteins are thought to move from one station to the next via the budding and fusion of small transport vesicles with subsequent cisternae, where they undergo various modifications such as carbohydrate modifications, acylation and sulfation catalysed by resident enzymes [337, 338]. VWF undergoes further modifications in the Golgi such as addition of O-linked carbohydrates [331].

Sorting of secretory proteins destined for the plasma membrane, secretory vesicles and lysosomes occurs in the Trans-Golgi Network (TGN) [339, 340], a

specialised reticulum of tubules derived from the trans-most cisterna of the Golgi involved in the final protein processing steps [337]. The TGN was firstly discovered by Novikoff in the 1960s and was thought to be a part of the ER that formed lysosomes (GERL- Golgi endoplasmic reticulum lysosomes) [341]. It was later renamed as the TGN by Griffiths and Simons [342]. The proteins reach the lumen of the TGN in a dilute solution and are progressively concentrated in a Ca^{2+}- and pH-dependent manner [343]. The TGN is thought to be slightly more acidic (~pH6.2-6.58 [344-347]) than the previous compartments, a feature that has a role in facilitating protein aggregation.

In the TGN the disulphide linked vWF dimer undergoes sulfation by sulfotransferases [348] and the endoproteolytic cleavage of proregion from the mature vWF by a furin-like activity [349]. The cleavage step was earlier thought to take place in the WPB where proregion and mature vWF are found in a 1:1 stoichiometry [350, 351]. However it was later found that the cleavage step occurs in the slightly more acidic TGN environment where a non-covalent association occurs between proregion and vWF [24, 34]. The vWF dimers then polymerise via disulfide bonds formed between the N-termini to generate high molecular weight multimers. The multimerization process also requires the acidic environment of the Golgi, high Ca^{2+} and the presence of proregion [334, 352, 353]. The latter may act as a disulfide isomerase at low pH, able to catalyze thiol protein disulphide interchange and support N-terminal disulphide bond formation essential for vWF multimerisation [354, 355].

The vWF tubules are packaged into the WPBs at the TGN in a highly ordered paracrystalline structure [26, 29]. The heterotetrameric adaptor protein 1 (AP-1) and clathrin coated membranes are reported to be important for WPB

biogenesis from the TGN [356] however the relationship between clathrin coat and formation of tubules is yet to be precisely determined. Clathrin is present on newly formed secretory granules including the WPB but is lost during their maturation. Clathrin mediated membrane budding is thought to lead to the removal of soluble and membrane proteins not needed in the mature organelle as well as recycling excess membrane back to the TGN [339]. This process of core and membrane remodelling leads to secretory granule maturation. The mature WPBs accumulate within the cytoplasm, ready to undergo exocytosis in response to secretagogue stimulation. There is evidence that vWF undergoes progressive condensation during WPB maturation as observed by EM of high-pressure frozen WPBs [27].

1.7.1.2 T-PA biosynthesis and non-WPB formation

The optical studies of the non-WPB secretion described in this thesis utilize a fluorescent fusion protein of one of its cargo molecules, tissue plasminogen activator (t-PA). The amino acid sequence of the t-PA precursor comprises 563 residues, including a signal sequence of 20-23 hydrophobic amino acids and a hydrophilic pro-sequence of 12-15 amino acids at the N-terminus [357]. In the ER the t-PA polypeptide chain is glycosylated and the signal and pro-sequence are cleaved from the newly synthesized enzyme [358]. No detailed data exist for the sorting at the TGN and formation of the t-PA containing non-WPB organelle. The cargo and regulation of secretion of the non-WPB organelle is less well understood and is discussed below.

1.7.2 Constitutive and regulated secretion

Segregation of proteins destined for constitutive or regulated secretion takes place at the TGN [359]. In contrast to the regulated pathway clathrin is not involved in the exit of constitutively secreted proteins from the TGN [360]. It is thought that upon arrival of material at the TGN destined for constitutive secretion, a signalling cascade involving protein kinase D (PKD) is triggered to locally produce diacylglycerol (DAG) [361]. The cargo is packaged into budding transport carriers which grow in size to encapsulate the cargo molecules, and the accumulated DAG catalyzes membrane fission to dissociate the transport carriers from the TGN (reviewed in [362]). The transport carriers are then trafficked to the plasma membrane. It was first though that secretion via the constitutive pathway was not altered by secretagogue stimulation [339, 359] however, there is evidence that under some conditions regulation of the constitutive pathway does occur [363], and other Ca^{2+} dependent trafficking steps [364-366]. Constitutively secreted proteins by definition are not stored within the cell, and consequently they do not accumulate within the cell in a time dependent fashion [359]. The release of constitutively secreted proteins can be rapidly blocked by inhibitors of protein synthesis [367, 368], by disruption of ER to Golgi trafficking by the antibiotic Brefeldin-A [369-371] or by decreasing the temperature below 20°C [372], while leaving regulated secretory storage granules largely unaffected. The half time for constitutive delivery to the plasma membrane of a GFP-tagged transmembrane protein expressed in COS cells was approximately 3.8min [373] and pulse labelling of constitutively secreted glycosaminoglycan chains (GAG) in CHO cells exhibited a half time for secretion of 12-14min [374]. Evidence from pulse-chase experiments shows that newly synthesized t-PA can be retained in the

cell for up to 4h [375]. Studies utilizing GAG chains have shown that constitutive secretion does not require any newly synthesized proteins suggesting recycling of components of the vesicle machinery [376].

Certain cell types also utilise the regulated secretory pathway [339]. Proteins destined for the regulated secretory pathway form a dense membrane bounded core of aggregated protein at the TGN, that becomes enveloped by a clathrin coat and buds off the TGN in an ATP dependent manner to yield a dense core immature secretory granule [340]. Regulated secretory proteins are concentrated into specialised membrane bound storage organelles, which are retained in large intracellular pools and their release is coupled to an extracellular stimulus [359]. Regulated exocytosis takes place in a controlled manner in which the time course, rates and quantity of bioactive molecules released varies in response to the strength or duration of stimulation. A fraction of protein sorted into the regulated pathway can be spontaneously secreted in the absence of a stimulus and this is called basal secretion [377].

VWF is sorted into both the constitutive secretory pathway [95] and the regulated secretory pathway (stored into WPB) [350] at the TGN. Constitutively secreted vWF appears to be in the form of smaller multimers originating from the ER [350]. It was originally thought that only 5-10% of vWF synthesized in cultured EC is stored in WPB and the rest is secreted constitutively [350]. Recently however it has been shown that the sorting efficiency is much higher, with perhaps > 50% of vWF sorted into the WPB [371]. There is not a clear distinction about which pathway the non-WPB belongs to.

1.7.3 The role of the cytoskeleton in exocytosis

The microtubules extend asymmetrically from the microtubule organizing centre around the nucleus (minus end) to the cell periphery (plus end) [378]. The microfilament network may anchor and stabilise the plus ends of microtubules at the plasma membrane [379]. It is thought that vesicle movement to the plasma membrane is facilitated by transport on microtubules [380], and vesicle interactions with microtubules have been observed in electronmicrographs [381]. Following microtubule depolymerisation, the secretion and polarization of newly synthesized material [382] along with regulated secretion of WPBs [383] is inhibited suggesting microtubules are important in trafficking of constitutive and regulated secretion. The viscous gel of the actin cortex acts to hinder vesicle motion at the subplasmalemmal area [384, 385] and prevent docking to the plasma membrane and subsequent fusion in the absence of a stimulus [359, 386-388]. Involved in this process are Rab27a and its effector protein MyRIP, which are thought to anchor WPBs to the actin cortex [57]. Disassembly of the cortical F-actin allows translocations of vesicles to the plasma membrane for fusion [389]. Both WPB and non-WPB trafficking is thought to be co-ordinated between microtubules and the actin cytoskeleton [390].

1.7.4 Pools of granules

In a population of regulated secretory granules different pools of granules are likely to exist at different stages in the secretory pathway. Immature secretory granules are found near the centre of the cell, in the vicinity of the TGN and mature secretory granules tend to be located in the periphery of the cell. Early work on neuronal synaptic vesicles has classed distinct granule pools depending

on their readiness to be released upon stimulation [391, 392]. In chromaffin cells these different pools of granules were seen as distinct components in membrane capacitance recordings [393-395]. It is thought that a pool of granules can be pre-docked at "active" sites on the plasma membrane, waiting for the appropriate stimulus for fusion. In many neuronal cells "active" sites have been shown to be enriched in Ca^{2+} channels [396]. This pool of granules is termed the "immediately readily releasable" pool, as opposed to the "slowly releasable" or "reserved" pools of granules that are found further away from the membrane, however there is a controversy surrounding the nature of the different pools of granules [397, 398].

It is suggested that Ca^{2+} is the messenger of communication between the pools of granules regulating their readiness to be released. Synaptotagmin 1 is thought to be the Ca^{2+} sensor only on the "immediately readily releasable" pool in adrenal chromaffin cells, regulating their fusion [399].

1.8 Molecular fusion machinery

1.8.1 Regulated exocytosis

Secretion, the discharge of the granules content into the extracellular space was originally called "membrane fusion" by Palade (1959) and later on "exocytosis" by de Duve (1963). Early work on stimulated secretion by Jamieson and Palade [343] revealed it is not the rates of synthesis and intracellular transport of secretory proteins that are enhanced by stimulation *in vitro*, but the final discharge steps and the preceding storage steps. This data implied that stimulated secretion is regulated at stages close to the point of fusion. The molecular machinery for exocytosis has been studied extensively in excitable cells. Although

the WPB and non-WPB fusion apparatus remains largely unknown, the classical view of exocytosis in neuroendocrine cells will be briefly described here. The granules are transported towards the plasma membrane where they undergo tethering, docking, priming, triggering and finally fusion.

Tethering describes the initial attachment between vesicles and the target membrane, required prior to docking. Docking involves SNARE proteins (soluble N-ethylmaleimide-sensitive factor (NSF) attachment protein receptors). These include a vesicular SNARE (v-SNARE) VAMP (vesicle associated membrane protein) (or synaptobrevin) [400]; a target membrane SNARE (t-SNARE) on the plasma membrane, such as SNAP-25 (Synaptosome Associated Protein) [401] and syntaxin [396]. These SNARE proteins assemble into a helix bundle to form the SNARE complex [402]. The SNARE complex assembly is prevented by Munc-18 (mammalian homologue of UNC-18 gene), which bind syntaxin stabilizing it in a closed conformation [403, 404]. Priming is considered to be the process which renders the vesicles fusion-competent and this includes the ATP- independent disruption of the Munc-18- syntaxin interaction by PKC phosphorylation to allow formation of the SNARE complex [405]. Priming also consists of an ATP-dependent step which involves the activation of the SNARE complex by binding of soluble protein α-SNAP (NSF attachment protein) [402]. The α-SNAP-SNARE complex then binds soluble NSF ATPase, an interaction that induces the hydrolysis of ATP [402]. NSF is considered to be the molecular motor of fusion since the energy from ATP hydrolysis is used for the dissociation of the SNARE complex, leading to the close apposition of the vesicle with the plasma membrane, proposed as a zippering effect occurring from the N-terminus of the SNARE motifs to the C-terminal membrane anchors of opposing membranes. This pulls

the membranes close together overcoming the energy barrier, the proximal lipid leaflets interact and an aqueous fusion pore opens [406]. Figure 1.4 illustrates a schematic of the classical SNARE fusion machinery however it is not known whether WPBs or non-WPBs undertake this pathway of fusion. After fusion the SNARE complex dissasembles so that the individual SNARE proteins can be recycled. Calmodulin (CaM) has been found to bind several proteins of the SNARE complex [125, 126] and has been implicated in regulation of exocytosis.

The triggering step of exocytosis can be Ca^{2+}-driven or GTP-driven. Ca^{2+}-triggered exocytosis involves Ca^{2+} sensor proteins such as synaptotagmins [407] and annexins [408, 409]. Synaptotagmins are found in excitable cells on vesicles at subplasmalemmal regions of high local $[Ca^{2+}]_i$, rich in voltage operated Ca^{2+} channels (VOCs) [280]. VOCs bind t-SNARES and this allows direct access of Ca^{2+} to the SNARE complex. Synaptotagmins bind to phospholipids in the SNARE complex and couple $[Ca^{2+}]_i$ rises to exocytosis [410]. Annexins are heterologously expressed in all cell types and are abundantly found in EC [411]. The annexins are a family of proteins that can bind to the plasma membrane and coordinate fusion events in a Ca^{2+} dependent manner [412, 413].

The GTP-dependent form of regulated exocytosis uses a distinct set of molecules including Ral GTPases [414, 415]. RalA is activated by cAMP- and Ca^{2+}- raising agents, although more efficiently by the latter, to coordinate the assembly of a complex called the exocyst that is composed of small GTPases thought to be involved in directing vesicles to their precise site of fusion (reviewed in [416]). Guanine exchange factors (GEF) enhance the conversion from the inactive GDP-bound to the active GTP-bound form of RalA on the donor membrane where Rabs orchestrate the recruitment of effectors. Activated RalA

interacts with several protein effectors such as Sec5 and Exo84 [417], via binding and activating phospholipase D1 [418]. The Rab27a effector MyRIP has been shown to associate with the exocyst [419]. After fusion, GTPase activating proteins promote the GTP hydrolysis to inactivate and dissociate Rabs from the respective membranes and to initiate a new cycle of fusion. A binding site for calmodulin on Ral has been detected, and calmodulin has been shown to enhance the binding of GTP to Ral [124, 420]. Figure 1.4 includes a schematic of the exocyst mode of exocytosis.

It is not clear whether WPB exocytosis is regulated by the SNARE complex or the exocyst as evidence exists to support both routes. Regarding the SNARE complex, one report has identified t-SNARE syntaxin4 to be involved in WPB exocytosis [421], for which likely binding partners are SNAP23 and synaptobrevin3 (SNAREs expressed in endothelial cells) [422, 423]. The same group proposed that PKC_{α} is responsible for the phosphorylation of syntaxin4 and Munc18c, thereby facilitating the formation of the SNARE complex and allowing WPB exocytosis [421]. Moreover there is evidence that NSF plays a role in WPB exocytosis [423], from work that showed NO S-nitrosylation and H_2O_2 inhibited the ATPase activity of NSF and this led to an inhibition of WPB exocytosis [422]. The Ca^{2+}-triggering step of WPB SNARE-mediated exocytosis could involve synaptotagmins or annexins. Although a vesicular synaptotagmin for the WPB has not been established, synaptotagmin1 was recruited to rod-shaped pseudo-granules in vWF expressing AtT-20 cells [424]. Annexins, have also been implicated in a role in EC exocytosis [412] and in particular WPB exocytosis [55]. There is also some evidence linking the exocyst with WPB exocytosis [124, 420,

425]. The Guanine exchange factor (GEF) for RalA for WPB exocytosis has been reported to be Ral-GDP dissociation stimulator (RalGDS) [124].

1.8.2 Constitutive exocytosis

Constitutive secretion is thought to use a similar molecular mechanism to the SNARE machinery [426]. However constitutive secretion is thought to follow vesicle docking without delay, subtracting the priming step. Fusion of reconstituted synaptic vesicles from neurons is shown to involve the formation of the SNARE complex in a Ca^{2+}-independent manner, despite the presence of Ca^{2+} sensors on the vesicles [427]. The molecular machinery of constitutive exocytosis remains mainly elusive.

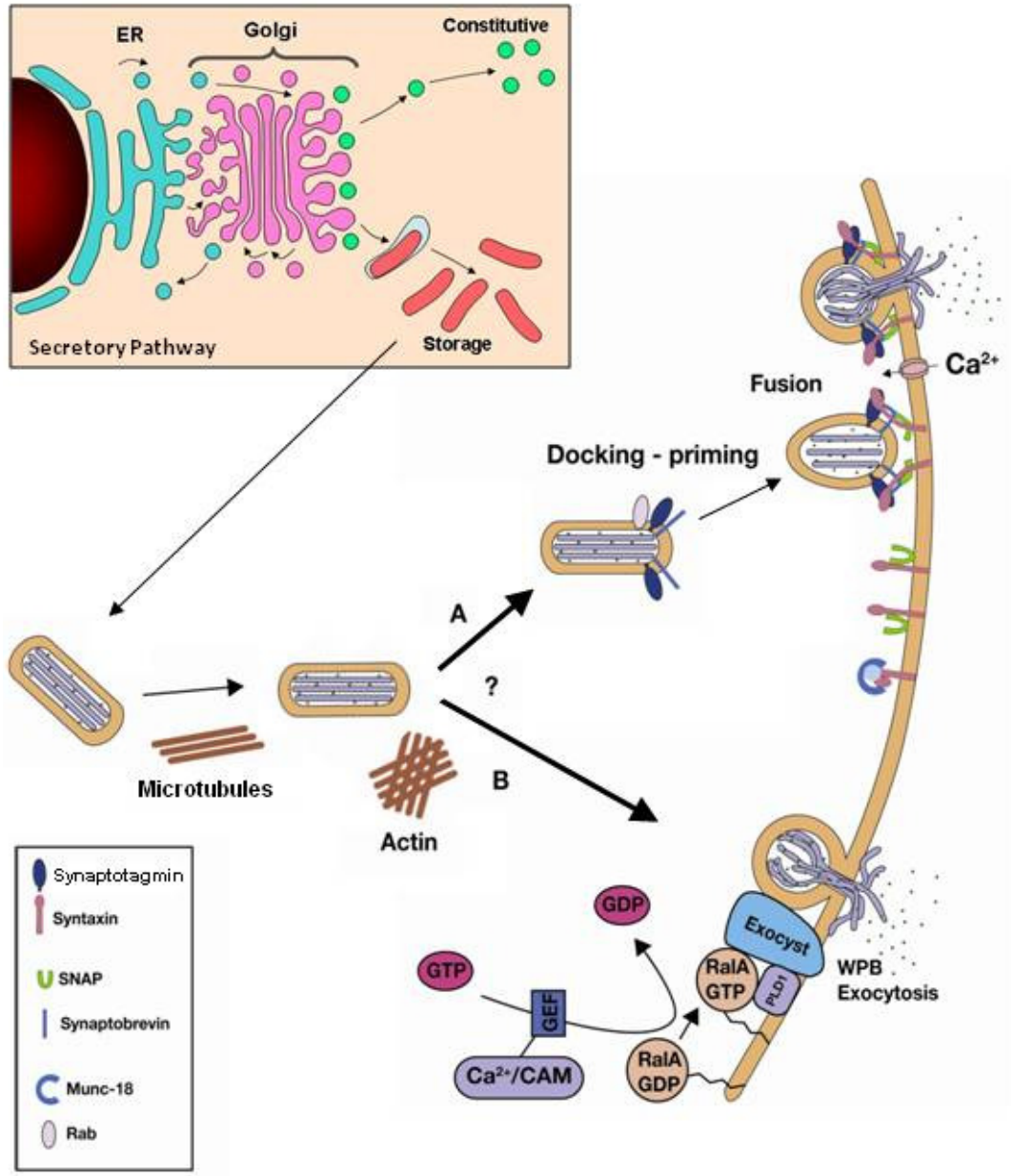

Figure 1.4 Possible secretory pathways of the WPB

VWF undergoes post-translational modifications in the ER and Golgi before driving the formation of WPBs at the TGN. The exocytotic machinery of WPBs is not yet established. In ***A*** *the classical neuronal SNARE exocytosis is described. Synaptobrevin3 has been reported on the WPBs and syntaxin4, SNAP23 and Munc-18 on the plasma membrane of endothelial cells.* ***B*** *The exocyst complex recruited by RalA-activated PLD1 may represent an alternative mechanism by which WPB exocytosis is controlled. The inactive GDP-bound form of RalA is converted to its active GTP-bound form via an interaction involving* Ca^{2+}*-bound Calmodulin and a guanine exchange factor (GEF) thought to be RalGDS.*

1.8.3 Modes of fusion

Granule exocytosis can be separated into full fusion during which all contents are released or incomplete fusion in which partial or selective release of cargo may occur. In the latter a transient fusion pore forms that can readily reseal and retract from the plasma membrane [428] known as "kiss-and-run" fusion [429]. This type of fusion was originally observed in neuroendocrine cells as flickering of the fusion pore [430] and later on in mast cells [431], chromaffin [432], eosinophils [433] and neutrophils [434]. Kiss-and-run events are thought to be a mechanism of regulating the amount and species of cargo released depending on their size [435-437]. These events support the existence of a reversible fusion machinery temporally coupled to the highly stable SNARE complex [438]. Although WPBs can undergo kiss-and-run fusion they also display long lived fusion pores through which small chemokines can exit while pro-coagulant vWF and proregion are retained in the granule [435]. A similar selective mechanism of release of small transmitters is thought to take place in neuroendocrine cells [439].

1.9 Haemostatic and inflammatory responses of the endothelium

The process of exocytosis of von Willebrand Factor (vWF) and tissue plasminogen activator (t-PA) was studied here. A brief description of haemostatic and inflammatory responses and the involvement of vWF and t-PA are described below and illustrated in Figure 1.5.

1.9.1 Involvement of WPB protein Von Willebrand Factor (vWF) in Haemostasis

Haemostasis is the cessation of blood loss from a damaged blood vessel that can be triggered by a physical or a chemical injury to the vessel. The process of haemostasis is often categorised into two phases termed primary and secondary haemostasis.

1.9.1.1 Primary Haemostasis

Primary haemostasis is characterised by platelet adhesion to the sub-endothelium, a process that is facilitated by binding to recruited vWF, their subsequent activation and formation of a platelet plug. VWF was discovered in 1971 as a Factor VIII binding antigen [440] and named after Professor Erich von Willebrand who first described the bleeding disorder von Willebrand disease in 1926 [441]. VWF is synthesized by EC [442] and secreted constitutively in small dimers [95] or by regulated secretion of WPBs where it is stored in large multimers [25]. It is also secreted by regulated exocytosis of α-granules in platelets [44, 443] or constitutively from megakaryocytes [444, 445]. Upon vascular injury EC are stimulated to secrete WPBs which release high molecular weight multimers of vWF. Under conditions of high shear WPB derived vWF can unravel revealing multiple interaction sites and increasing its binding potential [446]. The A3 domain of vWF contains a binding site for collagen that may facilitate its adhesion to the exposed subendothelium and the C1 domain contains a binding site for the vitronectin receptor ($\alpha_v\beta_3$) on the EC membrane [24, 37-39] that strengthens the attachment of endothelial cells to the basement membrane, forming a seal around the vascular injury [447]. Although WPB-derived large

multimers of vWF can bind more efficiently to the exposed subendothelium than constitutively secreted dimers that circulate in the plasma [448], the latter are essential for both primary and secondary haemostasis as seen by treatments of vWF disease [449] such as blood replacements [450, 451]. Binding of vWF to the subendothelium via the A3 domain triggers a conformational change that exposes the A1 domain containing the sequence Arg-Gly-Asp (RGD) that recognises the Glycoprotein (GP) Ib component of the integrin GPIb-IX-V receptor complex found on the platelet membrane [30, 452] promoting platelet adhesion at the site of vascular injury. The integrin receptors on resting platelets have high affinity for the corresponding ligands on vWF adherent on the basement membrane [453], extracellular matrix [454] or incorporated into a forming clot [455]. The initial platelet GPIb interaction with vWF A1 elicits platelet signals including $[Ca^{2+}]_i$ rises and activation of PKC and tyrosine kinases [456, 457] that lead to activation of integrin $GPII_b$-III_a ($\alpha_{IIb}\beta_3$) on the platelet surface [458]. This interaction induces platelet activation [459], shape change by cytoskeletal rearrangements and secretion of their α-granules which store ADP, vWF [460] and thromboxane A_2 (TXA_2), molecules required for further platelet activation and aggregation, forming a primary haemostatic plug [461, 462]. The $GPII_b$-III_a integrin is a receptor for further agonists such as plasma vWF [463, 464], fibrinogen and fibronectin [465, 466], adhesive proteins found in the extracellular matrix or released from the α-granules. Figure 1.5 illustrates platelet rolling on WPB-secreted vWF and platelet aggregation at the exposed subendothelium in a schematic of the inside of a vessel.

1.9.1.2 Secondary Haemostasis

Activated platelets, monocytes, EC and lymphocytes expose negatively charged phospholipids on their surface where circulating proteins in a precursor form are converted to active serine proteases in the presence of Ca^{2+}, during a series of stepwise proteolytic events [467, 468]. This is called the coagulation cascade, part of secondary haemostasis which leads to the formation of a fibrin clot that reinforces the platelet aggregate. Circulating low molecular weight vWF derived from either constitutive or basal secretion from EC [371], plays a role in secondary haemostasis by stabilizing coagulation Factor VIII in the circulation [469], binding with high affinity via domain D' to form a tight, non covalent complex that protects FVIII from proteolytic degradation [470, 471]. The end reaction of the coagulation cascade is the activation of factor Xa which assembles into a complex responsible for cleaving pro-thrombin (factor II) into thrombin (factor IIa) [472]. Thrombin is the most potent physiological activator of human platelets [473]. Thrombin also cleaves the soluble plasma protein fibrinogen (factor I) into insoluble fibrin monomers, which stick together to form fibrin polymers that form the scaffold of a developing clot [474, 475]. A forming fibrin clot is illustrated in Figure 1.5.

Haemostasis is tightly controlled by the endothelium through secretion of a combination of positive and negative regulatory molecules. Anticoagulant tissue factor pathway inhibitor (TFPI) is secreted by activated platelets and Thrombin-stimulated endothelial cells, to limit thrombin production [476, 477]. Also activated protein C, secreted by EC, inactivates factors of the coagulation cascade, in reactions catalysed by protein S [169, 478].

1.9.2 Tissue-Plasminogen Activator (t-PA)- Fibrinolysis

Fibrin clots are degraded by the action of serine proteases including urokinase and tissue plasminogen activator (t-PA) [479]. The mature t-PA protein contains 5 discrete structural domains including a fibronectin-like domain, an epidermal growth factor EGF-like domain and the serine proteinase catalytic domain [480]. Circulating t-PA binds fibrin and is activated to cleave plasminogen (incorporated in the newly formed fibrin clot) into the active non-specific serine protease plasmin which degrades fibrin and consequently dissolves the fibrin clot [481]. T-PA is secreted constitutively from endothelial cells, but its secretion is increased under conditions of vascular injury, exercise or presence of vasoactive substances *in vivo* [77, 78] and *in vitro* [84]. This may be a mechanism for delivering an additional pulse of t-PA to the site of injury ensuring its incorporation in the forming clot and the dissolution of fibrin at the initial stages of fibrin clot formation. *In vitro* t-PA is more potent in dissolving fibrin when it is incorporated into a clot during coagulation [482], because it forms a ternary complex with fibrin and plasminogen in the locality of the clot therefore the rate of activation of plasminogen by t-PA is higher in the presence of the polymerized fibrin [483, 484].

Degraded fibrin no longer binds plasmin or plasminogen, and is eventually inactivated by the respective inhibitors. The amounts of t-PA in the circulation are carefully balanced by plasminogen activator inhibitors PAI-1 and PAI-2, members of the serpin family that are also secreted from EC. These form a covalent bond with t-PA leading to its inactivation [485, 486]. PAI-2 is up-regulated in human plasma only under certain conditions such as pregnancy [76].

1.9.3 Inflammation

Endothelial cells play an important role in inflammatory processes. Stimulated WPB exocytosis from EC, along with vWF, also releases P-selectin on the EC plasma membrane. This type 1 membrane protein is responsible for mediating the initial adherence and rolling of leukocytes on the surface of the endothelium [487]. Stimulation of EC with Interleukin-1 (IL-1) and TNF-α (tumor necrosis factor-a) produced by infiltrating inflammatory cells, results in the up-regulation and cell surface expression of adhesion molecules including integrins, selectins, vascular cell adhesion molecule (VCAM-1), intercellular adhesion molecule (ICAM-1) and platelet endothelial cell adhesion molecule-1 (PECAM-1) [488-491]. These facilitate the attachment to the endothelium and subsequent trans-migration of leukocytes into inflamed tissue, facilitated by EC induced shape change, forming intercellular gaps. Physiological stimuli for EC gap formation are thrombin and histamine which induce cell retraction by formation and rearrangement of stress fibers composed of filamentous F-actin and myosin [191]. Moreover, IL-1 and TNF-α up-regulate EC expression of chemokines such as the neutrophil chemoattractant interleukin-8 (IL-8), eotaxin-3, monocyte chemoattractant protein-1 (MCP-1), growth-related oncogene protein-alpha (GRO-α) and RANTES (Regulated on Activation, Normal T Expressed and Secreted) which stimulate the chemotaxis of lymphocytes, neutrophils and monocytes to the site of inflammation and potentiate transendothelial migration (reviewed in [492]). Chemokines such as IL-8 and eotaxin-3 are reported to be sorted in the WPB [67], however, they may also exit the cell through the non-WPB organelle, along with other chemokines such as GRO-α and MCP-1 [92]. Sorting of chemokines to differentially regulated organelles in EC may allow for

their differential release to modulate inflammatory processes. An illustration of leukocyte rolling on the endothelium and transmigration to the inflamed tissue is shown in Figure 1.5.

Moreover recent findings that WPBs can be released in response to invading bacterial pathogens such as lipoproteins activating Toll-like Receptors on EC membrane [493] or by an antibody against human leukocyte antigen (HLA) [494] suggest that WPB exocytosis participates in innate immune responses or the pathology of transplant rejection respectively.

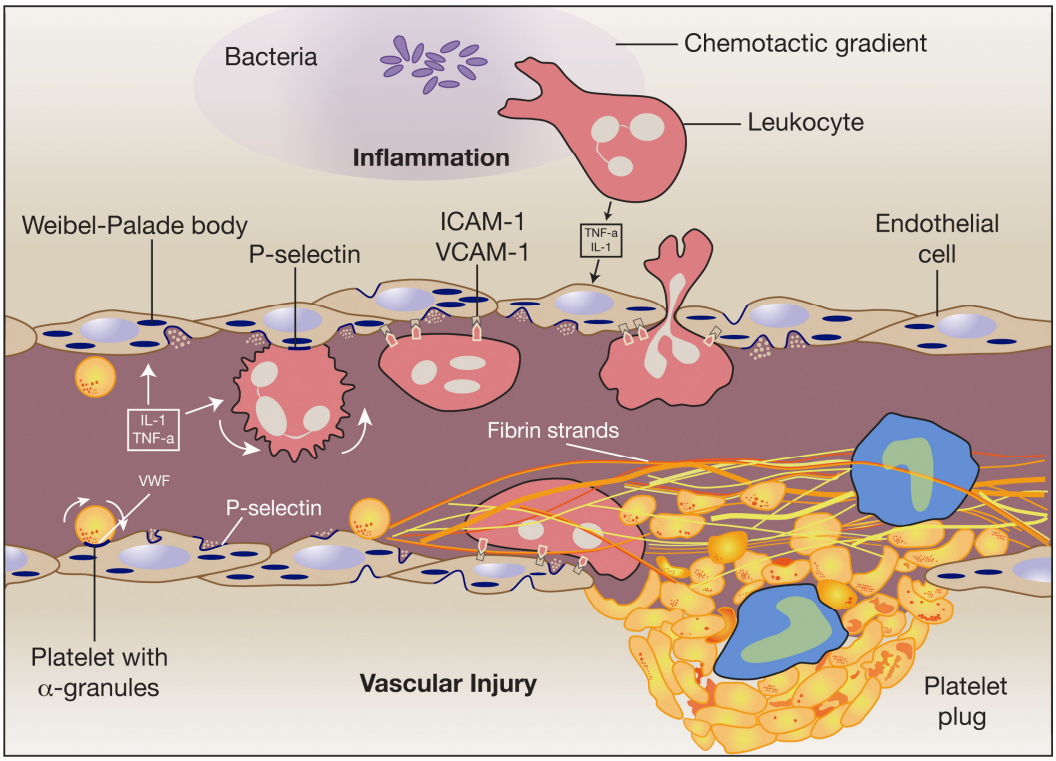

Figure 1.5 Inflammatory and haemostatic action of the endothelium

Upon vascular injury which involves the exposure of the subendothelium to plasma, or inflammation which involves the activation of leukocytes and subsequent secretion of interleukin-1 (IL-1) and tumour necrosis factor α (TNF−α); endothelial cells are stimulated to secrete von Willebrand Factor (vWF) and P-selectin from their Weibel Palade Bodies (WPB) and up-regulate the expression of membrane adhesion molecules vascular cell adhesion molecule (VCAM-1), intercellular adhesion molecule (ICAM-1) and others. VWF facilitates platelet rolling on the endothelium and platelet attachment to the site of injury with subsequent platelet activation and aggregation to form a platelet plug. Secreted vWF from α–granules of activated platelets promotes platelet-platelet adhesion. This process initiates the coagulation cascade on activated EC and platelet membranes which results in the formation of a fibrin mesh. P-selectin on the activated EC membrane and adhesion molecules VCAM-1 and ICAM-1 facilitates leukocyte rolling and attachment to the endothelium and subsequent translocation to the site of inflammation. Figure adapted from [487].

1.9.4 Defects in vWF or t-PA formation/ secretion lead to disease

Complications in the process of haemostasis (bleeding disorders) can occur due to defects or lack in the elements making up or regulating the processes underlying the primary or secondary haemostasis cascades [495, 496]. Here vWF and t-PA related diseases will be considered. Von Willebrand disease (vWD) is an autosomal dominant mutation which comes in many degrees of severity. In its mild form vWD has a 0.8% frequency of occurrence [497]. In its most severe form (VWD type III), absence of vWF leads to complications in haemostasis due to inability of platelets to adhere to the exposed subendothelium and form the platelet plug (primary haemostasis) [498] and a failure of the clotting cascade due to lack of factor VIII in the circulation (secondary haemostasis) [32, 499]. On the other hand there is evidence that high plasma levels of vWF can cause thrombotic complications in the circulation [500, 501]. Such complications may manifest in the development of atherosclerosis as shown from experiments on P-selectin and vWF-deficient mice that showed delayed onset and reduced extent and severity of atherosclerosis when placed on an atherogenic diet [502, 503]. Abnormal vWF levels are not only involved in the dysfunction of haemostasis, but it was also shown that vWF contains binding sites for tumour cell receptors such as glycoprotein I_b or the $\alpha_{IIb}\beta_3$ and $\alpha_v\beta_3$ integrins thereby providing a role in tumour metastasis [504].

In terms of the role of t-PA in disease, once coagulation occurs, inadequate dissolution of a fibrin deposit by t-PA may result in the obstruction of a blood vessel [481]. On the other hand excessive, premature fibrin degradation by t-PA can lead to bleeding [505]. T-PA is used clinically as a thrombolytic agent in the treatment of acute myocardial infarction and deep vein thrombosis.

1.10 Mitochondria

1.10.1 Mitochondria structure

Mitochondria are vital, dynamic organelles forming an interconnected network as observed by direct visualization of the organelle by specifically targeted GFPs (reviewed in [506]). The mitochondrial network in a single HUVEC expressing the mitochondrial targeted fusion protein mito-DsRed is shown in Figure 1.6, co-expressing proregion-EGFP (A) or t-PA-EGFP (B). Mitochondria are thought to have evolved from prokaryotic organisms that were phagocytosed by a eukaryote, and contain their own circular DNA (mtDNA) in their lumen [507]. Mitochondria have genetic continuity inherited maternally and are prone to mutations as mtDNA lacks histones and has limited capacity for repair [507]. The mitochondrial DNA is 15.5kb encoding 13 polypeptides, components of the complex inner mitochondrial membrane [508]. Their major role is to produce the cells energy (ATP) by oxidative phosphorylation in most cell types [509]. Endothelial cells however are mainly glycolytic cells, producing 75-99% of their energy by substrate glycolysis [510, 511]. Endothelial mitochondria are thought to be more important for various other functions including O_2 sensing [512], Ca^{2+} sequestration and production of NO (Nitric Oxide) and ROS (Reactive Oxygen Species) (reviewed in [513, 514]). ROS production, generated by a damaged respiratory chain, triggers apoptosis by releasing proteins that activate effector caspases in the cytoplasm (reviewed in [515]).

Mitochondria are delimited by two membranes, an inner mitochondrial membrane (IMM) and an outer mitochondrial membrane (OMM). The OMM is

readily permeable to small molecules (MW<10KDa) thanks to the abundance of a large conductance channel known as mitochondrial porin or voltage-dependent anion channel (VDAC). Therefore the OMM is not a limiting factor to Ca^{2+} diffusion. The IMM is an ion-impermeable membrane with much larger surface area due to folds extending into the internal space known as *cristae* [516]. The IMM contains the electron transport chain (ETC) or respiratory chain, the ATP synthase and specific carriers for metabolites [507]. The matrix space of the mitochondrial contains enzymes of the citrate cycle and β-oxidation [507].

Mitochondria are motile organelles that undergo continual cycles of fusion [517] and fission [518, 519] and the balance of these opposing processes regulates mitochondrial morphology, number and function. When fusion is blocked continuous fission causes the mitochondria network to fragment. Fusion in mitochondria is unique from other organelles in that it co-ordinates fusion of OMM, IMM, inter-membrane space and matrix [520].

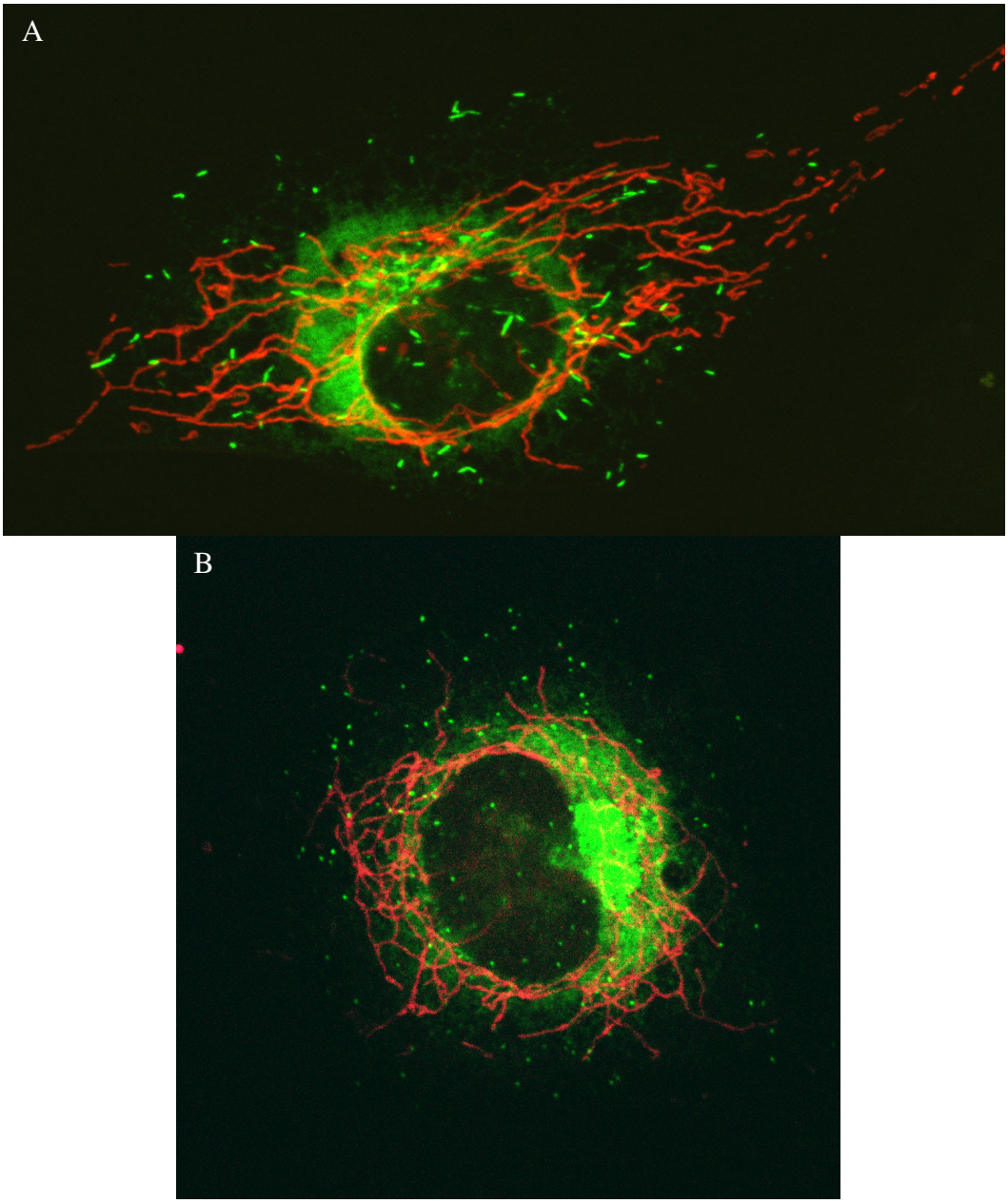

Figure 1.6 The mitochondrial network in HUVEC

*Single HUVEC co-expressing mito-DsRed which fluorescently labels the mitochondria and (**A**) proregion-EGFP which fluorescently labels WPBs or (**B**) t-PA-EGFP which fluorescently labels the non-WPBs.*

1.10.2 Oxidative phosphorylation

The cytosolic process of glycolysis produces a carbon chain substrate such as pyruvate that is supplied to the mitochondria to maintain the citric acid cycle (or tricarboxylic acid cycle (TCA)) (demonstrated by Denton, McCormack and Hansford in 1960s). During the TCA cycle the pyridine nucleotide NAD^+ and flavoprotein FAD are reduced to NADH and $FADH_2$ respectively and are then provided to the respiratory chain on the IMM. Electrons (e^-) from NADH are passed to complex I and from $FADH_2$ to complex II. Electrons are successively passed from either complex I or complex II via ubiquinone to complex III and via cytochrome C to cytochrome C oxidase (complex IV) which ultimately transfers e^- to oxygen to generate water. Cytochrome C transfers e^- in a cycle of Fe^{3+} reduction to Fe^{2+} when accepting e^- from complex III and a reverse oxidation of Fe^{2+} when donating e^- to complex IV. During the redox reactions of complexes I, III and IV, protons (H^+) are translocated across the IMM to the intermembrane space generating an electrochemical proton gradient 150-200mV negative to the cytosol ($\Delta\Psi_m$). This potential provides the driving force for proton influx through the F_1F_0-ATP synthase (ATPase) leading to the phosphorylation of adenosine diphosphate (ADP) to generate ATP which is then transported to the cytosol [509, 521]. Figure 1.7 shows a schematic of the oxidative phosphorylation process.

Thus ATP is synthesized by coupling two reactions, electron transport and phosphorylation. Metabolic uncouplers inhibit ATP synthesis by preventing the energy produced by redox reactions in the form of proton motive force to be used for phosphorylation [509]. Common uncouplers are hydrophobic weak acids such as carbonylcyanide-p-trifluoromethoxyphenylhydrazone (FCCP) which transport protons through H^+-impermeable membranes. Also any compound or physical

force such as osmotic shock that dissipates the pH difference and membrane potential can cause uncoupling.

1.10.3 Pathways of mitochondrial Ca^{2+} cycling

Studies in the 1960s on isolated mitochondria in suspension demonstrated their extraordinary ability to take up enormous quantities of Ca^{2+} when added to the bathing solution [522, 523]. Early experiments showed that isolated mitochondria accumulate up to 36mM Ca^{2+} without damage and up to 900mM Ca^{2+} accompanied by irreversible damage and morphological changes [524]. At the time the hypothesis existed that uptake was a passive process linked to the $\Delta\Psi_m$ [525, 526]. Later on a uniporter was identified, an inwardly rectifying Ca^{2+}-selective ion channel on the IMM [527]. The driving force for mitochondrial Ca^{2+} uptake via the uniporter is the $\Delta\Psi_m$ and its action is inhibited by ruthenium red and agents that collapse the $\Delta\Psi_m$ such as uncouplers [528, 529]. When $[Ca^{2+}]_i$ is above a threshold [530, 531], the uniporter, which has been shown to be half maximally activated around 10–20μM Ca^{2+}, can take up Ca^{2+} at high rates [311, 532-534]. Resting values of intra-mitochondrial Ca^{2+} are not thought to be much different from cytosolic Ca^{2+} levels (in the range of 80-200nM) as measured with loading dyes in both isolated and cellular mitochondria [535].

Ca^{2+} is removed from mitochondria at slow rates (30-400 times slower than the uniporter) by secondary transport [535]. The physiological Ca^{2+} cycling mechanism is achieved by the exchange of $2Ca^{2+}$ for $3Na^+$ via the Na^+:Ca^{2+} exchanger (NCE) [536, 537] and consequently the exchange of Na^+ for H^+ via the Na^+:H^{2+} exchanger (NHE) [311, 538, 539]. ROS production has been shown to inactivate the mitochondrial NCE and therefore cause $[Ca^{2+}]_i$ rises [540]. The

major mitochondrial Ca^{2+} handling pathways (the uniporter and the NCE) are illustrated in Figure 1.7.

Other pathways for mitochondria Ca^{2+} handling include the rapid uptake mode pathway (RaM) [541] and the permeability transition pore (PTP_m) pathway (reviewed in [542]). The latter consists of a multi-protein complex which assembles under pathological conditions such as mitochondria Ca^{2+} overload, oxidative stress or adenine nucleotide depletion [542]. The pore is a high conductance, non selective channel that allows maximal Ca^{2+} flux and initiates apoptotic pathways [543].

1.10.4 Mitochondrial Ca^{2+} homeostasis

The large capacity of mitochondria to sequester Ca^{2+} suggested that they could be major players in cytosolic Ca^{2+} homeostasis. Indeed estimates suggest they contribute to 25% of total cellular Ca^{2+} storage capacity in bovine aortic endothelial cells [209]. Initially it was thought that the sensitivity of the uniporter to Ca^{2+} was low, so that mitochondria would only participate in Ca^{2+} sequestration when $[Ca^{2+}]_i$ approached cytotoxic levels (see review [515]), however, it is now known that the threshold of activation of the uniporter is much lower (~300nM) [544-546]. Mitochondria can form clusters near the mouth of Ca^{2+} channels where high Ca^{2+} concentrations arise following channel activation [532]. While cytosolic Ca^{2+} near Ca^{2+} channels can be as high as 100μM, these levels can drop dramatically (below 1μM) even at 1-2μm further from the channels [547]. Mitochondrial clusters can form near IP_3Rs on the ER or near the plasma membrane (at a distance less than 100nm) [548] depending on the cell type [549]. In this way mitochondria are positioned to participate in Ca^{2+} uptake when

exposed to high Ca^{2+} microdomains. Data obtained using mitochondrial Ca^{2+} indicators showed that physiological stimuli acting on G_q-coupled receptors to elicit rises in $[Ca^{2+}]_i$, lead to a large rapid rise in mitochondrial Ca^{2+} concentration ($[Ca^{2+}]_{m)}$ in a variety of cell types [549, 550](reviewed in [551]). The $[Ca^{2+}]_m$ rises are shown to be significantly slower than the $[Ca^{2+}]_i$ rises and to outlast the cytosolic signal [535, 552-555]. Mitochondrial Ca^{2+} uptake is also thought to shape the decay phase of agonist-evoked Ca^{2+} transients. Evidence for this has come from studies in which uncoupled mitochondria dramatically prolong the depolarisation-induced $[Ca^{2+}]_i$ rises in chromaffin cells [547, 556-558], neurons [553, 559, 560], and pituitary gonadotropes [552, 561]. However in mouse skeletal muscle fibers, FCCP induced a drastic reduction of Ca^{2+} transient amplitude without any effect on the decay phase [562].

Clusters of mitochondria in the immediate vicinity of IP_3R have been found to regulate Ca^{2+} release from the stores. Ca^{2+} uptake into energized mitochondria lowers the local free $[Ca^{2+}]_i$ and regulates the Ca^{2+}-induced feedback activation or inhibition of IP_3R Ca^{2+} release [563]. In this way mitochondria control bulk $[Ca^{2+}]_i$ increases and modulate the rate and extent of Ca^{2+} signal propagation and consequently $[Ca^{2+}]_i$ oscillations [563, 564]. Uncouplers either dramatically slow the rate of $[Ca^{2+}]_i$ oscillations (e.g. in pituitary gonadotropes [552], in neurons [560, 565], and in rat cortical astrocytes [553]) or completely inhibit regeneration of $[Ca^{2+}]_i$ oscillations (e.g. in xenopus oocytes [566]).

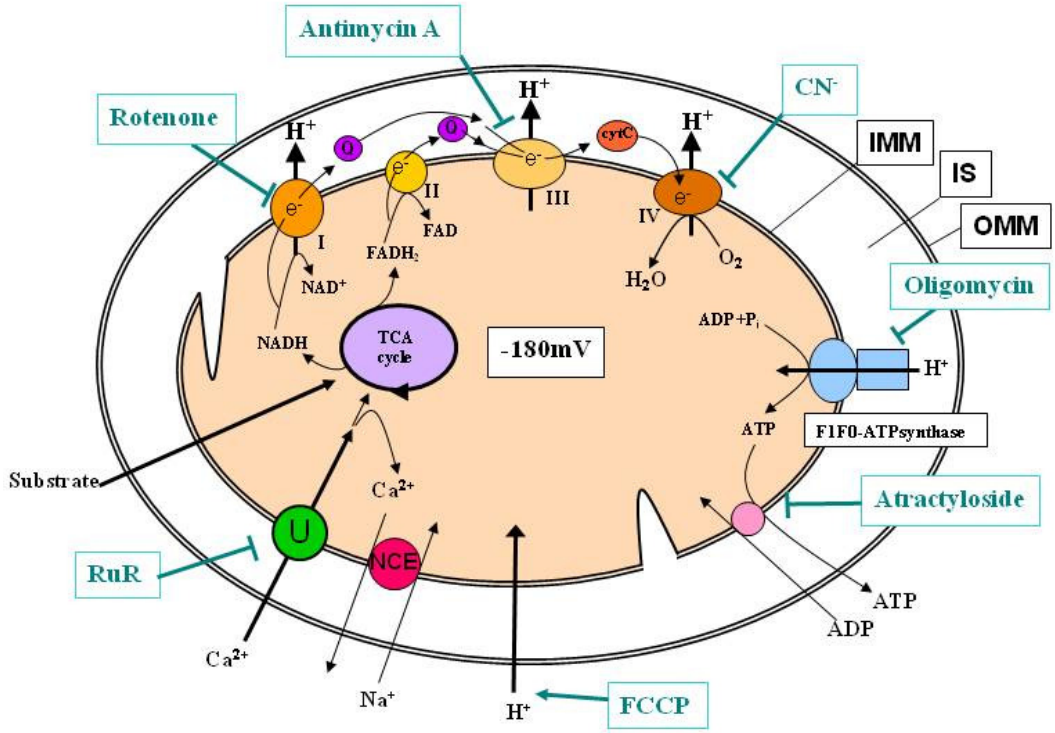

Figure 1.7 Mitochondrial Metabolism

A schematic of a mitochondrion illustrating the channels present on the inner mitochondrial membrane, including complexes I-IV of the electron transport chain, the F_1F_0-ATPase, the mitochondrial uniporter (U) and the Na^+/Ca^{2+} exchanger responsible for Ca^{2+} sequestration. The figure also highlights drugs that can be used for mitochondrial dysfunction including the uncouplers FCCP and antimycin A and the ATPase inhibitor oligomycin. (IMM=inner mitochondrial membrane, IS=intermembrane space, NCE=Na^+/Ca^{2+} exchanger, OMM=outer mitochondrial membrane, RUR=ruthenium red, U=Uniporter)

Mitochondria clusters have been found in close proximity to the plasma membrane Ca^{2+} channels in neurons [560], fibroblasts [567], T-cells [568] and endothelial cells [569, 570]. Subplasmalemmal mitochondria take up local Ca^{2+} and form microdomains of low $[Ca^{2+}]_i$ close to the plasma membrane. In this way during capacitative Ca^{2+} entry (CCE), the gradient for Ca^{2+} entry is increased and this is thought to help accelerate the transfer of Ca^{2+} into the cytosol for ER refilling (see 1.6.1) [570-573]. Inhibition of mitochondrial Ca^{2+} flux augmented agonist-evoked ER depletion and abolished ER refilling via CCE in endothelial cells [229, 568, 569, 573, 574].

1.10.5 Oscillatory $[Ca^{2+}]_m$ signals

$[Ca^{2+}]_m$ has been found to oscillate in phase with $[Ca^{2+}]_i$ oscillations in the case of anterior pituitary cells [552], xenopus oocytes [566], β-cells [575], adrenal glomerulosa cells [576] and hepatocytes [577]. In other cases $[Ca^{2+}]_m$ can increase accumulatively during $[Ca^{2+}]_i$ oscillations, due to the slow recovery of $[Ca^{2+}]_m$ [578]. In endothelial cells long lasting elevations in $[Ca^{2+}]_m$ are seen [549]. There is evidence that $[Ca^{2+}]_m$ oscillations are decoded into long term activation of dehydrogenases which translates into increased metabolism [577].

1.10.6 Mitochondria and secretion

Elevation of mitochondrial free Ca^{2+} up-regulates 3 major rate-limiting dehydrogenases of the TCA cycle (pyruvate, isocitrate and oxoglutarate dehydrogenase) which is paralleled by a rise in the reduced form of NADH [575], leading to an increase in ATP production [517, 579, 580]. Increased energy production by mitochondria may match the $[Ca^{2+}]_i$-triggered energy consuming

processes such as secretion in excitable cells [581], motion or Ca^{2+} re-extrusion. However this may not be significant in the glycolytic endothelial cells.

Extensive work has been done on secretion from chromaffin cells during inhibition of mitochondrial Ca^{2+} uptake. As mentioned above, clusters of mitochondria have been found concentrated in sub-plasmallemal regions rich in Ca^{2+} channels. These have been postulated to constitute active secretory zones where mitochondria buffer Ca^{2+}. Depending on the size of the local Ca^{2+} concentration after stimulation, mitochondria serve to limit the diffusional range of $[Ca^{2+}]_i$ and localise the secretory response [578]. It is proposed that mitochondria are involved in limiting the propagation of $[Ca^{2+}]_i$ and in controlling the traffic of vesicles at the plasma membrane between distinct pools [389, 582]. Indeed capacitance measurements of uncoupler treated chromaffin cells [552, 557, 578, 583, 584] and gonadotropes [552] showed no effect on the immediately releasable pool of granules but resulted in an enhancement of recruitment to the plasma membrane of granules in the reserve pool and consequently an overall increase in the secretory responsiveness. In addition an increased secretory response during the interpulse intervals and after cessation of the stimulus train was seen only in the presence of uncouplers in those studies. The opposite effects of uncouplers were seen in mouse chromaffin cells where a decline in $[Ca^{2+}]_i$ and secretion was observed [557]. Therefore, it appears as though different proportions of Ca^{2+} channel subtypes in each species work with mitochondria to determine the physiological response. At present there is no evidence to suggest that mitochondria play a role in regulating WPB or non-WPB exocytosis from EC.

1.10.7 Mitochondria in disease

Production of reactive oxygen species (ROS) (see reviews [585, 586]), mitochondrial DNA mutations [508] and inherited mitochondrial genetic defects [585, 587] lead to mitochondrial dysfunction. These encompass dissipation of $\Delta\Psi_m$ and consequently impairment of the mechanism by which mitochondria participate in Ca^{2+} homeostasis. As a result, this may lead to disruption of the fine tuning of spatiotemporal patterning of $[Ca^{2+}]_i$ signals by mitochondria, which in turn could affect the secretory response. Mitochondria are concentrated in neuronal synapses and significant alterations to synaptic mitochondrial localization, number, morphology, or function can be detrimental to synaptic transmission [585]. Dysfunctional exocytosis of neurotransmitters in the CNS caused by mitochondrial abnormalities is a common underlying phenomenon in the initial stages of some human neurodegenerative diseases [543, 585, 588]. The same concept could apply to endothelial cells and thus disruption of the exocytotic response of WPBs could be the link between mitochondrial dysfunction and chronic inflammatory diseases [589].

1.11 Thesis Aims

ECs control many important processes through the secretion of a wide range of molecules including peptides and proteins. Peptides and proteins are secreted by exocytosis from preformed membrane bound secretory organelles. In this thesis optical methods have been employed to fluorescently label and hence directly visualise two distinct populations of secretory granules, the WPB and a small organelle containing t-PA, the non-WPB. A main focus of this thesis will be to characterise the distinct nature of these two organelles. Using high speed multicolour imaging the kinetics of WPB and non-WPB exocytosis evoked by physiological and pharmacological $[Ca^{2+}]_i$-raising agents have been studied with sub second time-resolution. These data provide the first time-resolved analysis of the kinetics of secretion of these granule populations revealing new information about the inherent delays and rates of WPB exocytosis and their dependence on extracellular Ca^{2+}. Attempts were made to investigate whether $[Ca^{2+}]_i$ oscillations in cultured HUVEC might play a role in regulating WPB exocytosis, and whether mitochondrial Ca^{2+} uptake participates in shaping the $[Ca^{2+}]_i$ signalling in HUVEC and WPB exocytosis.

2 Experimental Methods

2.1 Protocols and Reagents

2.1.1 Tissue culture

Primary Human Umbilical Vein Endothelial Cells (HUVECs) were purchased from TCS Cellworks, Botolph, Claydon, UK and grown in HUVEC Growth Medium (HGM) (M199 +Earle's, +L-Glutamine, Invitrogen, Paisley, UK) supplemented with 20% fetal calf serum, 10 U/ml of heparin (Sigma, Dorset, UK), 30 µg/ml of Endothelial Cell Growth Supplement (Upstate, Dundee, UK) and 50 µg/ml Gentamicin (Invitrogen) under 5% CO_2 at 37°C as previously described [59].

2.1.2 Expression of fusion proteins by Nucleofection

HUVEC at passage 3 or 4 were transfected with 4-8µg of expression vector DNA using the Nucleofection™ device and buffers according to the manufacturer's instructions (Amaxa GmbH, Cologne, Germany) and as described in Erent et.al 2008. Briefly the cells were trypsinized and centrifuged at 1000rpm for 3min. The number of cells varied depending on the experiment. Roughly 60.10^6cells/ml were nucleofected per 6-well plate. The pellet was re-suspended in 100µl HUVEC nucleofector solution OLD and mixed with 4-8µg of the desired DNA. The mixture was transferred into a cuvette and placed in the Nucleofection device for the DNA to be electroporated to the nucleus of the cells using the program U-01 (appropriate for endothelial cells). The cells were plated in complete culture medium at confluent density onto 24 x 24mm square uncoated glass coverslips (Menzel-Glaser, Menzel GmbH Germany) for live cell imaging or onto gelatine-coated (incubate at 37ºC for 20min; 20%w/vol; Sigma fish skin gelatine) 9mm diameter glass coverslips (Griffiths & Nielsen, West Sussex, UK)

for immunocytochemistry. Cells were maintained without further medium changes until their use one to two days after Nucleofection.

Chimeric proteins provided and used for expression were vWF or its pro-polypeptide (proregion) fused to Enhanced Green Fluorescent Protein (EGFP), t-PA-EGFP, proregion-monomeric Red Fluorescent Protein (mRFP) and proregion-mEGFP made as previously described [35, 390, 590, 591] (Figure 2.1). Monomeric Enhanced Green Fluorescent Protein (mEGFP) was made by substituting Alanine at position 206 of EGFP with a lysine (A206K) to prevent possible dimerization without altering its spectral properties [591]. Cells were used 4 or 24hours post-Nucleofection for t-PA-EGFP and 48hours post-Nucleofection for vWF or proregion-EGFP or mEGFP.

In cells nucleofected with proregion-EGFP or mEGFP, 20-40% of cells had detectable EGFP fluorescence. In contrast only 5-20% of cells nucleofected with full length vWF-EGFP showed fluorescent WPBs presumably because it is more difficult for the cells to make the much larger full length vWF protein [1]. Nevertheless these levels of expression were more than sufficient for single cell optical studies of exocytosis and in the case of proregion-EGFP for biochemical studies of secreted GFP.

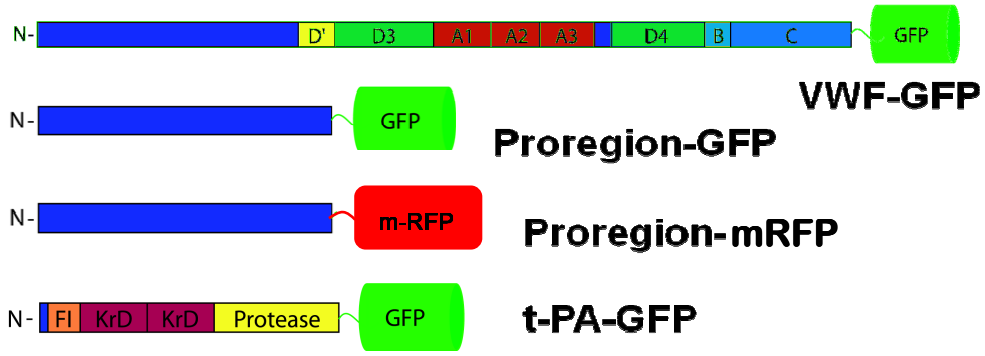

Figure 2.1 GFP-tagged constructs

GFP-tagged constructs were expressed in HUVEC by Nucleofection, including vWF-EGFP (top), proregion-EGFP or mEGFP (middle) and t-PA-EGFP (bottom).

2.1.3 Constructing mito-EGFP from mito-DsRed

A Ca^{2+}-insensitive fluorescent mitochondrial marker was constructed for control experiments to monitor intra-mitochondrial pH changes during pharmacological collapse of the $\Delta\Psi_{m.}$ This was achieved by exchanging the DsRed2 fluorescent protein of pDsRed2-Mito (BD biosciences Clontech, Oxford, UK, cat. No. 632421; see Figure 1.6) with EGFP (Figure 2.2). The vectors pEGFP-N1 (BD biosciences Clontech, cat. No. 6085-1) and pDsRed2-Mito (BD biosciences Clontech) were digested with BamHI and NotI (Roche, East Sussex, UK) according to manufacturer's instructions to cut out the fluorophores EGFP and DsRed2 respectively. The digestion products were separated by Agarose Gel electrophoresis as described in Sambrook, J., Molecular cloning 1989 [592]. The ~700bp fragment coding for EGFP and the ~4Kb fragment comprising the pDsRed2-Mito vector with the DsRed2 fluorophore removed (delta-pDsRed2-Mito) were identified using a 100bp and 1kb DNA ladders (New England BioLabs, Hertfordshire, UK); cut from the gel and purified using a QIAquick Gel Extraction Kit (QIAGEN, West Sussex, UK) according to manufacturer's instructions. The purified EGFP fragment and the delta-pDsRed2-Mito plasmid, in TE solution (Tris-EDTA; 10mM Tris-cl pH8, 1mM EDTA pH8) were ligated together using T_4 DNA ligase (New England BioLabs cat. No. M0202S) [593]. The ligated product was transformed into DH5α competent cells (Invitrogen, cat. No. 18263-012) using a 45sec heat shock in a 42ºC water bath according to instructions [594]. The transformed bacteria were plated on an L Agar Petri dish supplemented with a 1000 dilution of kanamycin from a stock concentration of 50mg/ml using sterile conditions and incubated overnight at 37ºC in humid conditions. Colonies were picked after 16hours and harvested in L Broth

supplemented with 50µg/ml kanamycin from a stock concentration of 50mg/ml in dH_2O for 16hours [595]. The cloned plasmid DNA was isolated from the transformed bacteria using the Alkali lysis method and dissolved in TE [595]. Figure 2.2A illustrates the cloning process and Figure 2.2B shows an epifluorescence image of a single HUVEC expressing this construct.

2.1.4 Antibodies, Reagents and Immunocytochemistry

For immunofluorescence localisation of endogenous vWF immunoreactivity in fixed HUVEC a rabbit polyclonal anti-human vWF antibody (Dako Ltd, Cambridgeshire, UK, catalogue number A0082) or a sheep polyclonal anti-human vWF (AbD Serotec, Oxford, UK cat. No. AHP062) were used at a 1:10000 dilution. For immunofluorescence localisation of endogenous t-PA immunoreactivity a sheep polyclonal anti-t-PA antibody (AbD Serotec, cat. No. 9020-0809) was used at a 1:300 dilution. Secondary antibodies coupled to fluorophores were purchased from Stratech scientific, Cambridgeshire, UK and used at a 1:200 dilution; donkey Cy-2 anti-rabbit (cat. No. 711-225-152), donkey Cy-2 anti-sheep (cat. No. 713-225-147), donkey Red-X anti-rabbit (cat. No. 711-295-152) and donkey Cy-5 anti-sheep (cat no 713-175-147). Cells were processed for immunofluorescence as previously described [35]. Briefly the cells were fixed with 3% (w/v) paraformaldehyde in PBS for 15min and permeabilized/quenched (Perm/quench) with 50mM NH_4Cl and 0.2% (w/v) saponin in PBS for 10min at room temperature. Perm/quench was replaced with PGAS (comprising of gelatine (0.2% (w/v)), saponin (0.02% (w/v)) and NaN_3 (0.02% (w/v)) in PBS) for 5min to block unspecific antibody binding sites. Cells were then incubated with 50µl of antibody appropriately diluted in PGAS; 45min in the primary followed by 40min in the secondary antibody. Coverslips were mounted onto Mowiol on a

microscope slide. The slides were stored for at least 4hours before being viewed using a 63x oil objective on a confocal microscope (Leica SP2 AOBS, Milton Keynes, UK).

2.1.5 GFP ELISA

Proregion-mEGFP expressing HUVEC were plated at confluency onto gelatine coated 6-well dishes (Fisher Scientific, Roskilde, Denmark). 48hours post-Nucleofection cells were incubated in serum free M199 Medium (+Earle's, +L-Glutamine, Invitrogen) supplemented with 20mM HEPES (Sigma, Dorset, UK) (S/FM199) for 1hour at 37ºC after which the medium was replaced with fresh S/FM199 for a further 10min at 37ºC (to ensure complete removal of secreted material released over the initial 60min incubation period). The medium was then changed to S/FM199 plus stimulus for 5min. Media samples were collected and centrifuged for 3min at 13000rpm and the pellet was discarded. The cells on the dish were washed with 1ml Lysis buffer made with 1% triton (TX-100, Sigma, Dorset, UK) in S/FM199 and 1:100 dilution of Protease Inhibitor cocktail (Sigma, Dorset, UK, cat no. P8340). Lysis samples were centrifuged for 5min at 13000rpm and the pellet was discarded. The experimental procedure is shown in Figure 2.3.

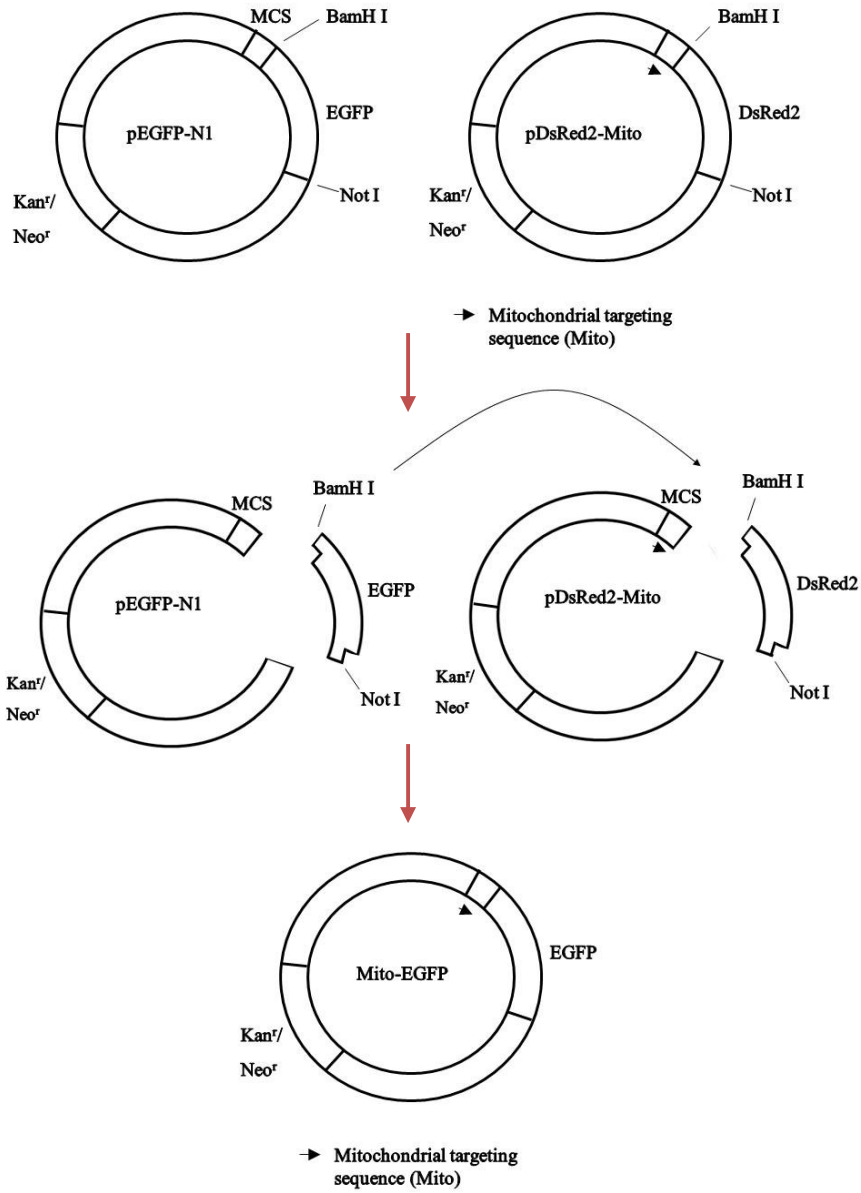

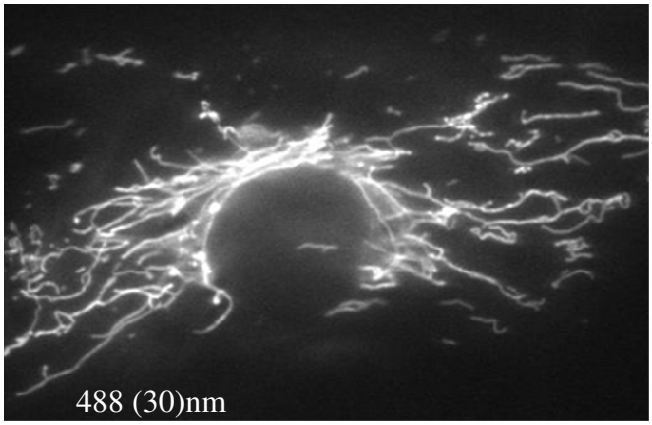

Figure 2.2 Constructing mito-EGFP from mito-DsRed

DsRed2 from vector pDsRed2-Mito was replaced with EGFP from vector pEGFP-N1. The bottom image shows a single HUVEC expressing mito-EGFP.

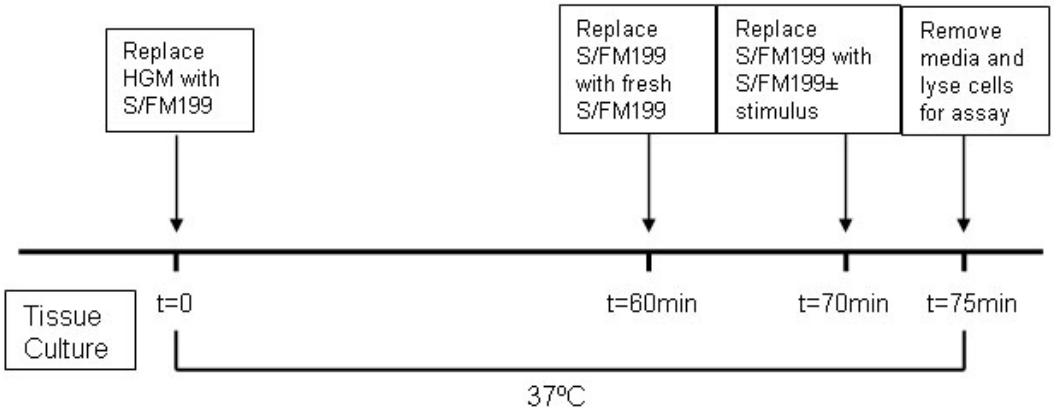

Figure 2.3 GFP ELISA

Experimental protocol for assessing stimulated secretion of GFP tagged proregion from HUVECs.

ELISA plates were coated overnight with 100µl of sheep anti-GFP antibody (AbD Serotec, Oxford, UK cat no. 4745-1051) diluted 1:1000 in PBS. Plates were blocked with 300µl of Tween-ELISA buffer (TWEB) (0.1% Tween-20, 0.2% gelatin and 1mM EDTA in PBS) for an hour before the samples were loaded. 100µl of standards, blanks and neat samples were added in duplicate, covered and mixed for 1hour. The standard curve was made from 1:2 dilutions of a recombinant bacterially produced GFP in S/FM199 (for the media samples) or in lysis buffer (for the lysate samples). The wells were then covered and incubated for 1hour on a mixer plate with 100µl of secondary rabbit anti-GFP (Invitrogen, Paisley, UK, cat no A11122) diluted 1:5000 in TWEB and then 100µl donkey anti-rabbit-HRP (horse radish peroxidase) conjugate (Stratech scientific, Cambridgeshire, UK, cat no 711-035-152) diluted 1:1000 in TWEB. The plates are washed with TWEB in between antibody incubations and with an additional PBS wash after the last incubation. The last wash is flicked off and replaced with 100µl chromogen O-Phenylediamine dihydrochloride (OPD, Sigma, Dorset, UK, cat no P8412) for GFP detection. OPD is prepared by dissolving 1.5mg/ml OPD tablets in CPT buffer pH6.2 (100mM citric acid, 0.2M Na_2HPO_4, 0.1% TX-100) for 10min before adding 1:50000 dilution of H_2O_2 for the colour change reaction to initiate. The assay is measured immediately kinetically at 450nm followed by an End point assay at 450nm approximately 5min after the H_2O_2 addition.

2.2 Imaging

2.2.1 Basic epifluorescence imaging apparatus

For experiments, cells seeded onto 24 x 24mm square uncoated glass coverslips (Menzel-Glaser, Menzel GmbH Germany) were transferred to the stage of an Olympus IX71 inverted fluorescence microscope where they were maintained at between 36-37ºC using a stage heater, an objective heater and an in-line solution heater (Harvard apparatus, Kent, UK). The imaging system comprised a monochromator (Optoscan; Cairn Research, Faversham, UK) capable of fast (~1 ms) wavelength switching and able to provide excitation light between 300–700nm at bandwidths between 2–30nm. The excitation light was passed through a 50% neutral density filter to reduce fluorophore bleaching before being reflected by a chromatic reflector onto the back aperture of an Olympus UPLSAPO x100 1.40NA objective to excite the specimen. Emitted light was transmitted through the chromatic reflector to be selected by an emission filter and sent to an Ixon EMCCD camera (Andor, Belfast, UK) operated in frame transfer mode at full gain and cooled to -65°C. Wavelength switching was synchronised with image capture using the free software WinFluor (http://spider.science.strath.ac.uk/sipbs/page.php?show=software_imaging) by Dr. John Dempster of Strathclyde University. Full frame (512 by 512 pixels) images were acquired as fast as 30frames/sec. A schematic of the basic setup configuration is shown in Figure 2.4. The filter sets used for each specific imaging configuration are illustrated in each following chapters.

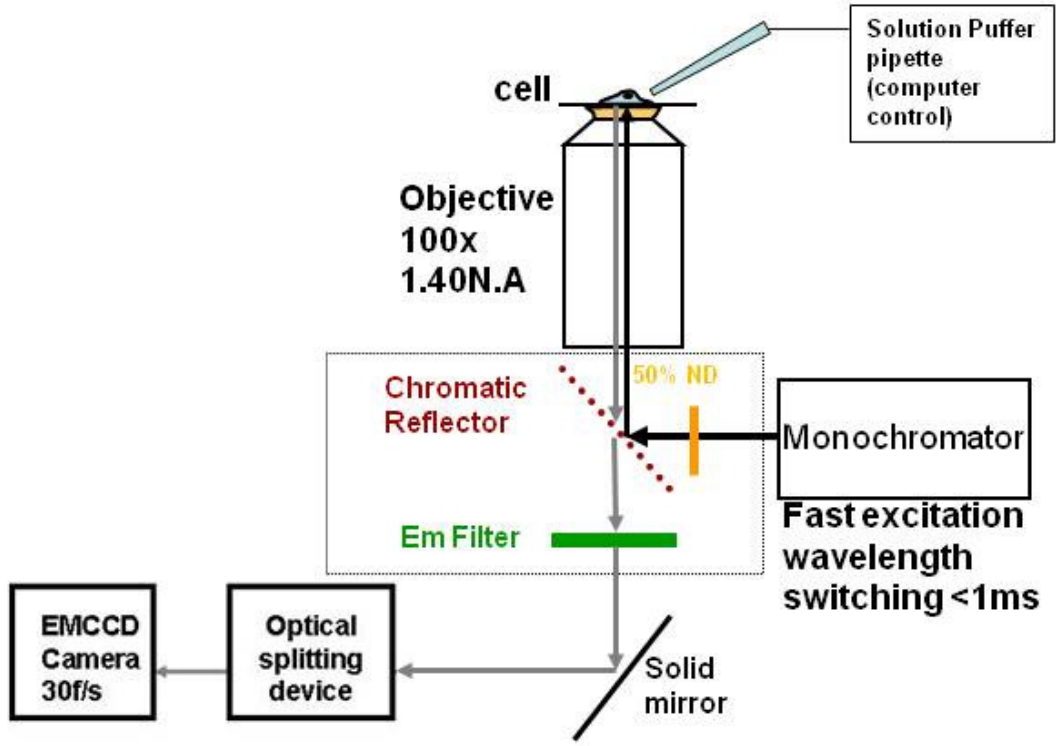

Figure 2.4 Basic configuration for imaging

The basic epifluorescence configuration used comprised a monochromator which sent the excitation light through a 50% neutral density filter to the chromatic reflector to be reflected onto the specimen. Emitted light was transmitted through the chromatic reflector and selected by an emission filter before sent to an EMCCD camera. The preparation is stimulated by a glass micropipette.

2.2.2 Total Internal Reflection Fluorescence Microscopy (TIRFM)

The TIRFM lasers were built around the epifluorescence microscope described above; a 488nm laser (20mW; I-Flex 2000, Point Source, Hamble UK), fitted with an acousto-optical deflector (AOD) allowing computer control of the laser power and a 561nm laser (50mW, 10Khz modulation; GLC-050-561, CrystaLasers, Nevada, USA) controlled by a pulse width modulation (PMW; 10KHz) and a range of neutral density filters to achieve optimum excitation with minimum photobleaching. Switching between laser and epifluorescence illumination was synchronized with image capture using Winfluor. Schematic Figure 2.5 describes the setup. A small mirror (≈3 mm diameter) was placed near the back aperture of the objective lens responsible for directing the laser beams to the specimen at a specific adjustable angle that will produce total internal reflection. The internally reflected beam is projected by another identical mirror, on the opposite side of the first one, onto a position-sensitive photodiode used for autofocus control. A similar configuration was previously used [596]. TIRFM is achieved by hitting the glass (high-refractive medium; n_2=1.518) – water (low-refractive medium; n_1=1.33-37) interface with excitation light at an angle (θ) above 61° to the normal which causes the light to undergo total internal reflection according to Snells' law. This produces an evanescence field of excitation with depth of penetration depending on the wavelength of light and the angle of incidence (the larger the angle the smaller the field penetration). Only material that enters the thin plane of the evanescent field is excited, giving rise to a high contrast image with minimal background fluorescence and no out-of-focus fluorescent material [596-598].

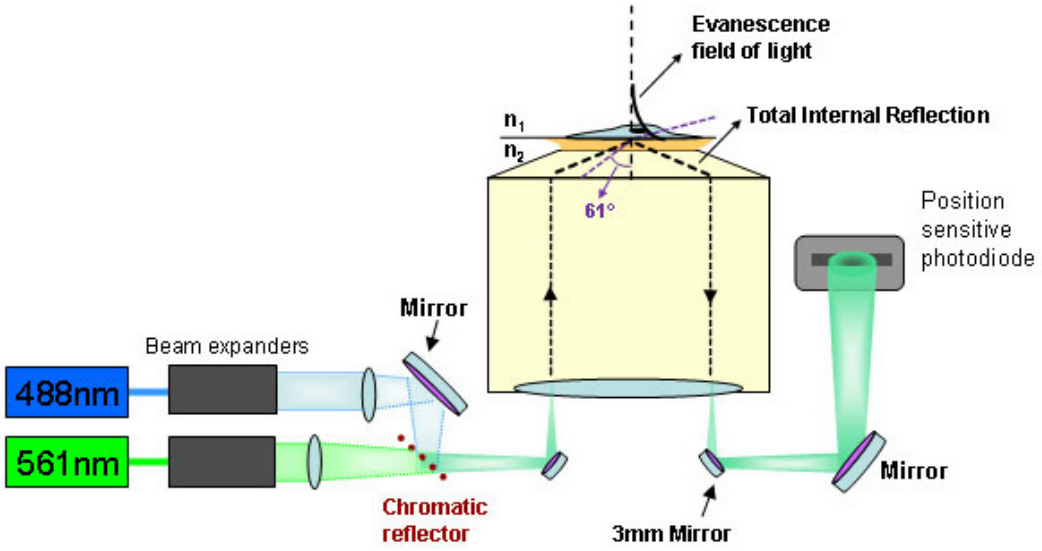

Figure 2.5 TIRFM

The 488nm and 561nm lasers were built around the epifluorescence microscope. The laser beam was directed to the specimen at a specific adjustable angle by a small mirror near the back aperture of the objective. At the glass- water interface, where the refractive index of glass is n_2=1.518 and of water n_1=1.33-1.37, the critical angle (θc) for total internal reflection is θc=61° defined by the equation $\theta c = \sin^{-1}(n2/n1)$. Above that angle an evanescence field of light is produced which excites a thin plane of the specimen at high contrast. The internally reflected light is directed by another mirror to the position sensitive photodiode for autofocus control.

2.2.3 Agonist stimulation of a single HUVEC

HUVEC grown on 24x24 coverslips were attached on a laminar-flow chamber (specially manufactured in the NIMR workshops) using silicon vacuum grease (Beckam cat no 335148-03) and bathed in physiological saline (PS) (140 mM NaCl, 5 mM KCl, 1.8 mM $CaCl_2$, 2 mM $MgCl_2$, 10 mM glucose, 10 mM HEPES-NaOH, pH 7.40). Ca^{2+}-raising agents dissolved in PS were applied to single cells by pressure injection from a glass micropipette (Warner Instruments, Kent, UK, cat no. 64-0804) positioned close to the cell (puffer application). A perfusion system was used to wash the stimulus off after each puffer application preventing stimulation of other cells on the coverslip. Figure 2.6 shows a picture of the stimulation configuration. Activation of the puffer controller was monitored by a +1V analogue telegraph output recorded simultaneously with image capture within the acquisition program WinFluor. Figure 2.7 shows a single proregion-EGFP expressing HUVEC in epifluorescence (A) and DIC (Differential Interference Contrast) (B) to illustrate the placement of the puffer. The distance between the pipette and the cell (typically 10-15µm), the width of the pipette tip (2µm) and the compressed air pressure (1psi) were adjusted to achieve fast agonist solution application but such that control solutions did not elicit a change in $[Ca^{2+}]_i$ due to fluid shear effects [21, 94]. Figure 2.8 shows an example of an experiment where the micropipette contains only PS to control for shear evoked elevation of $[Ca^{2+}]_i$ in a single HUVEC.

For the controlled repetitive puffing experiments, the puffer activation and deactivation was controlled with a voltage stimulus protocol within the WinFluor programme. For experiments where solutions were continuously perfused onto the cells, a 6 channel in-line perfusion system (fabricated by Dr Martin Stopps,

NIMR) connected to the cell chamber was used. Syringe valve switching was digitally controlled and recorded as an analogue signal in Winfluor during the experiments. The stimulation solutions passed through the in line solution heater (Harvard apparatus, Kent, UK) at about 37 ºC before arriving at the laminar-flow chamber. An aspirator on the opposite side of the chamber allowed removal of the applied solution. The average perfusion rate used that did not cause a shear $[Ca^{2+}]_i$ response was 2.5ml/min.

2.2.4 Determining the time-point of agonist arrival at the cell

To estimate the time-course of drug arrival at the cell during puffer application, experiments were carried out in which 10µM alexa-647 (Invitrogen) was included in the puffer pipette solution. A region of interest (ROI) was placed over the cell to measure the alexa-647 fluorescence change and the point of drug arrival at the cell was taken arbitrarily as the time-point corresponding to the 50% rise of Alexa-647 fluorescence. This was ~200ms (2 frames) post-activation of the puffer pipette (n=15 cells) (vertical dotted line in Figure 2.9) and was used as time=0s for defining subsequent delay times. Figure 2.9 illustrates an example of the temporal relationship between puffer application (A) and the detection of Alexa fluorescence (B) offset so that puffer activation occurs at t=0.

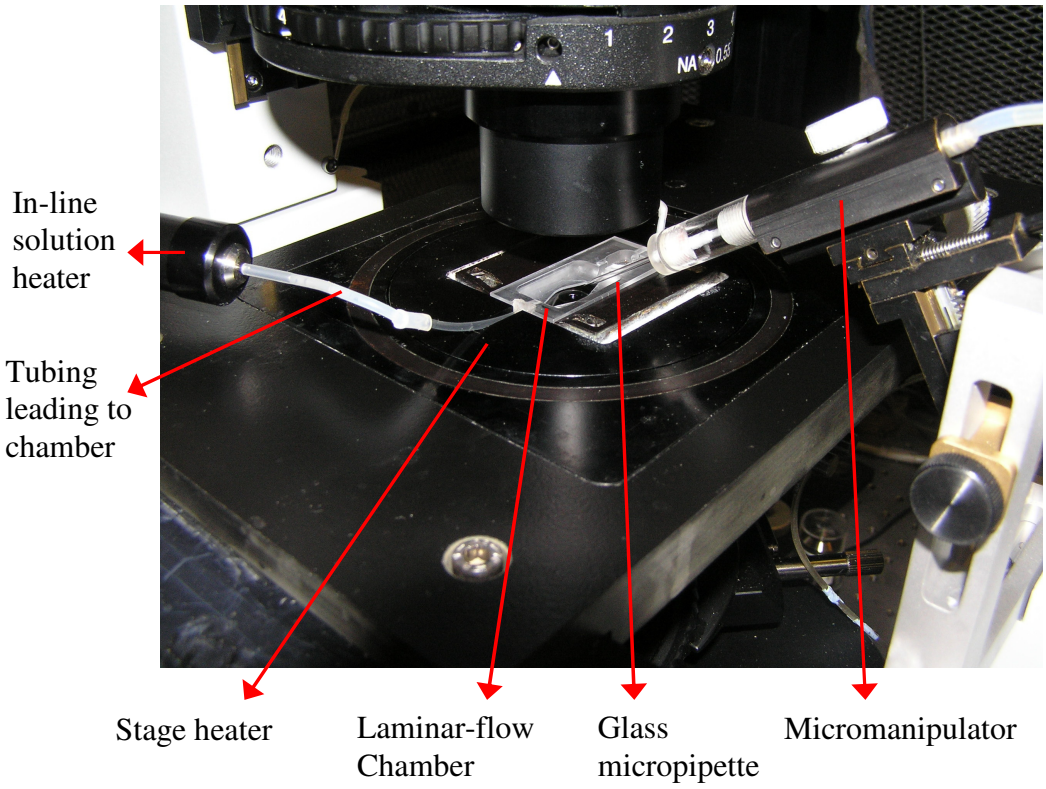

Figure 2.6 Agonist application setup

A picture of the cell stimulation setup showing the laminar-flow chamber, the puffer micropipette controlled by a micromanipulator, the in-line solution heater with the perfusion tubing leading to the chamber and the stage heater. An aspirator on the other side of the chamber allows flow of the applied solution.

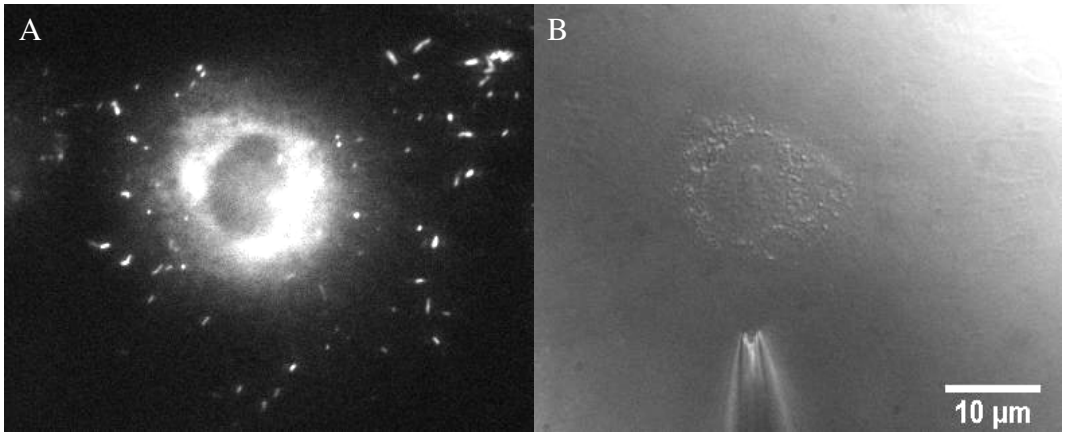

Figure 2.7 Agonist application

A. *Single proregion-EGFP expressing HUVEC in epifluorescence excited at 488nm.* ***B.*** *The same cell in DIC showing the placement of the puffer micropipette*

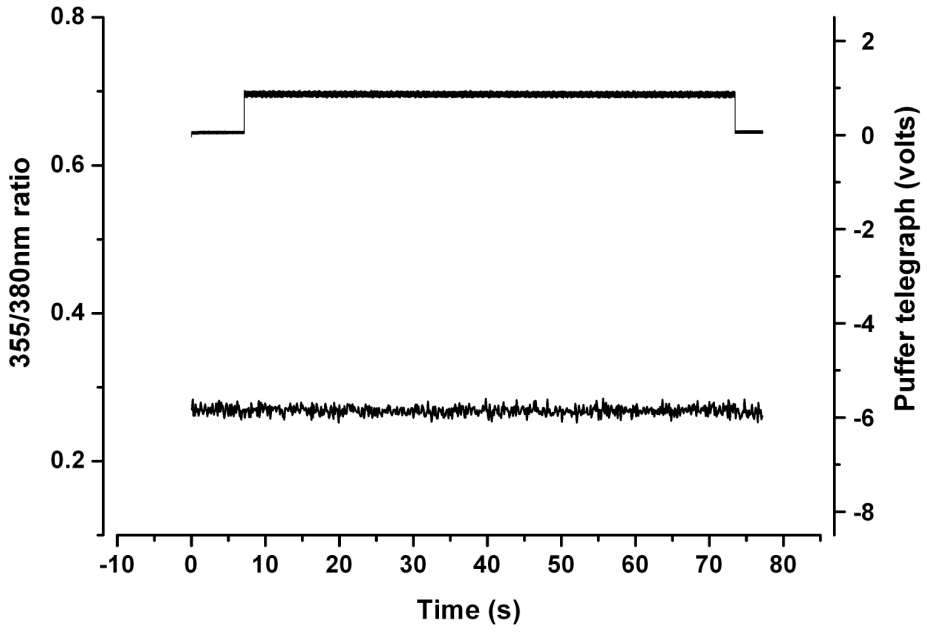

Figure 2.8 Effect of fluid shear due to puff application on resting $[Ca^{2+}]_i$ in HUVEC.

The top trace shows the analogue output signal and indicates activation and deactivation of the puffer micropipette. The lower trace shows the Fura-2 fluorescence which does not change during puff application of bath solution indicating there is no response due to fluid shear effects.

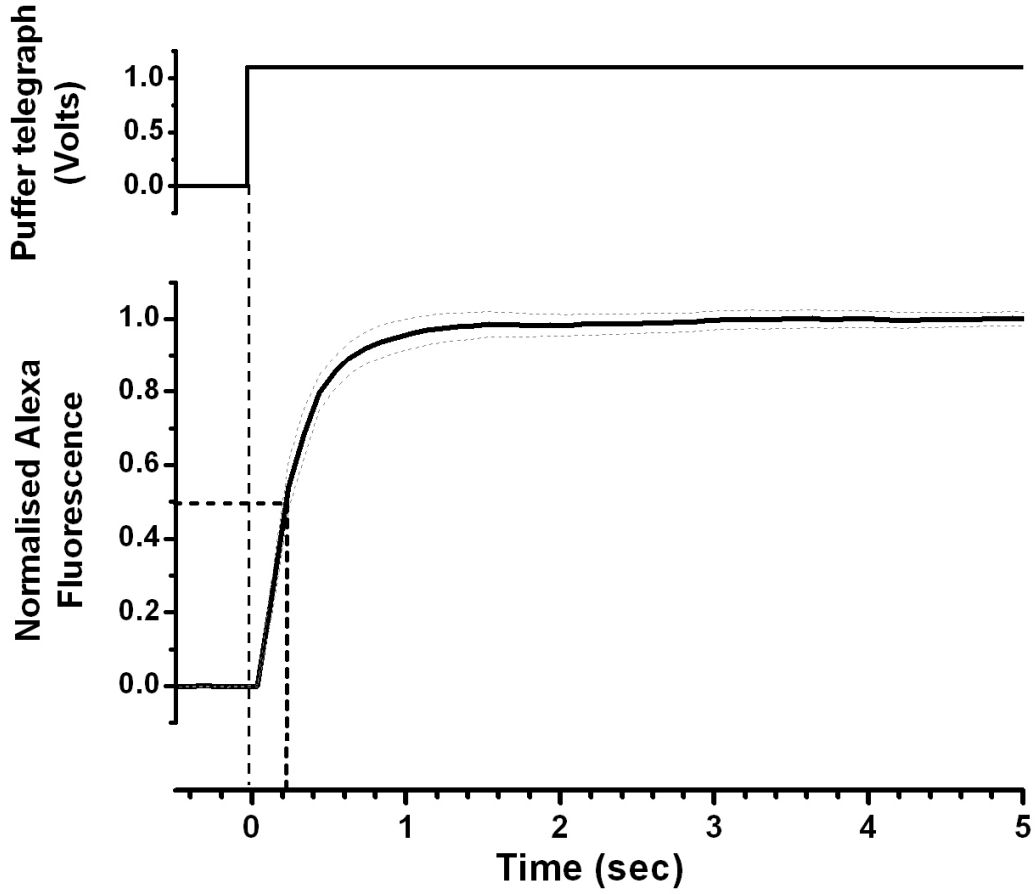

Figure 2.9 Defining the delay in drug arrival

The top panel shows the +1V analogue output from the micropipette solution puffer controller that signals activation of the device. The solid trace in the bottom panel represents the mean time-course of the fluorescence increase due to Alexa-647 in the puffer solution (normalised to the peak steady-state fluorescence level, n=15 cells), in a ROI placed over the cell. Dotted lines represent s.e., of mean. The time-point of drug arrival at the cell was taken arbitrarily as the 50% Alexa fluorescence increase (Vertical dashed line) and was ~200ms. This time-point was used to define time=0s for subsequent analysis of delay times.

2.2.5 Ammonium Chloride (NH_4Cl) pulse technique

NH_4Cl, a weak base, completely ionizes in solution to ammonium (NH_4^+) and Cl^-. NH_4^+ reacts with OH^- in solution to form ammonia (NH_3) and H_2O. NH_3 is cell permeable because it is uncharged and rapidly passes through lipid bilayers to bind protons in the lumen of organelles and form NH_4^+ until NH_3 and NH_4^+ reach equilibrium in the cell and its organelles (e.g. the secretory granules) [599]. This process alkalinises the granules transiently resulting in an increase of granule-targeted GFP fluorescence. The charged partner (NH_4^+) was originally thought to be cell impermeable from the early work by Overton in 1897 and by Jacobs in 1922 [599]. Later on it was discovered that NH_4^+ also passively enters the cell at a slower rate than NH_3, dissociating into NH_3 and H^+ and causing the cell to acidify [600, 601]. A simplified diagram of these reactions is illustrated in Figure 2.10A.

5mM NH_4Cl final concentration from 50mM stock in PS made up fresh and adjusted to pH7.4 with NaOH was added to the t-PA-EGFP and proregion-mRFP co-expressing HUVEC maintained in PS at 37°C. The EGFP fluorescence change upon NH_4Cl addition is used to calculate the $pH_{t\text{-}PA}$ by using the equation in 2.10B where the pK_a (pH at half-maximal fluorescence) is 5.84 and n_H (Hill coefficient) is 0.74 as derived from the *in vivo* pH titration of WPB EGFP fluorescence [1]. F represents the steady-state normalised EGFP fluorescence before NH_4Cl addition and F_{max} the peak of the normalised EGFP fluorescence.

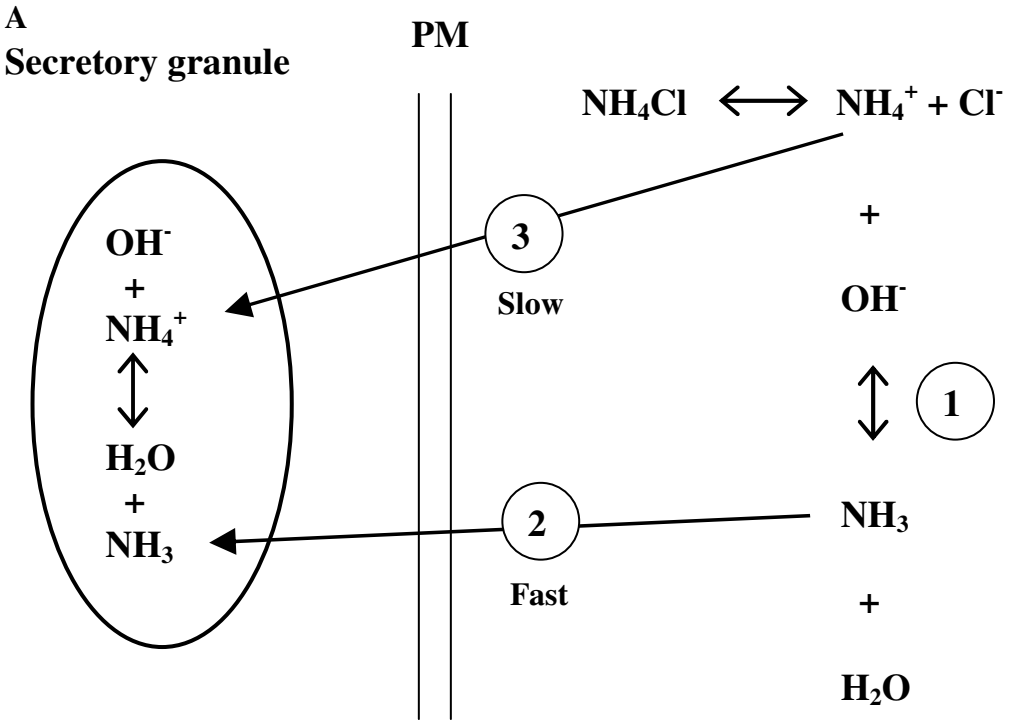

B $$pH = pKa - \frac{1}{n_H} \cdot \log\left(\frac{F_{\max}}{F} - 1\right)$$

Figure 2.10 NH_4Cl action on the secretory organelles

A. *Schematic diagram of the action of NH_4Cl on secretory granules. NH_4Cl completely ionizes in solution. Its charged moiety forms NH_3 which rapidly permeates membranes and binds H^+ inside the acidic lumen of secretory granules to form NH_4^+ until NH_3/NH_4^+ equilibrium is reached. Extracellular NH_4^+ slowly permeates the granule to re-acidify the lumen.*

B. *The equation used to calculate the intra-granule pH from the normalised luminal EGFP fluorescence during NH_4Cl addition. Where pK_a=5.84, n_H=0.74, F_{max}= normalised peak of EGFP fluorescence, F= steady-state normalised EGFP fluorescence.*

2.2.6 Data analysis and measurements

Image analysis was carried out using custom written plugins and macros in ImageJ software (http://rsb.info.nih.gov/ij/). Dataset plotting, fitting and analysis were performed in Excel, Microcal Origin 7 and GraphPad Prism. Results are expressed as mean±SD unless indicated otherwise. Statistical differences (at 95% confidence limit) between 2 population means were determined using a non-paired two way t-test or a one way ANOVA between more than 2 population means followed by a Tukey post test which compared all pairs of populations. The proportion of WPB that underwent exocytosis was determined in epifluorescence experiments. A 5 frame averaged image, taken prior to stimulation, was exported to ImageJ for counting WPBs using the *Pointpicker* plugin. The total number of WPBs within the cell were counted manually twice and the mean value taken. The number of WPBs that underwent exocytosis was determined (in ImageJ) from the time-lapse images. Changes in $[Ca^{2+}]_i$ were calculated as the ratio of background subtracted Fura-2 fluorescence at 355nm divided by that at 380nm within the WinFluor program. The time-point of $[Ca^{2+}]_i$ rise was determined as the first time point of the Fura-2 signal that was higher than the mean + 3 times the standard deviation of the pre-stimulated signal (>mean+3*SD).

For $[Ca^{2+}]_m$ changes, the analysis was done in ImageJ using a custom written average background subtraction macro (Nicolai Kiskin, NIMR). The average background was subtracted first from the cytosol and then from a ROI adjacent to the X-Rhod-1 loaded mitochondrial region that was being analyzed. A ROI was then placed over the chosen mitochondrial region to measure the change in X-Rhod-1 fluorescence. If the mitochondria happened to move during

stimulation i.e. contract, then a custom macro (written by Dr Victor Babitch, NIMR) was used to track the movement.

2.3 Description of Imaging

2.3.1 Imaging $[Ca^{2+}]_i$ changes with Fura-2

In order to determine the relationship between elevated $[Ca^{2+}]_i$ and secretion it is necessary to make simultaneous measurements of changes in $[Ca^{2+}]_i$ and WPB exocytosis. For measuring $[Ca^{2+}]_i$, the UV light excitable Ca^{2+} indicator Fura-2 (Invitrogen; Paisley, UK, cat. No. F1221) was used [602]. For intact cells the acetoxymethyl (AM) ester form was used that can passively diffuse across cell membranes where it is cleaved by cytosolic esterases to yield a charged molecule that becomes trapped inside the cell (Figure 2.11). Fura-2 is a high affinity ratiometric indicator (K_d=100nM) that allows measurements of $[Ca^{2+}]_i$ changes independent of variables such as indicator concentration, photo-bleaching, cell thickness and artefacts such as movement. Although this dye has a similar emission wavelength profile to that of GFP it is excited at very much shorter wavelengths. These characteristics, in conjunction with suitable optics allowed both fluorophores to be imaged within the same cell (setup Figure in chapter 4 Figure 4.1). The excitation and emission wavelengths of Fura-2 free of Ca^{2+} or Ca^{2+} bound are shown in Figure 2.11 along with the wavelengths chosen for imaging; 355nm and 380nm. The commonly used excitation wavelengths for Fura-2 are 380nm (for which emission light at 520nm is quenched upon Ca^{2+}-binding), and 340nm (for which emission light at 520nm increases upon Ca^{2+}-binding). However, microscope systems vary in their optical transmission properties and are often inefficient at transmitting light in the near UV. This is illustrated for the transmission properties of the objectives used in these studies

(Figure 2.12). To determine the optimal wavelengths for ratiometric measurements of Fura-2 for our optical setup, spectral imaging experiments were conducted using Winfluor software. 1μM Fura-2 loaded HUVEC were imaged at 30frames/s during which the centre wavelength for excitation light was varied frame by frame from 340nm to 400nm in 10nm steps (10nm bandwidth). The cells were stimulated with 3μM histamine to elevate $[Ca^{2+}]_i$. Figure 2.13 shows the background subtracted fluorescence at 520±40nm for each of the excitation wavelengths as a function of time. There was no signal for 340nm excitation light consistent with the poor transmission at this wavelength through the microscope objective (Figure 2.12). From the spectral data the wavelengths of choice for ratiometric measurements are 355nm, the iso-emissive wavelength (i.e. does not change in fluorescence upon binding to Ca^{2+}) and 380nm. Although at 390nm the Fura-2 signal was larger, this wavelength was not chosen in order to minimize cross talk with GFP excitation (which can be excited as low as 400nm).

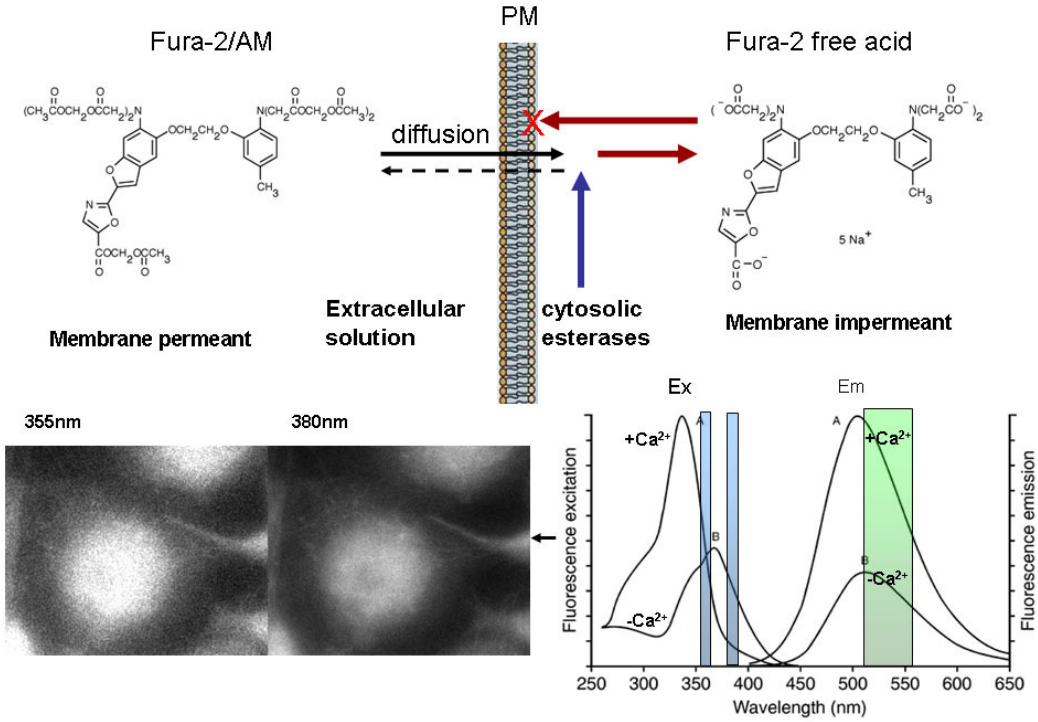

Figure 2.11 Chemical and Spectral properties of Fura-2

A schematic of the Fura-2/AM diffusion through the cell membrane and formation of a charged molecule that becomes trapped inside the cytosol, by removal of the ester moieties by cytosolic esterases. The lower panel on the right shows the excitation and emission wavelengths of Fura-2 in the Ca^{2+}-free and the Ca^{2+}-bound form. The excitation light for these experiments is 355nm and 380nm (blue bars) for ratiometric measurements and emission light is selected at 520±40nm (green bar). The next panel shows a single HUVEC loaded with 2.5µM Fura-2 imaged with the specific parameters.

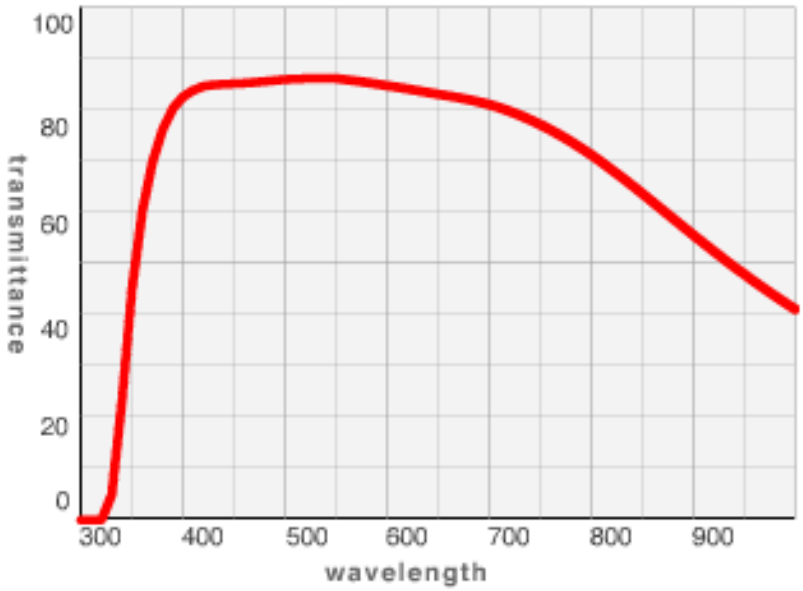

Figure 2.12 Transmission properties of* Olympus UPLSAPO x100 1.40NA and U-Plan-APO x100 1.35NA *objectives

http://microscope.olympus.com/uis2/UPLSAPO/100XO/

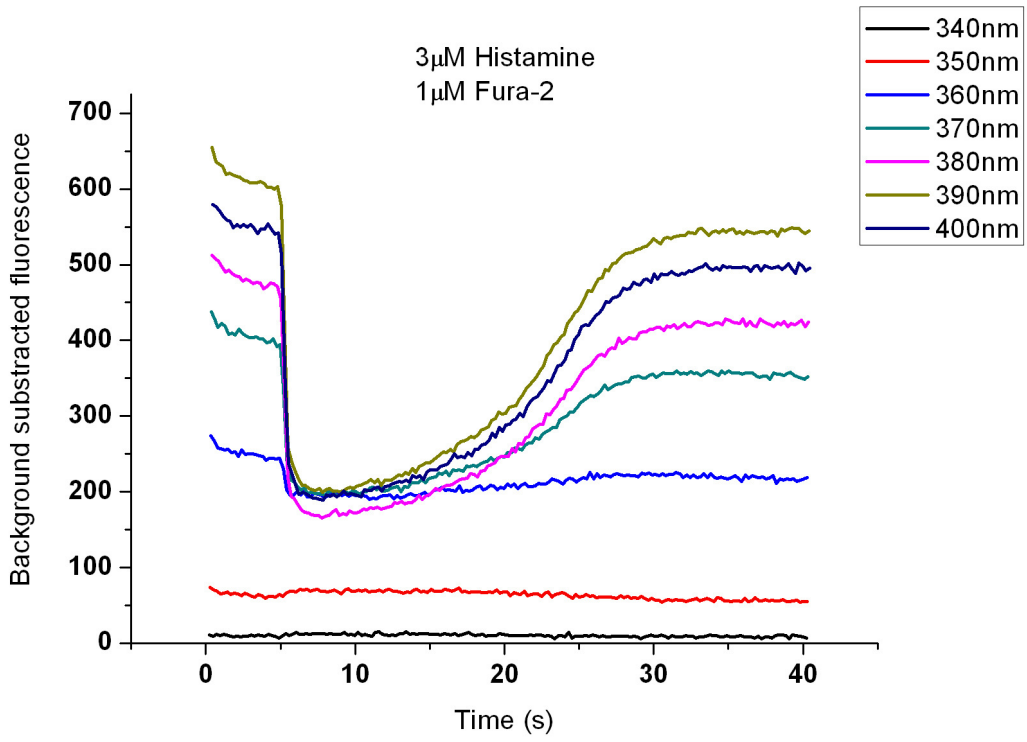

Figure 2.13 Excitation spectral imaging of Fura-2 loaded HUVEC

HUVEC loaded with 1μM Fura-2 and stimulated with 3μM histamine are imaged at 30frames/s for wavelengths between 340nm-400nm in 10nm steps (10nm bandwidth). Each trace represents the background subtracted fluorescence at 520±40nm for each of the excitation wavelengths indicated as a function of time.

2.3.2 Establishing Fura-2/AM loading conditions

Due to its Ca^{2+} binding properties Fura-2, at high cytosolic concentrations, may contribute to buffering, thus limiting the distance over which Ca^{2+} can diffuse and exert its effects. Changes in intracellular Ca^{2+} may be altered sufficiently to affect the kinetics of exocytosis. To ensure that Fura-2 did not interfere with hormone evoked exocytosis, the kinetics of exocytosis of fluorescent WPBs were compared between experiments using non-Fura-2 loaded cells (sham loaded) and cells loaded with different concentrations of Fura-2/AM (0.5-5μM; for 20min at room temperature; see below). Cells were stimulated either with a medium (3μM) or high (30μM) histamine concentration applied by pressure injection from a glass micropipette. Alexa-647 was included in the agonist solution in the control experiments to determine the time-course of drug arrival to the cell (2.2.4). Concentrations of Fura-2/AM of 2.5μM or less were found not to significantly alter the delays and rates of WPB exocytosis for the two concentrations studied. Figure 2.14 shows the histograms of WPB exocytotic events between sham loaded and 2.5μM Fura-2 loaded HUVEC stimulated with 3μM and 30μM histamine.

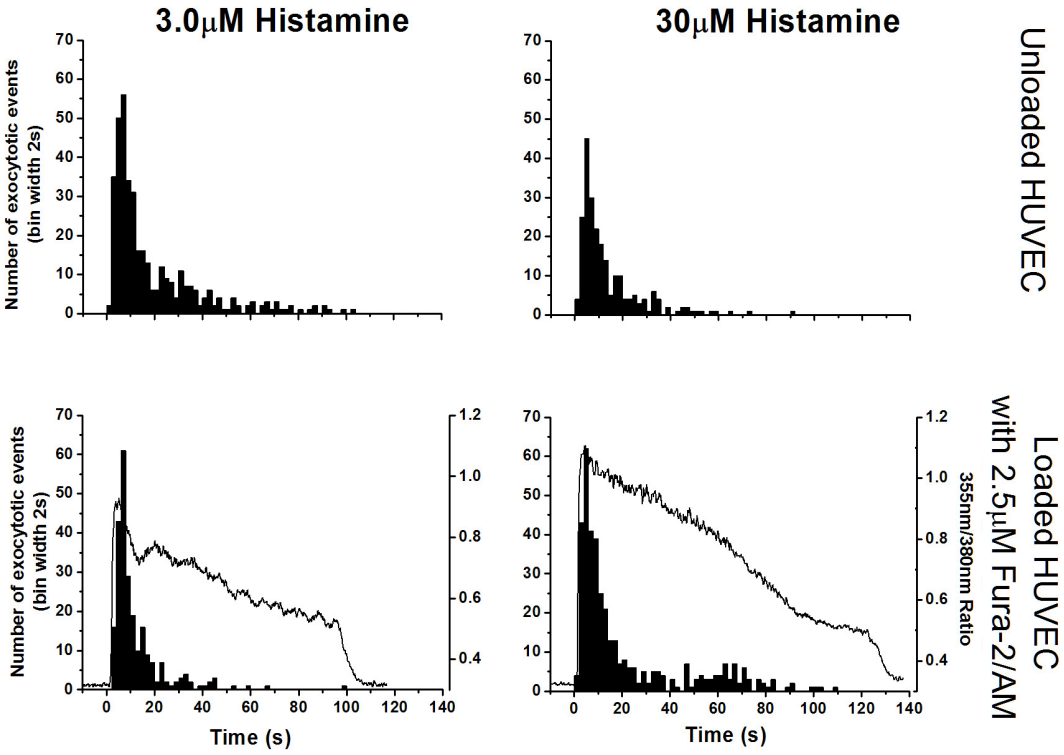

Figure 2.14 Fura-2 loading conditions

Upper panels show histograms of WPB fusion events, for control unloaded cells, offset so that puffer activation occurred at t=0. The lower panels show histograms of WPB fusion events and the Fura-2 fluorescence ratio for HUVEC loaded with 2.5μM Fura-2. Panels on the left are experiments stimulated with 3μM histamine and panels on the right 30μM histamine. Unloaded HUVEC histograms represent data pooled from 17 cells each (332 WPB for 3μM and 230WPB for 30μM Histamine stimulation). Fura-2 loaded HUVEC histograms represent data pooled from 18 cells (244 WPB) and 25 cells (388 WPB), stimulated with 3μM and 30μM histamine respectively.

For Fura-2 loading, nucleofected cells were transferred into Physiological Saline (PS) supplemented with 0.5-2.5μM Fura-2/AM diluted from a stock solution of 5mM Fura-2/AM in anhydrous DMSO (Dimethyl Sulphoxide; Sigma, Dorset, UK, cat no D2650) with 2.0% Pluoronic F-127 low UV absorbance (Invitrogen, Paisley, UK, cat no P-6867) a low-toxicity dispersing agent used to facilitate the solubilisation of water-insoluble dyes in PS. Cells were incubated at room temperature in the dark for 20min, then washed with fresh PS and further maintained in the dark at room temperature until use.

2.3.3 Imaging changes in $[Ca^{2+}]_m$ with X-Rhod-1

Changes in mitochondrial Ca^{2+} have been directly measured using targeted expression of Ca^{2+} sensitive photoproteins such as aequorin [550, 603] or mitochondrial specific fluorescent probes including rhodamine derivatives such as the Ca^{2+} indicator X-Rhod-1 [604]. X-Rhod-1 (Invitrogen; cat. No. X14210) has a K_d for Ca^{2+} of 700nM. The cell permeant acetoxymethyl (AM) form is positively charged and is preferentially concentrated into polarized mitochondria [604]. Once in the mitochondrial lumen its ester moieties become hydrolyzed and the resulting free acid remains trapped inside the mitochondria where it binds intra-mitochondrial Ca^{2+} and reports increases in $[Ca^{2+}]_m$ as an increase in fluorescence intensity (Figure 2.15). A portion of X-Rhod-1 fails to partition into the mitochondria and so remains in the cytosol where it reports $[Ca^{2+}]_i$ changes. X-Rhod-1 was chosen due to its long-wavelength emission characteristics (Figure 2.15) that allow its simultaneous detection with GFP with minimal crosstalk. In order to accommodate the optical arrangements, X-Rhod-1 was excited at 480nm to allow simultaneous excitation of GFP (setup Figure in chapter 6; Figure 6.1).

Figure 2.15 shows the X-Rhod-1 excitation and emission wavelengths used (blue and red bars respectively).

To establish localization of X-Rhod-1 in mitochondria, HUVEC were co-loaded with 0.2μM X-Rhod-1 and 50nM mito-tracker Green (Invitrogen) for 20min. Mito-tracker Green is a cell-permeant probe that passively diffuses across the plasma membrane and accumulates in mitochondria. It is excited at 490nm and emits light at 516nm. Figure 2.16A shows co-localization between mito-tracker Green and X-Rhod-1 indicating X-Rhod-1 efficiently partitions into the mitochondria. Figure 2.16B shows a single HUVEC expressing construct mito-EGFP (2.1.3) and loaded with X-Rhod-1. Similarly X-Rhod-1 fluorescence completely coincided with the mitochondrial in cultured HUVEC. In both panels 2.16 A and B, a portion of X-Rhod-1 remains in the cytosol. To remove the contribution of cytosolic changes in X-Rhod-1 fluorescence from mitochondrial derived X-Rhod-1 a background subtraction was made from a region adjacent to the mitochondrial ROI (2.2.6).

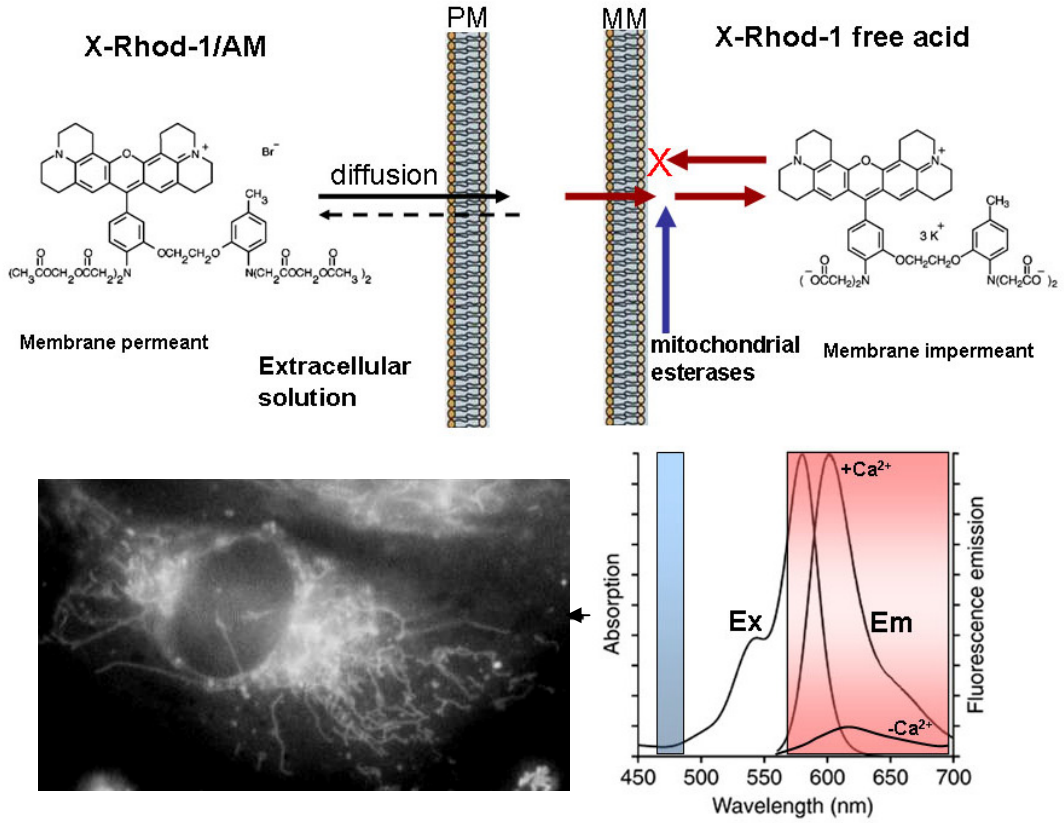

Figure 2.15 Chemical and Spectral properties of X-Rhod-1

The upper panel is a schematic of the X-Rhod-1 diffusion through the cell membrane and accumulation into the mitochondria where it becomes trapped by removal of the ester moieties by mitochondrial esterases. The lower panel on the right shows the spectral properties of X-Rhod-1 and the excitation (480nm; blue bar) and emission (615±25nm; red bar) wavelengths used to image X-Rhod-1 simultaneously with GFP in these experiments. The lower panel on the left shows a single HUVEC loaded with 0.2μM X-Rhod-1 imaged with the specific parameters.

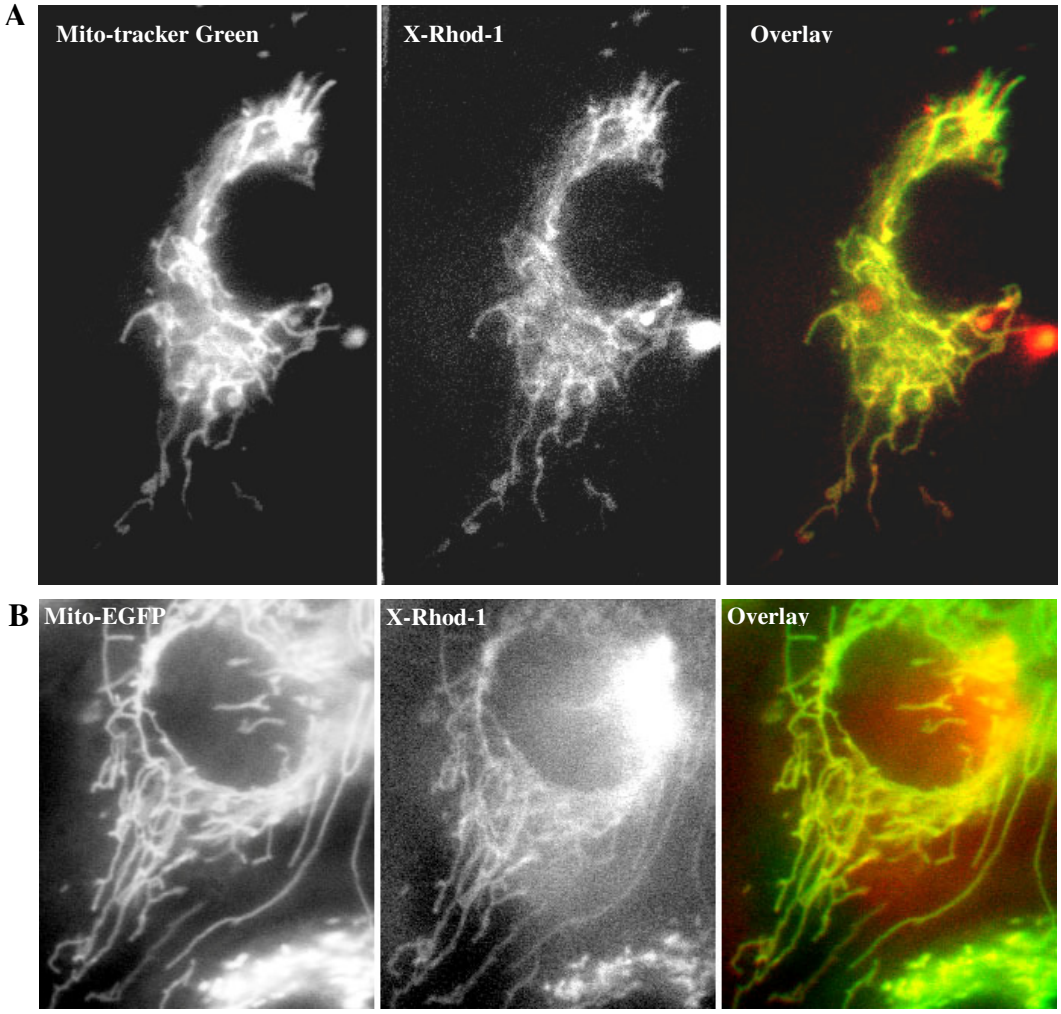

Figure 2.16 X-Rhod-1 co-localizes with mito-tracker Green and mito-EGFP

Live HUVEC were recorded at 6.6frames/s; excited at 480nm and emitted light was separated using an optical splitting device to be collected at 520±20nm and 615±25nm. ***A*** *shows single HUVEC co-loaded with 0.2μM X-Rhod-1 and 50nM mito-tracker Green and* ***B*** *shows single HUVEC nucleofected with mito-EGFP 24hours prior loading with 0.2μM X-Rhod-1. Left panel in* ***A*** *shows mito-tracker Green emission and left panel in* ***B*** *shows mito-EGFP. Middle panels in* ***A*** *and* ***B*** *show X-Rhod-1 emission and right panels the overlay. 0.2μM X-Rhod-1 efficiently labels the mitochondria with some dye remaining in the cytosol.*

2.3.4 Establishing dual-loading conditions for X-Rhod-1/AM and Fura-2/AM

X-Rhod-1 and Fura-2 are both Ca^{2+} buffers and their combined use for monitoring Ca^{2+} changes may interfere with physiological Ca^{2+} signalling and consequently with the kinetics of WPB exocytosis. Experiments were carried out to establish co-loading conditions that did not affect the kinetics of WPB exocytosis. The delay between $[Ca^{2+}]_i$ rise and the first exocytotic event and the maximal rate of WPB exocytosis stimulated with 30μM histamine was compared between HUVEC loaded with 2.5μM Fura-2 alone and HUVEC co-loaded with different concentrations of X-Rhod-1 and Fura-2. Data obtained from HUVEC co-loaded with 0.2μM X-Rhod-1 and 0.5μM Fura-2 were not significantly different from that obtained with 2.5μM Fura-2 loaded HUVEC (Figure 2.17).

The stock solution of X-Rhod-1 was made up to 1mM in DMSO (Sigma) with 2.0% Pluoronic F-127 (Invitrogen). HUVEC were co-loaded in 0.2μM X-Rhod-1 and 0.5μM Fura-2 in PS at room temperature in the dark for 20min and then washed with fresh PS and further maintained in the dark at room temperature until use.

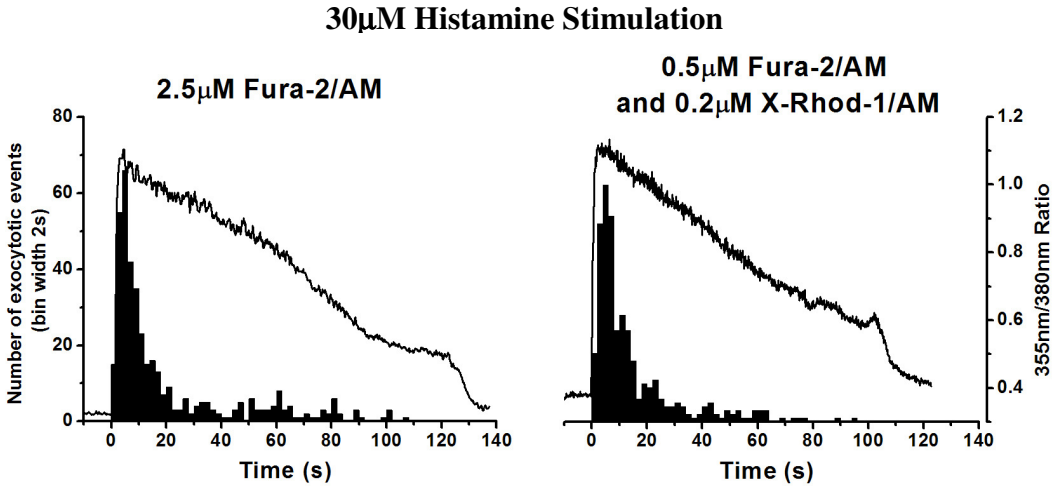

Figure 2.17 Establishing appropriate Fura-2 and X-Rhod-1 co- loading conditions.

Histograms of WPB fusion events and the Fura-2 fluorescence ratio for HUVEC stimulated with 30μM histamine; offset so that the Ca^{2+} rise occurred at t=0. Left panel are HUVEC loaded with 2.5μM Fura-2 and in the right panel HUVEC co-loaded with 0.5μM Fura-2 and 0.2μM X-Rhod-1. Histograms represent data pooled from 25 cells (388 WPB) for single loaded HUVEC and from 12 cells (379 WPB) for double loaded HUVEC

2.3.5 Imaging $\Delta\Psi_m$ Collapse with TMRE

The potentiometric dye tetramethylrhodamine ethyl ester (TMRE) is a fluorescent lipophilic cation widely used for $\Delta\Psi_m$ measurements as it accumulates in mitochondria in proportion to the standing electrochemical membrane potential gradient. The fluorescence change in response to $\Delta\Psi_m$ changes depends on the specific dye loading conditions and is reviewed in detail in [521]. Briefly as the dye reaches high concentrations inside the mitochondria its fluorescence becomes quenched. This auto-quenching of fluorescence is due to the individual dye molecules coming so close to one another at high concentrations that emitted photons from one molecule are absorbed by adjacent molecules. Depolarisation of $\Delta\Psi_m$ drives the dye out of the mitochondria, causing the molecules to separate, de-quench and increase in fluorescence. This leads to an abrupt increase in both mitochondrial and cytosolic TMRE fluorescence as the dye exits the mitochondria and enters the cytosol. The concentrations and loading times for reaching auto-quenching concentrations vary between cell types due to variability of the plasma and mitochondrial membrane potential [605]. This first method was called the de-quenching method and changes in TMRE fluorescence can be measured from the whole cell, as previously used in gonadotrope cells [552], chromaffin cells [584] and in neurons [553]. However if the dye is loaded in mitochondria at low concentrations, where it does not reach auto-quenching levels, upon $\Delta\Psi_m$ depolarisation and exit of the dye from mitochondria, the mitochondrial TMRE fluorescence signal decreases whereas the cytosolic signal increases as the dye enters the cytosol. We called this second method the redistribution method. Measurements of the TMRE signal in this case requires high resolution imaging to allow single mitochondrion fluorescence measurements as previously described in

endothelial cells [606, 607]. The basic principles of these two different loading methodologies are summarised in Figure 2.18. One potential problem of the high concentration, de-quenching method is that excitation of TMRE can lead to excessive ROS production that can damage the mitochondria leading to openings of the permeability transition pore (PTP_m) [608].

The concentration at which TMRE undergoes auto-quenching in our cells was determined by perfusing onto cultured HUVEC increasing concentrations of TMRE. Recordings were taken using a confocal Olympus BX50WI upright microscope with a 60x objective, in order to minimise the TMRE background fluorescence. TMRE was excited with a 543nm laser and collected using a 555-565nm emission filter at 0.4frames/s. The fluorescent signal measurements were analysed in Image J. In Figure 2.19A the cells were initially loaded with 0.01μM TMRE for 10min in the dark and then imaged for about 4min while perfused with 0.01μM TMRE (to prevent exit of the dye from the cell). The solution was then switched to 0.3μM TMRE, recorded for 4min, left to incubate for further 5min and then recorded again for another 4min before switching to the next concentrations; 1μM and 3μM TMRE, following the same protocol. This experiment shows the increase in mitochondrial TMRE fluorescence when a low concentration of TMRE is used (0.3μM) and a subsequent decrease (due to auto-quenching) as the concentration of TMRE is increased further to 3μM. To confirm that the dye was auto-quenched at 3μM TMRE, cells loaded in 3μM TMRE (for 10min in the dark) were imaged for 5min during perfusion with 1μM FCCP and 2.5μg/ml oligomycin to collapse the $\Delta\Psi_m$. There was an increase in TMRE fluorescence during application of the inhibitors consistent with de-quenching of TMRE fluorescence (Figure 2.19B). Although both methods were

attempted, we in the end used the second, redistribution method to avoid possible problems associated with photo-toxicity. Details of the redistribution method are described in more detail in chapter 6. Briefly cells were loaded in 0.3μM TMRE (Sigma, cat no 87917) from a stock of 100mM in DMSO, for 20min in the dark at room temperature before the start of the experiment and maintained in 0.3μM TMRE thereafter. TMRE is excited in epifluorescence at 480(7) and emitted light is collected at 615±25nm.

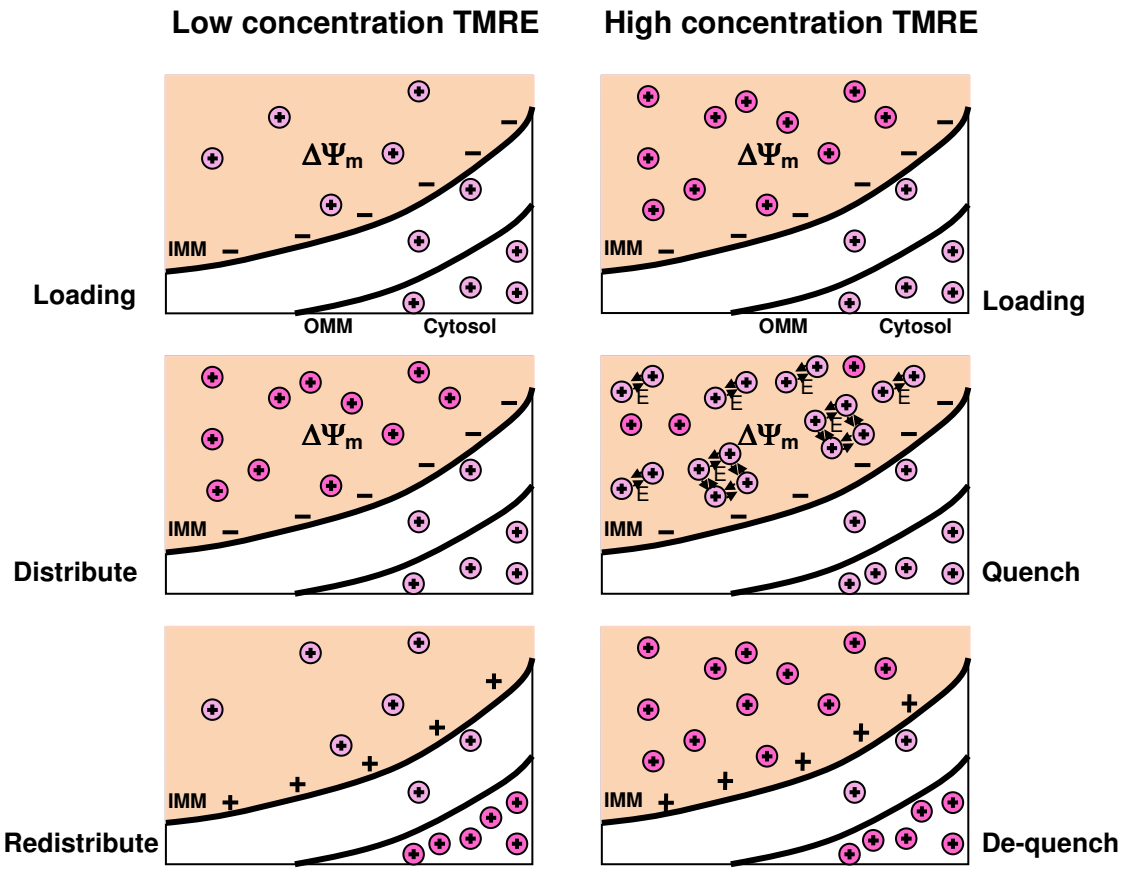

Figure 2.18 Loading conditions for TMRE

The panel on the left demonstrates the redistribution method for measuring TMRE fluorescence and on the right demonstrates the de-quenching method. In the first method TMRE is loaded at low concentrations (upper panel) and distributes (middle panel) in the mitochondrial lumen. Upon collapse of the $\Delta\Psi_m$ the dye exits the lumen into the cytosol therefore the TMRE fluorescence increases in the cytosol and decreases in mitochondria (lower panel). In the second method TMRE is loaded at high concentrations (upper panel) reaching auto-quenching levels in the mitochondrial lumen (middle panel). Upon $\Delta\Psi_m$ collapse TMRE molecules enter the cytosol de-quenching therefore increasing in fluorescence both in the mitochondrial lumen and the cytosol (bottom panel).

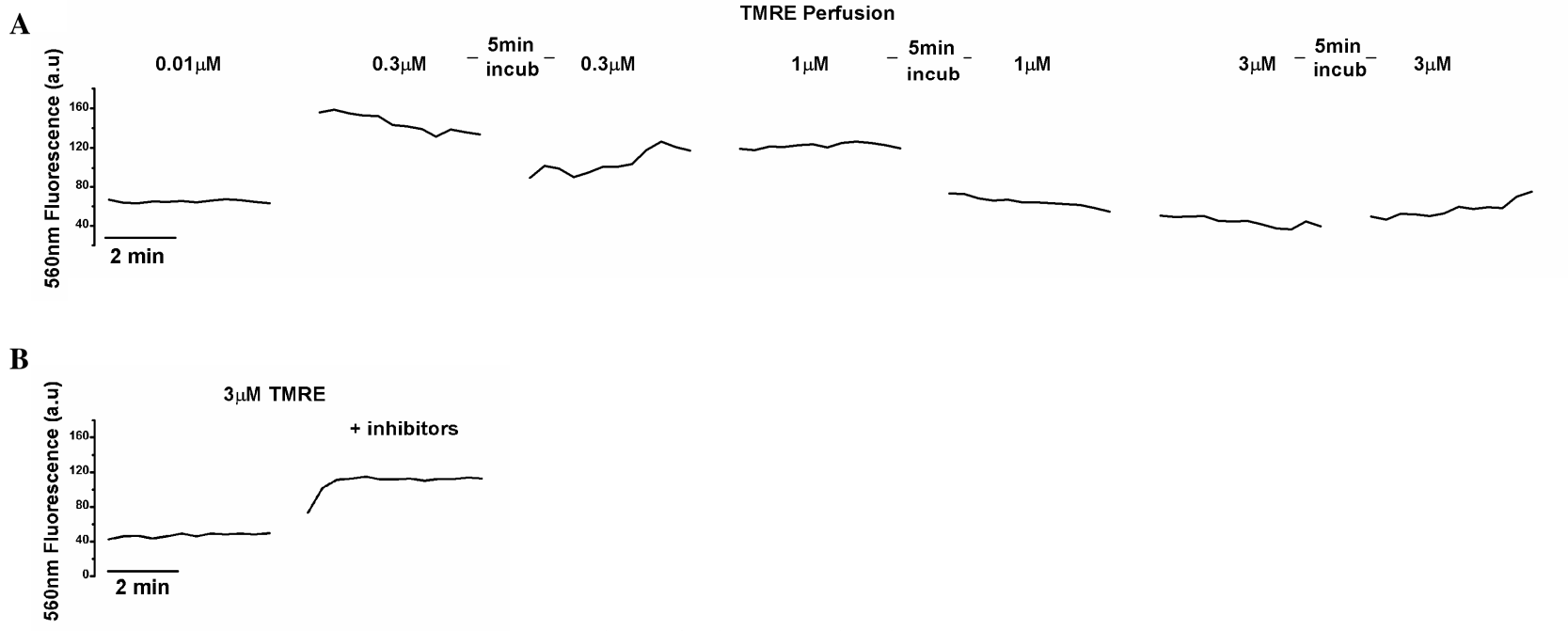

Figure 2.19 TMRE titration

A. *HUVEC loaded in 0.01μM TMRE for 10min were sequentially perfused with 0.01μM, 0.3μM, 1μM and 3μM TMRE and recorded at 0.4frames/sec with an Olympus BX50WI upright microscope using a 60x objective. TMRE is excited at 543nm and emitted light is selected with a 555-565nm emission filter. Each concentration was recorded for about 4min and there was a 5min incubation time between new concentrations as indicated.*

B. *Using the same optics 3μM TMRE loaded HUVEC for 10min were perfused sequentially with 3μM TMRE and 1μM FCCP with 2.5μg/ml Oligomycin as indicated, recorded for 4min each.*

RESULTS

3 GFP as a tool to probe changes in secretory granule pH and to determine the time of fusion pore formation during exocytosis of the non-WPB secretory organelle

3.1 Introduction

A major aim of this thesis was to characterise in detail the kinetics of exocytosis of two distinct secretory organelles found in endothelial cells (EC); the Weibel-Palade-Body (WPB) and the non-WPB organelle (Introduction 1.3). In order to study the kinetics of exocytosis as directly as possible both organelle populations needed to be visualised in living cells such that the fusion of individual granules could be determined accurately at high time resolution. To achieve this we used green fluorescent protein (GFP) targeted specifically to the two distinct secretory granule populations, taking advantage of the pH-dependent properties of this fluorescent protein to determine the point of granule fusion. Here I discuss the properties of GFP that make it suitable for this application and show that GFP tagged proteins targeted to endothelial secretory granules can be used to determine and compare the intra-granule pH and changes in this pH at different stages of organelle maturation.

3.1.1 GFP Structure

GFP is a fluorescent protein first identified in the hydroid jellyfish *Aequorea Victoria* as an accessory protein of the bioluminescence protein aequorin [609]. It absorbs blue light and emits green light [610] (Figure 3.1A). Cloning of GFP in the 1990s showed it to be a single 238 amino acid protein [611] of 27kDa molecular weight [612], that retains its fluorescence when heterologously expressed in prokaryotic and eukaryotic organisms [613]. GFP folds into a cylindrical structure composed of 11 stranded β-sheets linked together by proline-rich loops [614, 615]. Through the barrel runs an α –helix and both ends of the barrel are closed by short α –helices [614, 615] (Figure 3.1B). In the middle of the

central α –helix is the chromophore, formed by spontaneous cyclization and oxidation of 3 amino acids, Serine65- Tyrosine66 and Glycine67 occurring autocatalytically after the tertiary structure is formed (maturation) [611, 616, 617]. Moreover inside the barrel the chromophore is surrounded by 4 water molecules that participate in a hydrogen-bond network which permits proton transfer between the chromophore and the surrounding molecules [618, 619]. The configuration surrounding the chromophore is important for the fluorescence of GFP and its stability, rendering it a protease-resistant molecule only denatured under extreme conditions [620-622]. Variations in the configuration of the β-barrel or the chemical or physical interior environment can change the spectral characteristics of the protein [623]. Directed mutagenesis of the primary structure of GFP yielded various fluorescent molecules, with different properties including enhanced GFP (EGFP) [616, 624, 625]. GFP has a weak tendency to dimerise [626], however, mutations of any or all of 3 aa (Serine65, Tyrosine66 and Glycine67) removes this tendency giving rise to monomeric GFP (mGFP) that has essentially identical spectral properties to EGFP [591]. In these studies EGFP or mEGFP (obtained from EGFP mutations; see 2.1.2) were used as the fluorescent tags for WPB and non-WPB targeted proteins. No differences in the secretory kinetics of WPBs were observed with granules tagged with either GFP variant.

A

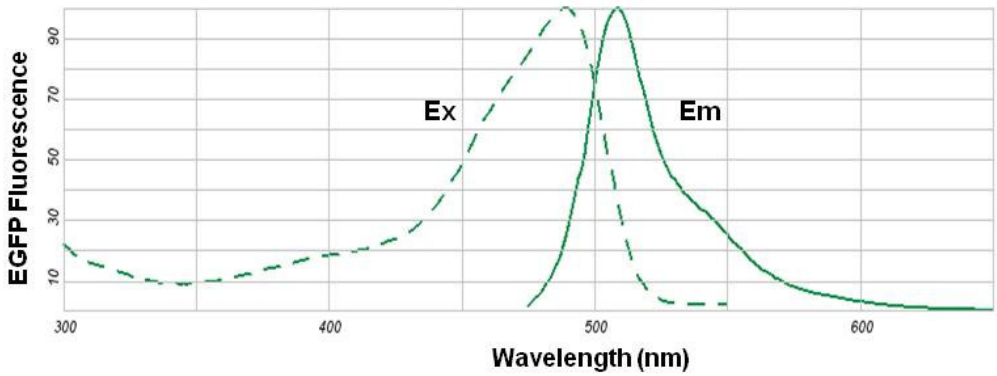

B

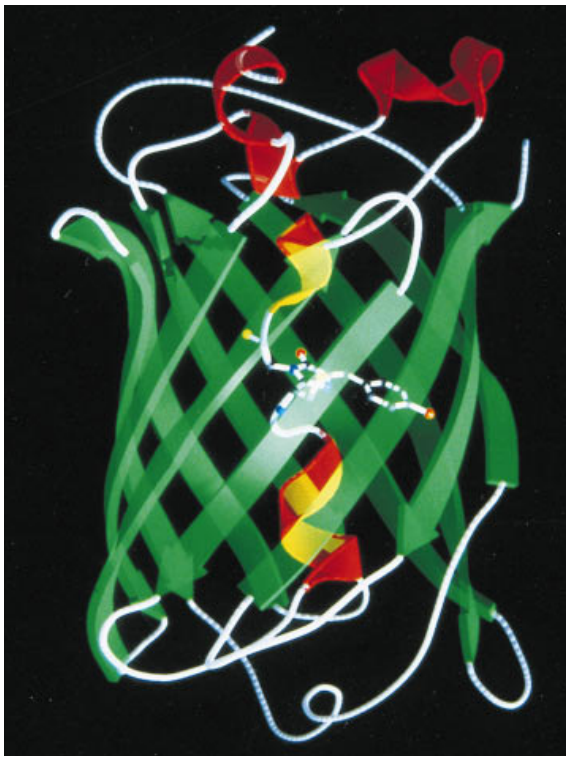

Figure 3.1 The GFP molecule

A. *Graph of the excitation (dotted green trace) and emission (green line) spectra of EGFP in pH7 buffer (taken from http://www.invitrogen.com/site/us/en/home/support/Research-Tools/Fluorescence-SpectraViewer.html).*

B. *A three-dimensional demonstration of the tertiary structure of GFP illustrating the GFP barrel formed by 11 β- sheets (green) arranged in a cylindrical order surrounding a middle α- helix (red) which contains the chromophore consisting of 3 amino acids (ball-and-stick model). Both ends of the barrel are closed by short α-helical sections. The Figure is taken from BREJC, K 1997 [618] and was produced by RASTER3D [627].*

3.1.2 The pH-sensitivity of GFP

The pH-sensitivity of GFP fluorescence was first noted by Ward in the early 1980s [620, 622] and characterised further by Verkman [628]. Verkman showed that the pH dependence of purified GFP *in vitro* and for GFP expressed in cells is nearly identical. Therefore GFP could be used as a reliable non-invasive and rapid cellular pH indicator capable of being genetically targeted to distinct sub-cellular compartments [629], a distinct advantage over other pH sensors such as acridine orange that distribute non-specifically into all acidic cellular compartments [630]. Cellular compartments to which GFP has been targeted include the cytoplasm, ER, Golgi, secretory granules, nucleus and mitochondria of a variety of cell types [345]. The GFP pH-sensitivity is thought to be due to protonation of the phenol group on the aromatic ring of tyrosine of the chromophore [622] at pH>5 and additional conformational changes below pH5 [628]. The two ground states of EGFP; protonated and uncharged states display different spectral characteristics and pH changes shift the equilibrium between the two states [631, 632].

3.1.3 pH in the secretory pathway

It is known that as soluble secreted proteins pass through the lumen of the secretory pathway there are progressive decreases in the intra-luminal pH that are thought to be important in facilitating protein aggregation and condensation (reviewed in [633, 634]). The pH of the ER is ~pH7.2-7.4 [634], similar to the cis-Golgi, while the medial compartments of the Golgi apparatus are thought to be mildly more acidic and at the TGN the pH drops to ~pH 6.2-6.58 [344-347]. This low pH is known to be important for the association of proregion and mature vWF, vWF condensation and multimerization and WPB formation [24, 34, 334,

635] (see introduction 1.7.1.1). Studies in endocrine cells indicate that secretory granules budding off the TGN undergo further acidification as they mature [343, 344, 636]. Average values of intra-luminal resting pH of secretory granules were determined using GFP targeted to immature granules of insulin-secreting cell lines (pH 6.22) [637] and in mature granules of PC12 cells (pH5.5) [638]; by determining the H^+ leak rates of secretory granules of the pituitary cell line AtT-20 cells (pH5.5) [344] and by loading mast cells with a pH-sensitive granule probe (pH5.5) [639]. In most studies the fluorescence measurements were taken from mean intensity levels of regions of interest as the density of granules and their small size precluded the possibility of determining the pH within individual granules [344, 637, 638]. However single granule pH (pH_g) measurements were possible in mast cells with very large granules [639].

3.1.4 GFP as a pH indicator in the secretory pathway of HUVEC

Based on pH studies on secretory organelles it has been speculated that WPBs would also acidify as they mature allowing progressive vWF condensation to form the highly ordered tubule like structures comprised of proregion and vWF [26, 27]. The pH-sensitivity of the EGFP fluorescence fused to vWF or proregion was determined in WPBs in living HUVEC and compared to that for the purified protein *in vitro* [1]. The pH titration of EGFP fluorescence *in vivo* was obtained from experiments where calibration solutions at different pH were perfused onto vWF-EGFP or proregion-EGFP expressing HUVEC cultures (Figure 3.2B). The EGFP fluorescence was normalized to that obtained with the pH8 calibration solution [637]. An example of such an experiment is shown in Figure 3.2B. The EGFP calibration curve derived from data such as that shown in Figure 3.2B is summarised in Figure 3.2A, fitted by a modified Hill equation [628]. The

behaviour of EGFP fused to either full length vWF or proregion alone was essentially identical to that of purified EGFP [1]. This suggested that the properties of EGFP (pH-sensitivity of fluorescence) are largely independent of what EGFP was fused to. From the information obtained in those experiments it was possible to use EGFP to measure the pH within the secretory pathway of HUVEC. The large size of the WPB allowed their pH to be determined (pH_{WPB}) in individual granules permitting the distribution of pH values within a secretory granule population to be determined for the first time (Figure 3.3). Using a morphological pulse chase approach, in which cells were imaged at different stages after expression of WPB targeted EGFP, it was possible to follow the changes in pH_{WPB} from newly formed immature granules through to fully mature organelles. These data show that WPBs, like secretory granules in other cells, undergo a time-dependent acidification of their lumen from pH6.2 for newly formed granules to 5.4 for the mature organelle (Figure 3.3) (pooled data from the secretion and NH_4Cl method, see below).

In contrast to the WPB, the intra-granule pH of the non-WPB ($pH_{non\text{-}WPB)}$ is not known. If this organelle is a true regulated secretory organelle it might be expected that the intra-granule pH might change in a generally similar fashion as described for the WPB.

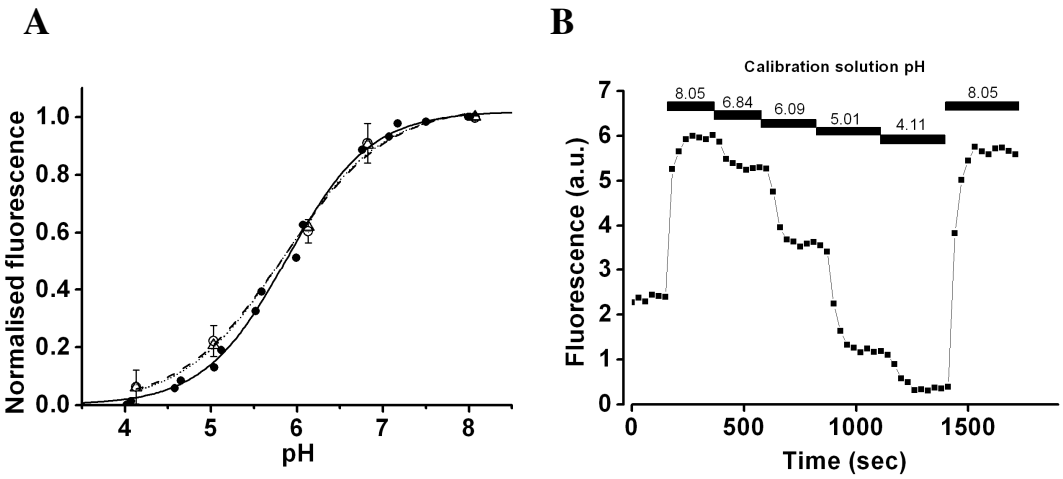

Figure 3.2 In vitro and in vivo pH titration of EGFP fluorescence (Adapted from Erent, M. et al. 2007)[1]

*Panel **A** shows the relationship between EGFP fluorescence and pH. The filled circles represent the fluorescence of purified EGFP in a SPEX fluoromax fluorimeter under different pH values. The dotted lines represent the fluorescence of EGFP* in vivo*; vWF-EGFP (open circles) and proregion-EGFP (triangles). Briefly HUVECs expressing vWF-EGFP or proregion-EGFP were perfused sequentially with cell-permeabilizing calibration solutions, titrated to different pH values, allowing sufficient time for fluorescence intensity to stabilize at each pH and imaged using epifluorescence imaging. A representative example of an individual WPB in a cell is shown in panel **B**. In each case (*in vitro *and* in vivo*), the EGFP fluorescence was normalized to that at pH8.0 (corresponding to F_{max} for EGFP) and plotted against the pH of the solution to generate the calibration curve in panel A. The data was fitted by a modified Hill equation with* in vitro *pKa and n_H for purified EGFP of 5.88 and 0.9 and* in vivo *(intra-WPB) mean pK_a and n_H values of 5.84 and 0.74 respectively.*

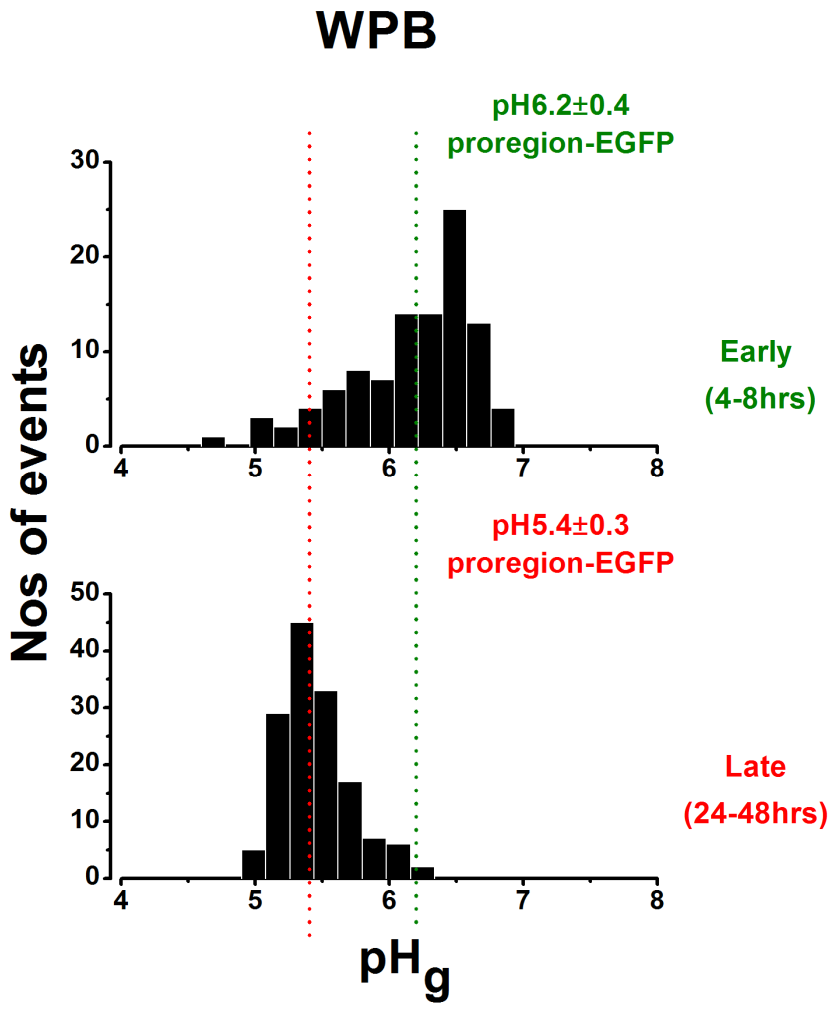

Figure 3.3 pH_{WPB} during maturation (Adapted from Erent, M. et al.2007)[1]

The two panels show the pH_g distributions of the immature WPB (4-8 hrs post-Nucleofection with proregion-EGFP) (upper panel) and the mature WPB (24-48 hrs post-Nucleofection with proregion-EGFP) (lower panel). The mean pH decreased during WPB maturation from pH6.16±0.45 (n=101 WPBs; mean±s.d.) to pH5.45±0.27 (n=303 WPBs; mean±s.d.).

3.1.5 GFP as a marker of fusion

The pH-sensitivity of GFP and the acidic lumen of secretory granules permits GFP targeted to the granular lumen to act as a marker of exocytosis. This is achieved due to the pH change during the formation of the fusion pore resulting in an abrupt increase in GFP fluorescence or 'flash' of light. Previous studies utilised GFP fusion proteins targeted to secretory granules to study exocytosis in PC12 cells [640, 641], insulinoma cells [642-644], chromaffin cells (see review [645]) and endothelial cells [89]. Similar flashes of light are seen on fusion of EGFP-tagged WPBs in HUVEC [35]. These 'flashes' of light mark the formation of the fusion pore and provide a basis for determining accurately the point of fusion for the WPB allowing the detailed analysis of the WPB secretory kinetics described later in chapter 4. Similar studies of the non-WPB granule have not been made.

3.1.6 Aim

In this chapter I describe experiments in which the pH within individual non-WPB organelles was determined using EGFP fused to t-PA. A morphological pulse chase experiment was carried out to determine the intra-granule pH at different times post Nucleofection and the data is compared to those previously determined for the WPB [1]. The data shows that the distribution of pH in the non-WPB organelle differs from that for WPBs in that there is no time-dependent acidification, characteristic of the maturation of regulated secretory granules. However, the changes in florescence seen on fusion of the non-WPB organelles can be used in the same way as for WPB-targeted GFP to mark the point of fusion of these organelles for kinetic studies (see chapter 5). s

3.2 Methods and Results

3.2.1 Targeted expression of EGFP or mEGFP to WPBs in living cultured HUVEC

WPBs in living cells were fluorescently labelled by Nucleofection™ with C-terminal fusion proteins of full length vWF or the vWF pro-polypeptide (Proregion) fused to EGFP [35] or mEGFP [591] (2.1.2). Figure 3.4 A and B show examples of HUVEC expressing proregion-EGFP or proregion-mEGFP counter stained with an antibody for vWF, an endogenous WPB marker. Some ER staining is also apparent. The red arrow in Figure 3.4B points to an example of a WPB that is not labelled with EGFP. During trypsinisation of HUVEC, a procedure carried out prior to Nucleofection, many, but not all WPBs are secreted [646, 647]. The non-fluorescent WPBs seen in cells expressing the fluorescent constructs most likely represent the small population of granules not released during the trypsinisation and Nucleofection process. These comprised ~22.2±16.1% of the total WPBs present in Nucleofected cells 24-48hours post Nucleofection [1].

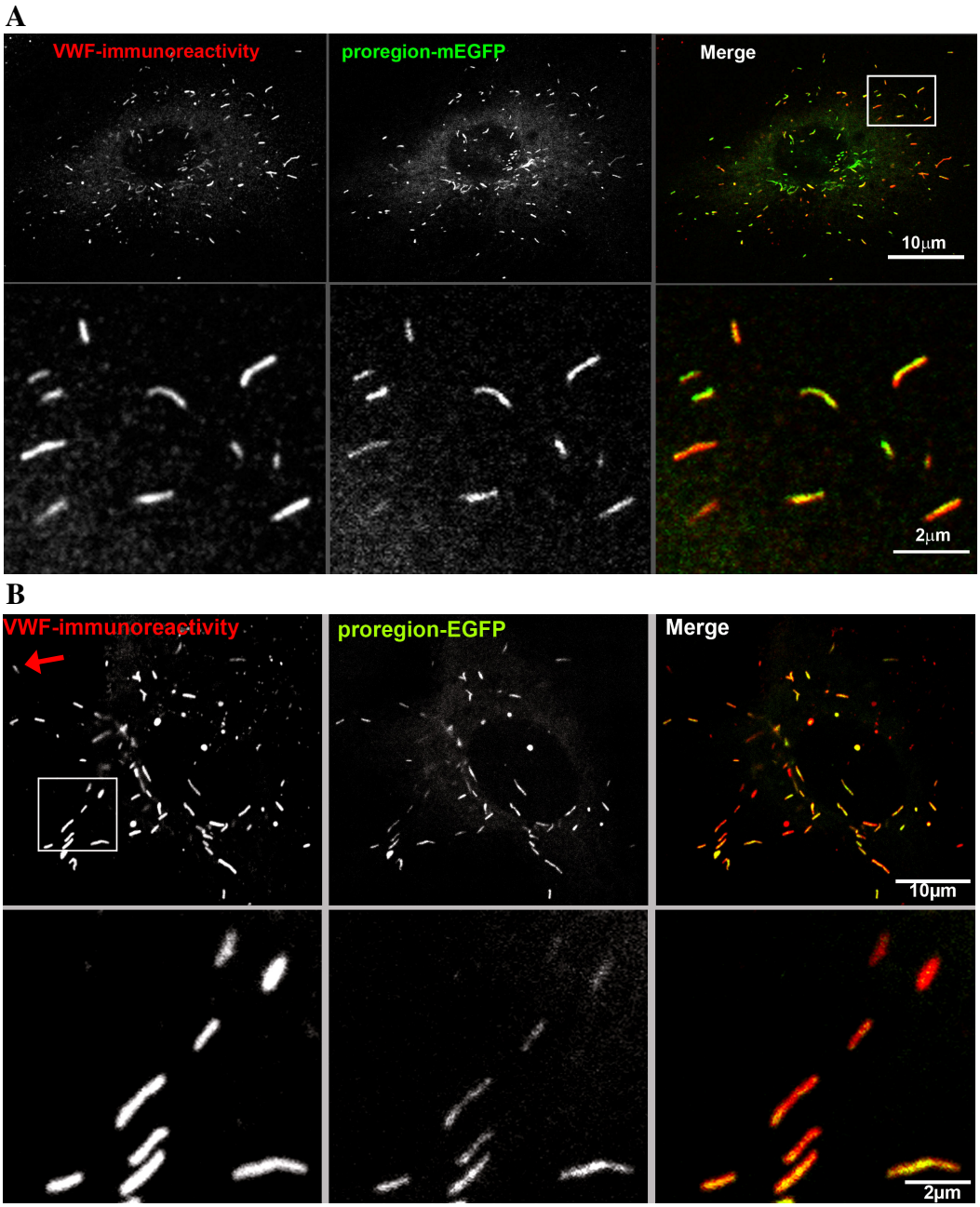

Figure 3.4 Expression of proregion-mEGFP and proregion-EGFP fluorescently label WPBs in cultured HUVEC

A *and* ***B*** *show endogenously expressed vWF (left panel), proregion-mEGFP (A) and proregion-EGFP (B) (middle panels), and merge images (right panel). The merge images confirm that the constructs when expressed in HUVEC by Nucleofection specifically label the WPB population of granules. The red arrow in B top left panel points to a WPB that is not expressing proregion-EGFP.*

3.2.2 EGFP Labelling of the non-WPB Organelle in cultured HUVEC

To fluorescently mark the non-WPB specifically requires a secreted protein exclusively sorted to this organelle and not the WPB. One possible candidate protein is the chemokine GRO-α [92]. GRO-α of the CXC chemokine family, is a small heparin-binding cytokine [648] that is not expressed to any extent in resting cells but can be up-regulated in HUVEC under inflammatory conditions such as following exposure to IL-1β or TNF-α [649]. Expression of EGFP-GRO-α in HUVEC led to specific labelling of the non-WPB (Figure I in supplementary material), however, there were potential problems associated with the use of this molecule in these studies. Following secretion from EC GRO-α can act in an autocrine or paracrine fashion via the G-protein coupled receptor CXCR2 on the cell surface of activated endothelial cells [650]. GRO-α activates CXCR2 by its recognition sequence Glu-Leu-Arg [651]. The consequence of activation of this receptor is activation of Rac, a small G protein, which regulates the formation of polymerized actin and leads to endothelial cell retraction and gap formation [652]. Moreover released GRO-α from EC is thought to bind to the surface of EC via the heparan sulphate proteoglycans where it serves to bind and/or activate monocyte adhesion to the EC surface [649, 653]. Over-expression of such a molecule could lead to the endothelial cells becoming 'activated'. This would make direct comparisons with 'non-activated' proregion-EGFP expressing cells potentially more complex. Ideally a molecule that is normally expressed in resting cells and therefore less likely to perturb the resting state of the cells would be preferable. For this purpose we decided to use t-PA that is expressed under resting conditions in HUVEC [76].

Expression of t-PA-EGFP in cultured HUVEC rapidly labels the non-WPB organelle (4hours post Nucleofection). Although t-PA is expressed in non-WPB organelles, it can also sometimes appear in WPBs [81], particularly at longer times following over-expression [70]; at ~24hours post-Nucleofection a small population of t-PA-containing WPBs can sometimes be seen (e.g. Figure 3.5 red arrow). Experiments were carried out both at 4hour post Nucleofection at which time no WPBs were t-PA-EGFP positive and at 18-28hour post Nucleofection. Therefore we had to develop a method for differentiating between the major population of small non-WPB granules and a variable but small number of WPBs labelled with t-PA-EGFP. WPBs that were morphologically distinctive could be readily identified and excluded from analysis, however, the distribution of sizes of vWF positive secretory organelles includes small almost spherical structures (<0.5μm diameter) [1] that were much more difficult to distinguish from the small organelles simply based on their morphology. To unequivocally distinguish these small 'WPBs' from the small non-WPB organelles, HUVEC were co-nucleofected with t-PA-EGFP and proregion-mRFP [590], the latter of which specifically targets all newly formed WPBs irrespective of their size or shape. Figure 3.5 shows a single HUVEC co-expressing t-PA-EGFP and proregion-mRFP and counter stained with an antibody to endogenous vWF. The Figure shows that endogenous vWF positive structures contain expressed proregion-mRFP, and although occasionally they might also contain t-PA-EGFP (arrow), the presence of proregion-mRFP allowed their identification as part of the WPB population.

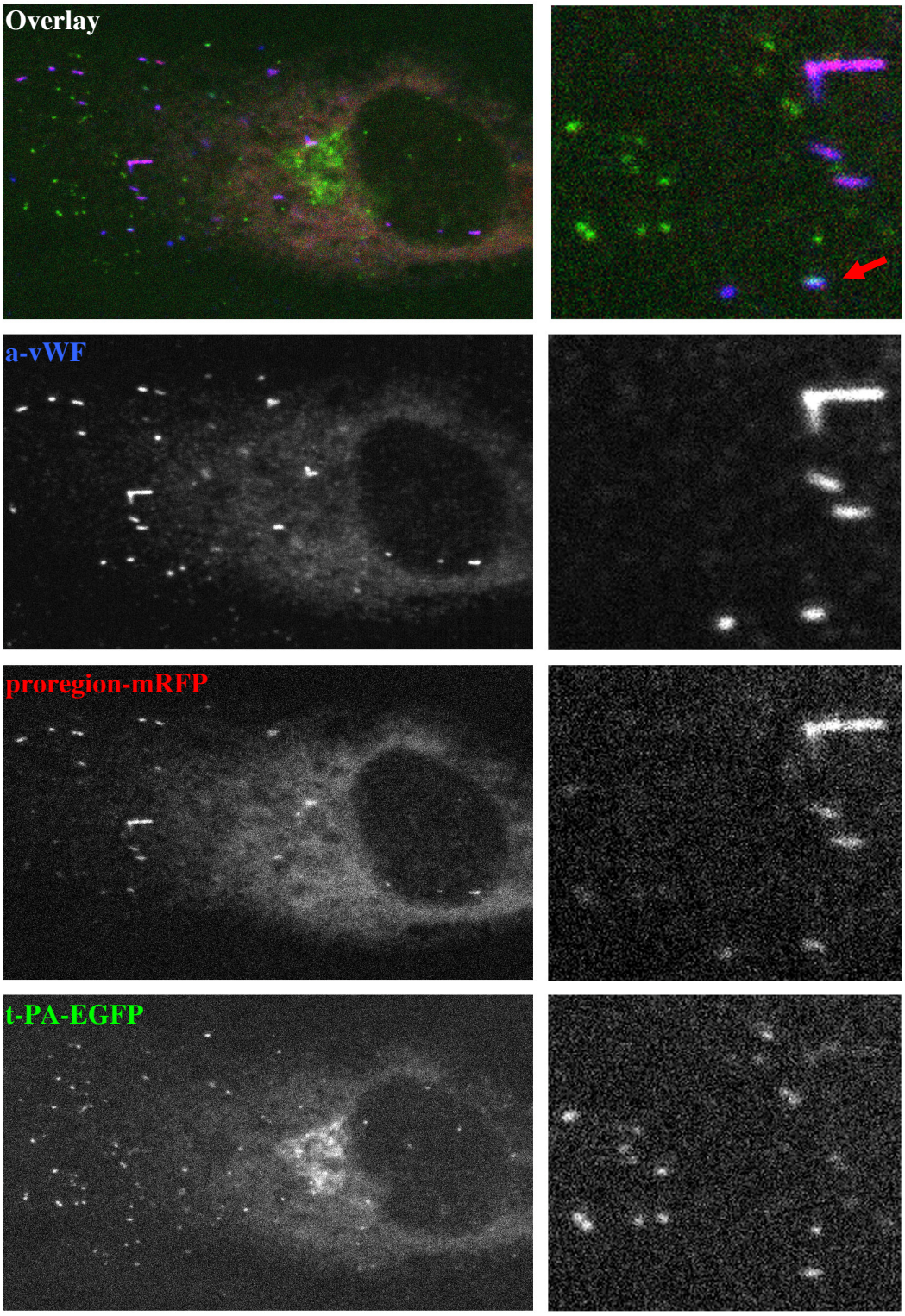

Figure 3.5 Co-expression of t-PA-EGFP and proregion-mRFP in single HUVEC stained with an antibody for vWF

From top: overlay of triple imaging, endogenously expressed vWF, proregion-mRFP and t-PA-EGFP. The red arrow points to an example of a small WPB that contains both proregion-mRFP and t-PA-EGFP.

3.2.3 Imaging

For pH measurements of WPBs and non-WPBs the experimental setup is shown in Figure 3.6 A and B respectively. T-PA-EGFP labelled WPBs were excited at 488nm in epifluorescence using an endow GFP bandpass emission filter set (Chroma, Vermont, USA, cat. no. 41017). For dual excitation of t-PA-EGFP and proregion-mRFP co-expressed in HUVEC, cells were imaged by TIRFM excited by the 488nm and 561nm lasers, passed through a custom made EGFP/DsRed filter set with a 400DCLP coating on the reverse side of the diachroic mirror to allow reflection of 355nm and 380nm light from the monochromator onto the cells for simultaneous Fura-2 imaging (Chroma, cat. no. 51019+) (set of experiments used for the kinetic studies of the non-WPB; chapter 5). TIRFM was used as it only excites a thin plane of field providing a better contrast imaging of the non-WPB granules against a high ER fluorescence signal [598, 654].

3.2.4 Determining the intra-granule pH of the non-WPB organelle.

The pH sensitivity of EGFP fluorescence for purified EGFP *in vitro* [628], EGFP alone targeted into cells [345] or when fused to a wide range of different cellular proteins expressed in cells (including vWF and Proregion [1]) is remarkably similar. This led us to think that the pH sensitivity of EGFP fused to t-PA would be essentially the same as EGFP fused to either full length vWF or proregion within the secretory pathway of living HUVEC. To test this hypothesis we made measurements of pH_{WPB} in WPBs expressing t-PA-EGFP (48hours post-nucleofection when t-PA-EGFP positive WPBs can sometimes be found). In this case WPBs were readily identified by their tubular morphology. Using EGFP to

calculate the resting pH within the WPBs requires knowing 1) the resting fluorescence of EGFP in the organelle, 2) the maximum fluorescence of EGFP (obtained at pH≥7.4) and 3) the relationship between EGFP fluorescence and pH. The latter has already been determined and is shown in Figure 3.2A [1]. The resting fluorescence is readily measured by direct imaging of the cells. The maximum fluorescence of EGFP can be determined in several ways; either by addition of an ionophore calibration solution at pH8.0 as previously described [637] or more simply by the addition of a weak base such as ammonium chloride (NH_4Cl) [599] (see methods section 2.2.5). Both the ionophore and NH_4Cl approaches have been used to determine the resting pH in WPBs containing proregion-EGFP and give identical results [1, 435]. Here we used the simpler NH_4Cl pulse methodology (acute application of 5-10mM NH_4Cl, to the cells see methods section 2.2.5) to calculate the pH of the mature WPB containing t-PA-EGFP and compared this data to the previously published values for pH_{WPB} obtained using vWF- or proregion-EGFP [1]. Application of NH_4Cl led to an abrupt increase in WPB t-PA-EGFP fluorescence due to alkalinisation of the granule (Figure 3.7A). The frame marked with a red square indicates application of NH_4Cl. The background subtracted EGFP fluorescence of single WPBs was measured in imageJ and normalised to the peak fluorescence (F_{max}) (Figure 3.7A). From the normalised EGFP fluorescence the pH_{WPB} can be calculated using the equation in Figure 3.7B taking the previously determined values for pK_a (pH at half-maximal fluorescence) and n_H (Hill coefficient) of 5.84 and 0.74 respectively [1]. Figure 3.7C upper and lower panels show histograms of the pH distributions for t-PA-EGFP and proregion-EGFP labelled WPBs respectively. The mean pH_{WPB} determined using EGFP fused to t-PA was identical to that obtained using

proregion-EGFP supporting the idea that the target protein to which EGFP is coupled has little influence on the pH-sensitivity of EGFP itself.

Taking this to be the case the resting pH in the t-PA-EGFP positive non-WPBs was determined at early (4-8hours) and late (18-28hours) time-points post-Nucleofection using the ammonium chloride pulse methodology. At early times the pH in newly formed non-WPBs (pH6.10±0.32; n=89 non-WPBs) was similar to that of the immature WPBs (pH6.16±0.45; n =101WPBs [1]) and corresponds to values close (but slightly lower than) to those determined for the TGN [34, 344-347]. However, at later times, where WPBs are more acidic (pH5.45±0.27 n=303 WPBs [1]), the pH within the non-WPBs organelles was unchanged (pH6.11±0.25; n=52 non-WPBs). Figure 3.8 compares the pH distributions of the WPB and non-WPBs at early and late time-points after Nucleofection of the EGFP-tagged proteins.

A

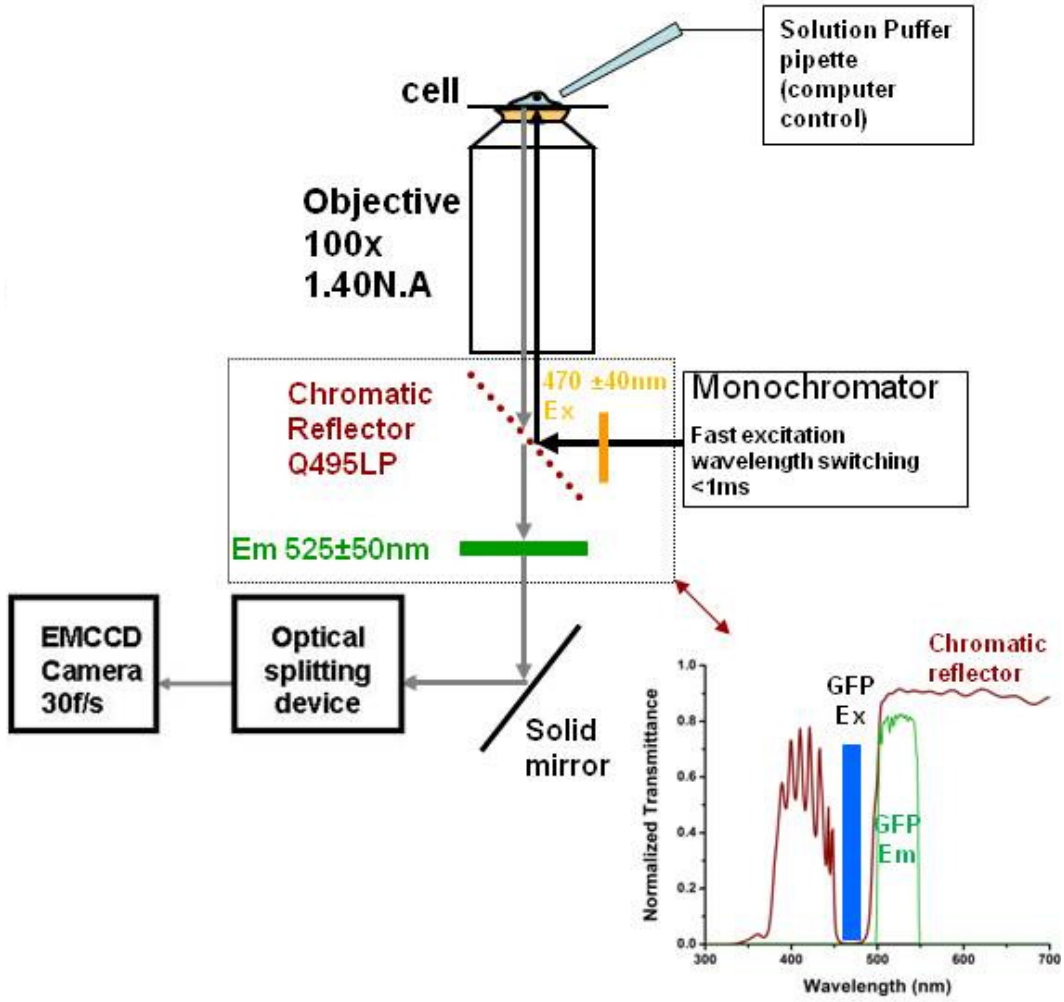
Solution Puffer pipette (computer control)
cell
Objective 100x 1.40N.A
Chromatic Reflector Q495LP
470 ±40nm Ex
Monochromator
Fast excitation wavelength switching <1ms
Em 525±50nm
EMCCD Camera 30f/s
Optical splitting device
Solid mirror
Chromatic reflector
GFP Ex
GFP Em
Normalized Transmittance
Wavelength (nm)

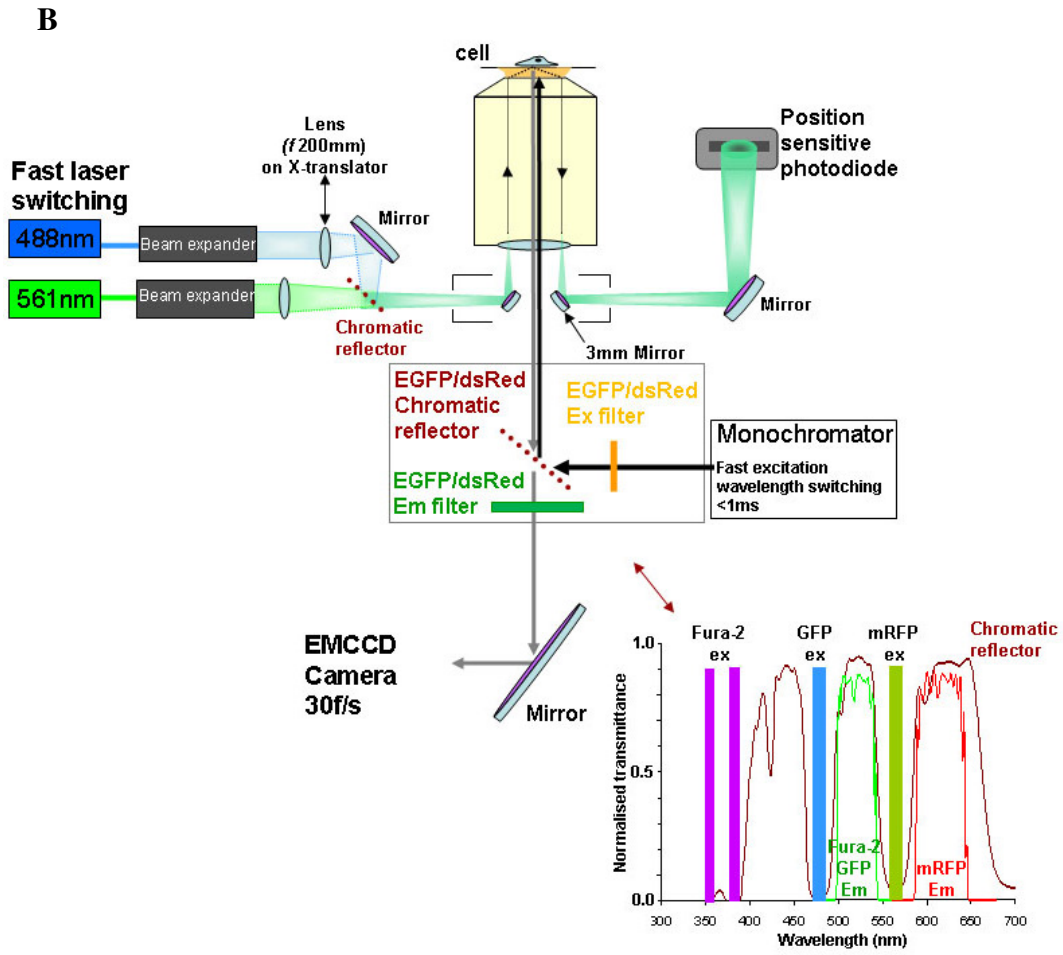

Figure 3.6 Optical arrangements for single granule fluorescent measurements

A. *For single t-PA-EGFP expressing WPB fluorescent measurements an endow GFP bandpass emission filter set was used.*

B. *For HUVEC co-expressing t-PA-EGFP and proregion-mRFP the fluorophores were excited with a 488nm and 561nm lasers in TIRF configuration. The emitted light passed through an EGFP/DsRed filter set with a 400DCLP coating on the reverse side of the diachroic mirror to allow excitation of Fura-2.*

A

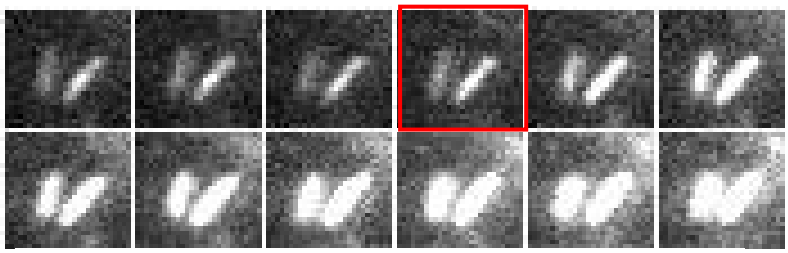

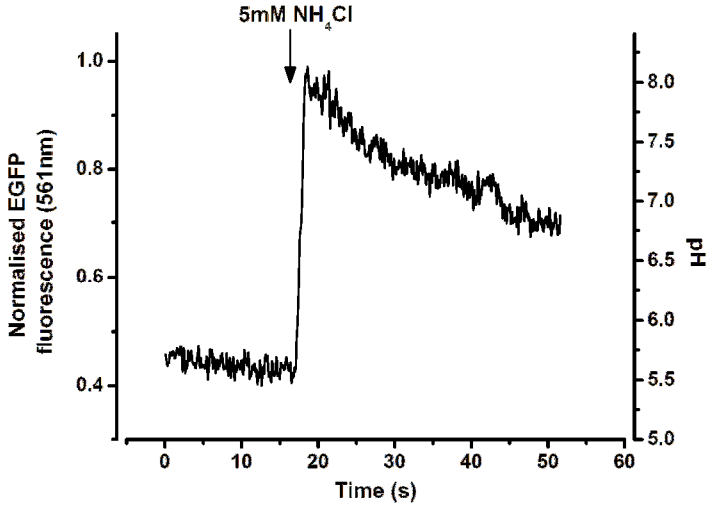

B

$$pH = pKa - \frac{1}{n_H} \cdot \log\left(\frac{F_{\max}}{F} - 1\right)$$

C

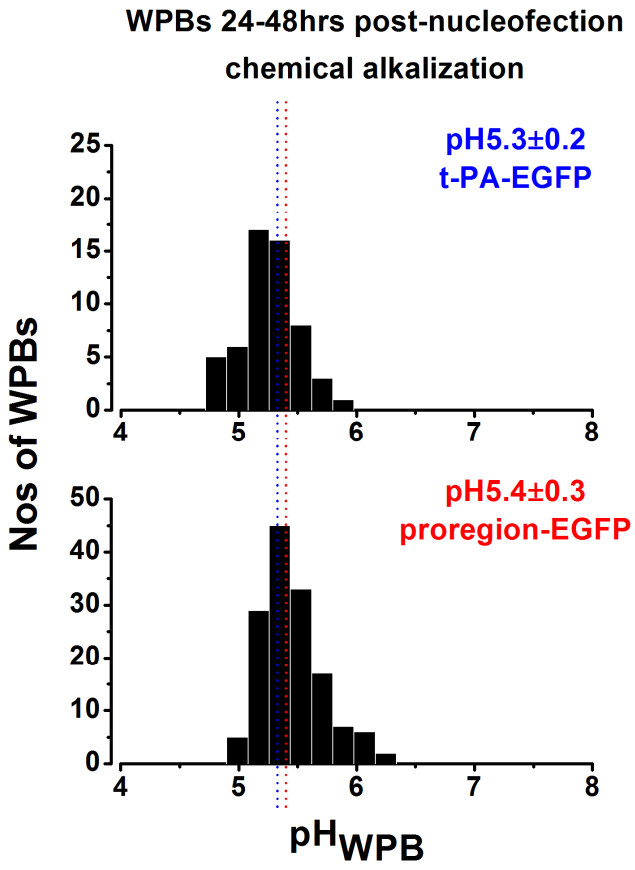

Figure 3.7 Measuring the pH_{WPB} using the NH_4Cl technique

A. *A montage of 2 t-PA-EGFP expressing WPBs 48hours post-Nucleofection subjected to 5mM NH_4Cl as indicated with the red square. The granules were imaged with an endow GFP bandpass emission filter at 33ms a frame and averaged twice. The plot below follows the normalised EGFP fluorescence measurements also plotted on a pH axis.*

B. *The equation used to calculate the pH_{WPB} from the normalised luminal EGFP fluorescence during NH_4Cl addition, such as in **A**. Where pK_a=5.84, n_H=0.74, F_{max}= normalised peak of EGFP fluorescence, F= steady-state normalised EGFP fluorescence.*

C. *The panel shows the pH distributions in Histograms of the mature WPBs at 24-48hours post-Nucleofection with t-PA-EGFP (pH5.27±0.23; n=56WPBs from 10 cells) (top panel) and proregion-EGFP (pH5.45±0.27; n=303 WPBs from 23 cells) (bottom panel).The vertical dotted lines pass through the mean pH of the two histograms and are colour coded. The pH_{WPB} of proregion-EGFP expressing WPBs was pooled from experiments using the chemical alkalization and the secretion method (see Figure 3.9).*

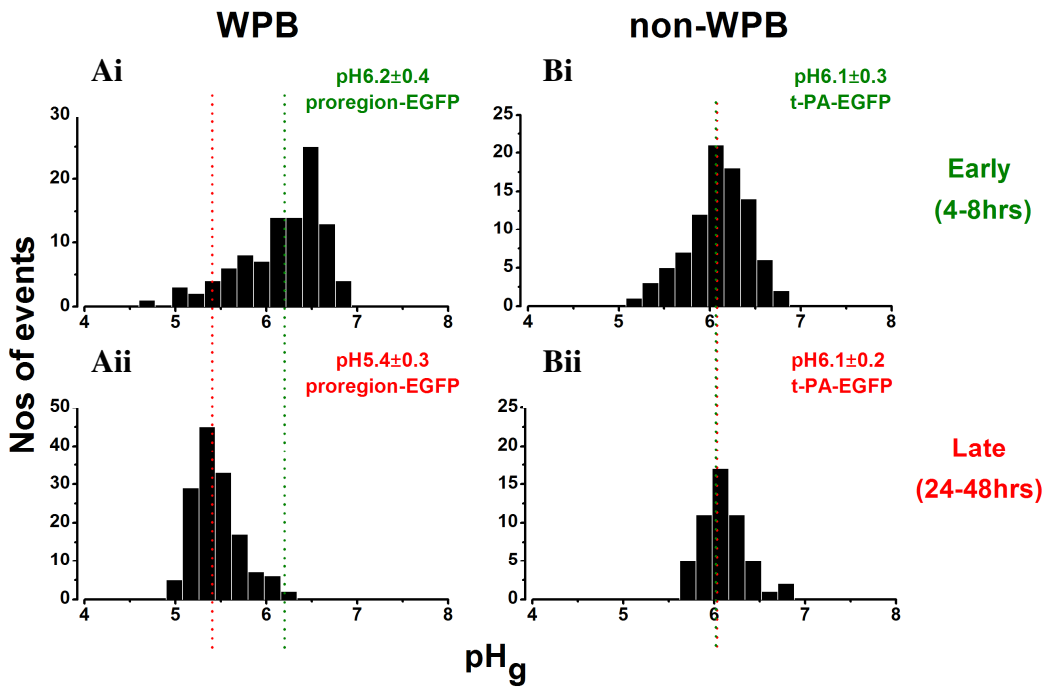

Figure 3.8 pH distributions of the WPB compared to the non-WPB organelle

*Panels show the pH_g distributions of **Ai** the immature WPB pH 6.16±0.45 (n=101 WPBs from 10 cells; mean±s.d.) calculated at 6-7hours post Nucleofection with proregion-EGFP; **Aii** the mature WPB pH5.45±0.27 (n=303 WPBs from 23 cells; mean±s.d.) 24-48hours post Nucleofection; **Bi** the non-WPB organelle 4-8hours post Nucleofection with t-PA-EGFP (distinguished from WPBs by co-expressing proregion-mRFP) pH6.10±0.32 (n=89 granules from 11 cells; mean±s.d.) similar to the pH of the **Bii** 24-28hours non-WPB organelle pH6.11±0.25; (n=52 granules from 4 cells; mean±s.d.).*

3.2.5 Determining the resting $pH_{non\text{-}WPB}$ from fluorescence changes during fusion

In addition to the NH_4Cl pulse methodology (methods 2.2.5) for identifying the $pH_{granule}$, here the Secretion method was also used for calculating the $pH_{non\text{-}WPB}$ as described below. The non-WPB organelle undergoes both unstimulated and stimulated exocytosis (described in detail in chapter 5). Following fusion pore formation in either case there is an increase in EGFP fluorescence that arises because the acidic granule lumen becomes exposed to the extracellular solution (see Figure 3.10B). The extracellular solution is buffered to pH7.4, and the increase in EGFP fluorescence under these conditions is ~97% of that at pH8.0 (where EGFP fluorescence is maximal) [1]. Taking the peak fluorescence change following granule fusion as a close approximation of the maximum fluorescence of EGFP (assuming no loss of EGFP from the granule at the initial point of fusion as is the case for the WPB [435]) we can use the equation in Figure 3.7B to calculate the pre-fusion resting pH within the non-WPB in the same way as described for the WPB (Figure 3.9 top left)[1]. The estimate of the resting pH for the non-WPB organelle obtained from analysis of fusion events (pH6.26±0.40, n=90 non-WPBs from 16 cells), was essentially identical to that obtained by the ammonium chloride pulse technique (pH6.10±0.30; n=141 non-WPBs from 15 cells pooled from Bi and Bii in figure 3.8) (Figure 3.9). The intra-granule pH of the population of non-WPBs undergoing stimulated exocytosis was the same as that for the population of organelles that undergo unstimulated fusion in resting cells (see chapter 5), suggesting they are part of the same population of organelles. In this respect these granules differ substantially from the more acidic mature WPBs [1] (Figure 3.9 left panels).

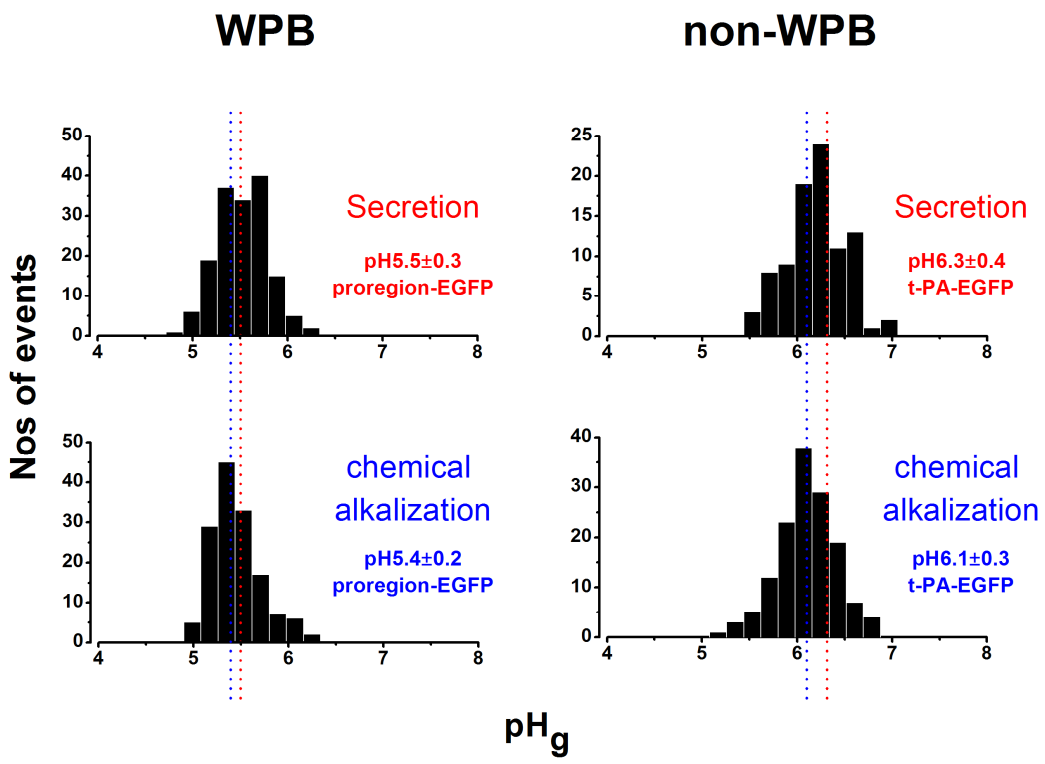

Figure 3.9 The t-PA-EGFP population of non-WPBs undergoing exocytosis differs from the mature WPB population in pH_g

Histogram plots of the pH_g distributions for proregion-EGFP expressing mature WPBs 24-48hours post-Nucleofection (left panels) and t-PA-EGFP expressing non-WPBs 24hours post-Nucleofection (right panels) determined using the Secretion method (described in 3.2.5) (top panels) or the chemical alkalization method with NH_4Cl (described in 2.2.5) (bottom panels). The pH of the two granuls was essentially identical determined with both methods. Top left panel: n=159 WPBs from 15 cells; bottom left panel: n=144 WPB from 8 cells; top right panel: n=90 non-WPBs from 16 cells; bottom right panel: n=141 non-WPBs from 15 cells (pooled from Bi and Bii in figure 3.8).

3.2.6 Determining the point of WPB and non-WPB fusion for kinetic studies

In order to analyse the kinetics of WPB and non-WPB exocytosis, the time for fusion of each exocytotic event needs to be determined as accurately as possible. The characteristic abrupt increase in fluorescence of EGFP/mEGFP labelled granules (producing a flash of light) upon formation of a fusion pore can be utilised as a convenient marker for fusion pore formation during exocytosis. In Figure 3.10 an example of such a WPB fusion event is shown (A) in comparison to that observed for the non-WPB (B). The fluorescence intensity plots are normalised to the peak increase. Qualitatively they are similar; in each case there is an abrupt increase in fluorescence to a peak followed by a decline as the EGFP fusion protein disperses away from the site of fusion; faster for proregion-mEGFP than t-PA-EGFP. The most striking difference between the two organelles is in the smaller magnitude of the fluorescence increase seen with the non-WPB, as illustrated in Figure 3.11. This shows the data in Figure 3.10 superimposed upon one another and aligned to the point of fluorescence increase. The smaller non-WPB fluorescence change upon fusion presumably reflects a smaller difference in the pH gradient between the granule lumen and the extracellular solution.

For the kinetic studies of WPB and non-WPB exocytosis in chapters 4 and 5 respectively, for each fusion event the mean background subtracted fluorescence was measured in ROIs enclosing the whole organelle and the mean fluorescence intensity for the organelle was determined prior to and during the fusion event. The time-point of fusion was taken as the first frame in which an increase (>3*SD of the mean resting fluorescence prior to fusion) in granule-EGFP fluorescence occurred (see Figure 3.10).

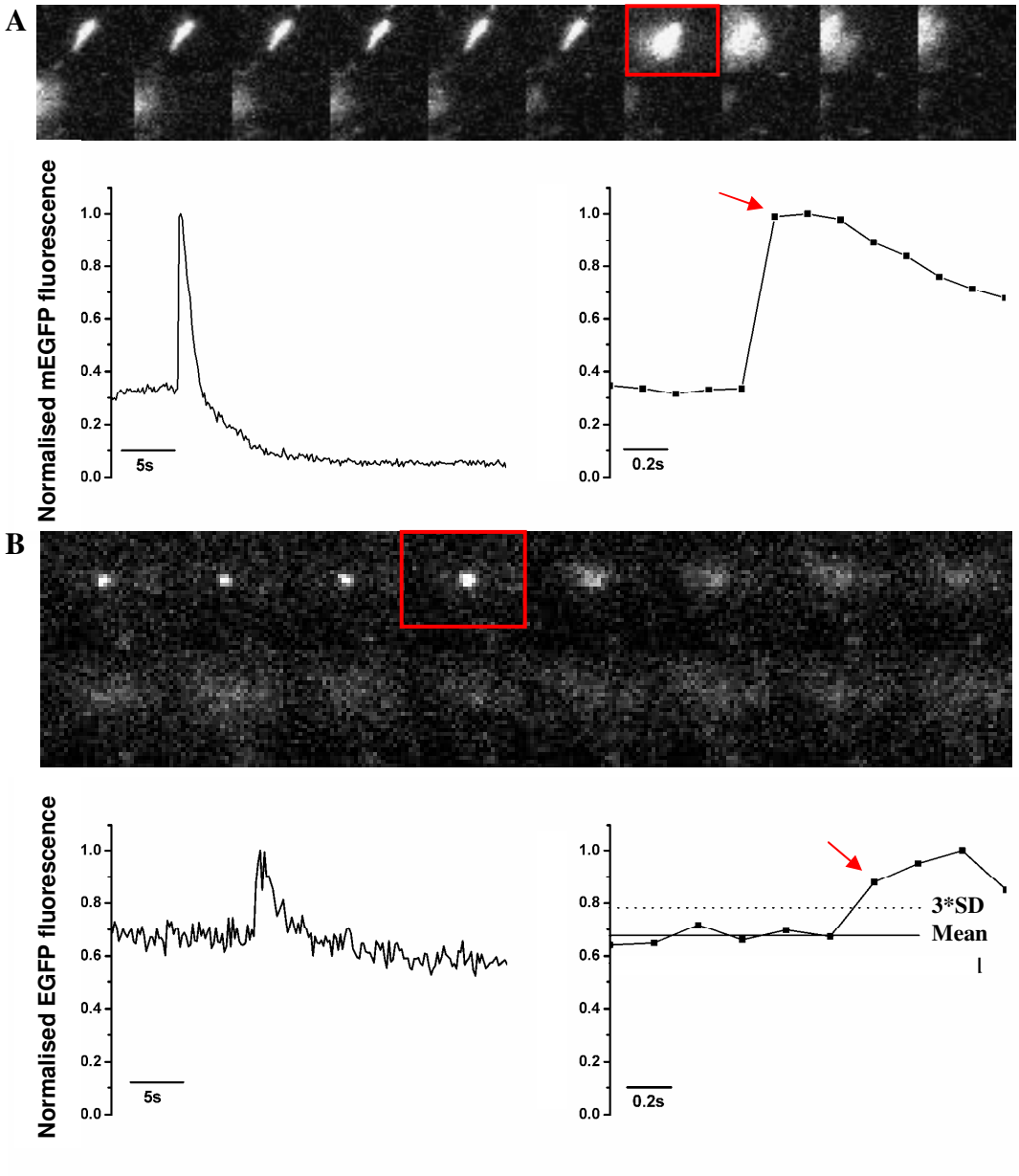
A
Normalised mEGFP fluorescence
1.0
0.8
0.6
0.4
0.2
0.0
5s
0.2s
B
Normalised EGFP fluorescence
3*SD
Mean

Figure 3.10 Determining the time-point of WPB or non-WPB fusion

*The first panel in **A** and **B** is a montage of images of a single proregion-mEGFP (**A**) and t-PA-EGFP (**B**) containing WPB and non-WPB respectively during stimulation with 100μM histamine undergoing exocytosis. The non-WPB fluorescence was smoothed x5 (adjacent averaging) to reduce noise. The example in **A** was imaged by epifluorescence at 6.66frames/s whereas the example in **B** was imaged in TIRFM at 5frames/s. The left panel below the montage in **A** and **B** shows the overall time-course of the normalised EGFP fluorescence change in a ROI around the WPB or non-WBP. The bottom panel on the right, in both **A** and **B,** shows the fluorescence increased on an expanded time-scale. The red arrow indicates the time-point taken as the point of fusion and corresponds to the montage frame marked with a red box. In **B** the mean steady-state fluorescence (solid line) and 3 times the standard deviation (dotted line) are shown to indicate the time-point of fusion is the first time-point above the mean+3*SD of the steady-state fluorescence.*

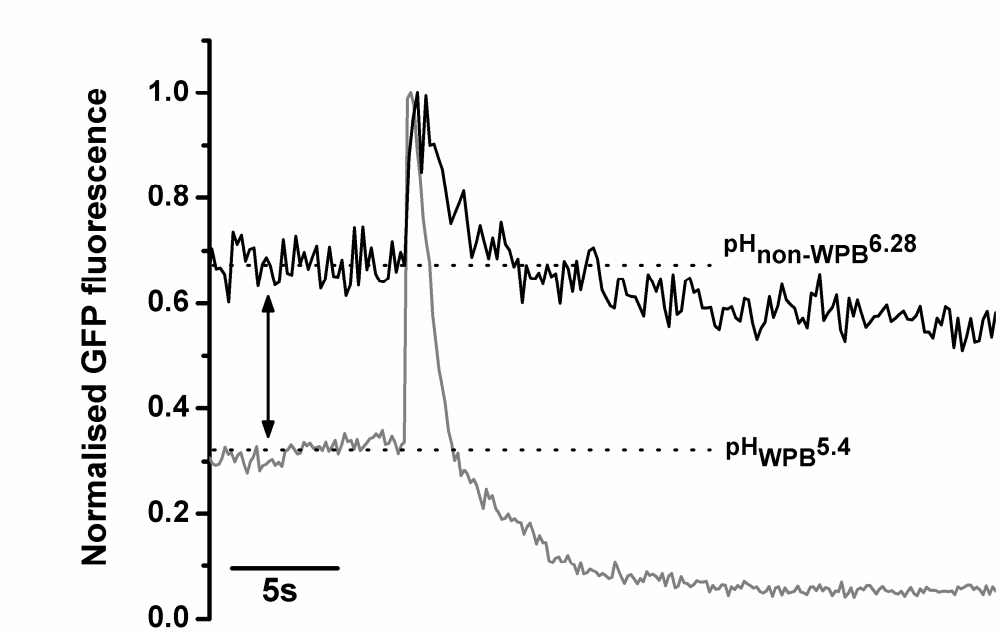

Figure 3.11 Comparison of the EGFP fluorescence between a single WPB and non-WPB organelle upon fusion

The normalised mEGFP fluorescence of a single mature WPB expressing proregion-mEGFP, 48hours post-Nucleofection (grey line) and a single non-WPB organelle expressing t-PA-EGFP, 24hour post-Nucleofection (black line) undergoing exocytosis. The black line was smoothed x5 (adjacent averaging) to reduce noise.

3.3 Discussion

3.3.1 EGFP as an indicator of exocytosis

GFP fusion proteins have been used extensively to investigate vesicular trafficking in the regulated and constitutive secretory pathways [89, 655, 656], exocytosis in neuroendocrine cells [640, 657] and diffusion dynamics of cargo proteins after exocytosis [89, 641, 642]. Data in other cell types [641, 658, 659] and here show that the abrupt increase in intra-organelle EGFP- fluorescence can be attributed to a rise in pH from an initial intra-granule acidic resting level (pH 5.4 for the WPB [1] and pH 6.2 for the non-WPB) to that of the extracellular solution (typically ~pH 7.40) upon formation of a fusion pore. The less acidic pH of non-WPBs gives rise to a smaller increase in intra-EGFP fluorescence upon fusion however this is still adequate for distinguishing exocytotic events.

The increased proregion-mEGFP fluorescence drops down to background levels during exocytosis as proregion diffuses away (Figure 3.10A). Proregion associates non-covalently with mature vWF inside WPB, in a pH dependent fashion [351]. Following exposure to physiological pH upon fusion, this association is lost resulting in the rapid dispersal of proregion from the site of exocytosis [35, 351]. The fusion-induced increase in t-PA-EGFP fluorescence however does not drop immediately after fusion because its dispersal kinetics are slower than for proregion and are dependent on the interaction with plasminogen activator inhibitor-1 (PAI-1) on the EC plasma membrane [89, 641]. During fusion events that don't fully exocytose but maintain an open fusion pore with the plasma membrane [429], the increased EGFP fluorescence upon fusion can be maintained in a plateau [435].

3.3.2 WPB fusion pore formation

The acidic lumen of secretory granules, maintains cargo proteins in a concentrated condensed form for storage [660], however, this packaging structure may hinder exocytosis of cargo proteins. Studies in excitable and non-excitable cells showed de-protonation is required for efficient release of the intra-vesicular contents during exocytosis [638, 661]. An example is the explosive release of mucin seen during epithelial Goblet cell exocytosis (reviewed in [662]). Mucins are a family of glycoproteins evolutionarily related to vWF [663]. Like vWF, Mucins form large molecular weight polyionic chains highly condensed within their storage granule shielded by Ca^{2+} [664, 665]. Upon Mucin granule fusion, cationic shielding is released and water entry results in a rapid swelling and an explosive release of Mucin untangled chains (reviewed in [662]). A similar process is likely to underlie the abrupt disordering of vWF and its subsequent explosive discharge. During WPB exocytosis, an abrupt change in morphology follows the increase in intra-WPB EGFP- fluorescence. Ultrastructural studies show that the major WPB core protein, vWF, is highly organized, forming discrete rod-like structures [24, 32], and the shape change seen is likely to reflect a change in the organization of this protein [35]. Although the nature of the shielding species in the WPB are not known, H^+ and Ca^{2+} are likely candidates.

3.3.3 Granular pH

At early times after Nucleofection the pH in WPBs and non-WPB organelles was similar (~pH6.2) and close to that of the TGN. Newly formed secretory granules are reported to have intra-granule pH close to that of the TGN [334, 343, 633, 634] and the data presented here is consistent with this. In mature

regulated secretory organelles, including the WPB, the pH is more acidic (~5.5) [638, 658, 659]. The acidic environment is thought to contribute to protein aggregation and structural organization of major core proteins, and this seems to be the case for vWF [27, 334]. Protein condensation is optimal at an environmental pH close to the isoelectric point (pI) of the cargo protein [666]. The calculated pI values for mature vWF and proregion are pH5.39 and pH4.99 respectively (predicted using the pI tool at Expasy http://us.expasy.org/tools/pi˙tool.html [1]), indicating that the WPB pH5.5 is optimal for aggregation of these proteins.

While the WPB lumen acidified in a time-dependent fashion ($pH6.2_{immature\ WPB}$ and $pH5.4_{mature\ WPB}$), the $pH_{non\text{-}WPB}$ was found to be identical when analysed at 4-6hours or 24-28hours after Nucleofection with t-PA-EGFP. The most likely reason for this difference is that WPBs are long term storage organelles that are designed to accumulate within the cell and maintain their cargo in a highly condensed state until released in response to stimuli. In contrast the non-WPB organelle is a short lived organelle with a half life of ~15min (T Carter personal communication). Thus at any particular time after Nucleofection the population of small non-WPB organelles represents a 'newly formed population' derived from the TGN. The lack of a time dependent acidification provides a further piece of evidence that the non-WPB population of granules are distinct from WPBs.

In conclusion this chapter demonstrates EGFP-fusion proteins targeted to WPBs or non-WPBs can be used to identify secretory events as 'flashes of light' and can be used to track changes in pH through the secretory pathway of these cells.

4 Concentration-dependence and kinetics of agonist-evoked WPB exocytosis

4.1 Introduction

Until recently the only means available to study WPB exocytosis were biochemical assays (e.g. ELISA or RIA) for soluble cargo molecules, principally vWF [97, 107], or the cell surface WPB membrane protein P-selectin [49]. However, biochemical assays for these secreted proteins suffer from a number of limitations that preclude a detailed analysis of the time-course for WPB exocytosis; vWF adheres strongly to the endothelial cell surface immediately following its release from WPB [35, 351, 446], and hence biochemical assays of soluble vWF are unlikely to reflect accurately the underlying kinetics or extent of WPB exocytosis. Assays based on cell surface P-selectin expression may provide more reliable data on the initial onset of WPB fusion [49], but cannot report the overall time-course or extent of the secretory response, and lack the sensitivity required for precise sub-second kinetic studies. A previous optical study of WPB exocytosis, using WPB targeted vWF-EGFP [128], was limited to a time resolution of about 1min, too slow to resolve the detail of individual fusion events that underlie the secretory time-course. Capacitance measurements may also provide time-resolved data [88] however it is difficult to be certain about the nature of the organelle undergoing exocytosis. Thus so far the underlying kinetics of WPB exocytosis have not been determined accurately.

In this chapter experiments are described in which the relationship between agonist evoked changes in $[Ca^{2+}]_i$, a major trigger for WPB exocytosis, and the onset, frequency and extent of WPB fusion was analysed at high time-resolution in single HUVEC by direct optical observation of individual WPB fusion events. To achieve this, WPBs were specifically labelled by expression of EGFP or mEGFP targeted chimeras of the soluble WPB protein proregion. The time-points

of individual WPB fusion events, identified by abrupt increases in WPB-EGFP fluorescence (flashes of light that arise due to pH changes within the WPB upon fusion- see chapter 3), were obtained from time-lapse movies of EGFP fluorescence in living HUVEC. WPB exocytosis was initiated by the physiological agents histamine or thrombin and the response was compared to a maximal concentration of the non-physiological secretogogue ionomycin, a Ca^{2+} ionophore. Changes in $[Ca^{2+}]_i$ were measured along with EGFP fluorescence with the ratiometric fluorescent Ca^{2+}-binding dye Fura-2 loaded into the cell using its acetoxymethyl ester. The parameters analysed were 1) the delay between agonist arrival at the cell membrane and the onset of the rise in free Ca^{2+}. This reflects the time taken for agonist to couple to intracellular Ca^{2+} release via the synthesis of the second messenger IP_3 [118, 267]. 2) The delay from the Ca^{2+} rise to the onset of WPB exocytosis; this parameter provides information about the coupling (e.g. recruitment to the membrane) between Ca^{2+} increases and WPB fusion [388, 428, 667]. 3) The rates of WPB exocytosis and 4) the extent of WPB degranulation. Prior to optical studies, the targeting of these constructs to WPBs was confirmed (see chapter 3) and the dose-response relation for histamine and thrombin evoked secretion of WPB-targeted EGFP was characterised using biochemical approaches. Together with previous biochemical studies of the dose-dependence of vWF secretion from WPBs [97, 108, 183] allowed the establishment in advance of the agonist concentration ranges needed for the single cell imaging experiments described below.

4.2 Methodology

4.2.1 Epifluorescence imaging of $[Ca^{2+}]_i$ and EGFP

For Fura-2/EGFP imaging Fura-2 was illuminated sequentially with 355±10nm and 380±10nm light and EGFP with 480±20nm light. Excitation light was reflected onto the specimen using a 500DCXRU dichroic mirror (Chroma) and the emitted light passed through a 520±40nm emission filter onto the chip of the EMCCD camera. The setup configuration and an example of a single HUVEC nucleofected with proregion-EGFP and loaded with 2.5μM Fura-2/AM imaged with this optics is shown in Figure 4.1.

4.2.2 Defining the delays of agonist evoked- WPB exocytosis

Single cells were stimulated using a puffer micropipette. Simultaneous time-resolved imaging of Fura-2 and EGFP expressing WPBs allowed for the direct analysis of exocytosis correlated with $[Ca^{2+}]_i$ increases. Delays in exocytosis were resolved into two components. Delay 1 (*D1*) which was due to the delay between drug arrival at the cell (defined as the 50% rise in Alexa-647 fluorescence; 207ms; see methods Figure 2.9) and intracellular Ca^{2+} release from Ca^{2+} stores, and delay 2 (*D2*) between the rise in $[Ca^{2+}]_i$ and WPB exocytosis. A cartoon of delays and the signalling cascades associated with them is shown in Figure 4.2D. Figure 4.2 illustrates an example of the temporal relationship between puffer application (A), the Alexa fluorescence (B), the evoked rise in $[Ca^{2+}]_i$, shown by the Fura-2 fluorescence ratio, and the first event of WPB fusion (C).

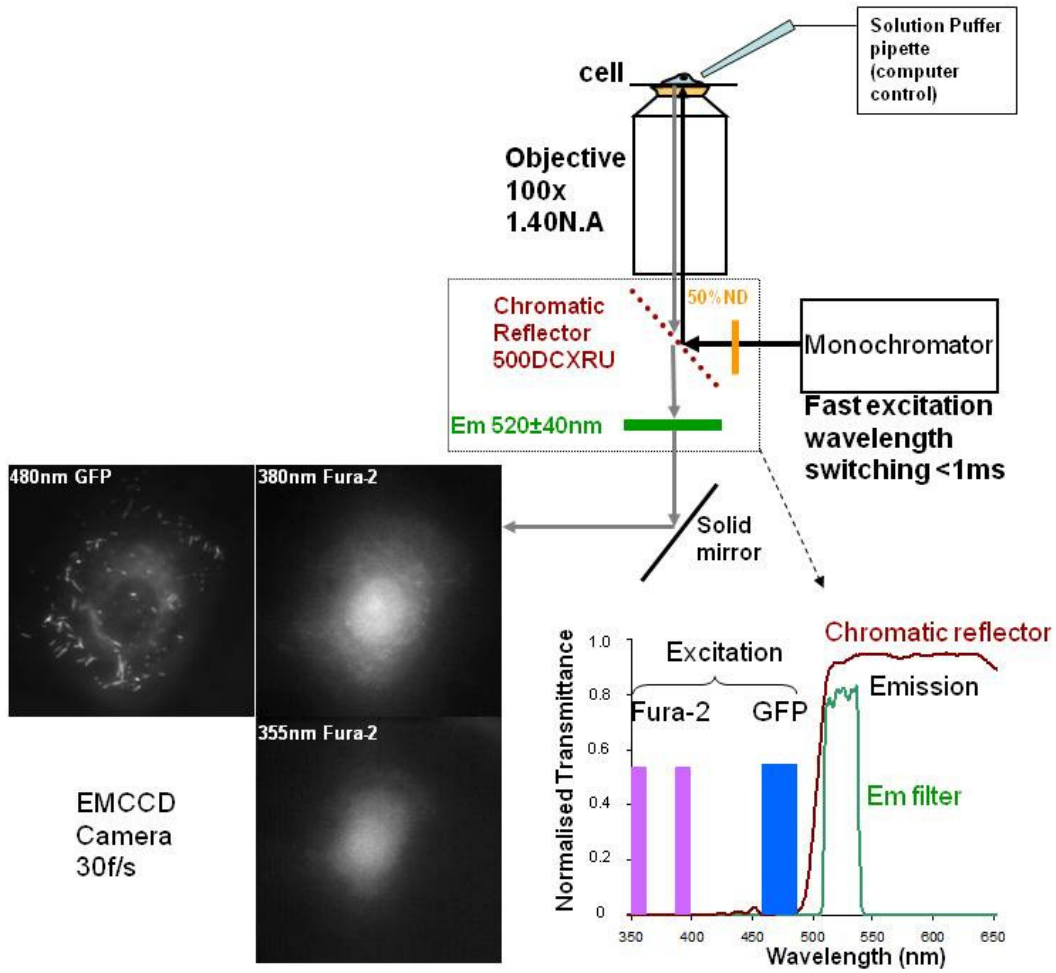

Figure 4.1 Setup schematic for simultaneous imaging of Fura-2 and EGFP.

The excitation light 480±20nm for EGFP and 355±10nm and 380±10nm for Fura-2, was sent from a monochromator source, through a 50% neutral density filter, to a 500DCXRU chromatic reflector to be reflected onto a single HUVEC nucleofected with proregion-EGFP and loaded with 2.5μM Fura-2/AM. The emitted light collected by the objective was passed through a 520±40nm emission filter onto the chip of the EMCCD camera. Each image is a single frame imaged sequentially at 30 frames/s (corresponding to 10 frames/s per wavelength).

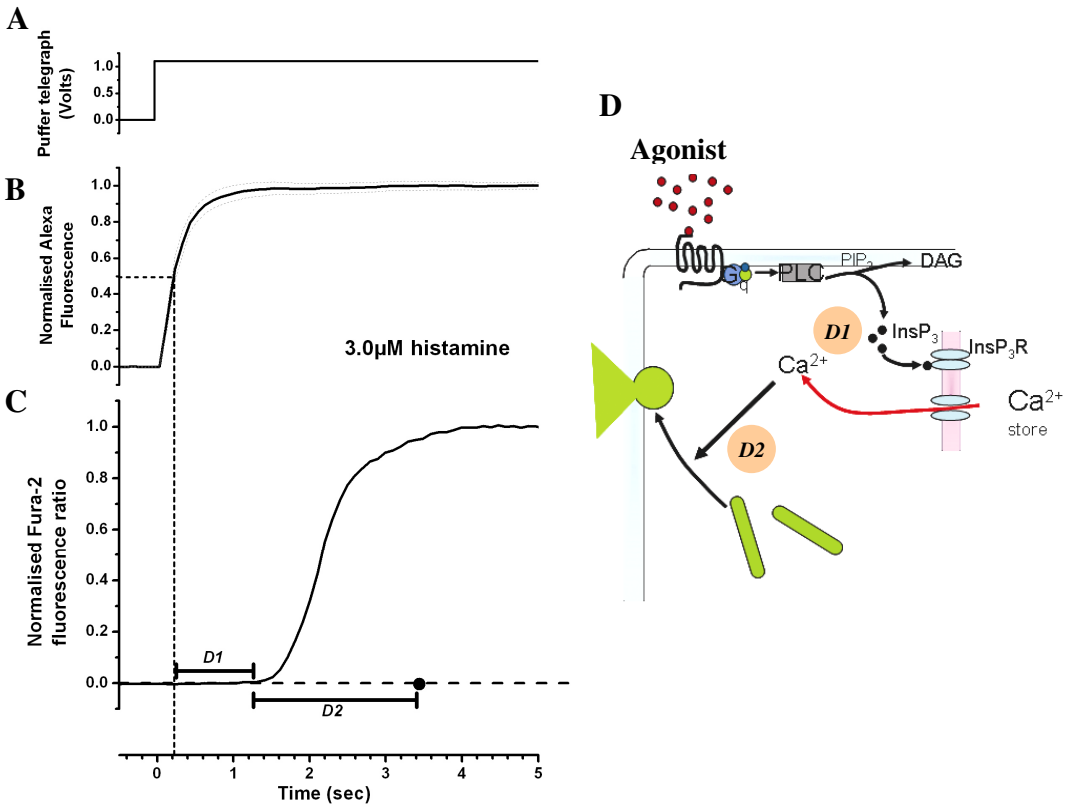

Figure 4.2 Defining the delays in drug arrival, Ca^{2+} rise and exocytosis.

A *Shows the +1V analogue output from the micropipette solution puffer controller that signals activation of the device.* ***B*** *The solid trace represents the mean time-course (normalised to the peak steady-state fluorescence level, n=15 cells) of the fluorescence increase due to Alexa-647 in the puffer solution, in a ROI placed over the cell. Dotted lines represent s.e., of mean. The time of application was taken arbitrarily as the 50% fluorescence rise of the Alexa signal (Vertical dashed line projecting in C).* ***C*** *shows a representative record of the increase in $[Ca^{2+}]_i$ evoked by 3μM histamine (solid trace) and the time for the first fusion event detected in this cell (solid circle). The delay between application and the rise in $[Ca^{2+}]_i$ was defined as D1 and between the rise in $[Ca^{2+}]_i$ and the first WPB fusion event was defined as D2 as indicated by the horizontal bars. A schematic of the signalling cascade taking place from hormone binding to a G-protein coupled receptor to exocytosis is shown in* ***D****.*

4.3 Biochemical detection of agonist-evoked secretion of WPB targeted EGFP

4.3.1 Secretion of WPB targeted EGFP in proregion-EGFP expressing HUVEC

A previous study had shown, using optical approaches, that WPBs containing proregion-EGFP could undergo exocytosis in response to maximal concentrations of histamine and the Ca^{2+} ionophore ionomycin [35]. However, an analysis of the dose-dependence of agonist evoked secretion of WPB-targeted-EGFP had not been carried out. To establish the dose-dependence of exocytosis of EGFP containing WPBs a specific ELISA for GFP that detects the appearance of soluble EGFP immunoreactivity in the media of cells expressing proregion-EGFP was used. Proregion-EGFP was chosen as this rapidly and completely disperses into the media at physiological pH upon WPB exocytosis [35, 351]. Cells were initially stimulated by a range of agonists that elevate $[Ca^{2+}]_i$, (histamine, thrombin, the PAR-2 2f-LIGRLO peptide and ionomycin) using maximally effective concentrations of these different agonists. In each case these agonists strongly evoked the secretion of EGFP immunoreactivity into the cell media (Figure 4.3). The percentage of secreted EGFP from the total EGFP in the cell was 34.28±3.30% for 100μM histamine, 35.85±3.03% for 10U/ml thrombin, 31.35±1.63% for 10μM 2f-LIGRLO and 46.37±5.83% for 1μM ionomycin (n=2 experiments in triplicates; mean±s.d.). The most effective secretogogue was the Ca^{2+} ionophore ionomycin, consistent with previous biochemical studies of WPB exocytosis using ELISAs for endogenous vWF [84].

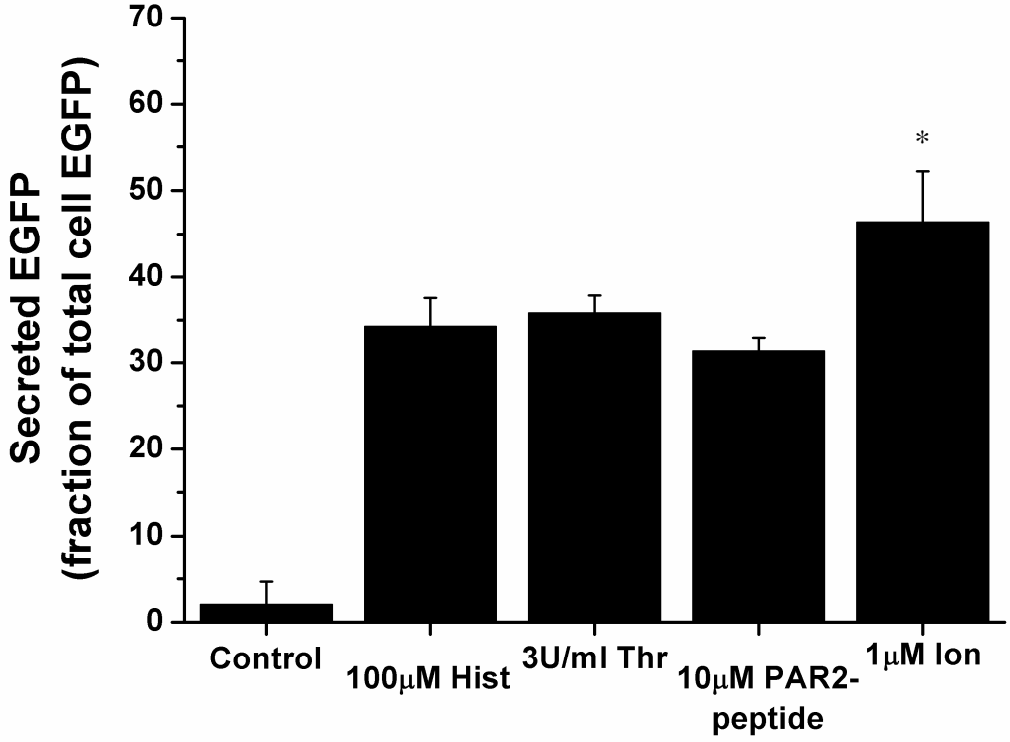

Figure 4.3 ELISA detection of secreted EGFP with maximal agonist concentration stimulation

HUVEC nucleofected with proregion-EGFP were stimulated with maximally effective concentrations of histamine (100μM), thrombin (3U/ml), PAR-2 peptide 2f-LIGRLO *(10μM) and ionomycin (1μM). A one way ANOVA and a Tukey's multiple comparison test showed that histamine, thrombin and PAR-2 peptide stimulation were not significantly different between them however ionomycin stimulation was significantly higher than the other secretagogues (*=P<0.0001).*

4.3.2 Dose-dependence of histamine or thrombin -evoked secretion of WPB targeted EGFP

Next, the dose-response relationship for agonist-evoked secretion of EGFP immunoreactivity was determined for the physiological secretogogues, histamine and thrombin. Histamine is reported to evoke secretion of vWF over the concentration range ~0.5-100μM [97], while thrombin-evoked vWF secretion is reported over the concentration range 0.03U/ml-3U/ml [84, 183]. Figure 4.4 shows that the dose-response relation for histamine (A) and thrombin (B) evoked secretion of EGFP in proregion-EGFP expressing HUVEC was in the same range as previously reported for vWF secretion suggesting the expressed granules behave similarly to the endogenous one. This concentration range was used next in the optical experiments on individual living HUVEC in order to determine more precisely dose-dependent effects of these agonists on the kinetics of WPB exocytosis. The EC_{50} of histamine calculated from the dose response graph is 6.2μM, assuming the maximal response is at 100μM histamine and the EC_{50} of thrombin is 0.09U/ml, assuming the maximal response is at 3U/ml.

4.4 Histamine-evoked WPB exocytosis.

4.4.1 Concentration-dependence of histamine-evoked WPB exocytosis

Using the concentration range determined in biochemical assays the effect of histamine on $[Ca^{2+}]_i$ and WPB exocytosis was determined in single Fura-2 loaded proregion-mEGFP expressing HUVEC. At 0.1μM histamine 12/14 cells studied exhibited a small increase in $[Ca^{2+}]_i$ however no WPB fusion events were detected. At 0.3μM histamine, 21/23 cells responded with an increase in $[Ca^{2+}]_i$, of these 9 cells underwent exocytosis. At concentrations >0.3μM all cells

responded with both an increase in $[Ca^{2+}]_i$ and exocytosis. The increase in Ca^{2+} concentration was dose-dependent, however, absolute quantification of the increases in free Ca^{2+} were not attempted as it had been shown previously that Ca^{2+} signals in HUVEC and other endothelial cells are large and Fura-2 is unlikely to report these changes reliably [267, 668]. Examples of single cells are shown in Figure 4.5A of the histamine-evoked increase in $[Ca^{2+}]_i$ (upper panel) and histograms of the times of WPB fusion, measured from the rise in $[Ca^{2+}]_i$, exposed to either 0.1, 0.3, 1.0, 3.0, 10, 30 or 100µM histamine (lower panel). The overall time-course for the WPB secretory response is summarized in Figure 4.5B, which shows the first latency distributions of WPB fusion events pooled from 15-29 cells in each case exposed to the histamine concentrations indicated.

4.4.2 Delays, rates and extent of histamine-evoked WPB exocytosis

Figure 4.6A shows examples of the $[Ca^{2+}]_i$ traces for each concentration studied on an expanded time-scale to illustrate the dose-dependent delay in rise, offset so that the arrival of histamine at the cell surface at each case occurred at t=0. Figure 4.6B summaries the delays *D1* and *D2* for histamine- evoked WPB exocytosis. At 0.1µM histamine there was a delay between application and the rise in $[Ca^{2+}]_i$ (*D1*) of 5.80±1.2s (s.e., n=12 cells) and at 0.3µM histamine of 2.95s±0.46s (s.e., n=9 cells). *D1* shortened with increase in histamine concentration reducing to 0.46±0.04s (s.e., n=15 cells) at 100µM. The *D2* delay (from $[Ca^{2+}]_i$ rise to onset of exocytosis) was also concentration dependent starting from 9.93±3.90s (s.e., n=9 cells) at 0.3µM histamine and reaching 1.62±0.21s (s.e., n=15 cells) at 100µM histamine.

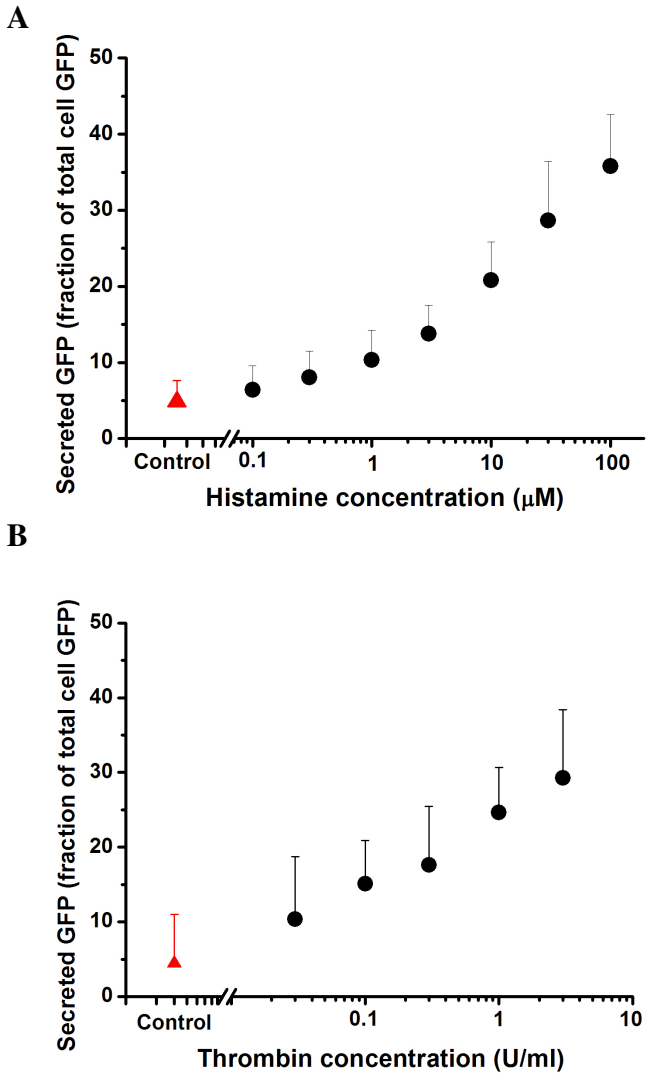

Figure 4.4 Dose response relations for histamine and thrombin evoked secretion of soluble EGFP

HUVEC nucleofected with proregion-EGFP were stimulated with histamine (A) or thrombin (B) at the concentrations indicated. Secreted EGFP in the media was expressed as the percentage of total EGFP. Each point is the mean±s.d. of triplicates from 2 experiments for histamine stimulation and 4 experiments for thrombin stimulation.

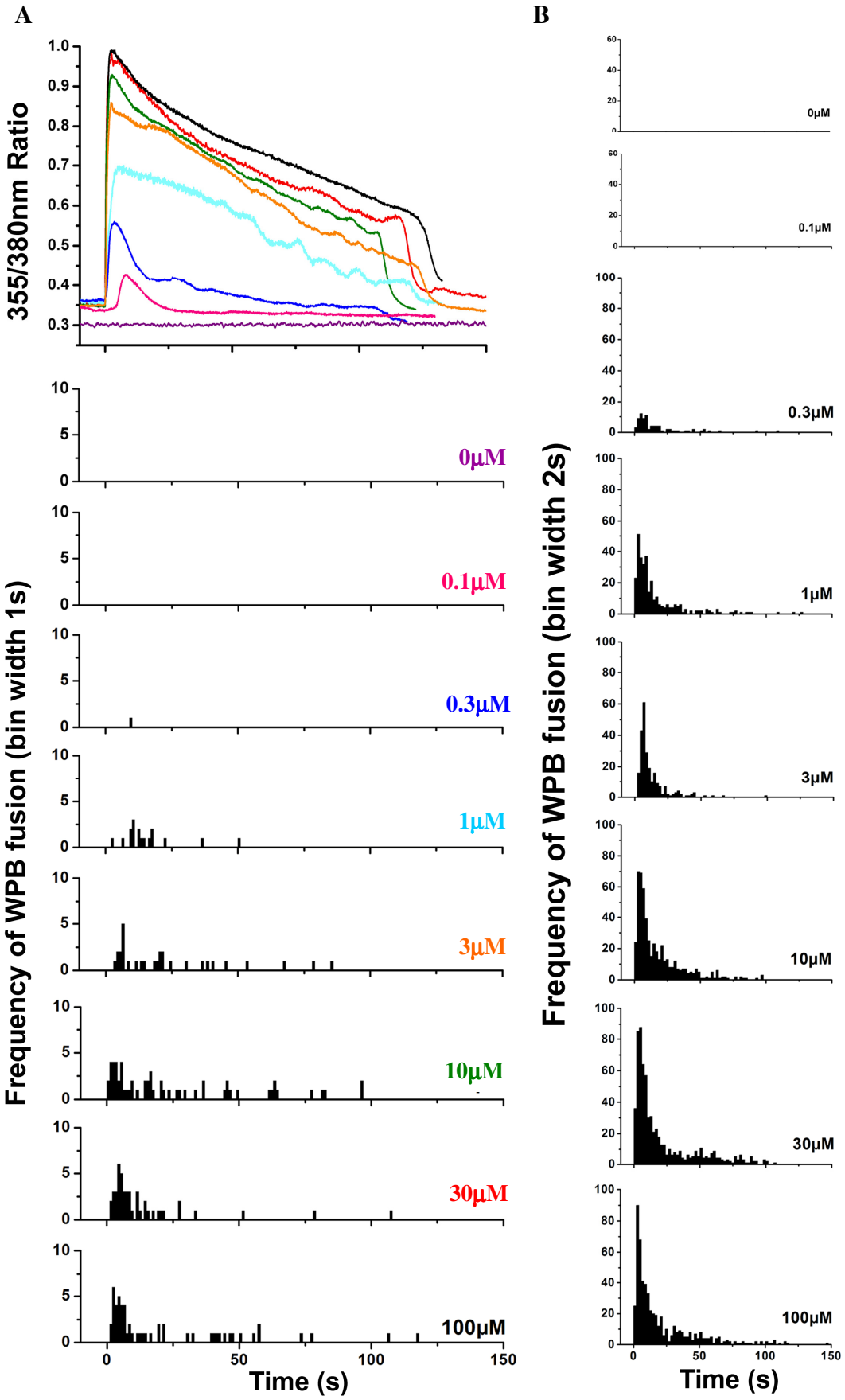
A
B
355/380nm Ratio
Frequency of WPB fusion (bin width 1s)
Frequency of WPB fusion (bin width 2s)
0μM
0.1μM
0.3μM
1μM
3μM
10μM
30μM
100μM
Time (s)

Figure 4.5 Concentration-dependence of histamine-evoked WPB exocytosis

A *(upper panel) shows representative records of the changes in Fura-2 fluorescence-ratio (355nm/380nm) in single HUVEC during stimulation with physiological saline (PS)(purple), 0.1 (pink), 0.3 (blue), 1.0 (cyan), 3.0 (orange), 10 (green), 30 (red) and 100μM (black) histamine. For comparison the Fura-2 traces were offset so that the increase in* $[Ca^{2+}]_i$ *in each case occurred at time=0.* ***A*** *(lower panel) shows the frequency of WPB fusion (bin width 1s) for each of the individual cells in* ***A*** *(upper panel). There was no secretion at PS or 0.1μM histamine stimulation. Panel* ***B*** *Summaries the frequency of WPB fusion (bin width 2s) with time (determined from the rise in* $[Ca^{2+}]_i$*) evoked by PS (n=10 cells), 0.1μM (n=14 cells), 0.3μM (n=9 cells, 81 WPB), 1.0μM (n=20 cells, 313 WPB), 3.0μM (n=18 cells, 244 WPB), 10μM (n=15 cells, 515 WPB), 30μM (n=29 cells, 654 WPB) and 100μM (n=15 cells, 549 WPB) histamine.*

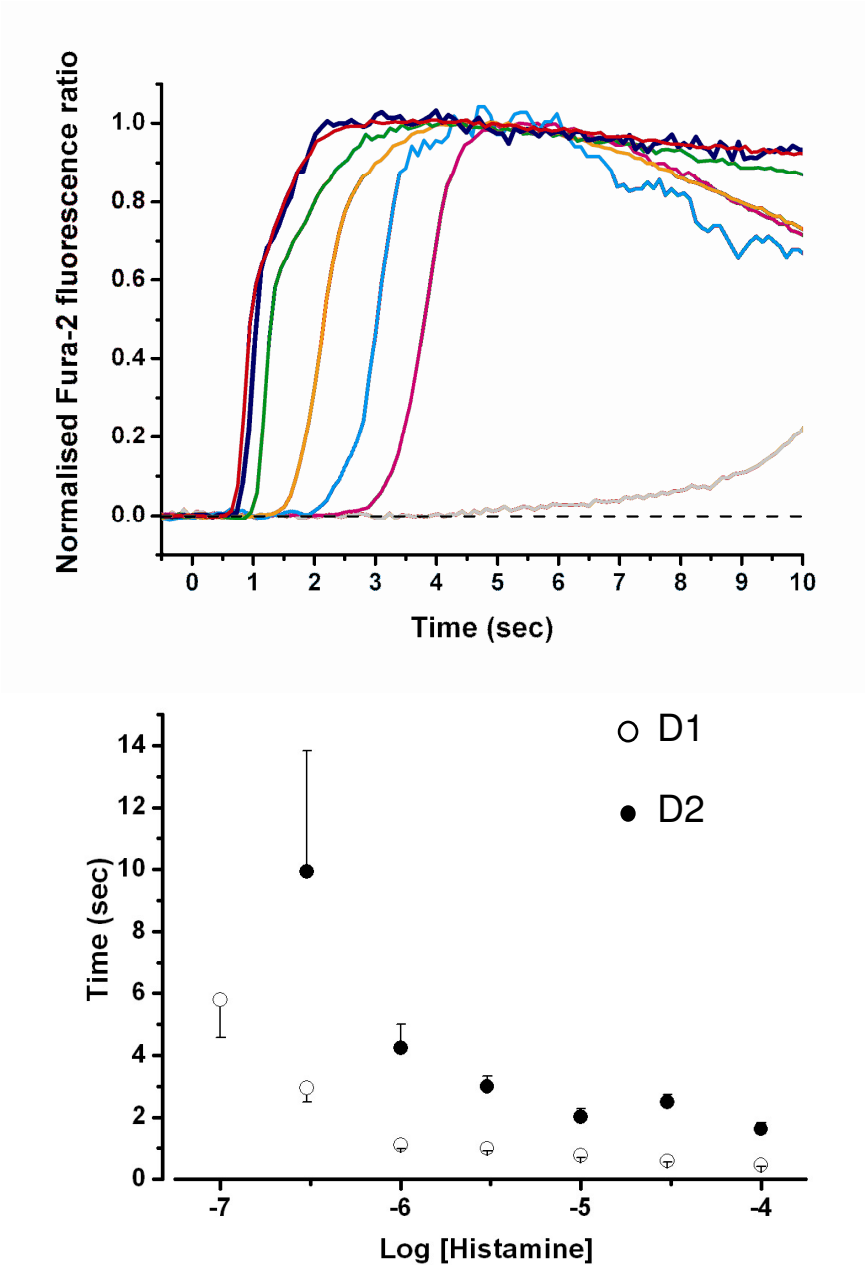

Figure 4.6 Delays of histamine-evoked WPB exocytosis.

A *Examples of the time-course of Fura-2 fluorescence increases evoked by 0.1μM (grey trace), 0.3μM (pink trace), 1.0μM (blue trace), 3.0μM (orange trace), 10μM (green trace), 30μM (black trace) and 100μM (red trace) histamine. Histamine was applied at t=0.* ***B*** *Summarises the delays between histamine arrival at the cell and the rise in* $[Ca^{2+}]_i$ *(D1; open circles) and between the rise in* $[Ca^{2+}]_i$ *and exocytosis (D2; closed circles) over the histamine concentration range indicated. (mean±se; n=9 cells at 0.3μM, and from between 15 to 29 cells at each of the higher concentrations).*

The exocytotic response comprised an initial rapid increase in fusion frequency which reached a maximum between 2 to 5 seconds after the rise in $[Ca^{2+}]_i$ before declining to a lower frequency in the continued presence of histamine. Exocytosis ceased by ~500s. Maximal rates were calculated for cells that secreted more than 6 WPBs by plotting the number of WPB fusion events against the time point of fusion for each cell and taking the steepest slope of the graph as the maximal rate of fusion. The maximal rate of WPB fusion increased from 1.2±0.16 WPB s^{-1} (mean, s.e., n=8 cells) at 0.3µM to 3.66±0.45 WPB s^{-1} (s.e., n=15 cells) at 100µM histamine (Figure 4.7). The highest rate of exocytosis recorded for histamine (30µM) was 12WPB s^{-1}.

The percentage of EGFP-tagged WPBs that exocytosed was analysed in cells exposed to 0.1, 1.0 or 100µM histamine. The extent of histamine-evoked degranulation increased from zero at 0.1µM, to 19.63 ±13.9% (n=20 cells, range 0.6- 50%) at 1.0µM and to 47.8±21.7% (*n*=15 cells, range 7.5-90.0%) at 100µM (Figure 4.8). About 90% of the exocytosed WPBs released their contents within 60s after stimulation.

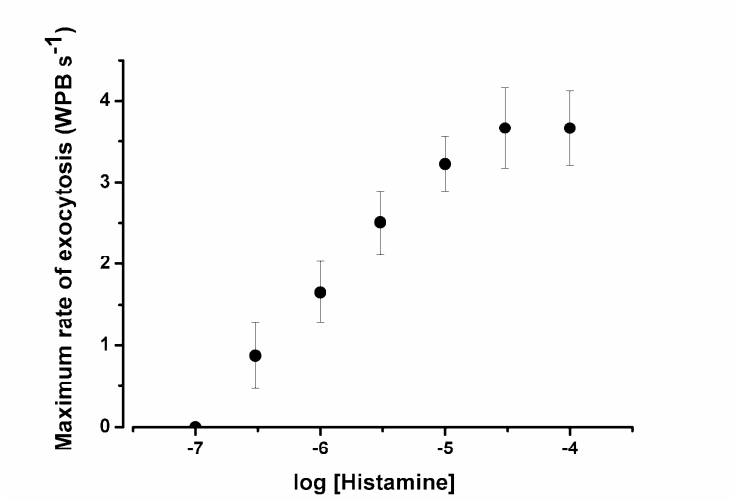

Figure 4.7 Rates of histamine-evoked WPB exocytosis.

Shows the maximal rates of WPB exocytosis for histamine stimulation over the concentration range indicated. The maximal rate at 0.3μM was 0.87±0.40, at 1.0μM 1.65±0.38, at 3.0μM 2.51±1.65, at 10μM 3.22±1.28, at 30μM 3.66±3.00 and at 100μM 3.66±1.76 WPB s^{-1} (mean ±se, n=8 cells at 0.3μM, and from between 15 to 24 cells at each of the higher concentrations).

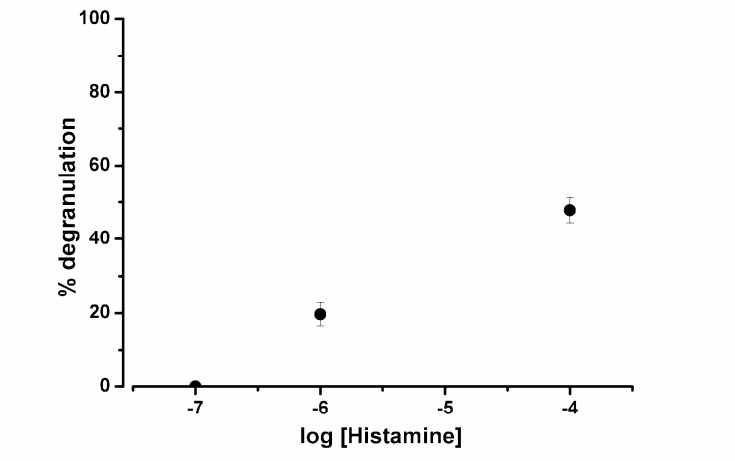

Figure 4.8 Extent of histamine-evoked WPB degranulation.

Summaries of the percentage of the total number of fluorescent WPB that underwent exocytosis in response to histamine at the concentrations indicated. There was no exocytosis at 0.1μM, at 1.0μM there was 19.63±13.9% (n=20 cells, range 0.6- 50%) and at 100μM 47.8±21.7% (n=41 cells, range 7.5-90.0%).

4.5 Thrombin-evoked WPB exocytosis

4.5.1 Concentration-dependence of thrombin-evoked WPB exocytosis.

The extent of secreted EGFP in response to 1U/ml thrombin was not significantly different from that produced by 3U/ml (see Figure 4.4B), suggesting that this was a maximally effective concentration. This was consistent with previously published biochemical data [97]. Therefore the dose range for the optical experiments used was limited to between 0.03 and 1U/ml. Thrombin evoked $[Ca^{2+}]_i$ increases and WPB exocytosis in a dose-dependent manner. Figure 4.9A shows representative $[Ca^{2+}]_i$ traces in single cells stimulated with thrombin concentrations 0.03, 0.3 and 1U/ml (upper panel) and their corresponding histograms of the first latency distributions of WPB fusion events (lower panel). Figure 4.9B shows the histograms of WPB fusion events pooled data for 0.03U/ml (n=5 cells), 0.3U/ml (n=15 cells) and 1U/ml (n=12 cells) thrombin stimulation. At 0.03U/ml thrombin stimulation there was either no $[Ca^{2+}]_i$ change or a small increase and only 5 out of 16 cells analysed responded with secretion. Above that concentration there was both a $[Ca^{2+}]_i$ response and WPB fusion in all cells.

4.5.2 Delays, rates and extent of thrombin-evoked WPB exocytosis

Figure 4.10 summaries the delays in thrombin-evoked WPB exocytosis at the concentrations indicated (mean±s.e.). Thrombin evoked a $[Ca^{2+}]_i$ rise with a delay *D1* of 10.08±4.50s (mean±s.d., n=6 cells) at 0.03U/ml which decreased to 4.18±1.65s (mean±s.d., n=12 cells) at 1U/ml. The longest delay *D2* was seen at 0.03U/ml thrombin, 20.93±10.49s (mean±s.d., n=5 cells) and decreased to a minimum of 5.78±2.639s (mean±s.d., n=12 cells) at 1U/ml stimulation.

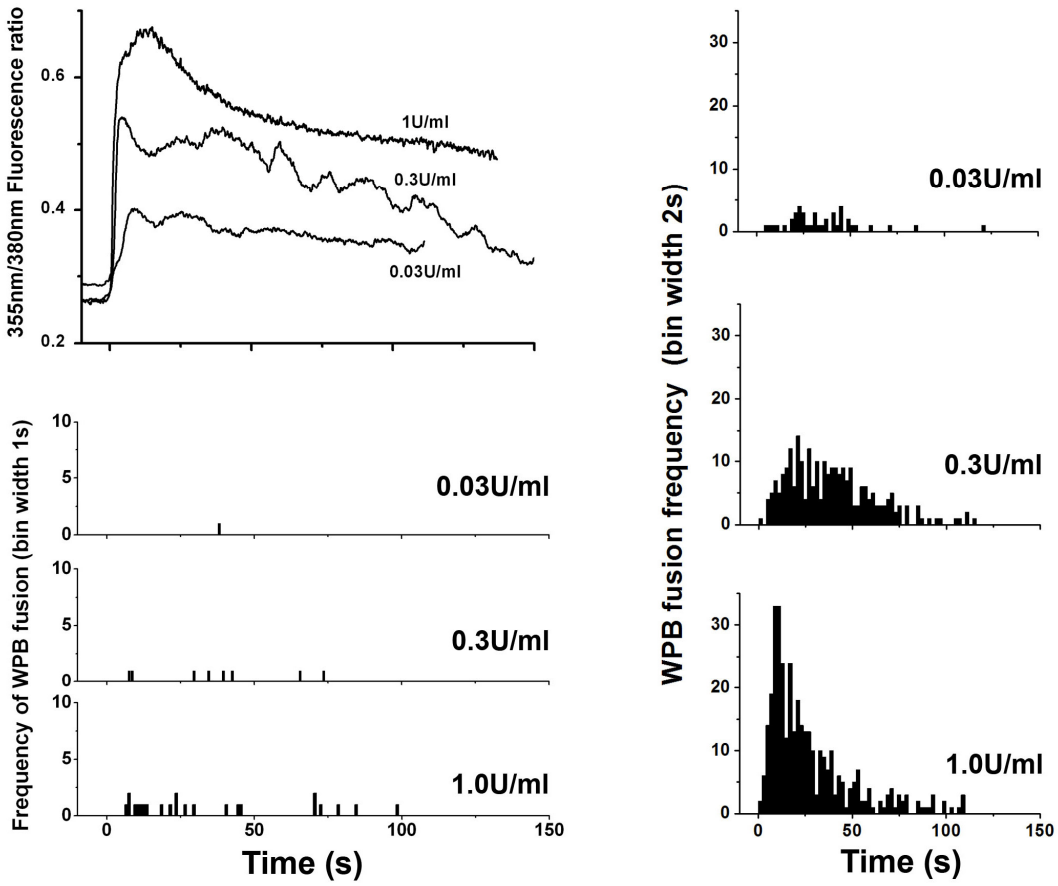

Figure 4.9 Concentration-dependence of thrombin-evoked WPB exocytosis

A *(upper panel) shows representative records of the changes in Fura-2 fluorescence-ratio (355nm/380nm) in single HUVEC during stimulation with 0.03, 0.3 and 1.0U/ml thrombin as indicated. For comparison the Fura-2 traces were offset so that the increase in* $[Ca^{2+}]_i$ *in each case occurred at time=0.* ***A*** *(lower panel) shows the frequency of WPB fusion (bin width 1s) for each of the cells in* ***A*** *(upper panel). Panel* ***B*** *Summaries the frequency of WPB fusion (bin width 2s) with time (determined from the rise in* $[Ca^{2+}]_i$*) evoked by 0.03U/ml (n=5 cells, 42 WPB), 0.3U/ml (n=15 cells, 251 WPB) and 1U/ml (n=12 cells, 362 WPB) Thrombin.*

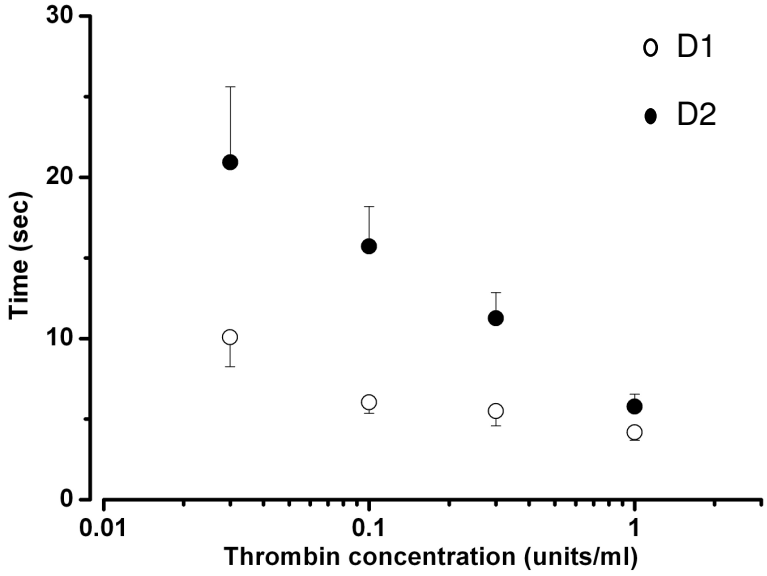

Figure 4.10 Delays of thrombin-evoked WPB exocytosis.

Summaries the delays between application and the rise in $[Ca^{2+}]_i$ (D1; open circles) and between the rise in $[Ca^{2+}]_i$ and exocytosis (D2; closed circles) on a logarithmic scale over the thrombin concentration range indicated. (mean ±se, n=5 cells at 0.03U/ml, n=16 cells at 0.1U/ml, n=15 cells at 0.3U/ml and n=12 cells at 1U/ml).

The gross time-course for the exocytotic response was similar to the histamine response however the initial increase in frequency of fusion was not as high as with histamine. For 0.03U/ml thrombin the maximum rate of WPB fusion was 1.25±0.92WPB s^{-1} (mean±s.d., n=3 cells); for 0.1U/ml 2.27±2.03WPB s^{-1} (mean±s.d., n=13 cells); for 0.3U/ml 1.54±0.88WPB s^{-1} (mean±s.d., n=11 cells) and for 1U/ml 3.64±2.28WPB s^{-1} (mean±s.d., n=11 cells). Data is summarised in Figure 4.11 (mean±s.e.). The highest rate of exocytosis recorded for thrombin was 7.6WPB s^{-1} at 1U/ml.

The percentage of EGFP fluorescent WPBs that underwent exocytosis was determined for thrombin concentrations 0.03, 0.1 and 1U/ml. At 0.03U/ml thrombin there was fusion of 11.96±7.31% of fluorescent WPBs (n=5 cells, range 3.22-21.74%); at 0.1U/ml 18.48±8.50% (n=16 cells, range 4.42-34%) and at 1U/ml 28.97±13.07% (n=12 cells, range 9.10-53.46%) (Figure 4.12).

4.5.3 Comparison of histamine and thrombin evoked WPB fusion

It was found that histamine (100μM) evoked WPB exocytosis with shorter delays than thrombin (1U/ml). Representative examples of Ca^{2+} traces in single cells evoked by 100μM histamine (grey) and 1U/ml thrombin (red) are shown in Figure 4.13A upper panel and the corresponding histograms of fusion events in the lower panel. Figure 4.13B shows the same examples on an expanded time scale, to emphasize the longer delay for thrombin (red trace) compared to histamine (grey trace), measured from puff application (t=0) to the $[Ca^{2+}]_i$ rise (*D1*) (upper panel); and from $[Ca^{2+}]_i$ rise to the first exocytotic event (*D2*) (lower panel).

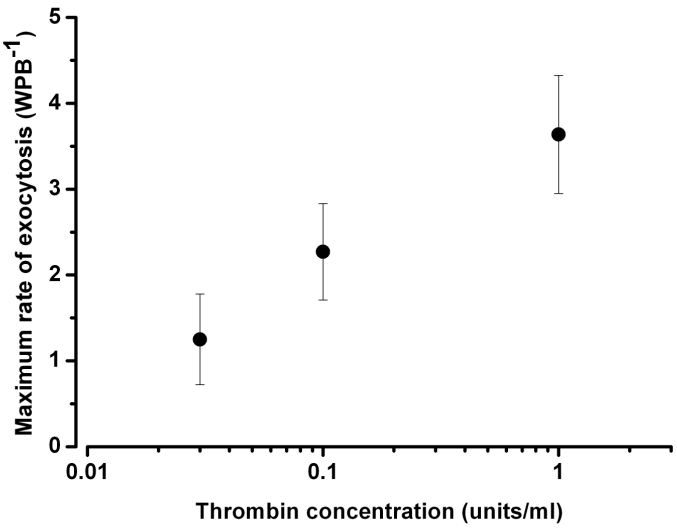

Figure 4.11 Rates of thrombin-evoked WPB exocytosis.

Summaries the maximal rates of WPB exocytosis for thrombin over the concentration range indicated (mean ±se, n=3 cells at 0.03U/ml, n=13 cells at 0.1U/ml and n=11 cells at 1U/ml).

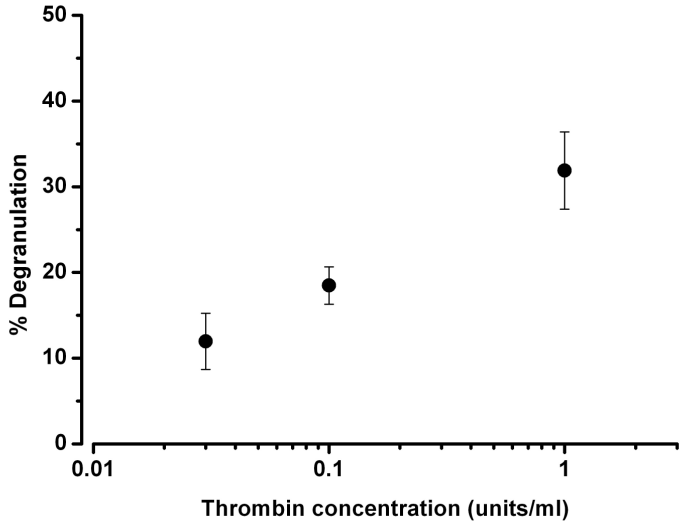

Figure 4.12 Extent of thrombin-evoked WPB degranulation.

Summaries the percentage of the total number of fluorescent WPB that underwent exocytosis in response to thrombin at the concentrations indicated. At 0.03U/ml thrombin there was 11.96±7.31% (n=5 cells, range 3.22-21.74%); at 0.1U/ml 18.48±8.50% (n=16 cells, range 4.42-34%) and at 1U/ml 28.97±13.07% (n=12 cells, range 9.10-53.46%).

A

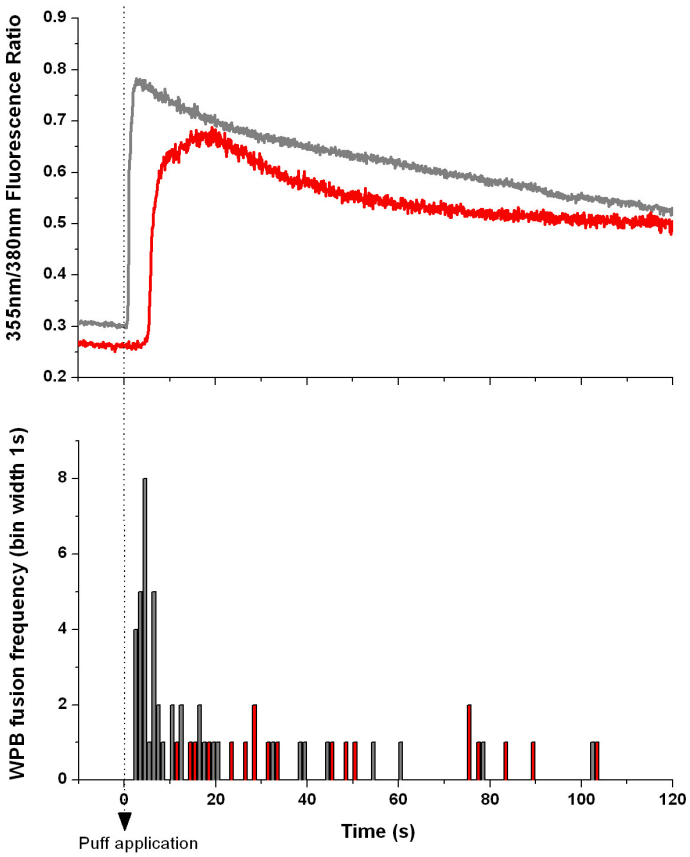
355nm/380nm Fluorescence Ratio
0.9
0.8
0.7
0.6
0.5
0.4
0.3
0.2
WPB fusion frequency (bin width 1s)
8
6
4
2
0
0
20
40
60
80
100
120
Time (s)
Puff application

B

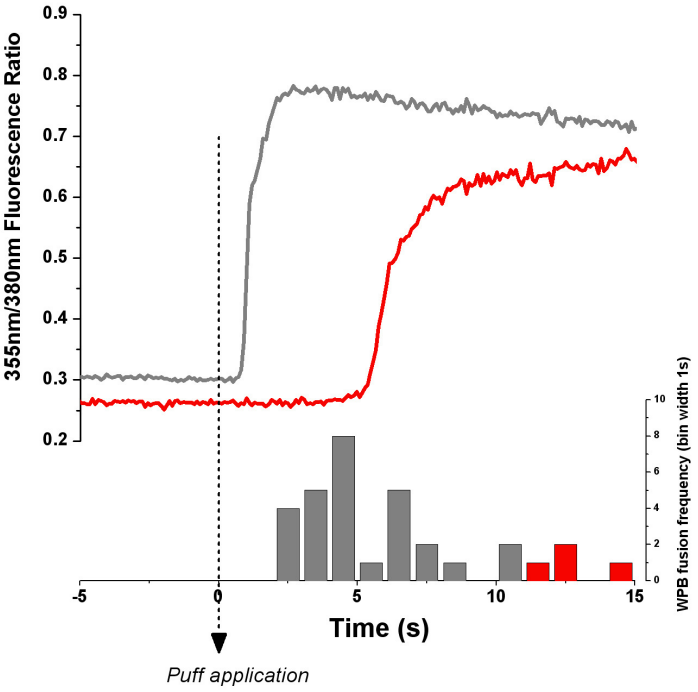
355nm/380nm Fluorescence Ratio
0.9
0.8
0.7
0.6
0.5
0.4
0.3
0.2
WPB fusion frequency (bin width 1s)
10
8
6
4
2
0
-5
0
5
10
15
Time (s)
Puff application

Figure 4.13 Comparison of D1 and D2 in representative single cell examples stimulated with 100μM histamine and 1U/ml thrombin.

A *(upper panel) Overlay of representative records of the changes in Fura-2 fluorescence-ratio (355nm/380nm) in single HUVEC stimulated with 100μM histamine (grey trace) and 1U/ml thrombin (red trace). The Fura-2 traces were offset so that puff application occurred at time=0 (vertical dotted line). The corresponding frequency of fusion events determined from puff application for each cell are shown in the lower panel in a grey histogram for histamine and in a red histogram for thrombin (bin width 1s).* ***B*** *Shows the same graphs as in* ***A*** *on an expanded time-scale to highlight the difference in the time-course of action of the two agonists.The ensembled data of the comparison of the histamine and thrombin- evoked kinetics of WPB exocytosis is shown in figure 4.15.*

4.6 Time-course and extent of ionomycin-evoked WPB exocytosis

Ionomycin is a strong secretogogue known to generate large increases in $[Ca^{2+}]_i$ in HUVEC [206]. Ionomycin (1μM) evoked a large, fast rising and maintained increase in $[Ca^{2+}]_i$ (Figure 4.14A solid trace) with a mean delay *D1* of 0.10±0.10s (n=6 cells) and delay *D2* of 1.67±0.24s (n=6 cells). The frequency of WPB exocytosis in epifluorescence experiments was high during the first 1-3 seconds after the onset of exocytosis with a mean maximal rate of 10.66±6.59 WPB s^{-1} (range 3.0-22 WPB s^{-1}, n=6 cells), before declining over the next 10-20 seconds to a low level that was maintained in the continued presence of ionomycin (Figure 4.14B histogram). In TIRFM experiments the maximal rate (10.01±10.67 WPB s^{-1}, range 0.47-42.50 WPB s^{-1}, n=28 cells) and over-all time-course of exocytosis determined for 1μM ionomycin was not significantly different from that of epifluorescence experiments [1]. TIRFM data showed that ionomycin released on average 66.5±17.6% (n=25 cells, range 16- 94%) of fluorescent WPB, a value significantly higher than that for 100μM histamine (P=0.0006).

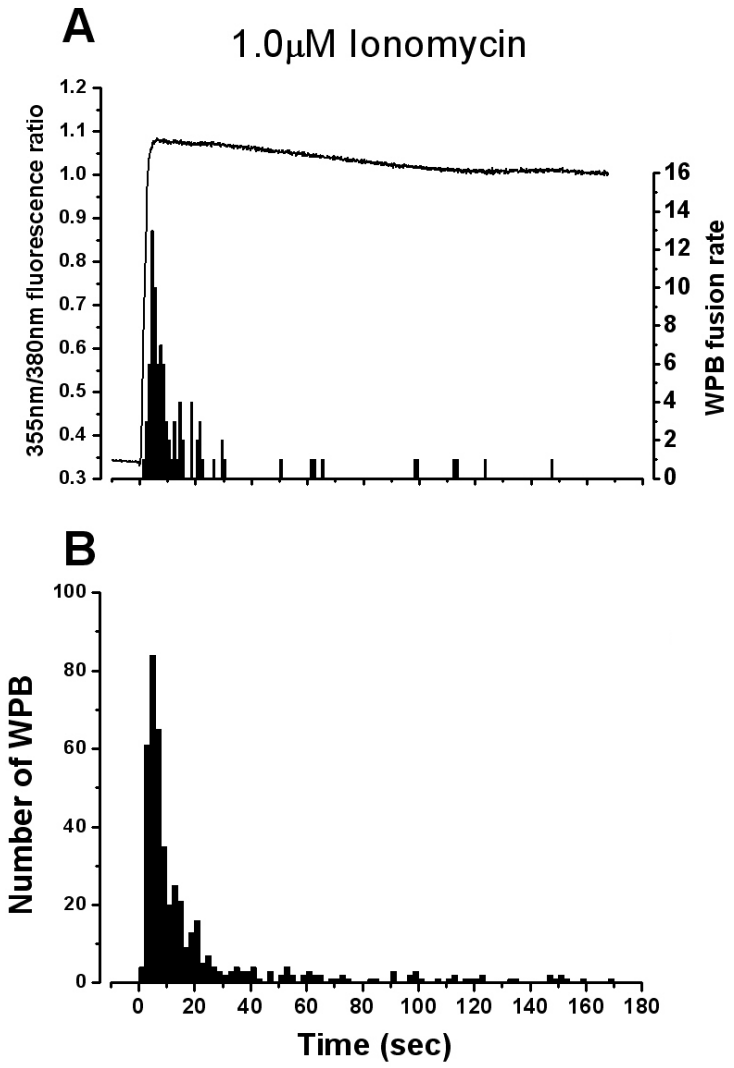

Figure 4.14 Time-course and extent of ionomycin-evoked WPB exocytosis

A *Representative record of a single HUVEC during stimulation with 1μM ionomycin, showing the change in Fura-2 fluorescence-ratio (355nm/380nm) (solid trace) and the frequency of WPB fusion shown as a histogram (bin width 1s); offset so that the increase in* $[Ca^{2+}]_i$ *occurred at time=0..* ***B*** *Summaries the frequency of WPB fusion with time, determined from the rise in* $[Ca^{2+}]_i$ *in 6 cells in the epifluorescence experiments (447 WPB, 1s bin widths).*

4.7 Comparison of secretagogue-evoked WPB exocytosis

Even though thrombin evoked WPB fusion was delayed in onset compared to histamine, the maximal rates of exocytosis were comparable. The Ca^{2+} ionophore Ionomycin is a stronger secretagogue than both histamine and thrombin, driving exocytosis with shorter delays, higher rates, and at higher extent of degranulation. Figure 4.15 summaries the delays *D1* (black) and *D2* (red), maximal rates (blue) and percentage of degranulation (green) in WPB exocytosis between maximal effective concentrations of physiological secretagogues histamine (H) and thrombin (T) and pharmacological secretagogue ionomycin (I).

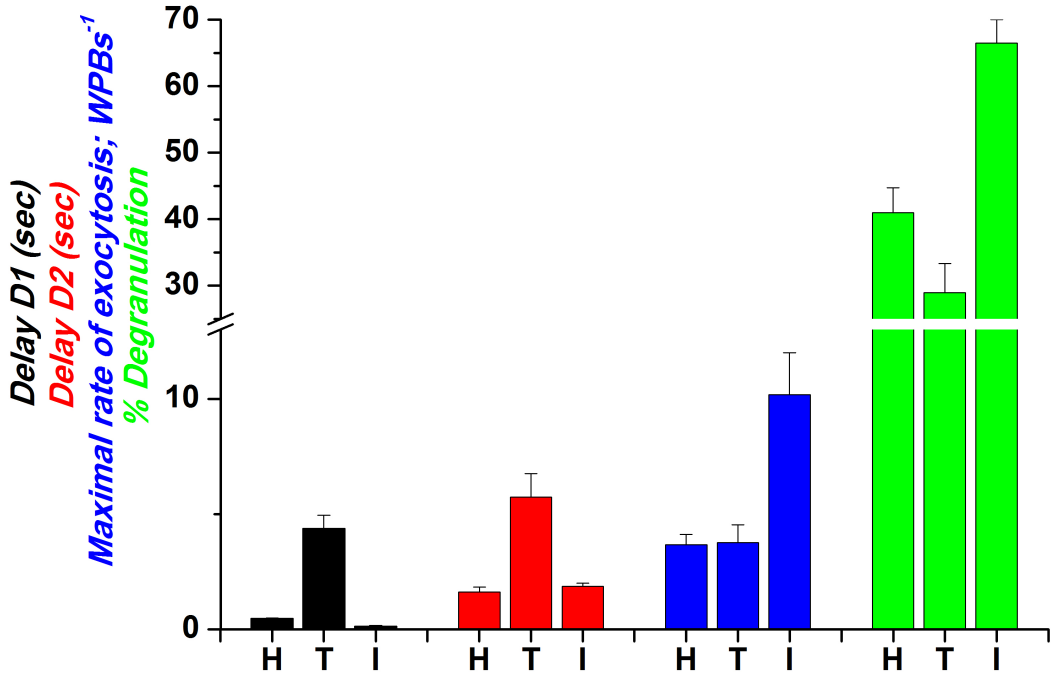

Figure 4.15 Rates, delays and magnitude of WPB release evoked by histamine, thrombin and ionomycin.

Summaries the delays D1 (black bars) and D2 (red bars), maximal rate of WPB exocytosis (blue bars) and extent of degranulation (green bars) for 100μM histamine (H) (n=15 cells), 1U/ml thrombin (T) (n=11-12 cells) and 1μM ionomycin (I) (n=6 cells for D1, D2 *and maximal rates and n=25 cells for % degranulation).*

4.8 Discussion

4.8.1 Biochemical detection of secreted EGFP.

Data from the GFP ELISA illustrates that cultured HUVEC expressing proregion-EGFP respond to stimulation by a range of Ca^{2+}-elevating agonists with EGFP secretion. Secreted EGFP detected during control (unstimulated) conditions was low in the range of 2-5% of total GFP. This is likely to be due to basal secretion, the spontaneous release of regulated granules, or due to fluid shear-stimulated secretion of WPBs during media changes in the experimental protocol [94]. For both histamine and thrombin the secretion of GFP immunoreactivity was dose-dependent, with effective concentrations ranges similar to that previously shown for vWF secretion [97, 108, 183]. We used proregion-EGFP in these pilot experiments because this protein, unlike vWF, does not bind strongly to the cell surface after secretion but rather disperses readily into solution. The efficient delivery of EGFP into solution provided excellent signal to noise in the assay allowing secretion to be clearly observed even with short stimulation times (5min). Does the EGFP ELISA data (Figure 4.3 and 4.4) provide an accurate readout of the extent of WPB degranulation? This is unlikely because proregion-EGFP is found not only in WPBs but also in the ER (the biosynthetic compartment). A better readout would be to assay release of endogenous proregion, as this molecule is found exclusively in the WPB, however, an ELISA assay for this molecule was not available at the time these studies were done.

4.8.2 Evidence for a threshold for Ca^{2+}-driven WPB exocytosis

Optical imaging experiments on single cells showed that in the absence of a rise in Ca^{2+} no WPB exocytosis was observed, even over periods of up to 20min with or without low concentrations of stimulus (0.1μM histamine). With 0.3μM histamine a rise in Ca^{2+} was observed, however, not all cells secreted during these small $[Ca^{2+}]_i$ rises indicating that there is a threshold for Ca^{2+}-driven WPB exocytosis. However, a quantitative analysis of the Ca^{2+}-threshold for WPB exocytosis was not possible with Fura-2 in these experiments as this dye will tend to saturate and therefore not provide reliable data on free $[Ca^{2+}]_i$ during hormone action [668]. Studies using lower affinity Ca^{2+} indicators are needed to directly address such questions. Previous biochemical studies in permeabilised HUVEC have shown that vWF secretion only occurred when $[Ca^{2+}]_i$ was elevated >0.8μM and that secretion increased steeply in the range of 10-20μM free $[Ca^{2+}]_i$ [183, 669] again consistent with a threshold for Ca^{2+}-driven WPB exocytosis. Similar observations were made in studies where secretion was measured as changes in membrane capacitance; 5-20μM $[Ca^{2+}]_i$ was required to evoke exocytosis in HUVEC [88, 103]. Both hormone evoked and direct IP_3-evoked Ca^{2+} release from internal stores can reach between 1 to 30μM free Ca^{2+}, as shown by quantitative Ca^{2+} measurements in endothelial cells from various vessels, using the low affinity Ca^{2+} indicator Furaptra [103, 267, 668] suggesting that this concentration range (>1-30μM) is likely to be physiologically relevant for driving WPB exocytosis, with lower levels ineffective.

4.8.3 Kinetics of agonist evoked-elevations of $[Ca^{2+}]_i$ and WPB exocytosis

4.8.3.1 Delays in agonist evoked WPB exocytosis

The analysis of the time-course of exocytosis shows that there are distinct delays in the secretory process and these can be modified by agonist concentration. The first step involves the coupling of receptor activation into the rise in $[Ca^{2+}]_i$. Here there was a delay (defined as *D1*) that most likely represents a composite of the times taken for agonist binding to the G-protein coupled receptor and the processes that lead to generation of intracellular IP_3, followed by the time taken for IP_3 to induce Ca^{2+} release from the stores (see introduction 1.4 for details of the signalling steps). Flash photolysis studies of caged-IP_3 have identified a minimum delay between IP_3 generation to $[Ca^{2+}]_i$ rise of <10ms in porcine aortic EC [267], <20ms in cerebellar Purkinje neurones [670] and 25ms in Xenopus oocytes [671]. Even low IP_3 concentrations produce Ca^{2+} release on the scale of 100-200ms in endothelial cells [267]. These delays are much shorter than the 0.5s seen here for maximally effective concentrations of histamine suggesting that slow signalling steps upstream of IP_3 action (e.g. coupling between receptor and G-protein, coupling of activated G-protein to PLC and the actions of PLC on PIP_2 to produce IP_3) are likely to be responsible for the majority of the delay seen between agonist application and the rise in $[Ca^{2+}]_i$ evoked by either histamine or thrombin. For both agonists the delays decreased in a concentration dependent fashion to a minimum of 0.5s at 100μM histamine and 4s for 1U/ml thrombin.

The delay between thrombin application and the rise in Ca^{2+} was much longer than that seen for histamine. Both agonists are thought to couple to IP_3 production through activation of PLCβ. As already mentioned most of the delays

at this stage in the signalling cascade are likely to arise from processes up stream of IP_3 generation [672]. Therefore the longer delay with thrombin presumably reflects even slower process at this stage. This could be due to differences in the mechanism of receptor activation between histamine (acting at the HR_1) and thrombin (acting at the PAR-1 receptor). PAR-1 activation requires a proteolytic cleavage of the extracellular amino-terminal domain of the receptor following Thrombin binding [176] unlike the activation of HR_1 by histamine, and this step in PAR-1 activation may contribute to the slightly delayed action of thrombin (see Figure 1.2 and section 1.5 in the introduction) .

Following the rise in Ca^{2+} there was a further delay of several seconds before WPB fusion was observed, (defined here as *D2*). Delays between Ca^{2+} increase and exocytosis have been observed in many other secretory cell types using electrophysiological or optical approaches. Minimum delays evoked by high Ca^{2+} are typically in the range of milliseconds to tens of milliseconds; in astrocytes [673], Chinese hamster ovary fibroblasts [674], chromaffin cells [675, 676], pituitary melanotrophs [677] and in pancreatic β-cells [678, 679]. This data suggests that WPB exocytosis is somewhat slower (minimum delay from Ca^{2+} rise of 1.6s) than vesicle secretion from neuroendocrine cells and this may reflect slow steps in recruiting of the granules to the cell membrane by the cytoskeleton [390]; in the tethering of the large in size WPB to the plasma membrane [428] and perhaps in the Ca^{2+}-sensitivity of the apparatus responsible for these processes and fusion itself. More work is needed to identify the molecular basis for slow steps in WPB exocytosis.

4.8.3.2 Maximal rates in agonist evoked WPB exocytosis

The maximal rate of WPB exocytosis increased with increasing agonist concentration, and was associated with an increase in the $[Ca^{2+}]_i$ signal. The rates of rise and amplitudes of the Fura-2 fluorescence changes versus WPB fusion were not formally analysed due to uncertainties in our ability to interpret the Fura-2 fluorescence changes reliably (due to dye saturation) in terms of free Ca^{2+}. The highest mean rate of exocytosis was ~4 $WPBs^{-1}$ with 30-100μM histamine, but was variable between single cells, not inconsistent with previous findings using capacitance recordings [88]. ~20% of the total WPBs in a cell expressing proregion-EGFP are not fluorescent [1] so the measurements of the rates of exocytosis may be modestly underestimated (assuming the non-fluorescent WPBs behave the same way as the proregion-mEGFP labelled WPBs). Correcting the rates to take account of these non-fluorescent WPBs gives mean maximal rates of 1.5 WPB/s at 0.3μM (rather than ~1.2 WPB/s) and ~4.7 WPB/s at 100μM histamine (rather than ~3.7 WPB/s).

Excitable cells show exocytosis of secretory vesicles at much higher rates than for the WPB, in the range of hundreds to thousands granules/s in pituitary cells [280, 677], pancreatic β-cells [679] depending on the stimulus strength and up to 40,000 vesicles/s in chromaffin cells [676] (reviewed in[680]). These very high rates may be due to very high local free $[Ca^{2+}]_i$ at release sites on the plasma membrane produced by clustering of Ca^{2+} permeable ion channels at active zones [280, 681]. Alternatively the Ca^{2+} sensitivity of the fusion apparatus might be different between excitable cells and WPBs in HUVEC. Secretory vesicles from neuroendocrine cells release their cargo into the circulation to be delivered on disparate tissues around the body therefore high rates of secretion may be

essential to overcome dilution, sequestration and clearance effects. On the contrary, the cargo of WPBs acts locally once secreted, at the surface of EC (vWF, P-selectin) or at the site of vascular injury (cytokines) where exocytosis is elicited. Perhaps the large size of WPBs and the highly condensed nature of intra-granule vWF mean that the slower rates of WPB exocytosis may be sufficient to deliver material efficiently to the cell surface to control processes such as platelet adherence.

4.8.4 High concentrations of histamine and thrombin fail to release all WPBs

Neither histamine nor thrombin was effective at releasing more than ~50% of WPBs. In contrast a maximally effective concentration of the receptor-independent agonist ionomycin (1μM), which acts directly on the ER to release Ca^{2+} [206] independent of IP_3 production [682], was able to drive exocytosis significantly more efficiently than either agonist studied. This suggests the existence of a reserved capacity in the secretory ability of endothelial cells, inaccessible to histamine or thrombin, which may come into play under conditions of severe $[Ca^{2+}]_i$ elevations such as cell injury. Under such conditions it is likely that the cellular free $[Ca^{2+}]_i$ levels rise much higher than those seen during agonist action, suggesting that the Ca^{2+}-sensitivity of WPB exocytosis extents to high levels.

5 Optical analysis of exocytosis of the non-WPB secretory organelle

5.1 Introduction

The non-WPB organelles are small structures that in the light microscope appear as diffraction limited punctae (Figure 1.1B). They lack the major WPB cargo proteins vWF, Proregion, P-selectin and CD63 [87](T Carter personall communication). Data suggests that they undergo continuous release [82] but may also undergo regulated exocytosis in response to secretagogues. In some studies in which t-PA release was used as a biochemical marker for release from these organelles, the secretion of t-PA appeared to be co-ordinated with that of vWF [70, 79, 80] while in other studies the time-course differed from that of vWF secretion [82-86]. Because t-PA can be present in WPBs under some conditions, the precise kinetics of exocytosis of these organelles has been difficult to establish using the indirect biochemical assay of t-PA secretion. In addition the time-resolution of biochemical studies of t-PA secretion from HUVEC are typically ~1min at best [82, 87], a time-course not fast enough to extract the underlying rates, delays or extent in stimulated non-WPB organelle exocytosis.

The aim of the experiments described in this chapter was to define more precisely the kinetics of stimulated exocytosis of the non-WPB organelle by direct observation of the organelles and their fusion and to compare these kinetics with that of the WPB. A time-resolved TIRFM (total internal reflection fluorescence microscopy) assay was used to investigate the kinetics of secretion of the non-WPB organelle population labelled by expression of t-PA-EGFP under resting conditions and during stimulation with histamine or ionomycin in single HUVEC. Cells were co-transfected with proregion-mRFP to label all newly formed WPBs, some of which can, particularly at later times after transfection, contain some t-PA-EGFP (see chapter 3).

5.2 TIRF live cell imaging of t-PA-EGFP and proregion-mRFP co-expressing HUVEC

Double nucleofected (t-PA-EGFP and proregion-mRFP), Fura-2 loaded HUVEC were imaged with TIRFM in conjunction with epifluorescence excitation of Fura-2 to monitor $[Ca^{2+}]_i$ changes. For EGFP excitation a 488nm laser was used and for mRFP excitation a 561nm laser. Switching between laser and epifluorescence illumination was synchronized with image capture using Winfluor software. Figure 5.1 shows a schematic of the setup described. The dichroic used was a custom made GFP/DsRed dual band dichroic mirror with a 400DCLP coating on the reverse side to allow reflection of 355nm and 380nm light from the monochromator on the cells (Chroma, cat. no. 51019+). The emission light was selected through an EGFP/DsRed emission filter (Chroma). Figure 5.1 shows an example of a single HUVEC co-expressing t-PA-EGFP and proregion-mRFP and loaded with Fura-2, imaged with this configuration.

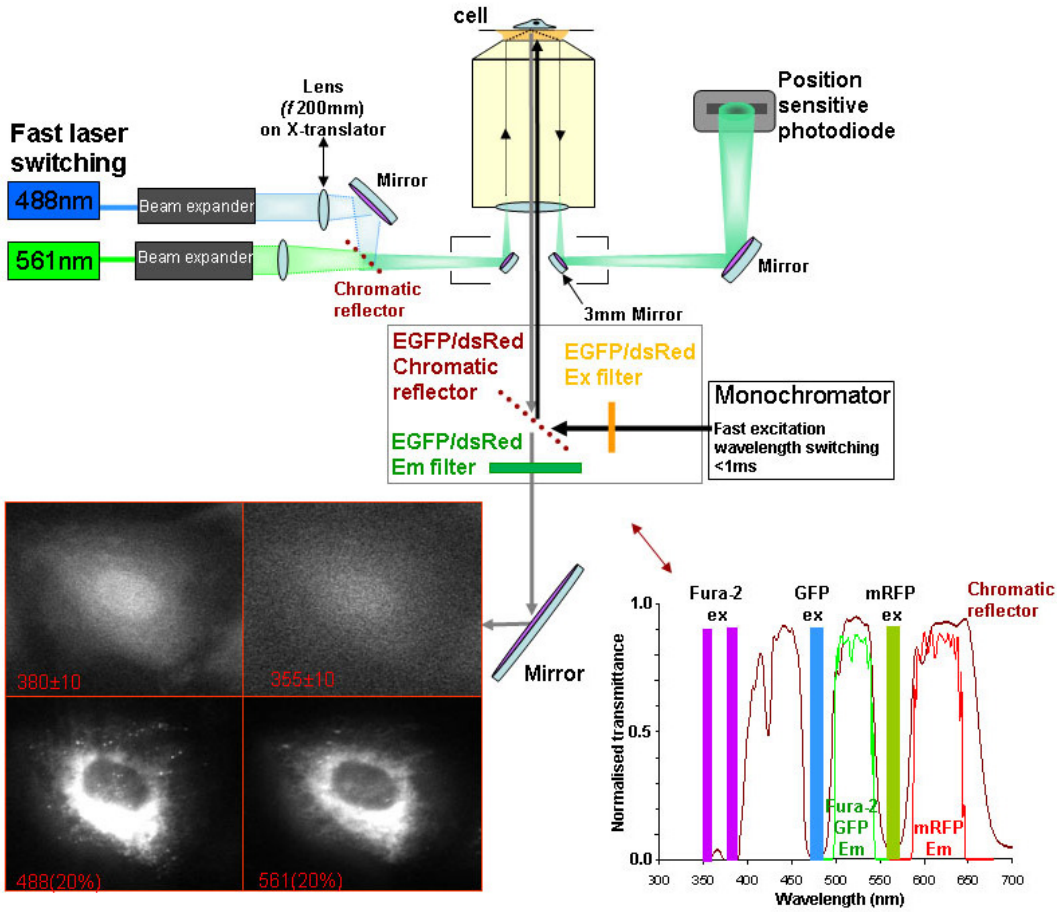

Figure 5.1 TIRF/EPI setup schematic

The blue and green laser light is co-aligned and focused into the back aperture of the objective so as to produce total internal reflection at an angle of 64^{o} at the glass coverslip-saline interface. A shallow evanescent field excitation is produced which excites only fluorophores at or near the basal cell membrane. Fura-2 is excited (purple) by epifluorescence illumination. The laser beam bypasses the chromatic reflector and a dual band emission filter selects for GFP (green) and mRFP (red) emission wavelengths. HUVEC co-nucleofected with t-PA-EGFP and proregion-mRFP loaded with 0.5µM Fura-2/AM are imaged sequentially at 30 frames/s (corresponding to 10frames/s per wavelength).

5.3 Spontaneous fusion of the non-WPB organelles in unstimulated HUVEC

Initially Fura-2 loaded HUVEC co-expressing t-PA-EGFP and proregion-mRFP were recorded for 2-4min under resting non-stimulated conditions to determine the unstimulated rate of non-WPB exocytosis. A representative resting $[Ca^{2+}]_i$ trace and the histograms of non-WPB fusion events pooled from 14 cells are shown in Figure 5.2A. For comparison no unstimulated release of WPBs was seen over periods of up to 15min (n=10) (Figure 5.2B). The events appear less frequent after the first minute or so because not all recordings were of the same length of time. Figure 5.3 shows the recording period of the 14 individual cells. The mean rate of the non-WPB spontaneous fusion calculated from individual cells was 0.02±0.01 non-WPBs^{-1} (n=14). Only 14 out of 25 (56%) cells recorded showed unstimulated fusion events.

5.4 Histamine-evoked non-WPB organelle exocytosis.

5.4.1 Concentration-dependence of histamine-evoked non-WPB organelle exocytosis.

The non-WPB organelle frequency of fusion increased during histamine stimulation in a dose dependent fashion. Figure 5.4A shows the $[Ca^{2+}]_i$ traces and the times of fusion events for representative examples of single HUVEC stimulated with either 1, 10 or 100μM histamine. Figure 5.4B shows the histograms of fusion events for data pooled from between 15-18 cells. The frequency of fusion events increased at the highest histamine concentration. The vertical dotted line in Figure 5.4B, aligned with the $[Ca^{2+}]_i$ rise, illustrates spontaneous fusion events occurring before the stimulus application in many

cases. At 1μM histamine only 61% of cells studied showed stimulated secretion (n=26), while at 10μM this was 54% (n=33) and at 100μM 62% (n=24) of cells. The percentage of cells that secreted non-WPBs were not significantly different between histamine concentrations.

5.4.2 Delays and rates of histamine-evoked non-WPB exocytosis

The delay from the Ca^{2+} rise to the onset of exocytosis (*D2*) for the non-WPB organelle at 1μM was 8.5±7.0s, at 10μM 5.5±5.0s and at 100μM it was 4.4±3.4s (n=15-18 cells at each concentration; mean±s.d.) (Figure 5.5A; mean±s.e.). The delays of the non-WPB exocytosis appear to decrease with increasing histamine concentration however due to their large variability they are not significantly different from one another as calculated by ANOVA (P=0.11).

The maximal rates of histamine evoked exocytosis for the non-WPB were 0.6±0.6 non-WPB $^{-1}$ at 1μM, 0.6±0.5 non-WPB $^{-1}$ at 10μM and 2.5±2.4 non-WPB $^{-1}$ at 100μM (n=9-12 cells at each concentration; mean±s.d.) (Figure 5.5B; mean±s.e.). ANOVA calculations show that the mean rate of exocytosis at 100μM histamine was significantly different from the mean rate at 10 and 1μM histamine (P=0.008), however the rates at 10μM and 1μM histamine were not significantly different.

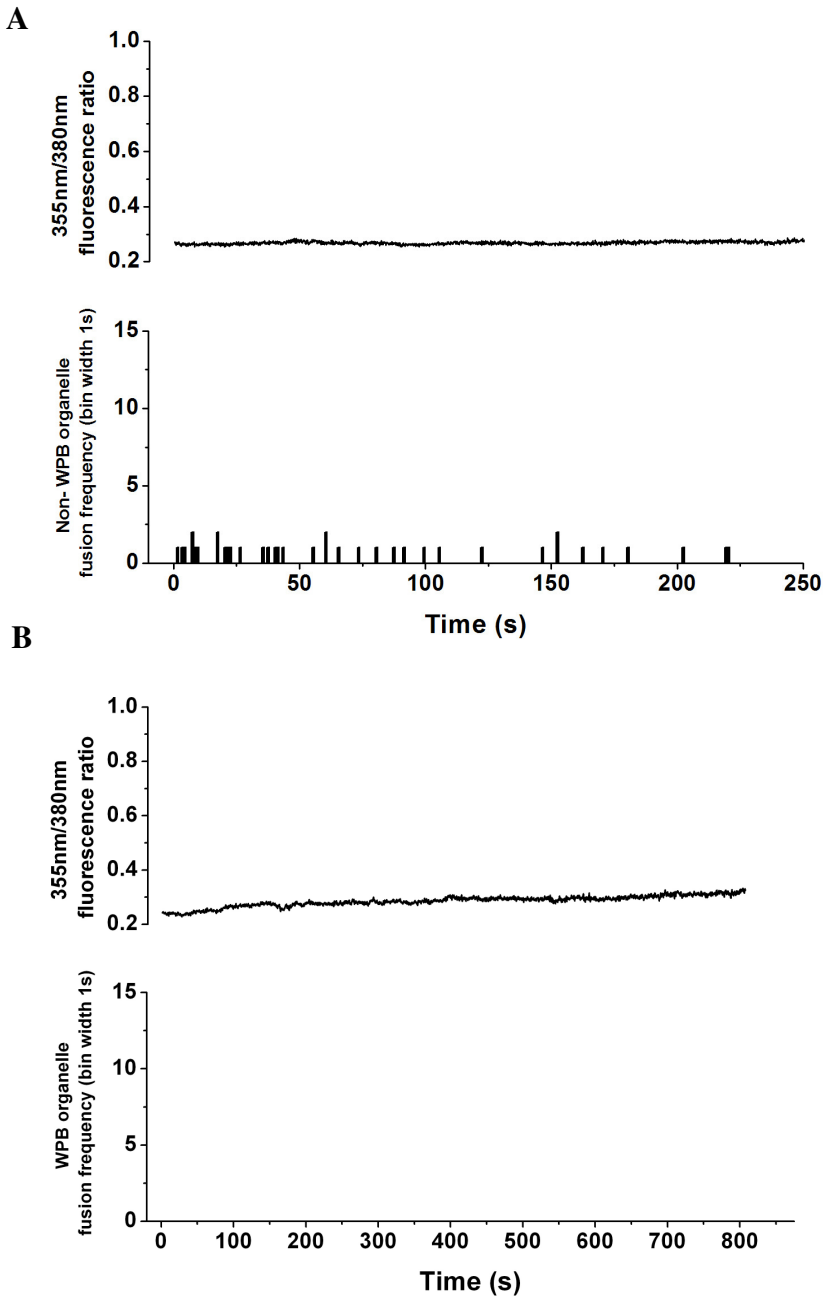

Figure 5.2 There is no unstimulated release of WPBs in contrast to the non-WPB organelle

*Upper panel in **A** and **B** shows a representative Ca^{2+} trace for unstimulated HUVEC recorded for approximately 250s (**A**) or 800s (**B**). The lower panel in **A** and **B** shows the histogram of the first latency distributions of fusion events for the non-WPB organelle (14 cells; 39 fusion events) (**A**) and the WPB (10 cells; no fusion events) (**B**), during basal $[Ca^{2+}]_i$ levels.*

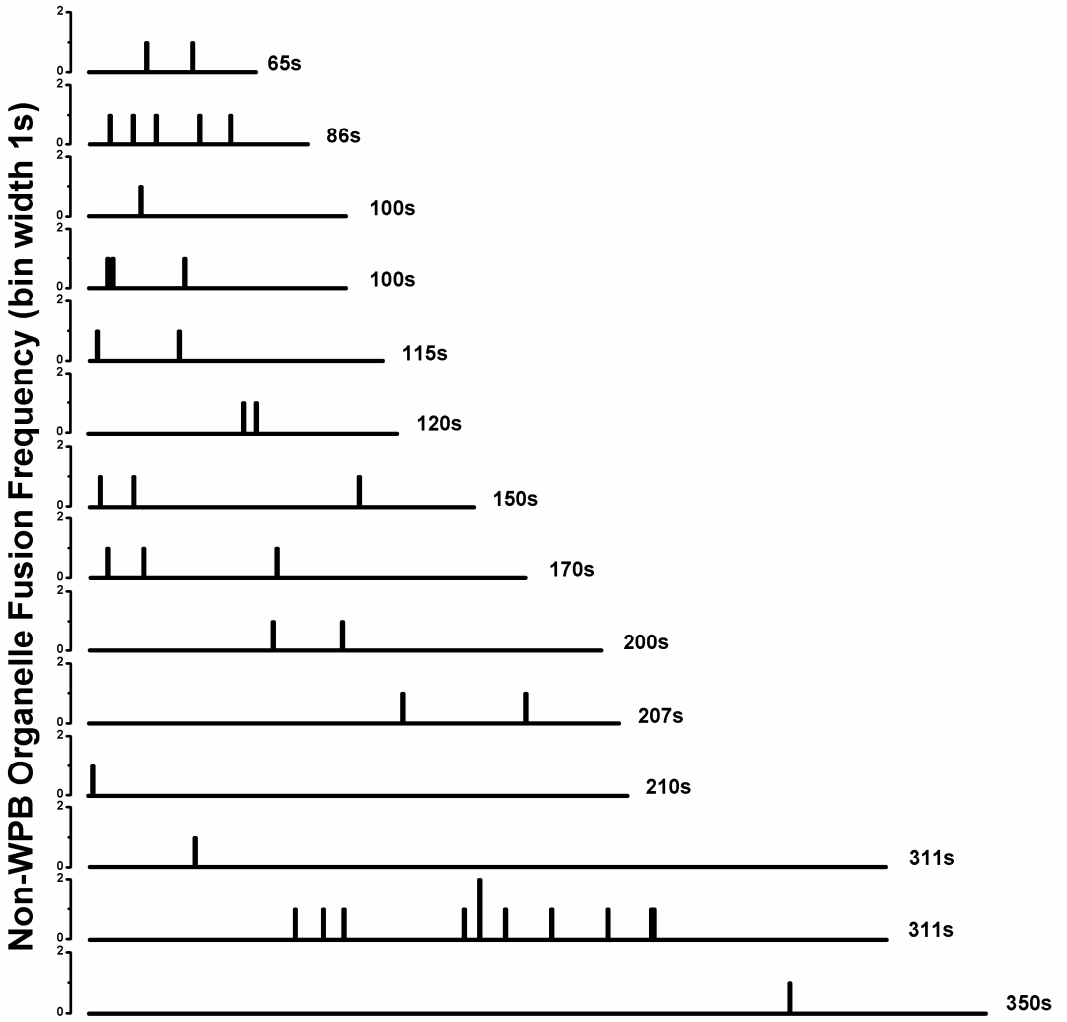

Figure 5.3 Time-course of individual experiments recorded during unstimulated conditions

The first latency distributions of the non-WPB fusion events from the experiments pooled in figure 5.2 are plotted separately for the individual cells studied. The time at the end of each experiment indicates the time-course of recording of each experiment to show the variability and to illustrate the spontaneous non-WPB fusion events are arbitrary and sporadic.

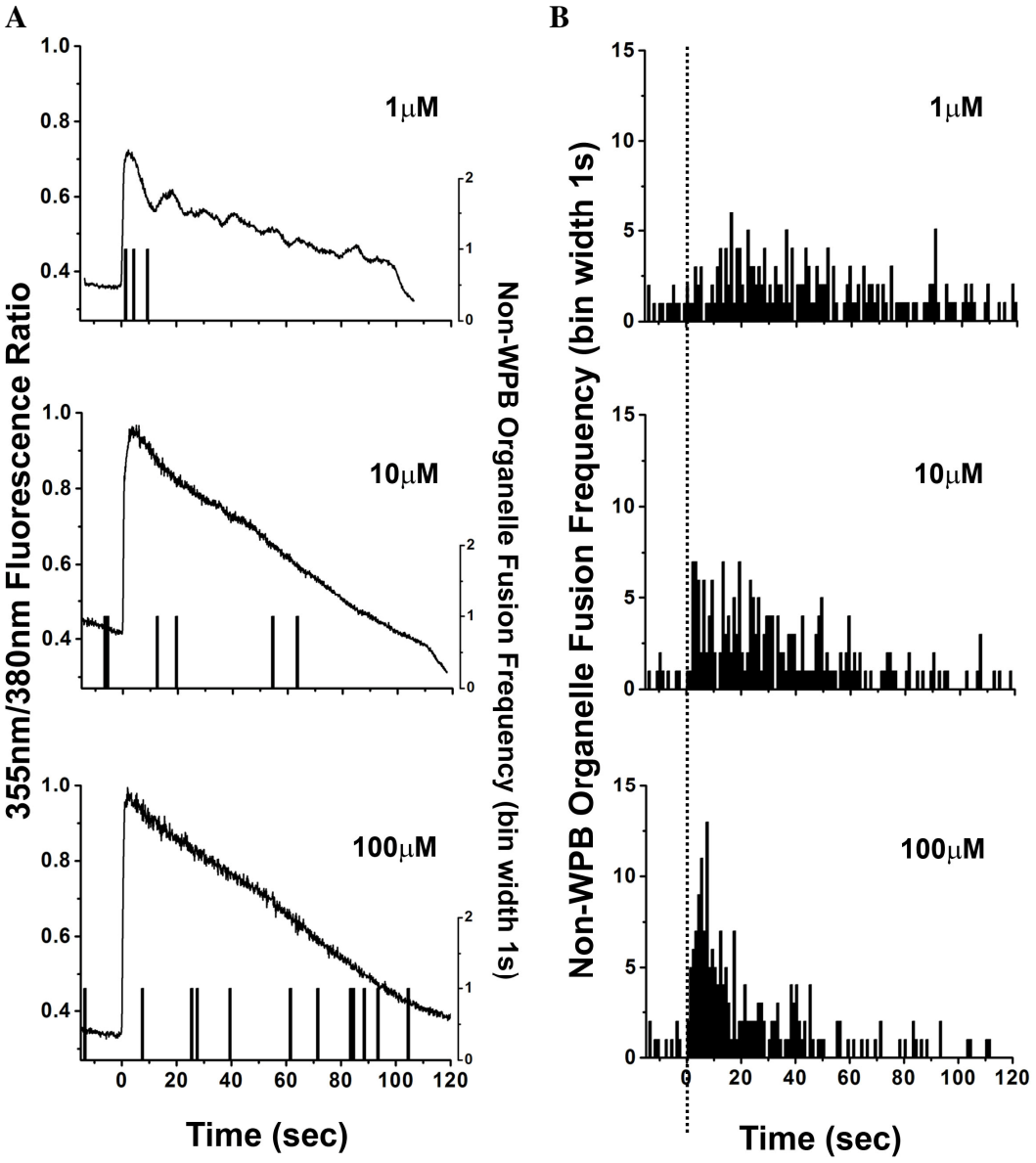

Figure 5.4 Concentration-dependence of histamine-evoked non-WPB exocytosis

*Each panel in **A** shows the changes in Fura-2 fluorescence ratio (355/380nm) in single HUVEC during stimulation with histamine at the concentrations indicated, and the corresponding frequency of fusion events. The Fura-2 traces were offset so that the increase in $[Ca^{2+}]_i$ in each case occurred at time=0 and the fusion events are determined from the rise in $[Ca^{2+}]_i$. **B** shows the first latency distributions of pooled events evoked by 1μM (n=15 cells, 217 non-WPB), 10μM (n=18 cells, 216 non-WPB) and 100μM (n=16 cells, 200 non-WPB) histamine determined from the rise in $[Ca^{2+}]_i$ (vertical dotted line).*

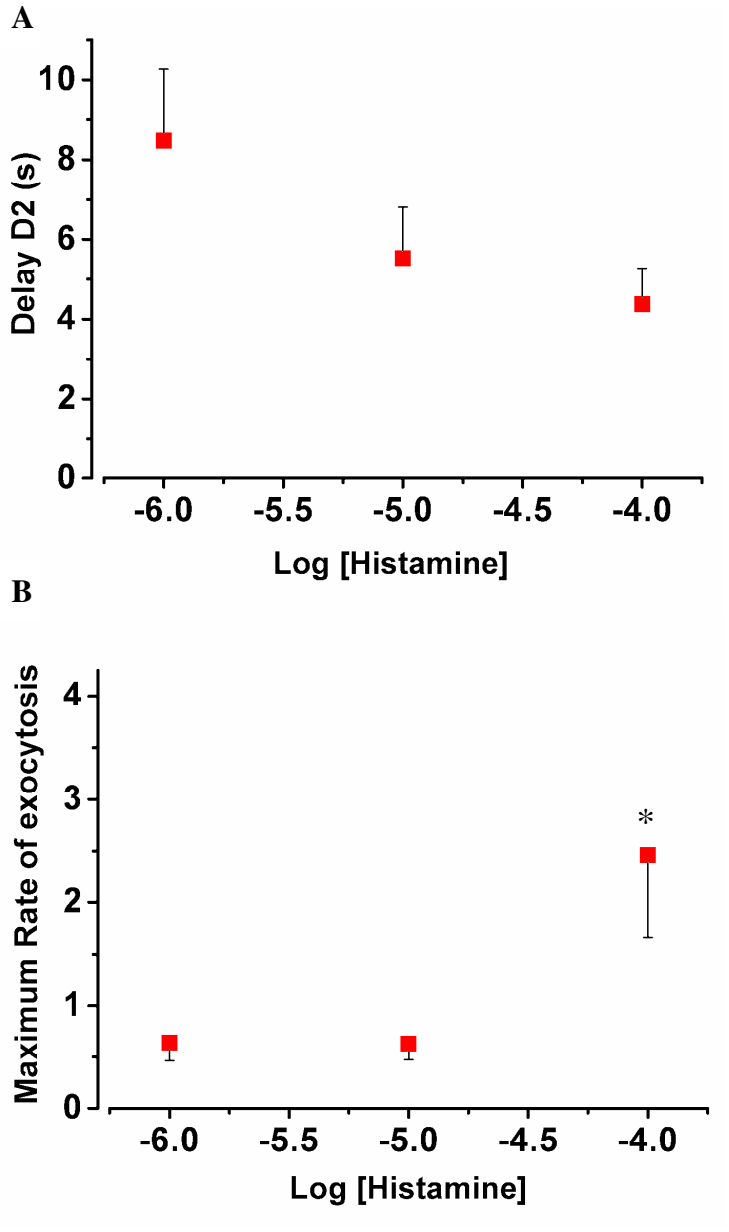

Figure 5.5 Delays (D2) and maximal rates of histamine-evoked non-WPB exocytosis

A. *The non-WPB stimulated exocytosis initiated with a delay from* $[Ca^{2+}]_i$ *rise of 8.5±1.8s at 1μM; 5.5±1.3s at 10μM and 4.4±0.9s at 100μM histamine (n=15-18 cells in each case; mean±se). The delays* D2 *are not significantly different between them (P=0.11).* ***B.*** *The maximal rates of the non-WPB stimulated exocytosis were 0.6±0.2 non-WPB*$^{-1}$ *at 1μM; 0.6±0.2 non-WPB*$^{-1}$ *at 10μM and 2.5±0.8 non-WPB*$^{-1}$ *at 100μM histamine (n=9-12 cells in each case; mean±se)(*=P=0.008 compared to the other rates).*

5.5 Ionomycin-evoked non-WPB organelle exocytosis

In order to examine the secretory behaviour of the non-WPB population of granules during severe conditions, as might occur during vascular injury, the kinetics of non-WPB secretion were determined with ionomycin. A representative example of a single HUVEC co-expressing t-PA-EGFP and proregion-mRFP stimulated with 1μM ionomycin is shown in Figure 5.6 (upper panel). The lower panel shows the first latency distributions of the non-WPB exocytotic events from 13 cells during ionomycin stimulation.

Figure 5.7 summaries the maximal rates and delays from the $[Ca^{2+}]_i$ rise to the onset of exocytosis (*D2*) of the non-WPB for 1μM ionomycin and 100μM histamine stimulation. The evoked kinetics of non-WPB exocytosis for the two secretagogues are not significantly different between them indicating that unlike the WPB (see chapter 4) the non-WPB stimulated exocytosis cannot be driven faster or at higher rates than a maximally effective hormone concentration.

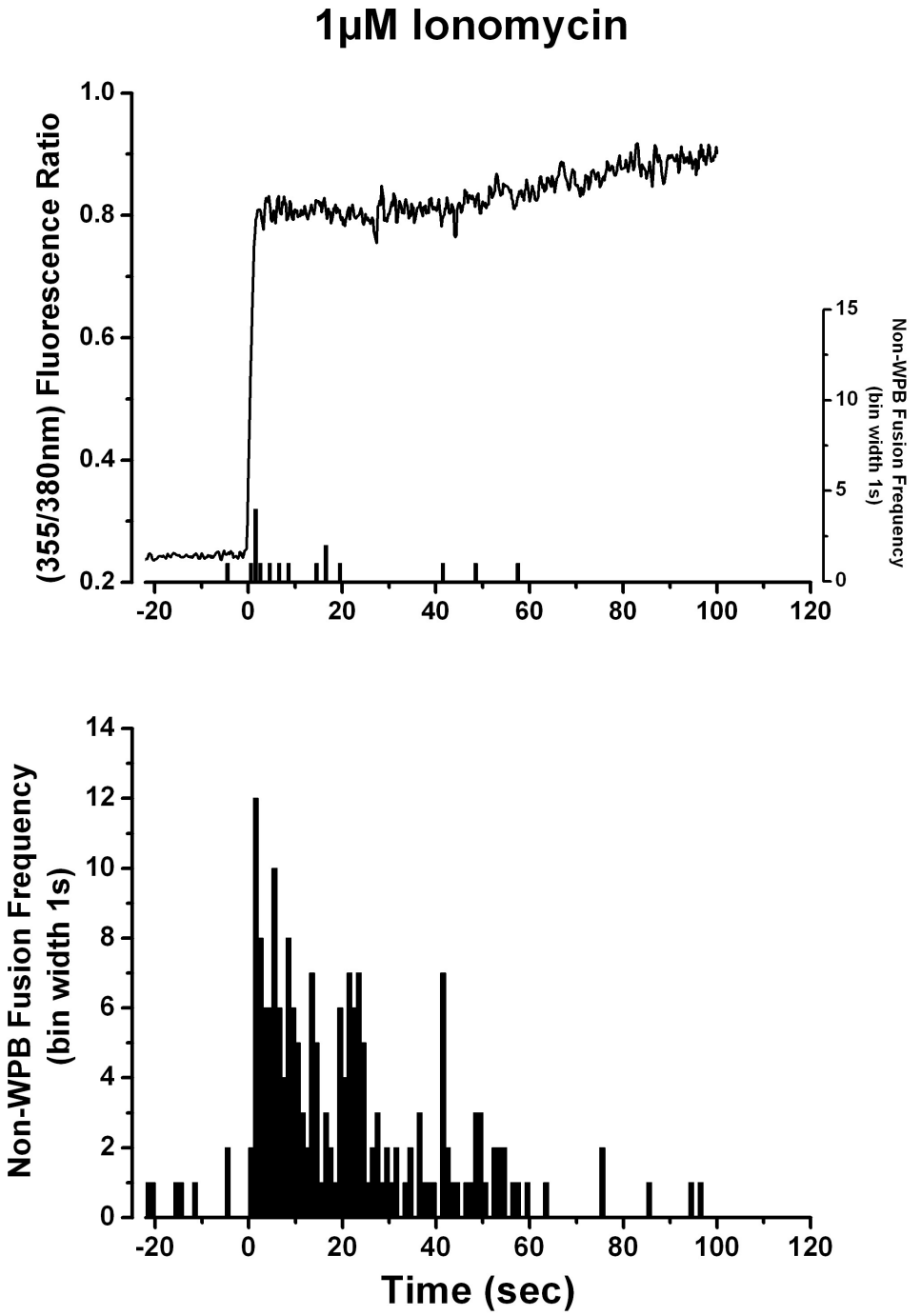

Figure 5.6 Ionomycin-evoked non-WPB exocytosis

Upper panel shows a representative Fura-2 fluorescence ratio (355nm/380nm) and the frequency of non-WPB fusion events, offset so that the $[Ca^{2+}]_i$ rise occurs at t=0, of a single HUVEC stimulated with 1μM ionomycin. The lower panel shows the frequency of fusion events from the rise in $[Ca^{2+}]_i$ of pooled TIRF experiments (13 cells, 198 non-WPB).

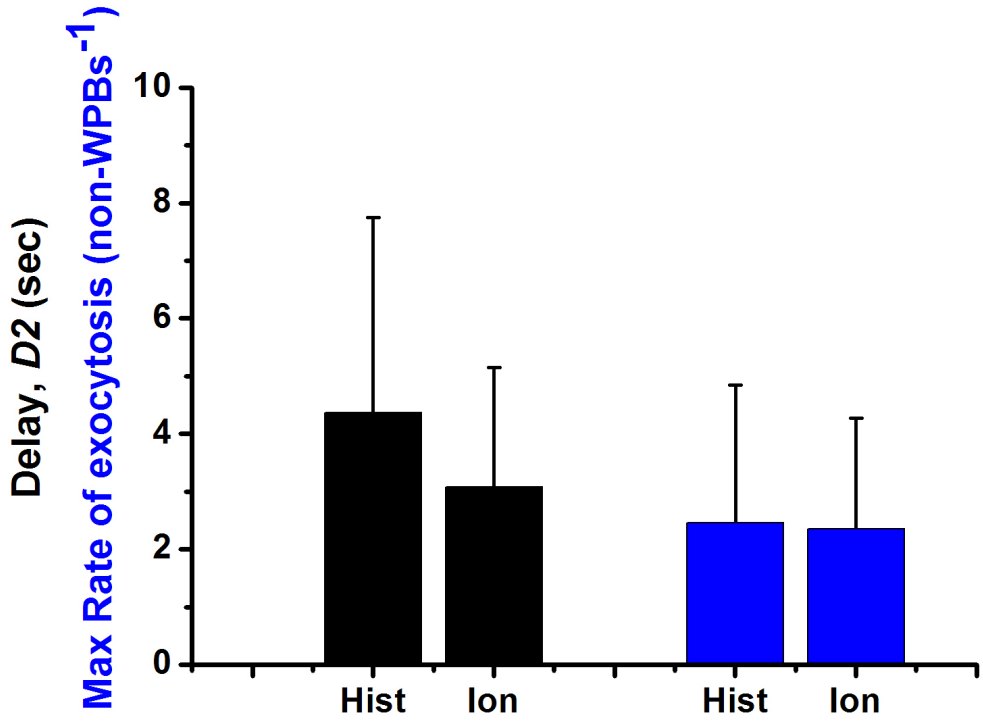

Figure 5.7 Comparison of the kinetics of non-WPB exocytosis stimulated with 100μM histamine and 1μM ionomycin

The black bars represent delays (D2) from $[Ca^{2+}]_i$ rise to the first non-WPB fusion event stimulated with 100μM histamine (Hist) 4.372±3.37s (mean±s.d.; n=16 cells) and 1μM ionomycin (Ion) 3.08±2.07s (mean±s.d.; n=13 cells). The blue bars represent the maximal rates of non-WPB exocytosis evoked by 100μM histamine 2.46±2.38 non-WPB^{-1} (mean±s.d.; n=9 cells) and 1μM ionomycin 2.36±1.92non-WPB^{-1}(mean±s.d.; n=9 cells). The D2 and maximal rates evoked by the two secretagogues were not significantly different.

5.6 Discussion

Previous studies have suggested that t-PA either resides in WPBs [70, 80] or in a unique secretory organelle [87] that we call the non-WPB organelle. Biochemical studies of the secretory kinetics of t-PA in endothelial cells have been complicated by the possibility that t-PA could be contained in both granule populations. In this work the non-WPB was labelled with t-PA-EGFP and visually distinguished from the t-PA-containing WPBs by co-expressing proregion-mRFP to enable a kinetic analysis of histamine-evoked non-WPB exocytosis directly.

5.6.1 Kinetics of the histamine-evoked exocytosis of the non-WPB organelle

The delay from $[Ca^{2+}]_i$ rise to the first exocytotic event (D_2) for the non-WPB organelle decreased with increasing histamine concentrations, yet due to the large variability in the delays, these values were not significantly different from each other. An additional complication and one that could account in part for the variability seen is that the non-WPB organelle can undergo unstimulated fusion. As a result no clear conclusions could be drawn about the concentration dependence of the delays in histamine evoked non-WPB fusion. The magnitude of the delays were however, significantly longer than those seen for the WPB, particularly at high histamine concentrations (~4.5 s versus 1.6 s for the WPB) suggesting that the Ca^{2+}-dependent recruitment and or fusion of these two organelles differs. Figure 5.8A compares the *D2* of the non-WPB to the WPB at the histamine concentrations indicated.

ANOVA analysis showed that the rates of non-WPB fusion stimulated with 1 and 10μM histamine were not significantly higher than the unstimulated rate of

fusion however the rates increased significantly at 100μM histamine (P=0.0001). At 100μM histamine the rates were similar to that seen for the WPB. Figure 5.8B compares the maximal rates of non-WPB exocytosis to the WPB at the histamine concentrations indicated. Despite taking great care to ensure that WPBs were excluded from this analysis could it be that some of these fusing organelles were in fact WPBs? Evidence against this comes from the determination of the resting pH within these organelles from intra-granule EGFP-fluorescence changes upon fusion (described in detail in chapter 3). The intra-granule pH of the non-WPB is ~pH6.1 irrespective of the time-point (4h-24h) after which cells were Nucleofected with t-PA-EGFP. Similarly, the estimate of the resting pH in non-WPBs that underwent fusion (either unstimulated or stimulated; data obtained from the experiments described in this chapter) was also ~pH 6.3, significantly higher than would be expected for mature EGFP containing WPBs (either proregion-EGFP or t-PA-EGFP; see chapter 3).

5.6.2 Extent of stimulated fusion of the non-WPB organelle

Figure 5.9 compares the time-course of exocytosis between the two granules. The percentage of degranulation for the non-WPB population could not be precisely determined because the number of non-WPB organelles in a single cell was typically too large to be counted accurately. However, rough estimates of the proportion of non-WPBs exocytosed, at 100μM histamine, indicated that significantly less than 5% of the total number of non-WPBs underwent fusion. This compared to ~50% of WPBs fusing with 100μM histamine. Similarly, with ionomycin <5% of the population of non-WPBs appear to undergo fusion compared to >60% for WPBs.

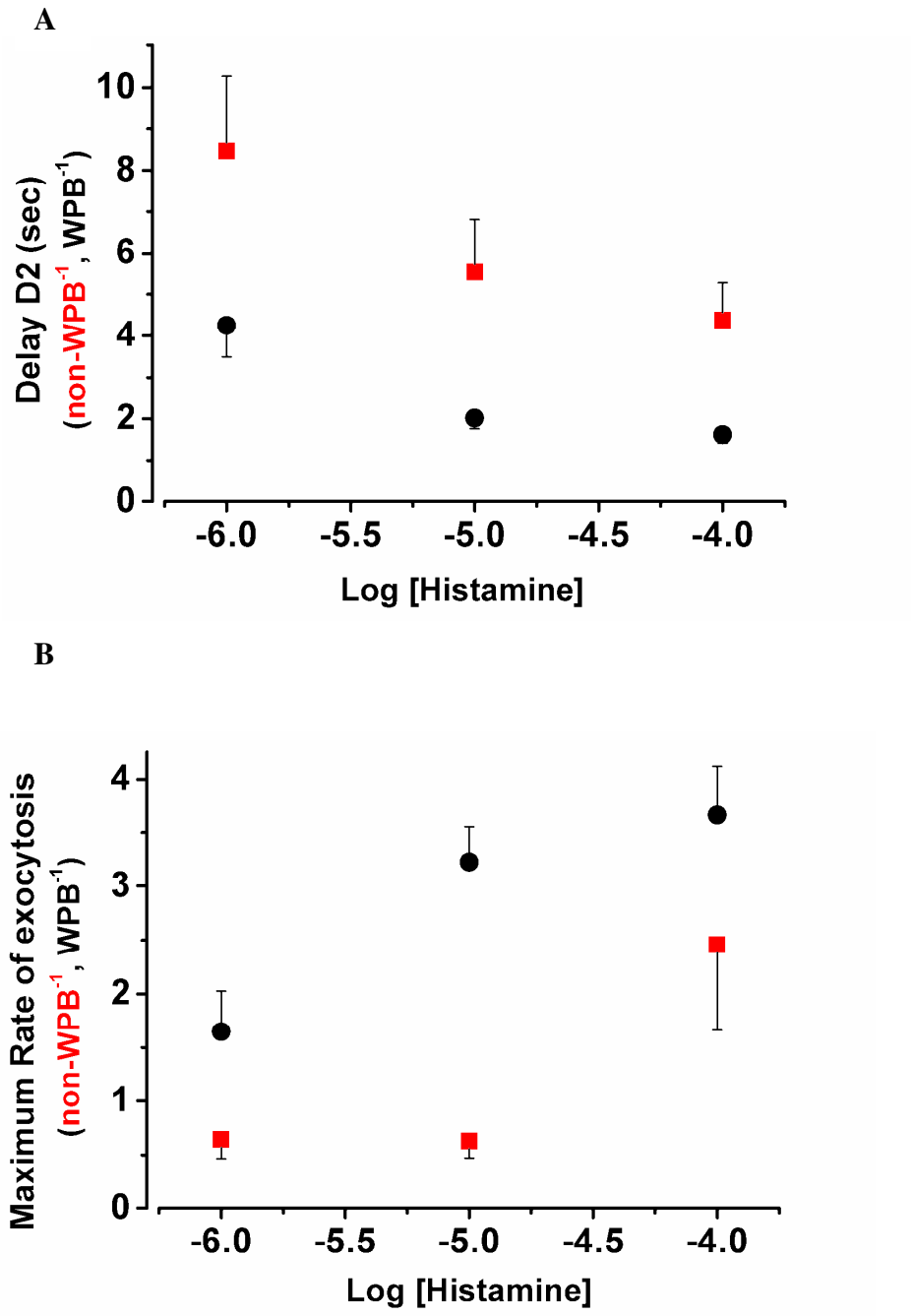

Figure 5.8 Delays (D2) and maximal rates of the non-WPB and WPB histamine-stimulated exocytosis

A. *The delays from the $[Ca^{2+}]_i$ rise to the onset of exocytosis were slower for the non-WPB than the WPB at the histamine concentrations indicated.* ***B.*** *The maximal rates of stimulated exocytosis for the non-WPB were lower than the WPB.*

WPB fusion rate
Non-WPB fusion rate
100μM
10μM
1μM
WPB
Non-WPB
Time (s)
355nm/380nm fluorescence ratio

Figure 5.9 Comparison of histamine stimulated secretion frequencies between WPBs and non-WPB organelles

Summarises the first latency distributions of WPBs (black histograms) and non-WPB organelles (red histograms) determined from the rise in $[Ca^{2+}]_I$, stimulated with histamine concentrations 1, 10 and 100μM. In each case the histograms represent pooled events from 15-20 cells. The top trace represents a Fura-2 Ca^{2+} trace offset so that the increase in $[Ca^{2+}]_i$ in each case occurred at time=0. The dotted line is aligned with the first time-point of Ca^{2+} increase (t=0). Events occurring before Ca^{2+} increase in the non-WPB population signify spontaneous secretion.

5.6.3 Comparison of WPB and non-WPB organelle exocytosis

The WPB and the non-WPB differ in their morphology, cargo, and intragranular pH (see chapter 3). Here we show that there were also differences in the initial kinetics of exocytosis and in the extent of degranulation between the two organelles. The differences between the two organelles are summarised in table 1. Data in this chapter shows, first; that the non-WPB undergoes spontaneous exocytosis, something that was not detectable in optical measurements of fluorescent WPBs (Figure 5.2). Second, although both organelles show Ca^{2+}-triggered exocytosis, the onset for fusion for non-WPB organelles was slower than for the WPB (Figure 5.8A) and at low histamine concentrations the rates of fusion were also lower; although they were similar at 100μM histamine (Figure 5.8B). Third, the extent of fusion was dramatically lower for the non-WPB, and finally, ionomycin was not capable of evoking a stronger non-WPB secretory response than 100μM histamine (Figure 5.7). This last piece of data indicates that the two organelles may exhibit different sensitivities to $[Ca^{2+}]_i$, something that had previously been suggested [82, 84]. Do they utilise different molecular machinery of exocytosis? The fusion apparatus of the non-WPB can operate at resting $[Ca^{2+}]_i$ levels [82] whereas WPB exocytosis is only stimulated above a certain threshold $[Ca^{2+}]_i$ [183, 669]. This indicates that the fusion apparatus for the non-WPB is likely to be more sensitive to Ca^{2+}. The rate and extent of stimulated exocytosis of the non-WPB saturates at lower $[Ca^{2+}]_i$; indicated by the inability of ionomycin to evoke a stronger response. This data suggests that the two granule populations are likely to contain Ca^{2+}-sensors with different affinities for Ca^{2+}. Although in other systems, mainly neuroendocrine cells, the $[Ca^{2+}]_i$ sensing apparatus has been extensively studied [399, 683-686]; in

endothelial cells it remains unclear. In excitable cells sensor proteins required for Ca^{2+}-triggered exocytosis include the synaptotagmins [410, 685] and annexins [408, 409, 687]. What evidence is there for the molecular identity of the Ca^{2+}-sensor in WPB exocytosis? One study identified the recruitment of synaptotagmin 1 to pseudo-WPBs in vWF expressing AtT-20 cells [424] suggesting a possible involvement of synaptotagmins in WPB exocytosis, although this could be an AtT-20 specific effect. Synaptotagmins exist in different isoforms with different Ca^{2+} affinities [688] suggesting combinations of multiple synaptotagmin isoforms could potentially fine tune the Ca^{2+} sensing machinery for exocytosis of different populations of granules. Annexins are heterologously expressed in all cell types and are abundantly found in endothelial cells [411]. They are either found in the cytoplasm as monomers or bound to phospholipids on the plasma membrane in a heterotetrameric complex [408]. The latter is thought to control Ca^{2+} homeostasis by controlling Ca^{2+} channel trafficking on the plasma membrane in endothelial and epithelial cells [411, 689]. Moreover annexins are thought to be involved in exocytosis when activated by Ca^{2+} in endothelial cells [412] and chromaffin cells [413]. Annexins have high affinity for Ca^{2+} [409]. Disruption of the annexin complex on the plasma membrane does not completely inhibit exocytosis in endothelial cells as observed with capacitance measurements [412]. Other work showed that down-regulation of the annexin A_2 complex interfered with vWF secretion but not t-PA secretion from endothelial cells when stimulated with histamine or ionomycin [55]. The same group showed that the GTP-bound conformation of Rab3D mutants, involved in the exocytotic machinery [690], were recruited to vWF-containing WPBs but not t-PA-containing organelles and its over-expression interfered with WPB formation and exocytosis whereas t-PA

exocytosis was unaffected [55]. Other membrane proteins recruited to the WPB but not the non-WPB include Rab27a and its effector MyRIP [54], thought to be involved in anchoring mature WPBs to peripheral actin and thus preventing WPB exocytosis prior to maturation [57]. Further differences identified in the secretory pathway of the two organelles come from studies showing that phospholipase D1 knock down in HUVEC, a molecule shown to regulate the recruitment of the exocyst complex (also reported to be involved in WPB exocytosis [418]), inhibited WPB exocytosis but did not affect t-PA secretion [691].

The data presented here strengthen the concept that fusion of the WPB and non-WPB organelles are regulated differently. Further work is needed to elucidate the differences in the molecular machinery that give rise to the formation, trafficking and fusion of these two different organelles.

Table 1: Differences between WPB and non-WPB

Feature	WPB	Non-WPB
Morphology	Small spherical structures through to large cigar shaped organelles	Exclusively small spherical structures
Cargo	vWF, proregion, P-selectin, CD63, Angiopoietin-2, Osteoprotegerin (under certain conditions ; IL-8, eotaxin-3, t-PA) [64, 68]	t-PA (under certain conditions ; IL-8, eotaxin-3, MCP-1, GROα)
Early pHg	pH6.2	pH6.1
Late pHg	pH5.4	pH6.1
Storage	Yes	No
Molecules possibly involved in exocytosis	Rab27a and effector MyRIP, Rab3D, phospholipase D1, annexin A2	No evidence
Spontaneous release	No	Yes
Regulated exocytosis	Yes	Yes
Kinetics of exocytosis	D2=1.62 ± 0.21s Max rate=3.7±1.8 $WPBs^{-1}$ Perc.Degr.=47.8±21.7%	D2=4.37±0.90s Max rate=2.5±0.8non$WPBs^{-1}$ Perc. Degr.<5%
Potential Ca^{2+}-sensitivity	Low	High
Efficiency of Histamine vs Ionomycin evoked exocytosis	Histamine < Ionomycin	Histamine = Ionomycin

6 Mitochondria and WPB exocytosis

6.1 Introduction

Mitochondria are the major source of energy production in most cells [692], however ECs are thought to use the process of anaerobic glycolysis (metabolism of glucose in the cytosol) to satisfy their energy demands [510, 511, 513, 514]. As a consequence, mitochondria in endothelial cells are thought to be important for other processes such as oxygen sensing [512], production of NO and ROS [513, 514], and intracellular Ca^{2+} buffering [571, 573]. How do mitochondria regulate cytosolic Ca^{2+}? During increases in cytosolic $[Ca^{2+}]_i$ mitochondria are able to accumulate Ca^{2+} [528, 533, 565] using a high affinity uniporter (Kd=2nM) [527] which selectively transports Ca^{2+} into the mitochondria [527, 545]. This ability of mitochondria to sequester Ca^{2+} has been shown to lead to modifications of cytosolic Ca^{2+} signaling patterns including Ca^{2+} oscillations [552, 553, 566], to facilitate capacitative (CCE) Ca^{2+} entry [572, 573], to suppress the positive feedback of local Ca^{2+} on the IP_3R involved in Ca^{2+} propagation [563], and to facilitate Ca^{2+} clearance from the cytosol [558] in a variety of cell types. Ca^{2+} is a major second messenger coordinating many cellular functions, including secretion [97] and its modulation by mitochondria would potentially have consequences on the secretory kinetics. Previous studies, using pharmacological inhibition of mitochondrial Ca^{2+} uptake, have shown that stimulated secretion of catecholamines from chromaffin cells was increased [578, 583, 584] as was the release of gonadotropins in pituitary gonadotropes [552]. In other instances however mitochondrial Ca^{2+} uptake inhibition led to a decrease in catecholamine secretion from mouse chromaffin cells, suggesting differences between species and cell types [557].

In this chapter the role of mitochondrial Ca^{2+} uptake in modifying histamine-evoked $[Ca^{2+}]_i$ changes and the kinetics of WPB exocytosis was examined by dissipating the mitochondrial membrane potential ($\Delta\Psi_m$), the driving force for Ca^{2+} uptake via the uniporter, and observing the effects on mitochondrial free Ca^{2+}, cytosolic free Ca^{2+} and WPB exocytosis simultaneously in single cells. To achieve the collapse of the $\Delta\Psi_m$, the metabolic uncoupler FCCP (Carbonyl cyanide-p-trifluoromethoxyphenylhydrazone) was used. This drug transports protons across the mitochondrial membrane down the electrochemical gradient collapsing in this way the $\Delta\Psi_m$ and uncoupling respiration from oxidative phosphorylation [509], leading to the block of Ca^{2+} uptake via the uniporter (reviewed in [693]). Oligomycin was used in combination with FCCP to inhibit the consumption of cytosolic ATP as a result of reversal of the F_1F_0 ATPase on the IMM after dissipation of the membrane potential [694].

Little work has been done on mitochondrial disruption and WPB exocytosis in endothelial cells. Because there is evidence of links between mitochondrial diseases and vascular diseases such as atherosclerosis (for reviews see [513, 589]) it was of interest to establish whether mitochondria might play any role in modifying Ca^{2+} signals and secretion of WPBs.

6.2 Epifluorescence imaging of WPB exocytosis and changes in $[Ca^{2+}]_i$ and $[Ca^{2+}]_m$

For monitoring $[Ca^{2+}]_m$, the membrane permeant form of X-Rhod-1 (X-Rhod-1/AM) was used in combination with Fura-2 (see methods section 2.3.3). Excitation light for Fura-2 380±10nm and 355±10nm and light for exciting both X-Rhod-1 and mEGFP 480±20nm was sent to a 500DCXRU dichroic mirror. The emitted light was sent to an optical splitting device containing a DC560 dichroic mirror that separated the Fura-2 and mEGFP light from that of X-Rhod-1 prior to band pass filters centred at 520±40nm and 615±25nm respectively. The imaging setup and an example of a single HUVEC expressing proregion-EGFP and loaded with Fura-2 and X-Rhod-1 is shown in Figure 6.1.

6.3 Simultaneous Measurements of $[Ca^{2+}]_i$ and $[Ca^{2+}]_m$ in single HUVEC

6.3.1 Is X-Rhod-1 measuring changes in $[Ca^{2+}]_m$?

X-Rhod-1 is a Ca^{2+} -sensitive fluorescent rhodamine derivative that becomes selectively trapped in mitochondria due to the highly negatively charged inner mitochondrial membrane (IMM) and has been used extensively to report changes in $[Ca^{2+}]_m$ [552, 584, 695]. X-Rhod-1 was used here to report changes in $[Ca^{2+}]_m$ during mitochondrial inhibition and histamine action. To confirm the partitioning of the X-Rhod-1 into mitochondria, HUVEC were co-loaded with X-Rhod-1 and mitotracker green, a fluorescent mitochondrial marker that preferentially accumulates in mitochondria regardless of the mitochondrial membrane potential. In separate experiments HUVEC expressing mito-EGFP which specifically marks the mitochondria, were loaded with X-Rhod-1. In both cases the X-Rhod-1 fluorescence signal co-localised with these mitochondrial

specific markers (Figure 2.16). X-rhod1 is not a ratiometric Ca^{2+} indicator, and as such is potentially susceptible to movement artefacts and to changes in mitochondrial morphology (e.g. swelling / shrinking) that could give rise to changes in the optical path length or volume of the organelle. Such morphological changes might give rise to spurious changes in fluorescence intensity un-related to changes in $[Ca^{2+}]_m$. To determine if such changes might occur and thus contribute to measurements of $[Ca^{2+}]_m$, mitochondria were labelled with both X-Rhod-1 and a second Ca^{2+}-insensitive fluorescence marker (mito-EGFP or mitotracker green). Changes in the fluorescence of these markers should report Ca^{2+}-independent changes in parameters such as swelling. Figure 6.2 shows a typical experiment in which the mitochondrial fluorescence change of mito-EGFP, X-Rhod-1 and the $[Ca^{2+}]_i$ change reported by Fura-2 were recorded during histamine stimulation. The background subtracted (blue ROI in A) EGFP (green trace) and X-Rhod-1 (red trace) fluorescence were measured from the same region of interest (shown in green and red ROIs in A). While X-Rhod-1 responds with an increase in fluorescence, mito-EGFP fluorescence remained stable, suggesting changes in X-Rhod-1 fluorescence reflect changes in $[Ca^{2+}]_m$, presumably due to mitochondrial Ca^{2+} uptake.

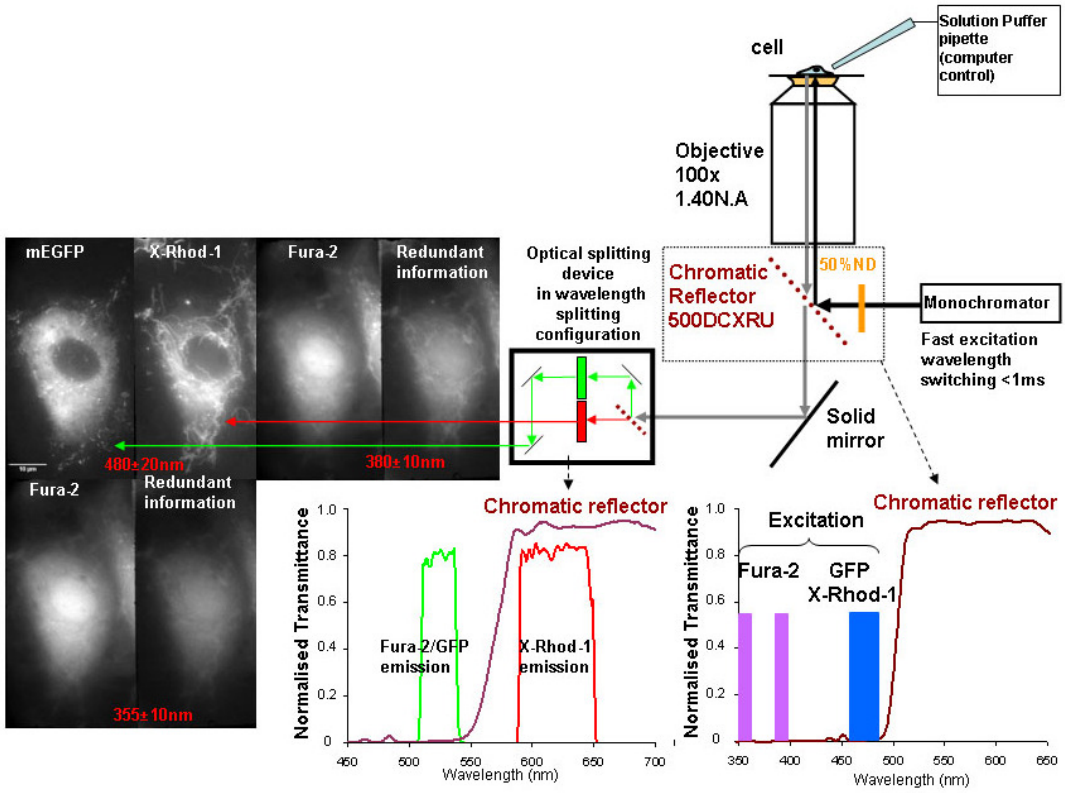

Figure 6.1 Setup schematic for imaging Fura-2, EGFP and X-Rhod-1.

The excitation light sent from the monochromator, 480±20nm for EGFP and X-Rhod-1 and 355±10nm and 380±10nm for Fura-2, passed through a 50% neutral density filter and was then reflected onto the specimen by a 500DCXR chromatic reflector. The emitted light was separated using an optical splitting device to be collected at 520±40nm for Fura-2/EGFP and 615±25nm for X-Rhod-1. An example of the images obtained on the EMCCD camera of a single HUVEC nucleofected with proregion-EGFP and loaded with 0.5µM Fura-2/AM and 0.2µM X-Rhod-1/AM is shown. Each image is a single frame imaged sequentially at 30 frames/s (corresponding to 10frames/s per wavelength).

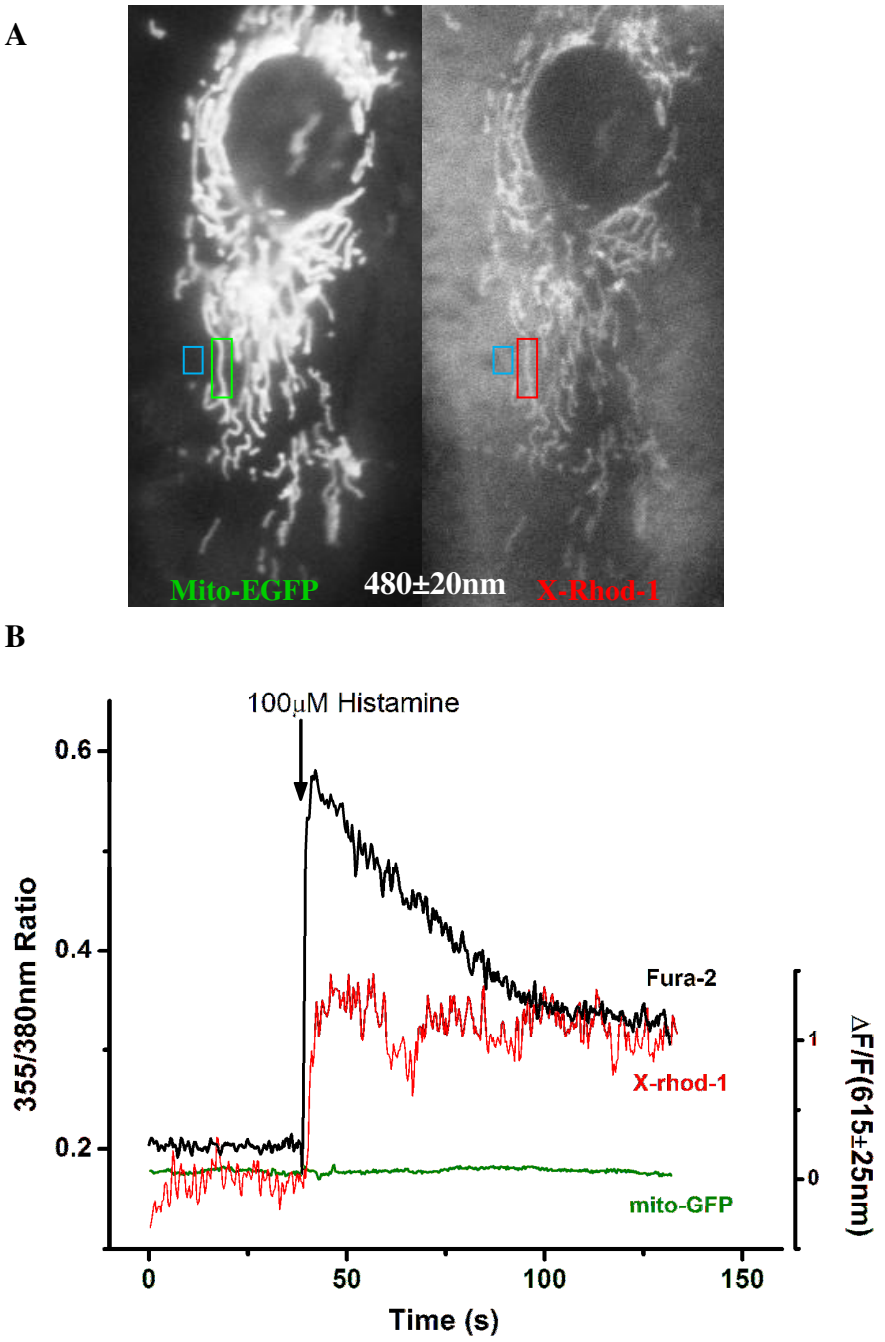

Figure 6.2 Mito-EGFP signal is independent of histamine stimulation

A. *A single HUVEC expressing mito-EGFP and loaded with 0.5μM Fura-2 and 0.5μM X-Rhod-1 imaged using the setup described in figure 6.1 and stimulated with 100μM histamine.* ***B.*** *The fluorescent measurements of the background subtracted Fura-2 ratio (black trace), the background subtracted X-Rhod-1 (red ROI minus blue ROI in* ***A****) and the EGFP fluorescence (green ROI minus blue ROI in* ***A****).*

Another consideration is that mitochondria contain auto-fluorescent proteins such as flavoproteins which participate in oxidative phosphorylation and are excited optimally at 450nm and emit broadly with a peak at ~550nm. Flavoproteins increase in fluorescence when oxidised during increases in the mitochondrial respiration rate and have been used to measure the up-regulation of the TCA cycle [577]. This will occur for example during collapse of mitochondrial $\Delta\Psi_m$ by FCCP. Since X-Rhod-1 is excited at 475(20)nm and emission light is collected at 615±25nm, there was a small possibility of some overlap between the tail end of the flavoprotein autofluorescence emission spectra and the emission filter used for X-Rhod-1. To identify if there was any bleed through cells not loaded with X-Rhod-1 were imaged with the same optical arrangement during incubation with uncoupler FCCP. During such recordings there was no detectable signal due to mitochondrial autofluorescence changes observed (data not shown).

6.3.2 Stimulus-evoked $[Ca^{2+}]_m$ changes

Figure 6.3 shows a representative experiment of a live HUVEC expressing proregion-mEGFP and loaded with 0.2μM X-Rhod-1 during stimulation with a maximally effective (30μM) histamine concentration. The top panel shows the raw X-Rhod-1 changes from a mitochondrial region (red trace; red region of interest (ROI) on the cell image), and from a cytosolic region (blue trace), measured from a ROI adjacent to the mitochondrial ROI (blue ROI on cell image). The middle panel shows the background subtracted Fura-2 ratio (black trace) and the mitochondrial X-Rhod-1 signal from the red ROI after subtraction of the background signal and the cytosolic signal from the blue ROI that includes some cytosolic X-Rhod-1 (red trace). The black histogram in the lower panel

represents the first latency distribution of the fusion events in this cell. This data shows that changes in both cytosolic and mitochondrial Ca^{2+} could be measured along with WPB fusion in single cells.

At what histamine concentration are mitochondrial Ca^{2+} signals observed? With low histamine concentrations (0.3μM) no clear changes in X-Rhod-1 fluorescent were seen despite small increase in $[Ca^{2+}]_i$ (Figure 6.4). However, at histamine concentrations ≥ 1μM there was a slow rise in $[Ca^{2+}]_m$ that started with a delay after the $[Ca^{2+}]_i$ rise. At high concentrations (30-100μM) the delay between $[Ca^{2+}]_i$ rise and $[Ca^{2+}]_m$ was on average 2.06±1.45s (mean±sd, n=7) (Figure 6.4). To summarise, the $[Ca^{2+}]_m$ signal reported by X-Rhod-1 increased with a delay with respect to the $[Ca^{2+}]_i$ signal, it was slower to rise and was more prolonged than the $[Ca^{2+}]_i$.

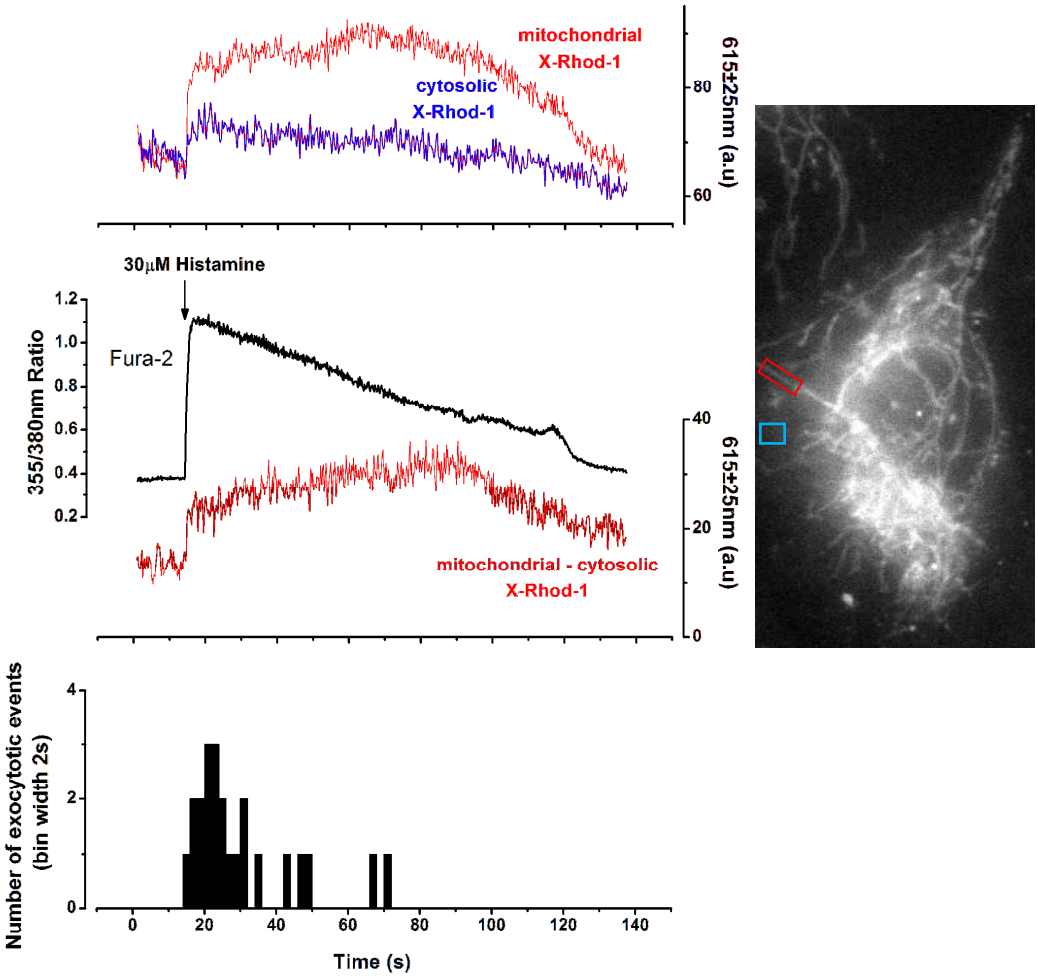

Figure 6.3 Simultaneous monitoring of $[Ca^{2+}]_i$, $[Ca^{2+}]_m$ and exocytosis.

An example of $[Ca^{2+}]_i$, $[Ca^{2+}]_m$ and WPB exocytosis monitored in a single HUVEC loaded with 0.5μM Fura-2 and 0.2μM X-Rhod-1 and stimulated with 30μM histamine. The top panel represents the raw X-Rhod-1 measurements from a mitochondrial ROI (red trace; red ROI on cell image) and an adjacent cytosolic ROI (blue trace; blue ROI on cell image). The middle panel shows the background subtracted Fura-2 ratio fluorescence measuring $[Ca^{2+}]_i$ (black trace) and the background subtracted X-Rhod-1 signal from the red ROI (red trace) after subtraction of the cytosolic X-Rhod-1 signal from the blue ROI. The lower panel shows the histogram of the WPB fusion events.

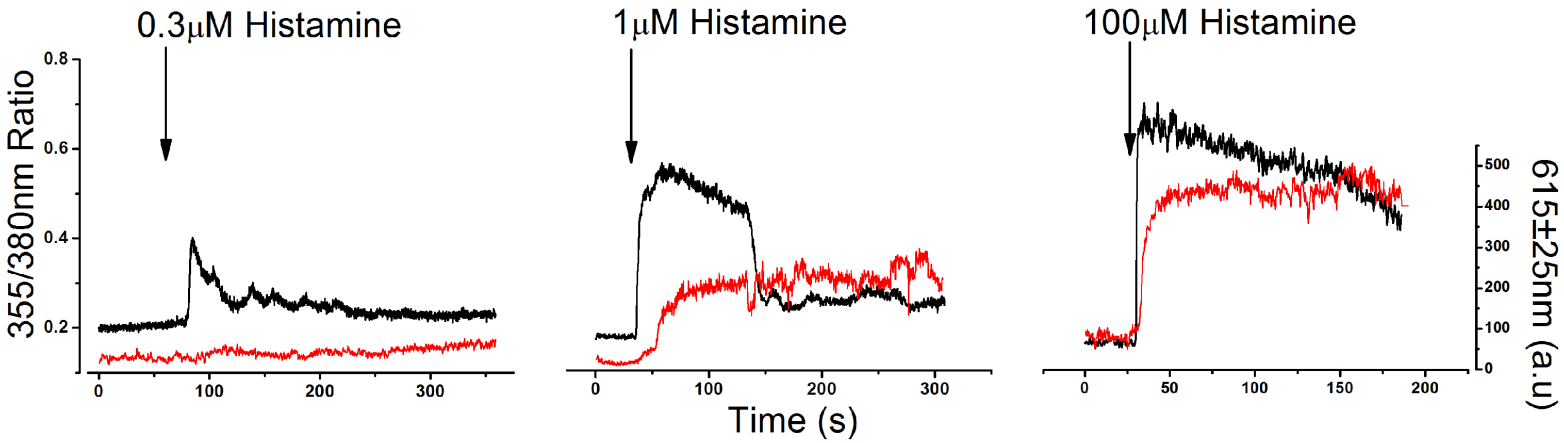

Figure 6.4 $[Ca^{2+}]_m$ increases are significant above 0.3μM Histamine stimulation

Measurements of the background subtracted Fura-2 ratio (black traces) and the X-Rhod-1 signal (red traces) in single HUVEC loaded with 0.5μM Fura-2 and 0.2μM X-Rhod-1 and stimulated with 0.3 (left panel), 1 (middle panel) and 100μM histamine (right panel).

6.4 Action of FCCP

6.4.1 FCCP collapses the mitochondrial $\Delta\Psi_m$

FCCP was used at 1μM in combination with 2.5μg/ml oligomycin. Initially, to ensure that this concentration of FCCP efficiently collapsed the $\Delta\Psi_m$ and to determine the time-course of its action, changes in $\Delta\Psi_m$ were measured using the fluorescent dye TMRE [521]. TMRE is a fluorescent lipophilic cation that accumulates in mitochondria in proportion to the magnitude of $\Delta\Psi_m$. The properties of the dye and how it can be used are described in detail in Methods section 2.3.5. The method used here was the "redistribution" method where the cells were loaded at low TMRE concentrations that did not reach auto-quenching levels. As the mitochondrial membrane depolarises, TMRE exits the mitochondrial lumen and enters the cytosol. This results in a decrease in the specific mitochondrial signal [521]. TMRE was used in combination with mito-EGFP as described below.

Mito-EGFP comprises a mitochondrial targeting sequence derived from subunit VIII of human cytochrome C oxidase (COX) located on the inner mitochondrial membrane with the EGFP directed to the mitochondrial matrix [696, 697]. During oxidative phosphorylation the electron transport chain provides the energy for proton transport via the complexes I, III and IV on the inner mitochondrial membrane (IMM) from the mitochondrial lumen to the inter-membrane space (see Introduction Figure 1.7 for a cartoon of the electron transport chain on the mitochondria). The FCCP protonophore carries protons down their electrochemical gradient from the inter-membrane space into the mitochondrial lumen leading to a rise in the inter-membrane space pH and a drop

in the luminal pH. The mitochondrial matrix pH is alkaline at ~pH8 [345] and FCCP will equilibrate this to the cytoplasmic pH (~pH7.2). This small pH drop is not sufficient to give a detectable EGFP fluorescence change as at pH7.2 the GFP fluorescence is approaching maximum as described by the pH-GFP fluorescence relationship in figure 3.2. Although in this case EGFP cannot be used as a pH indicator, it can be used to determine any mitochondrial morphological changes due to FCCP perfusion.

TMRE fluorescence ($\Delta\Psi_m$ measurements) and mito-EGFP fluorescence (morphological changes) were recorded simultaneously using the same imaging configuration as in Figure 6.1. Figure 6.5A shows a single HUVEC expressing mito-EGFP and loaded with TMRE, both fluorophores being excited at 480nm, perfused with FCCP/oligomycin, and with TMRE present in the perfusate to prevent any loss of cellular dye. The red ROI indicates the region of the mitochondria used for the EGFP and TMRE measurements and the blue ROI the region used for background subtraction. A montage of the EGFP fluorescence of mitochondria in 6.5B shows an apparent condensation of the mitochondria and formation of rings as previously reported with the mito-GFP construct in mammalian cells [696] (upper montage) and the decrease in TMRE fluorescence (lower montage). The time-course of the background subtracted TMRE fluorescence changes are plotted in 6.5C. The gray trace shows the TMRE signal decreasing as the uncoupler is perfused on, signalling a drop in the mitochondrial membrane potential. The cytosolic signal should increase in fluorescence as TMRE leaves the mitochondria, however this signal was too weak to be measured.

A

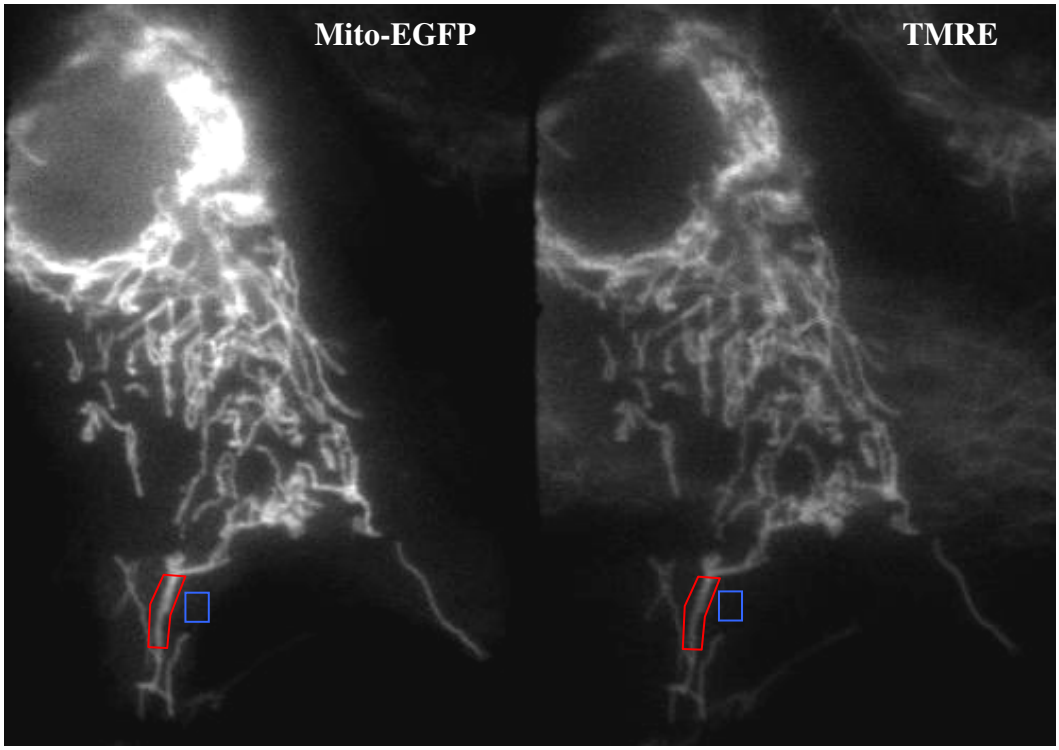

B

EGFP

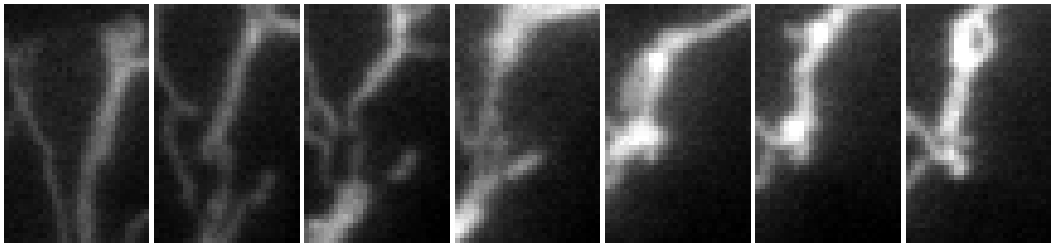

TMRE

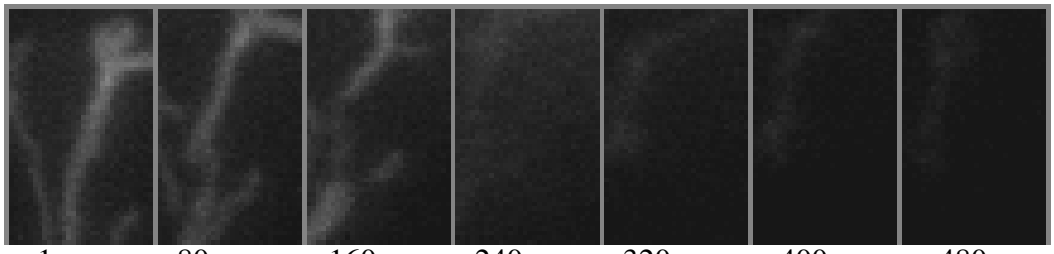

1s 80s 160s 240s 320s 400s 480s

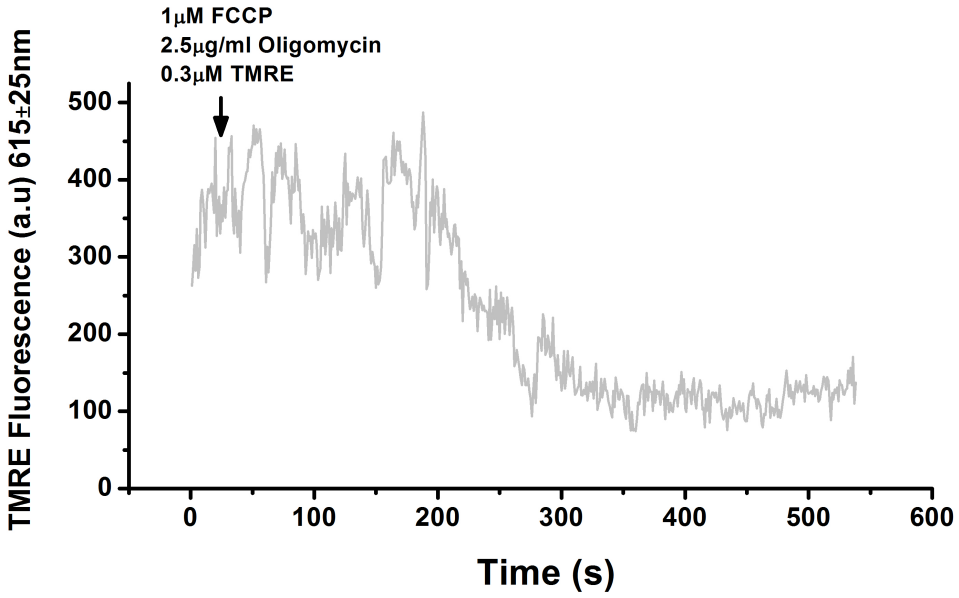

Figure 6.5 FCCP collapses $\Delta\Psi_m$

A *Image of a single HUVEC expressing mito-EGFP 24hours post-nucleofection and loaded with 0.3μM TMRE imaged using the configuration in Figure 6.1. Both fluorophores were excited at 480(7)nm and emitted light was separated using an optical splitting device to be collected at 520±40nm for EGFP and 615±25nm for TMRE. The cell was perfused with 1μM FCCP, 2.5μg/ml oligomycin and 0.3μM TMRE recorded at a time lapse of 1 second to reduce bleaching. The red diagram is the mitochondrial ROI selected for the TMRE and mito-EGFP measurements and the blue diagram the background ROI.*

B *Montage of the red ROI shown in* ***A****, after background subtraction (blue ROI), for mito-EGFP fluorescence (top panel) and TMRE fluorescence (bottom panel), taken every 80s.*

C *Background subtracted time-course of TMRE fluorescence during perfusion of inhibitors added as indicated with the arrow.*

6.4.2 FCCP causes an increase in proregion-mEGFP fluorescence

When cells become exposed to FCCP, the protonophore collapses H^+ gradients across all membranes. In the case of the WPB the result is a rise in WPB lumen pH and consequently a rise in WPB-targeted mEGFP fluorescence. Figure 6.6 shows an example of a single HUVEC perfused with FCCP /oligomycin for 1min prior to stimulation with 1μM histamine. The top panel shows the background subtracted Fura-2 ratio (black trace) and the first latency distributions of the WPB fusion events (histogram). The time-course of the background subtracted mEGFP fluorescence of a single WPB (indicated by the vertical black arrow in A) is measured in Figure 6.6B. The fluorescence was normalised to the peak fluorescence at the point of fusion. As can be seen the WPB associated mEGFP signal increases slowly while the cell is exposed to FCCP indicating a rise in the WPB pH. This is illustrated in Figure 6.6C which shows the pH_{WPB} time-course derived from the mEGFP fluorescent measurements using the equation in Methods Figure 2.10B. The pH_{WPB} reached during FCCP perfusion calculated between the two black asterisks was pH6.0, increasing from the average resting pH_{WPB} of 5.4 [1]. This value varied between different WPBs presumably due to differences in the buffering capacity of individual WPBs [1]. Figure 6.6D shows the same normalized mEGFP fluorescence trace on an expanded time-scale to highlight exocytosis. A montage of images of the individual WPB undergoing exocytosis is shown in Figure 6.6E. Frames marked with a number correspond to the numbers with arrows in red in B and the red asterisk corresponds to the time-point of fusion indicated with a red asterisk in D.

Detection of the point of WPB exocytosis relies on the flash of light caused by the abrupt increase in mEGFP fluorescence during fusion. Under conditions of

FCCP exposure, although the mEGFP fluorescence change is smaller in amplitude, it was still adequate to mark the point of exocytosis.

6.4.3 FCCP treatment blocks mitochondrial Ca^{2+} uptake

Having established that FCCP efficiently transports protons and collapses the $\Delta\Psi_m$, I then went on to confirm the effect of FCCP on agonist evoked $[Ca^{2+}]_m$ changes. A short (1min) and a long (10min) duration of pre-treatment with FCCP/oligomycin was used prior to histamine stimulation, in order to determine the time-course for the effects of these inhibitors on mitochondrial Ca^{2+} uptake. Figure 6.7 shows the effects of a 1min and 10min pre-treatment period on $[Ca^{2+}]_i$ and $[Ca^{2+}]_m$. In both cases (1 and 10min), the inhibitors abolished the mitochondrial Ca^{2+} uptake (Figure 6.7). The noisier Fura-2 signal seen with the 10min recordings was due to a reduction in the bandwidth of the Fura-2 excitation light from 10nm to 5nm to reduce Fura-2 bleaching during longer recordings.

In order to ensure mitochondrial Ca^{2+} uptake was blocked throughout the cell the X-Rhod-1 fluorescence from several different peripheral ROIs were selected within individual cells. Figure 6.8 shows that the mitochondrial Ca^{2+} uptake produced following stimulation with 1μM histamine is inhibited in all selected ROIs (orange, green and blue trace) in a single HUVEC after treatment with the inhibitors for 10min. Together this data suggests that mitochondrial Ca^{2+} uptake was efficiently blocked under the conditions used. Occasionally the application of inhibitors alone induced some $[Ca^{2+}]_i$ changes (see Figure 6.7B), these are discussed in more detail below.

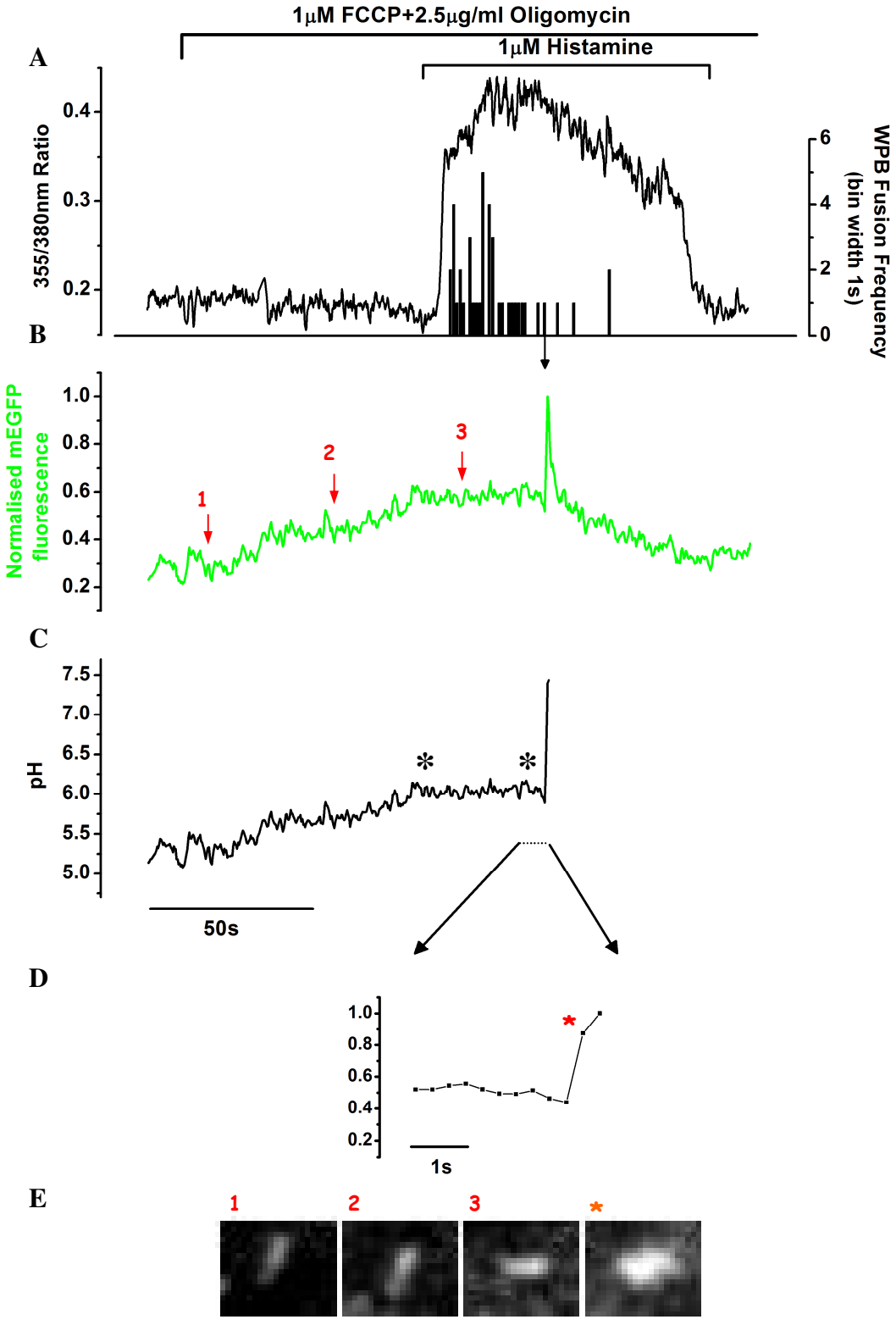
1μM FCCP+2.5μg/ml Oligomycin
1μM Histamine
A
355/380nm Ratio
0.4
0.3
0.2
WPB Fusion Frequency
(bin width 1s)
6
4
2
0
B
Normalised mEGFP
fluorescence
1.0
0.8
0.6
0.4
0.2
1
2
3
C
pH
7.5
7.0
6.5
6.0
5.5
5.0
50s
D
1s
E
1
2
3
*

Figure 6.6 WPBs undergo pH changes due to FCCP action

A single proregion-mEGFP nucleofected HUVEC recorded at 20frames/s (6.66frames/s per wavelength) perfused with 1μM FCCP and 2.5μg/ml oligomycin and stimulated with 1μM histamine. ***A*** *Background subtracted fluorescent traces of Fura-2 (black) and the first latency distribution of the WPB fusion events presented in a histogram.* ***B*** *The normalised mEGFP fluorescence of a single WPB fusion event (arrow from* ***A****) averaged by 2 and* ***C*** *the corresponding intra-WPB pH obtained using the equation described in [1] from the mEGFP fluorescence. The normalised mEGFP trace slowly increases in fluorescence when exposed to FCCP and it reaches a plateau before undergoing exocytosis. The mean* pH_{WPB} *calculated between the two black asterisks is pH6.0.* ***D*** *shows the normalised mEGFP fluorescence on an expanded timescale indicated by the arrows from* ***C****. The montage images of the individual WPB are shown in* ***E*** *averaged by 2 and smoothed. The numbers on the single frames of the montage correspond to the time-points indicated with numbered arrows on the fluorescent time course in* ***B*** *and the red asterisk indicates the frame of fusion corresponding to the time-point marked similarly on the expanded time-scale in* ***D****.*

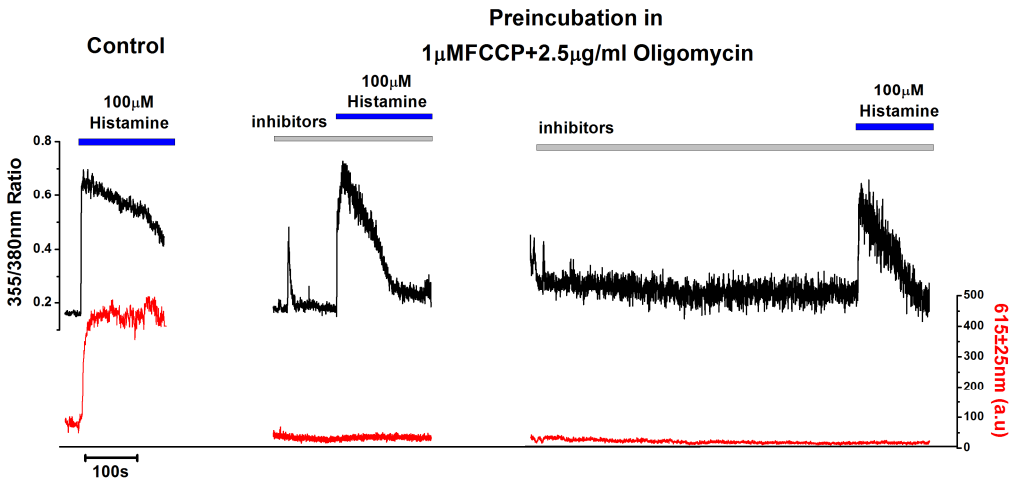

Figure 6.7 FCCP inhibits mitochondrial Ca^{2+} uptake

Single HUVEC loaded with 0.5μM Fura-2 and 0.2μM X-rhod-1 were stimulated with 100μM histamine. The panel on the left shows the un-treated control whereas the middle and right panels were treated with 1μM FCCP and 2.5μg/ml for 1 and 10min respectively before histamine stimulation. The black traces represent the background subtracted Fura-2 ratio and the red traces the background and cytosol subtracted X-Rhod-1 changes. The mitochondrial Ca^{2+} uptake was inhibited in the presence of the drugs.

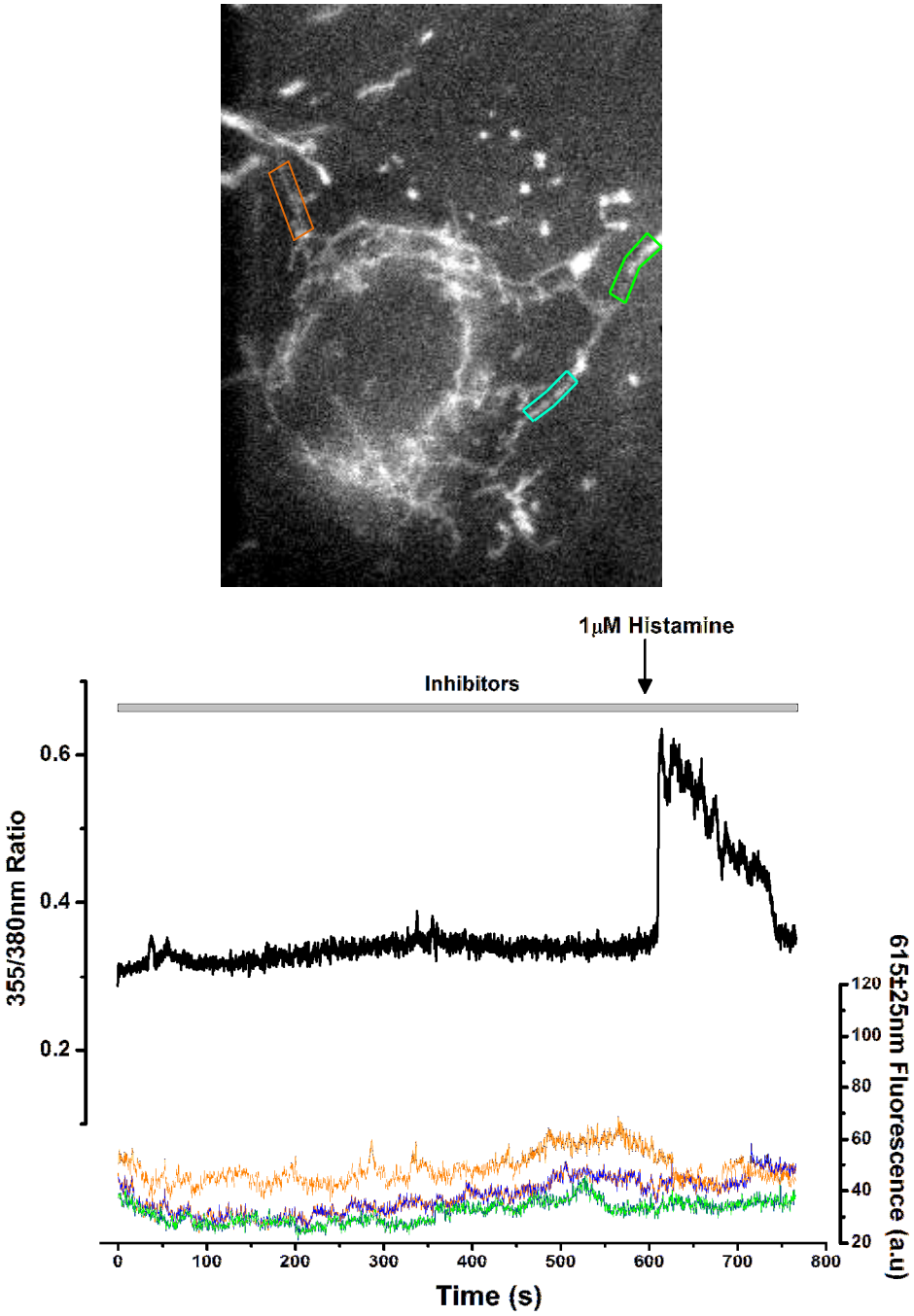

Figure 6.8 The inhibitors prevent mitochondrial Ca^{2+} uptake throughout the cell network of mitochondria

Upper panel shows a single HUVEC loaded with 0.2μM X-rhod-1 and 0.5μM Fura-2 and incubated in 1μM FCCP and 2.5μg/ml oligomycin 10min before stimulation with 1μM histamine. The lower panel shows the Fura-2 fluorescent changes (black trace) and the background and cytosol subtracted X-rhod-1 measurements from the corresponding ROIs shown in the HUVEC picture above (orange, blue and green).

6.5 Measuring $[Ca^{2+}]_m$, $[Ca^{2+}]_i$ and secretion under conditions of mitochondrial Ca^{2+} uptake inhibition

6.5.1 Effect of Inhibition of mitochondrial Ca^{2+} uptake on histamine evoked increases in $[Ca^{2+}]_i$

The mean Fura-2 ratio change obtained with either 1 or 100μM histamine from a number of cells was compared between controls and inhibitor treated cells pre-incubated for either 1 or 10min. Figure 6.9 summaries the effect of the inhibitors on the amplitude of the Fura-2 ratio evoked by histamine. For both 1 and 100μM histamine the amplitude of the Fura-2 ratio change was significantly decreased for 10min pre-incubation time in inhibitors.

6.5.2 Effect of Inhibition of mitochondrial Ca^{2+} uptake on histamine evoked WPB exocytosis

In ~50% of the cases application of the inhibitors alone caused a small $[Ca^{2+}]_i$ change usually in the form of a brief $[Ca^{2+}]_i$ spike (Figure 6.7 middle panel). This was associated with a limited exocytotic response comprising at most ~5.0±3.4% (mean±sd, n=10) of fluorescent WPBs over a 10min pre-treatment period. This effect of the inhibitors would reduce slightly the population of WPBs available for subsequent release by histamine.

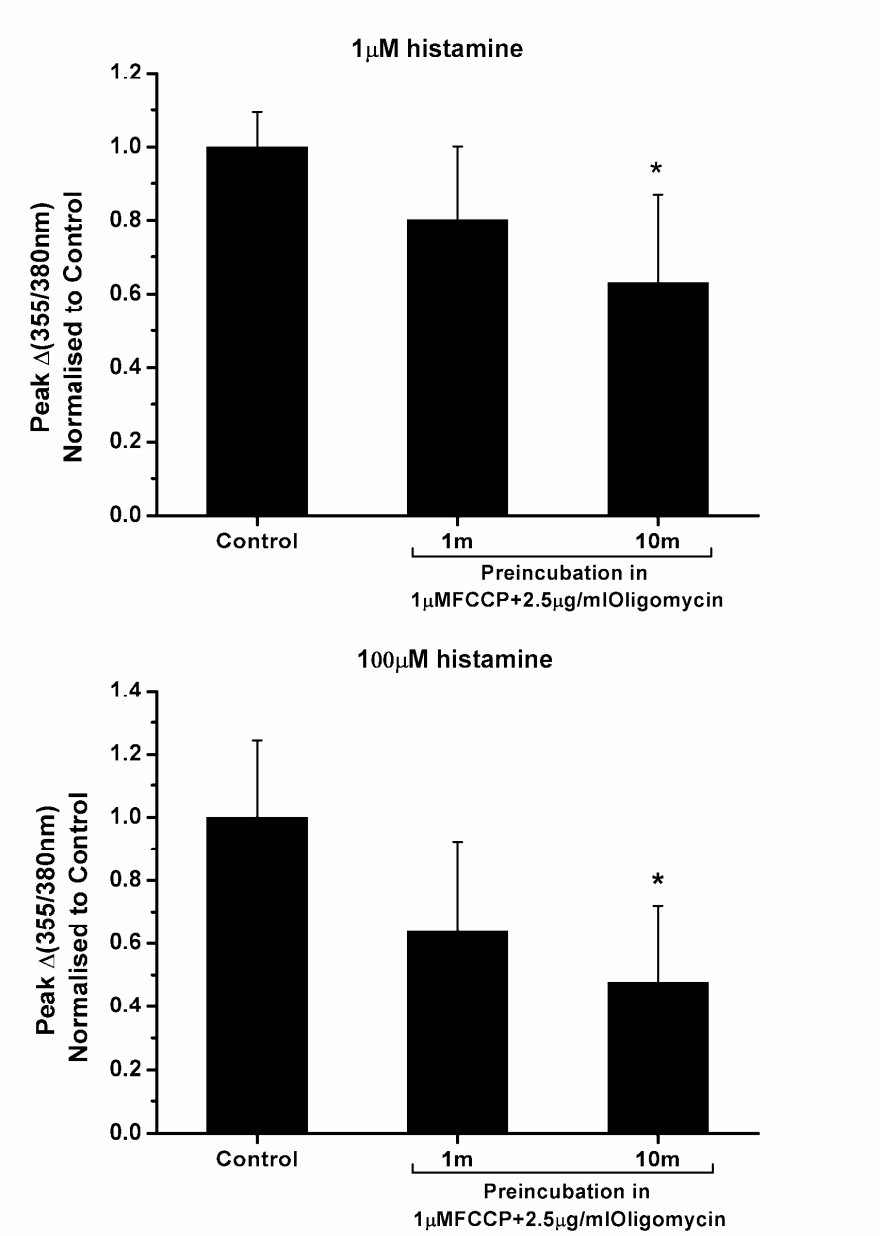

Figure 6.9 Presence of inhibitors decreases the histamine induced $[Ca^{2+}]_i$ changes

Pooled Δ(355/380nm) amplitudes of stimulated Fura-2 fluorescent changes with 1 (upper panel) and 100μM (lower panel) histamine, for un-treated control cells and cells incubated in inhibitors for the indicated time prior to stimulation (mean±sd; n=4-5 cells in each case) normalised to control. There is a significant decrease in stimulated $[Ca^{2+}]_i$ changes when pre-treated with inhibitors for 10min evoked with 1μM (p=0.03) and 100μM histamine (p=0.015).

Figure 6.10 shows histograms of the first latency distributions of the WPB fusion events in control cells and cells stimulated with 1μM (A) or 100μM (B) histamine after 1 or 10min pre-incubation with the inhibitors to partially or completely block mitochondrial Ca^{2+} uptake respectively. The kinetics of WPB exocytosis; delays from the histamine evoked $[Ca^{2+}]_i$ rise (*D2*) (red bars), maximal rates (blue bars) and the percentage of WPB degranulation (green bars) are summarised in the lower panels of Figure 6.10 A and B. Any exocytosis that occurred prior histamine stimulation, during pre-incubation in the inhibitors, is neglected in these calculations in order to selectively study stimulated exocytosis. Following inhibition of mitochondrial Ca^{2+} uptake, there was a reduction in the extent of WPB exocytosis evoked by 1μM histamine for 10min inhibitors pre-incubation ($p=0.058$) and a significant reduction of WPB exocytosis evoked by 100μM histamine for 1 ($p=0.015$) and 10min ($p=0.0014$) pre-incubation in inhibitors.

6.6 Discussion

In this chapter conditions for measuring $[Ca^{2+}]_i$, $[Ca^{2+}]_m$ and exocytosis simultaneously, and conditions for efficiently blocking mitochondrial Ca^{2+} uptake have been determined. Preliminary data from the optical imaging assay suggests a decrease of the extent of histamine-evoked WPB exocytosis when mitochondrial Ca^{2+} uptake was disrupted.

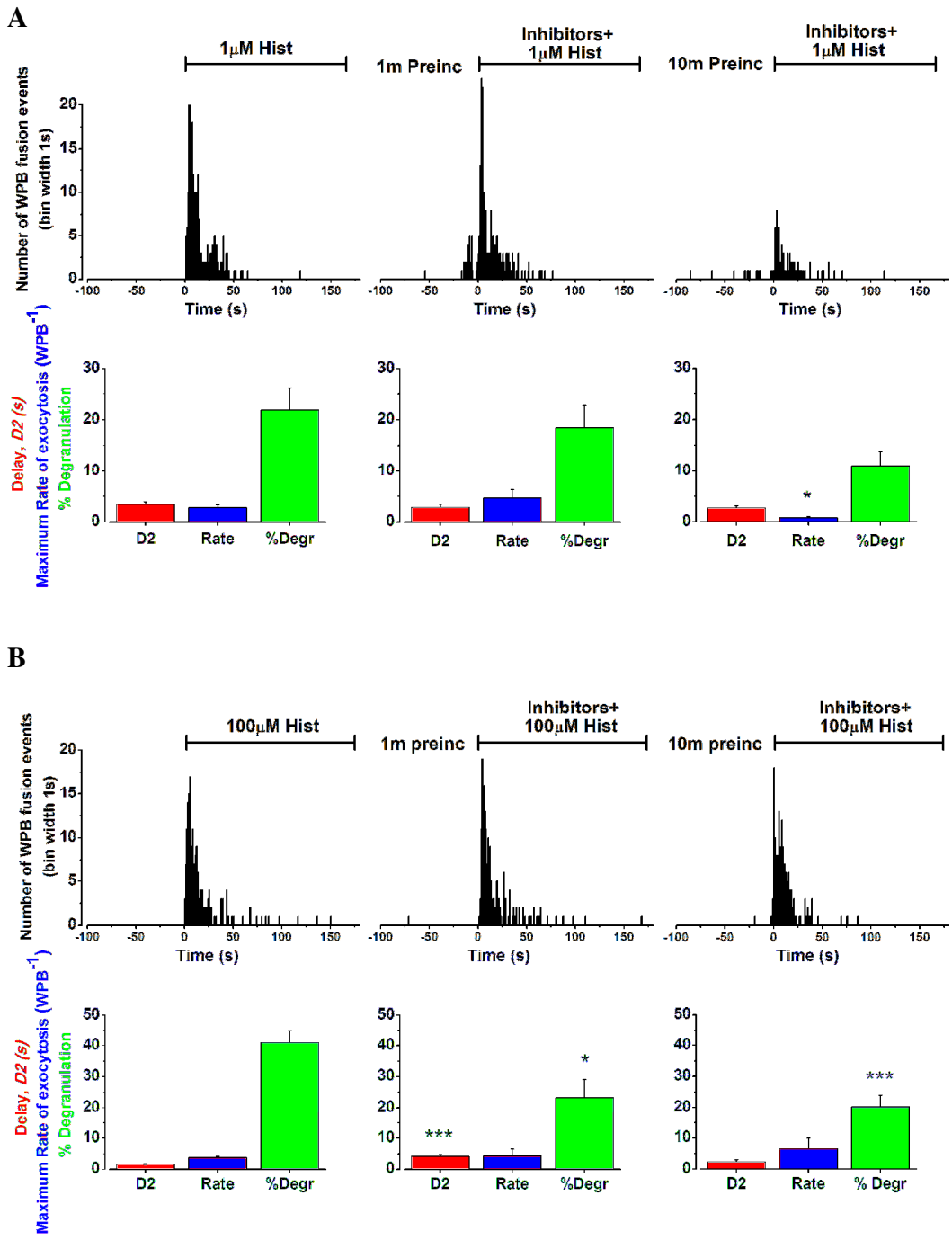
A
1μM Hist
1m Preinc
Inhibitors+ 1μM Hist
10m Preinc
Inhibitors+ 1μM Hist
Number of WPB fusion events (bin width 1s)
Time (s)
Delay, D2 (s)
Maximum Rate of exocytosis (WPB-1)
% Degranulation
D2
Rate
%Degr
*
B
100μM Hist
1m preinc
Inhibitors+ 100μM Hist
10m preinc
Inhibitors+ 100μM Hist
***
*
***
% Degr

Figure 6.10 Summaries kinetics of stimulated WPB exocytosis during mitochondrial Ca^{2+} uptake inhibition.

Summaries the kinetics of WPB exocytosis of proregion-mEGFP nucleofected HUVEC co-loaded with Fura-2 and X-Rhod-1. The upper panels in ***A*** *and* ***B*** *show the first latency distributions of the WPB fusion events (bin width 1s) for control cells (left panels) and cells perfused with 1μM FCCP and 2.5μg/ml oligomycin for 1 (middle panels) or 10min (right panels) prior to 1μM (upper panel) or 100μM (lower panel) histamine stimulation. The lower panels in* ***A*** *and* ***B*** *summary the corresponding delays (D2) from the histamine-evoked $[Ca^{2+}]_i$ rise to WPB exocytosis (red bars), the maximal rates of histamine-evoked WPB exocytosis (blue bars) and the percentage of histamine-evoked WPB degranulation (green bars). In each case the data sets were pooled from 6-16 cells and represent 100-220 WPBs plotted as mean±se.*

6.6.1 Using X-Rhod-1 to measure mitochondrial Ca^{2+}

X-Rhod-1 is a rhodamine-based mitochondrial Ca^{2+} indicator, and was chosen for these studies because it has a low affinity for Ca^{2+} (K_d=700nm) compared to other members of this family of indicators. The lower affinity would help to limit buffering of $[Ca^{2+}]_m$ allowing changes in $[Ca^{2+}]_m$ to be more reliably tracked. Moreover its spectral properties allowed simultaneous measurements with EGFP and Fura-2 (see X-Rhod-1 spectrum wavelengths in Methods Figure 2.15). The main disadvantage of using X-Rhod-1 is that it lacks a spectral shift upon Ca^{2+} binding, precluding ratiometric measurements. Thus the absolute X-Rhod-1 fluorescence change depends on the amount of dye present in different regions of the mitochondrial network, and the thickness of mitochondria. X-Rhod-1 efficiently enters mitochondria (Figure 2.16), and by background subtraction from adjacent regions of cytosol, the $[Ca^{2+}]_m$ changes could be measured independently of $[Ca^{2+}]_i$ changes (Figure 6.3). Using mito-EGFP or mitotracker green it was shown that changes in X-Rhod-1 fluorescence were unlikely to be due to artefacts such as movement or volume changes (Figure 6.2) providing further evidence that the signals seen reflect changes in $[Ca^{2+}]_m$. FCCP inhibited these $[Ca^{2+}]_m$ changes during agonist stimulation (Figure 6.7).

6.6.2 Mitochondrial Ca^{2+} uptake during histamine action in HUVEC

The threshold for mitochondrial Ca^{2+} uptake is estimated to be ~300nM [544-546], with a half maximal (EC_{50}) activation of the uniporter at 10-20μM [698]. This is well within the range of $[Ca^{2+}]_i$ elevations evoked by histamine and thrombin in HUVEC [97, 103, 105]. During stimulation with histamine, changes in $[Ca^{2+}]_m$ occurred with a distinctive time-course. The kinetics of the increase in

$[Ca^{2+}]_m$ comprised a delay after the $[Ca^{2+}]_i$ increase, followed by a slow rise to a maintained plateau. In most cases the increase in $[Ca^{2+}]_m$ persisted after the $[Ca^{2+}]_i$ increase had declined to pre-stimulated levels. Similar kinetics for changes in $[Ca^{2+}]_m$ have been previously observed in a variety of cell types including HeLa cells [550], hepatocytes [563], epithelial cells [554], neurons [546, 553], smooth muscle cells [555] and endothelial cells [549]. Increases in $[Ca^{2+}]_m$ have been shown to be dependent on stimulus strength [546], and this was also the case here, with $[Ca^{2+}]_m$ changes increasing in amplitude above 0.3μM histamine (Figure 6.4).

The sustained $[Ca^{2+}]_m$ signal during stimulation with IP_3-elevating agonists is thought to reflect the high buffering capacity of mitochondria [552], enabling accumulation of large Ca^{2+} loads (up to 36mM) without damage [524]. The main $[Ca^{2+}]_m$ buffer is thought to be phosphate, which forms insoluble Ca^{2+}-phosphate complexes within the mitochondrial matrix [546, 584, 699, 700].

6.6.3 Possible effects of mitochondrial inhibitors on cellular ATP levels

The movement of cellular organelles by molecular motors within the cell, requires energy in the form of ATP (reviewed [701]). Complete or partial ATP depletion could have consequences on Ca^{2+} signalling and the secretory kinetics. Although not quantified here, observation of the motility of mito-EGFP expressing mitochondria or proregion-EGFP labelled WPBs, suggested that transport was not severely altered by exposure of the cells to FCCP and oligomycin, for up to 15min. This suggests that these inhibitors did not cause a severe depletion of cytosolic ATP levels during the experiments. A verification of

this would be by direct measurements of cytosolic ATP concentrations; however this was not carried out here.

6.6.4 FCCP and the fluorescence of WPB targeted EGFP

The fluorescence of EGFP-tagged vesicles and EGFP in the mitochondrial matrix increased upon FCCP exposure indicating a rise in pH within these compartments (sections 6.4.2 and 6.4.3). This provided a useful additional indication that the FCCP had induced proton translocation across cellular membranes in these experiments. The acidic pH_{WPB} is thought to facilitate protein aggregation during granule formation and is important for formation of proregion and vWF as tubules that are responsible for the elongated WPB shape [334]. Increased pH causes the proregion and vWF to dissociate and collapses the WPB shape [35]. FCCP action on the pH_{WPB} did not appear to affect the WPB shape; the likely reason for this is that the increases in pH_{WPB} seen (up to ~pH6.0) was still less than that within the TGN (~pH 6.4) where vWF and proregion are thought to associate [26]. Despite the increase in pH_{WPB} the changes in fluorescence upon WPB fusion were still clearly evident after FCCP treatment and could be used to mark the point of WPB fusion.

6.6.5 FCCP–induced $[Ca^{2+}]_i$ rises

In ~50% of single cells studied exposure to FCCP and oligomycin alone caused a small rise in cytosolic Ca^{2+} levels. An example of such experiment is shown in Figure 6.11B. Why might this be? This phenomenon has been observed in a variety of other cell types and interpreted as leak of Ca^{2+} from mitochondria via the mitochondrial Na^+/Ca^{2+} exchanger (NCE) [562, 702-706]. For instance, in mouse skeletal muscle fibers FCCP caused a continuous increase in basal $[Ca^{2+}]_i$

independent of external Ca^{2+} [562] whereas in endothelial cells uncouplers showed no effect on the steady state $[Ca^{2+}]_i$ [549]. Other pathways by which Ca^{2+} may exit mitochondrial during FCCP action is by transient spontaneous openings of the mitochondrial permeability transition pore (PTP_m) [707].

Alternatively the small FCCP-induced $[Ca^{2+}]_i$ increases may arise from extracellular Ca^{2+} entry. FCCP is reported to reduce cytosolic pH [708]. The molecule responsible for the control of intracellular pH in EC is the Na^+/H^+ exchanger suptype 1 (NHE) [709, 710]. Extrusion of intracellular H^+ by the NHE and import of Na^+ is coupled to the activity of the Na^+/Ca^{2+} exchanger (NCE) [305, 711]. The direction of both exchangers depends on the ion gradient across the PM. It has been suggested that during FCCP action, NHE activity is increased to extrude excess protons carried inside the cell by FCCP, leading to an increase of intracellular Na^+. This in turn leads to an increase in the NCE activity leading to an excess influx of extracellular Ca^{2+}. This hypothesis is consistent with work on neurons that showed that FCCP induced an intracellular Na^+ rise [712]. To investigate the origin of the increased $[Ca^{2+}]_i$ seen during exposure to the inhibitors requires further experiments. The reason for only 50% of cells responding in this way is not clear, however it may be due to the cellular heterogeneity in ion channels and $[Ca^{2+}]_i$ responses of EC [713].

6.6.6 FCCP effects on histamine-evoked Ca^{2+} signalling.

The imaging experiments reveal a time-dependent decrease in histamine evoked $[Ca^{2+}]_i$ responses after pre-incubation in FCCP (Figure 6.9). Inhibition of mitochondrial Ca^{2+} uptake is reported to have differential effects on $[Ca^{2+}]_i$ responses in different cell types [557]. The influence of mitochondrial Ca^{2+}

buffering on cytosolic Ca^{2+} responses is thought to be dependent on the position of the mitochondria. Mitochondrial Ca^{2+} uptake near IP_3 channels on the ER (<700nm) [714] is thought to influence the initial kinetics of the $[Ca^{2+}]_i$ response, whereas mitochondrial Ca^{2+} uptake in the subplasmallemal regions influences the sustained and declining phase of $[Ca^{2+}]_i$ responses [573].

At the ER, activation of IP_3-gated Ca^{2+} channels is facilitated by low local Ca^{2+} levels and inhibited by high Ca^{2+} levels [268, 273, 715, 716]. The threshold for activation and inhibition of the IP_3R may vary from one cell type to another and may contribute to periodic fluctuations in cytosolic Ca^{2+} signals such as Ca^{2+} oscillations that are commonly observed in many non-excitable cells [267]. Removal of mitochondrial $[Ca^{2+}]_i$ buffering by uncouplers can lead to an increase in agonist-evoked Ca^{2+} release from the ER such as is seen in hepatocytes [563], pituitary gonadotropes [552] and chromaffin cells [578]; or a decrease in agonist-evoked Ca^{2+} release such as in HeLa cells [564, 717]. These different effects may arise due to a two-fold role of mitochondrial Ca^{2+} buffering on Ca^{2+} signalling mediated via the IP_3R receptor [532]; local Ca^{2+} buffering close to the IP_3R can both suppress or increase IP_3R activation. Suppression of Ca^{2+} release may arise because Ca^{2+} is required for the initial activation of the IP_3R. By buffering Ca^{2+} to very low levels the mitochondria can prevent or reduce the sensitivity of the IP_3R to activation by IP_3. In contrast an enhanced $[Ca^{2+}]_i$ response may arise if local buffering interferes with the mechanism of Ca^{2+}-inhibition of the IP_3R following receptor activation.

At the subplasmallemal level, mitochondria are thought to facilitate capacitative-Ca^{2+}-entry by generating low $[Ca^{2+}]_i$ microdomains and directing in this way the influx of extracellular Ca^{2+} towards the ER for refilling [229, 570,

572, 573]. Depolarised mitochondria may slow the recovery of ER Ca^{2+} levels and thus affect the amplitude and duration of the agonist-evoked $[Ca^{2+}]_i$ rises [573].

6.6.7 FCCP decreases stimulated WPB exocytosis

The imaging experiments described here show a decrease in histamine-evoked WPB exocytosis following inhibition of mitochondrial Ca^{2+} uptake, consistent with the decreased histamine-evoked $[Ca^{2+}]_i$ response. Whether $\Delta\Psi_m$ collapse has any effect on the molecular machinery of WPB exocytosis is not clear. Collapsing $\Delta\Psi_m$ increases mitochondrial ROS production [515] including H_2O_2 which is thought to inhibit the ATPase activity of NSF and consequently inhibit WPB fusion [422] (see 1.8.1 in Introduction for a review of the fusion machinery). Low levels of ROS production have been implicated as vasoprotective, whereas excess levels may contribute to the pathogenesis of vascular disease in diabetes, hypertension and atherosclerosis [589].

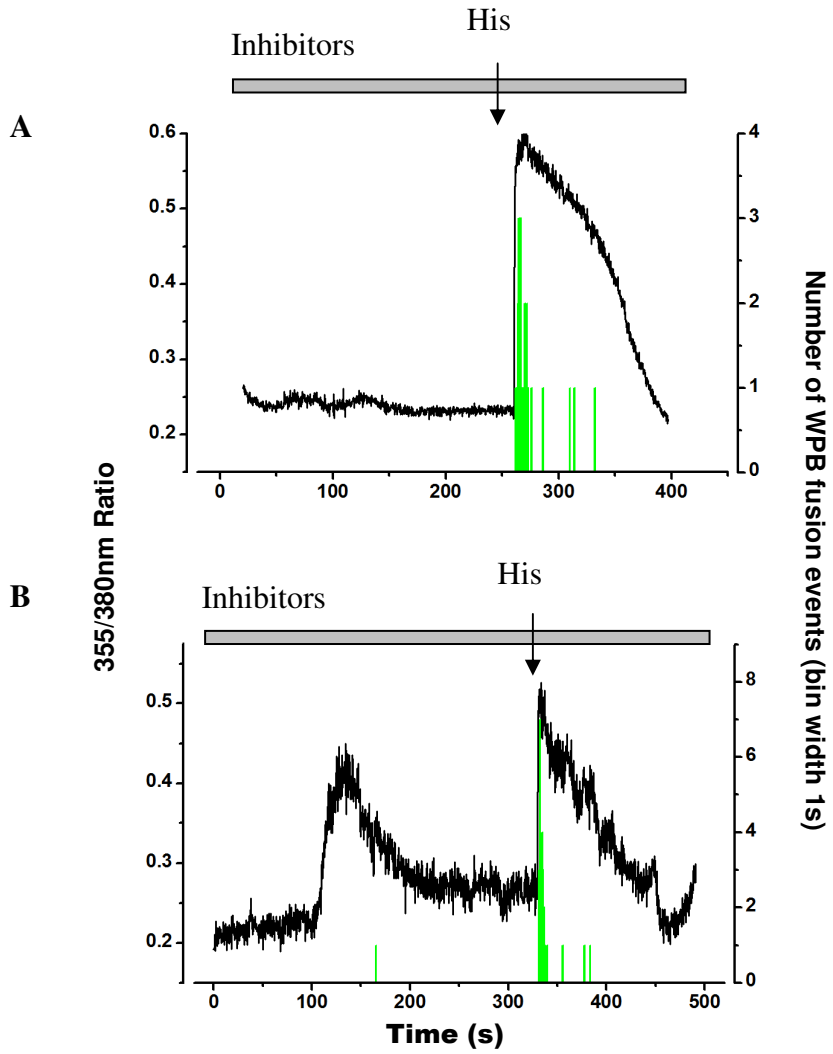

Figure 6.11 Perfusion of inhibitors alone induced exocytosis which correlated to $[Ca^{2+}]_i$ rises

Fura-2 ratio changes (black trace) and number of WPB fusion events (green histograms) of proregion-mEGFP expressing cells perfused with 1μM FCCP and 2.5μg/ml oligomycin for the duration of the recordings and stimulated with 1 or 100μM histamine as indicated with the arrow. ***A.*** *Shows a single cell example where the inhibitors alone did not elicit a change in the Fura-2 ratio fluorescence or WPB exocytosis.* ***B*** *Example where the inhibitors alone elicited an increase in the Fura-2 ratio fluorescence in the form of a slow rise and WPB exocytosis.*

7 Ca^{2+} Oscillations and WPB exocytosis in human endothelial cells

7.1 Introduction

The agonist-evoked $[Ca^{2+}]_i$ response in ECs is biphasic consisting of an initial transient response due to Ca^{2+} release from internal stores and a second phase, dependent on extracellular Ca^{2+} that can be prolonged in the continued presence of an agonist [152, 268]. In Chapter 4 and 5 the early kinetics of WPB and non-WPB exocytosis were described, that result largely from the initial Ca^{2+}-release from the internal stores. During more prolonged exposure to physiological agonists the patterns of Ca^{2+} signalling can take a number of different forms, either a sustained $[Ca^{2+}]_i$ plateau, a return to basal $[Ca^{2+}]_i$ levels, or more commonly $[Ca^{2+}]_i$ oscillations [152, 215]. $[Ca^{2+}]_i$ oscillations can regulate exocytosis in electrically excitable secretory cells [281-283, 718]. In non-excitable cells, early work demonstrated $[Ca^{2+}]_i$ oscillations in hepatocytes [227] and later on in a variety of cell types shown to regulate different cellular processes including glycogenolysis in hepatocytes [227] and cell contraction in smooth muscle cells [288]. In endothelial cells (EC) $[Ca^{2+}]_i$ oscillations, are typically induced by low to medium concentrations of $[Ca^{2+}]_i$-elevating agents such as bradykinin [216, 266], histamine [152], ATP [100, 215] and thrombin [183]. The function of $[Ca^{2+}]_i$ oscillations in EC is not clear however it has previously been suggested that secretory events driven by extracellular Ca^{2+}, such as PGI_2, NO and endothelin may be regulated by $[Ca^{2+}]_i$ oscillations [289]. A possible role of $[Ca^{2+}]_i$ oscillations in the release of secretory granules such as the WPB and the non-WPB population has not been carefully analysed. While a large maintained increase in Ca^{2+} drives WPB exocytosis strongly, brief transient $[Ca^{2+}]_i$ elevations may constitute a mechanism to limit WPB exocytosis, either to help maintain the secretory response for longer periods of time in the face of a limited pool of

secretory granules, or to limit WPB exocytosis altogether. The latter might help to prevent excessive release of vWF under conditions of mild stimulation and help prevent unwanted haemostasis. In one study an attempt to correlate vWF secretion from populations of HUVEC, with single cell measurements from cells within those populations, was interpreted as $[Ca^{2+}]_i$ spikes having little role in driving WPB exocytosis [183].

Parameters of $[Ca^{2+}]_i$ oscillations such as spike amplitude, frequency and duration may be a mechanism for regulating multiple signals for various cellular processes such as observed in other systems [291-294]. In endothelial cells, as in many other cell types, the frequency of $[Ca^{2+}]_i$ oscillations is modulated by agonist concentration suggesting a possible role for frequency modulation of Ca^{2+}-dependent processes [100, 152, 183, 215, 266].

The aim of this chapter was to use direct optical observation of WPB fusion events to try and determine whether $[Ca^{2+}]_i$ oscillations might play a role in regulating WPB exocytosis. This was carried out by simultaneously monitoring $[Ca^{2+}]_i$ and exocytosis, induced by low to medium concentrations of histamine. Technical difficulties in the end meant that a definitive analysis of the relationship between $[Ca^{2+}]_i$ spike frequency and WPB exocytosis was not achieved, however, conditions were identified that might allow such an analysis in the future.

7.2 Histamine evoked Ca^{2+}-oscillations in cultured HUVEC

To observe the patterns of Ca^{2+} signalling in HUVEC, Fura-2 loaded, non-transfected cells were imaged during exposure to different concentrations of histamine using the imaging setup described in chapter 4 (Figure 4.1). The cells were sequentially perfused with physiological saline containing increasing concentrations of histamine, with ~3min intervals between each exposure during which the cells were perfused with stimulus free saline to recover the $[Ca^{2+}]_i$ levels. Examples of $[Ca^{2+}]_i$ responses from three single cells to histamine are shown in Figure 7.1 (0.3, 1, 3 and 10μM for A and B and PS, 0.03, 0.1 and 0.3 for C). The arrows indicate the application (upwards arrow) and removal (downwards arrow) of histamine by perfusion.

At 0.3μM histamine 77% of cells studied (n=70) exhibited $[Ca^{2+}]_i$ oscillations; 13% showed a sustained response and 10% showed a single transient $[Ca^{2+}]_i$ spike that returned to pre-stimulated $[Ca^{2+}]_i$ levels. At 1μM histamine 49% of cells (n=70) exhibited $[Ca^{2+}]_i$ oscillations and the remaining 51% exhibited a sustained $[Ca^{2+}]_i$ response. The proportions of cells showing $[Ca^{2+}]_i$ spikes decreased further as the histamine concentration increased, reducing to 26% (n=70) at 3μM and 10% at 10μM histamine (n=70). In each case the remaining fraction of cells showed a sustained $[Ca^{2+}]_i$ plateau. At 1 and 3μM histamine the $[Ca^{2+}]_i$ oscillations were often fast and superimposed on an elevated $[Ca^{2+}]_i$ level; for example see graphs in Figure 7.1A at 3μM histamine and 7.1B at 1μM histamine.

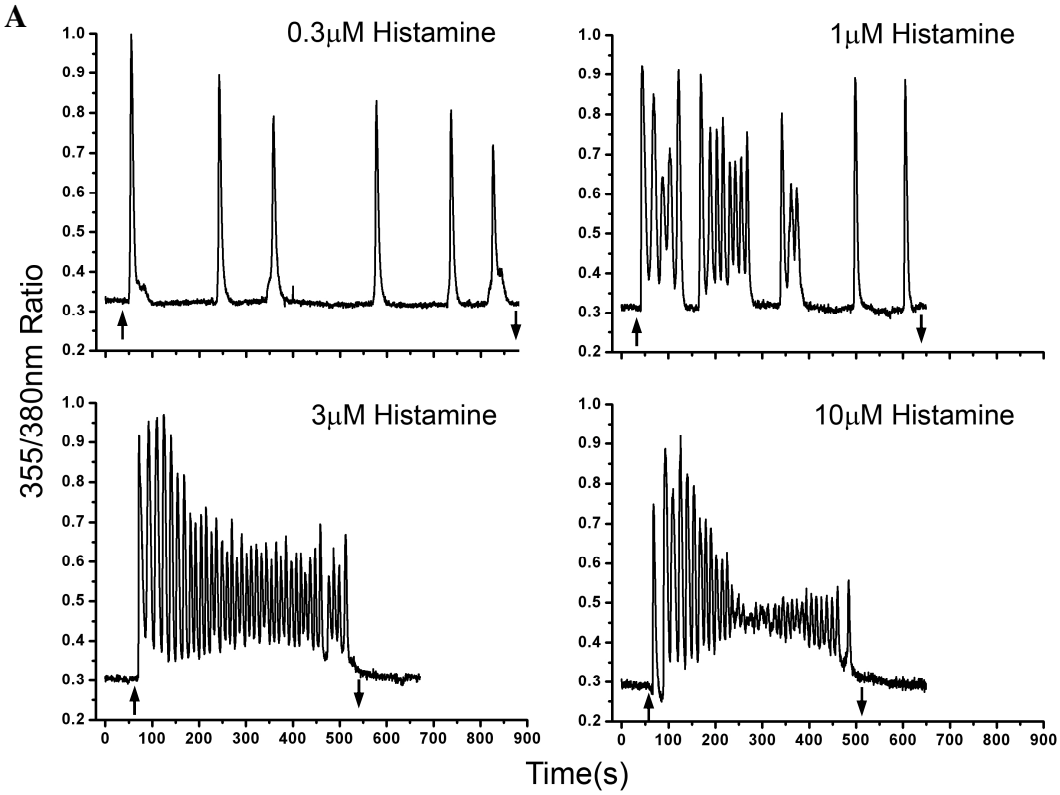
A
0.3μM Histamine
1μM Histamine
3μM Histamine
10μM Histamine
355/380nm Ratio
Time(s)

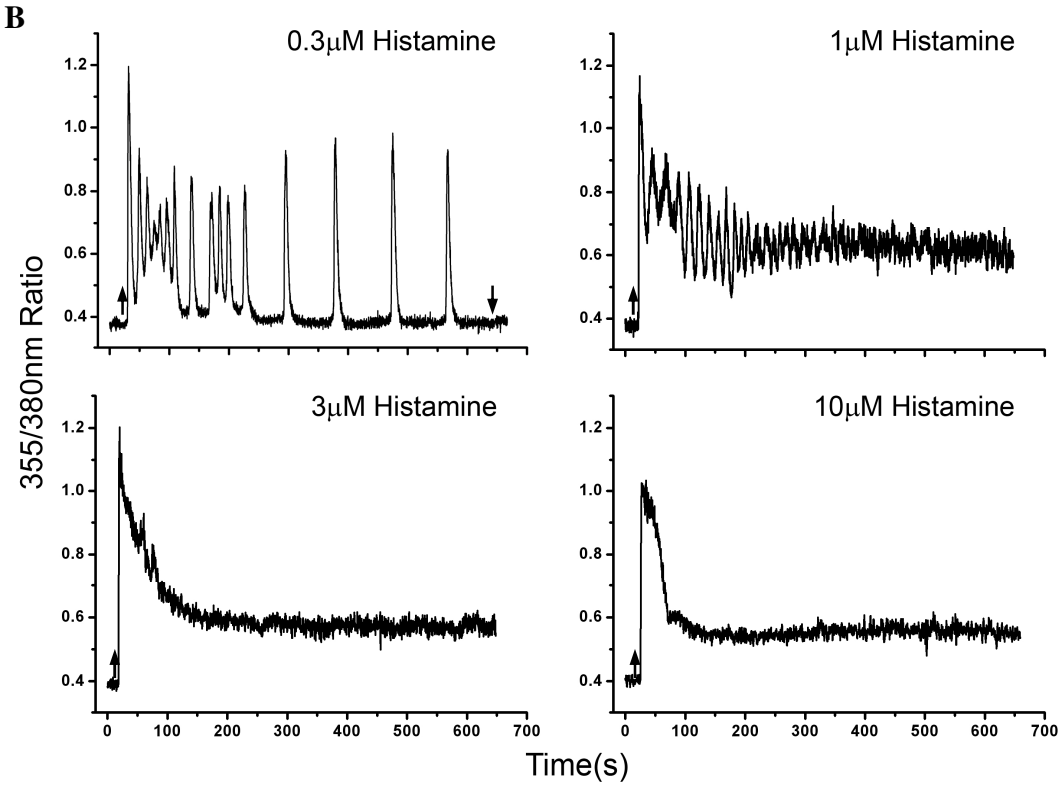
B
0.3μM Histamine
1μM Histamine
3μM Histamine
10μM Histamine
355/380nm Ratio
Time(s)

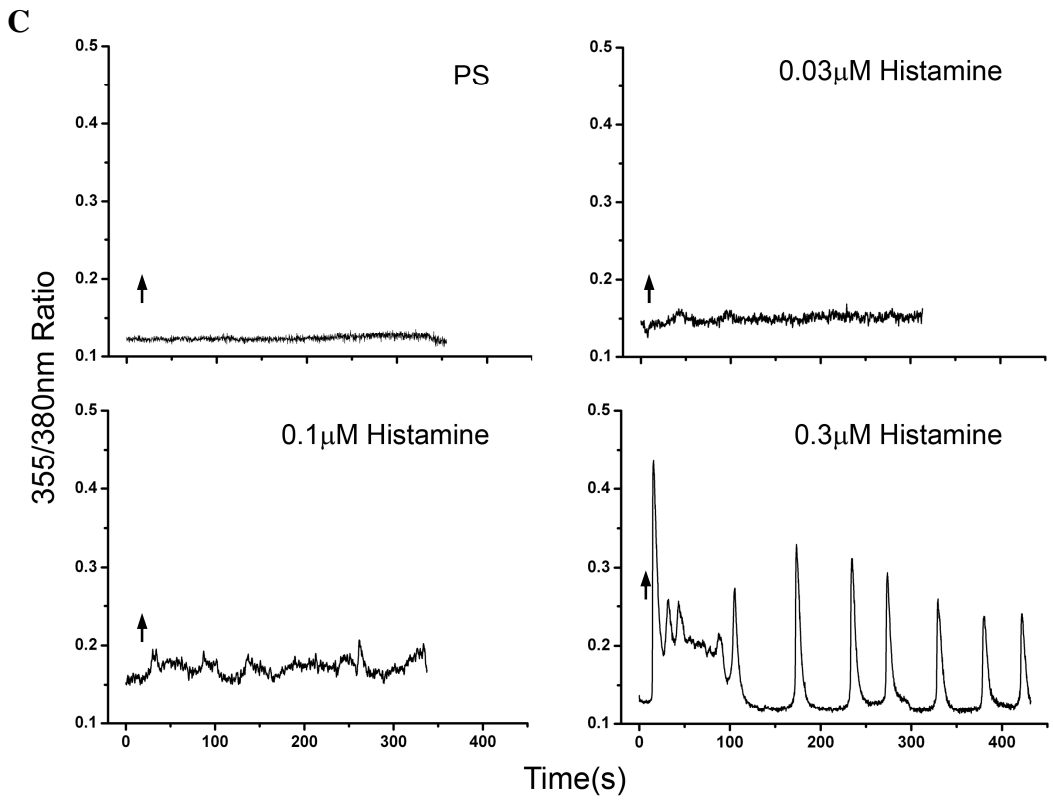

Figure 7.1 $[Ca^{2+}]_i$ patterns generated by continuous stimulation with increasing histamine concentrations within individual HUVEC

*Examples **A, B** and **C** show individual non-nucleofected cells imaged with a 40 times objective, perfused with increasing concentrations of histamine to observe the $[Ca^{2+}]_i$ responses. **A** and **B** are examples of single cells perfused with 0.3μM, 1μM, 3μM and 10μM histamine as indicated, whereas **C** shows an example of a cell perfused with Physiological Saline with no stimulus, 0.03μM, 0.1μM and 0.3μM Histamine as indicated. Between stimulations the cells were washed with no additive physiological saline for a few minutes to bring the $[Ca^{2+}]_i$ levels back to pre-stimulated levels. Spikes were seen at lower concentrations, whereas increased concentrations of histamine evoked higher frequency spikes and/or a sustained plateau. Different patterns of $[Ca^{2+}]_i$ oscillations were observed in different cells. The arrows indicate activation (upwards arrow) and inactivation (downwards arrow) of perfusion.*

Histamine-induced $[Ca^{2+}]_i$ responses recorded by Fura-2 showed a degree of concentration dependence as previously observed [100, 152, 183, 215, 266] and the individual cell $[Ca^{2+}]_i$ responses were very heterogeneous. This may reflect a combination of the source of cells, culture conditions and experimental conditions used.

7.3 Extracellular Ca^{2+}-dependence of the prolonged histamine-evoked $[Ca^{2+}]_i$ phase

The $[Ca^{2+}]_i$ response is biphasic, consisting of an initial phase that reflects release of Ca^{2+} from internal stores and a second extracellular Ca^{2+}-dependent phase [100]. To confirm this, experiments were performed at 0mM extracellular Ca^{2+} in the presence of 0.2mM EGTA, a Ca^{2+} chaletor (Figure 7.2). In the absence of extracellular Ca^{2+} the initial Ca^{2+} spike was mainly unaffected however, the maintained phase of the $[Ca^{2+}]_i$ response was absent.

To investigate the contribution of extracellular Ca^{2+} in defining the time-course of WPB exocytosis, proregion-mEGFP expressing HUVEC were stimulated with 30μM histamine in the presence or absence of extracellular Ca^{2+} (Figure 7.3). In the absence of external Ca^{2+} the delays *D1*, *D2,* and the maximal rates of WPB exocytosis were not significantly different from those in the presence of external Ca^{2+}, suggesting removal of external Ca^{2+} had little effect on the initial kinetics of WPB exocytosis consistent with the initial burst of secretion being due primarily to release of Ca^{2+} from internal stores. However, in the absence of external Ca^{2+}, following the initial burst of exocytosis, there was a more rapid termination (after approximately 30s) and a reduced extent of the secretory response (almost 60% reduction in exocytosis), demonstrating that there

is some dependence on external Ca^{2+} for the low level of WPB fusion seen at longer times.

The observation that WPB exocytosis occurred during the brief transient rise in Ca^{2+} observed in the absence of extracellular Ca^{2+} suggested that WPB fusion might occur during Ca^{2+} spikes seen at lower agonist concentrations. Although the HUVEC used here responded to low histamine concentrations with $[Ca^{2+}]_i$ oscillations, the patterns of $[Ca^{2+}]_i$ oscillations were very heterogeneous. In order to try and study the relationship between Ca^{2+} spikes (in particular their frequency) and WPB fusion, we tried two separate experimental approaches, the first was to simply observe different patterns of Ca^{2+} signalling and to try to correlate WPB exocytosis with Ca^{2+} spiking patterns in single cells. The second was to develop a system in which we could simulate Ca^{2+} spiking patterns in such a way that the inter spike interval could be controlled in a systematic fashion. Together it was hoped that these approaches might help shed light on the role, if any, of Ca^{2+} spikes and in particular the frequency of Ca^{2+} spiking in the regulation of WPB exocytosis. The latter approach was attempted first and will be described next. Technical difficulties with both approaches meant that in the end few hard conclusions could be drawn from these studies.

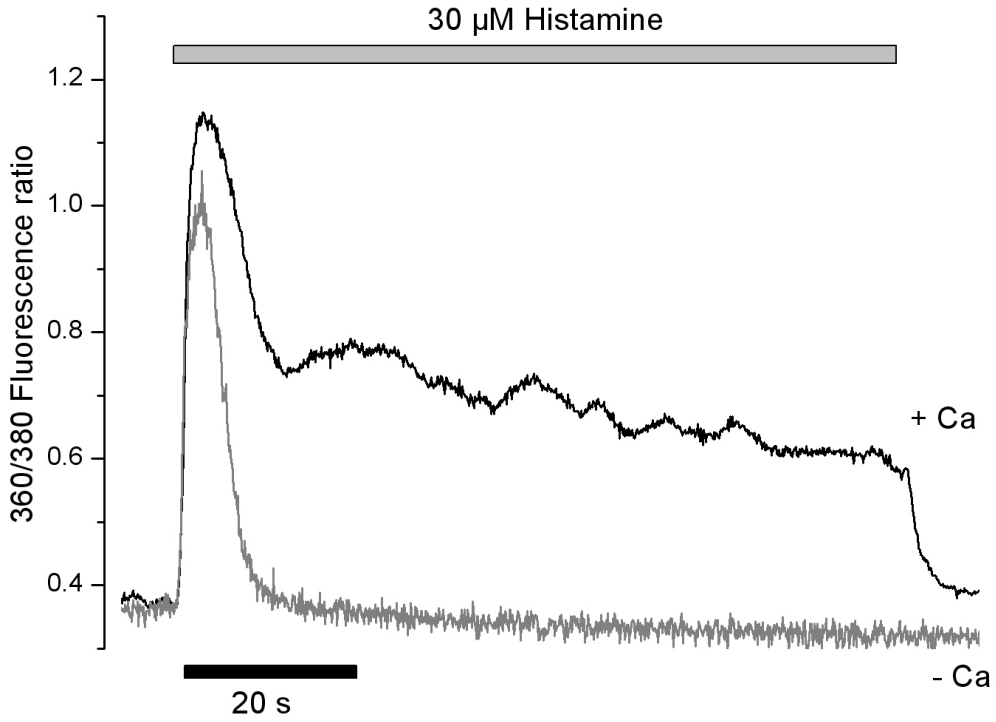

Figure 7.2 The sustained phase of the histamine-evoked $[Ca^{2+}]_i$ response depends on extracellular Ca^{2+}

The Fura-2 traces from two single HUVEC stimulated with histamine in the presence (+Ca; black trace) and absence (-Ca; grey trace) of extracellular Ca^{2+}.

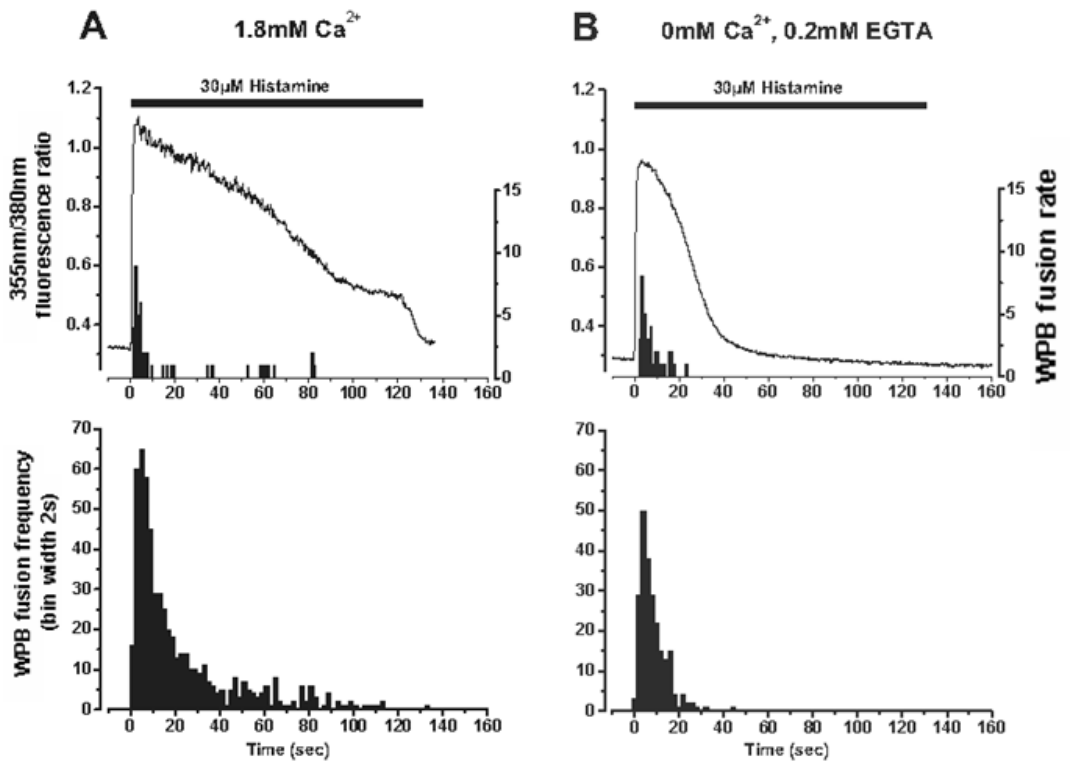

Figure 7.3 Extracellular Ca^{2+}-dependence of histamine-evoked WPB exocytosis.

*Upper panels in **A** and **B** show examples of the changes in Fura-2 fluorescence ratio (355nm/380nm) (solid traces) and the frequency of WPB fusion (solid histograms, bin width 1s) evoked by 30μM histamine in the presence (A) or absence (B; plus 0.2mM EGTA) of 1.8mM external Ca^{2+} in single HUVEC. The Fura-2 traces were offset so that the increase in $[Ca^{2+}]_i$ occurred at time=0. The lower panels in A (n=637 WPB) and B (n=232 WPB) summaries the frequency of WPB fusion determined from the rise in $[Ca^{2+}]_i$ (2s bin widths) for 28 cells in each case.*

7.4 Simulating Ca^{2+} spikes with well defined intervals by controlled puff application of histamine

In order to study the relationship between Ca^{2+} spikes (in particular their frequency) and WPB fusion in intact cells, a system was developed in which transient $[Ca^{2+}]_i$ elevations, mimicking Ca^{2+} oscillations in their size and shape, could be generated with well defined intervals in different cells. To do this $[Ca^{2+}]_i$ spikes were produced by brief periodic application of a $[Ca^{2+}]_i$-raising agonist by a puffer micropipette placed close to the cell. Precise timing for the activation of the puffer pipette was controlled from within WinFluor using the stimulus protocol editor (http://spider.science.strath.ac.uk/sipbs/software_imaging.htm).

Initially ionomycin was used, first because its action is reported to be readily reversible on removal (by perfusion) and second, because it bypasses hormone signalling pathways and thus its use could avoid complications such as receptor desensitization that might arise during hormone action. Figure 7.4A shows the average of 12 Ca^{2+} spikes from 6 cells normalised to the peak amplitude induced during continuous perfusion of 0.3µM histamine onto a single un-transfected HUVEC (black trace). This average time-course was used as a 'reference' waveform for a typical Ca^{2+} spike for comparison with a typical averaged (4 spikes) time-course for the Ca^{2+} spike produced by a 2s puff application of 1µM ionomycin (on a proregion-mEGFP expressing HUVEC (red trace)). Ionomycin produced Ca^{2+} spikes of longer duration (about 70s) than the ones seen with low agonist concentrations (about 20s), even when brief periods of puff application were used (2s) under flow conditions. As a consequence this secretagogue was abandoned.

We then tried histamine although as mentioned above this has the possible drawback of being susceptible to processes such as desensitization during repeated puff application. Different concentrations of histamine (0.3-3μM) were used along with different durations of puff application in order to identify conditions that would elicit a transient Ca^{2+} spike of similar amplitude and time-course to the 'reference' $[Ca^{2+}]_i$ spike (Figure 7.4A). Puff application of 0.3μM histamine for 2s to proregion expressing cells generated Ca^{2+} spikes of amplitudes typically lower than the 'reference' $[Ca^{2+}]_i$ spike (data not shown). Higher concentrations, 1μM and 3μM histamine were then used. Figure 7.4B shows the comparison between the reference Ca^{2+} spike and a typical Ca^{2+} spike produced by a 10s puff application of 3μM histamine (on a proregion-mEGFP expressing HUVEC (red trace)). Application of 3μM histamine for 10s generated Ca^{2+} transients of longer duration than the reference Ca^{2+} spike, however, a shorter period of application, 2s, did produce transient Ca^{2+} increases with a similar time-course to the reference spike (Figure 7.4C). This condition, 2s puff duration of 3μM histamine, was then used in subsequent experiments to try and generate repetitive brief Ca^{2+} spikes with well defined intervals in the range seen during continuous hormone action.

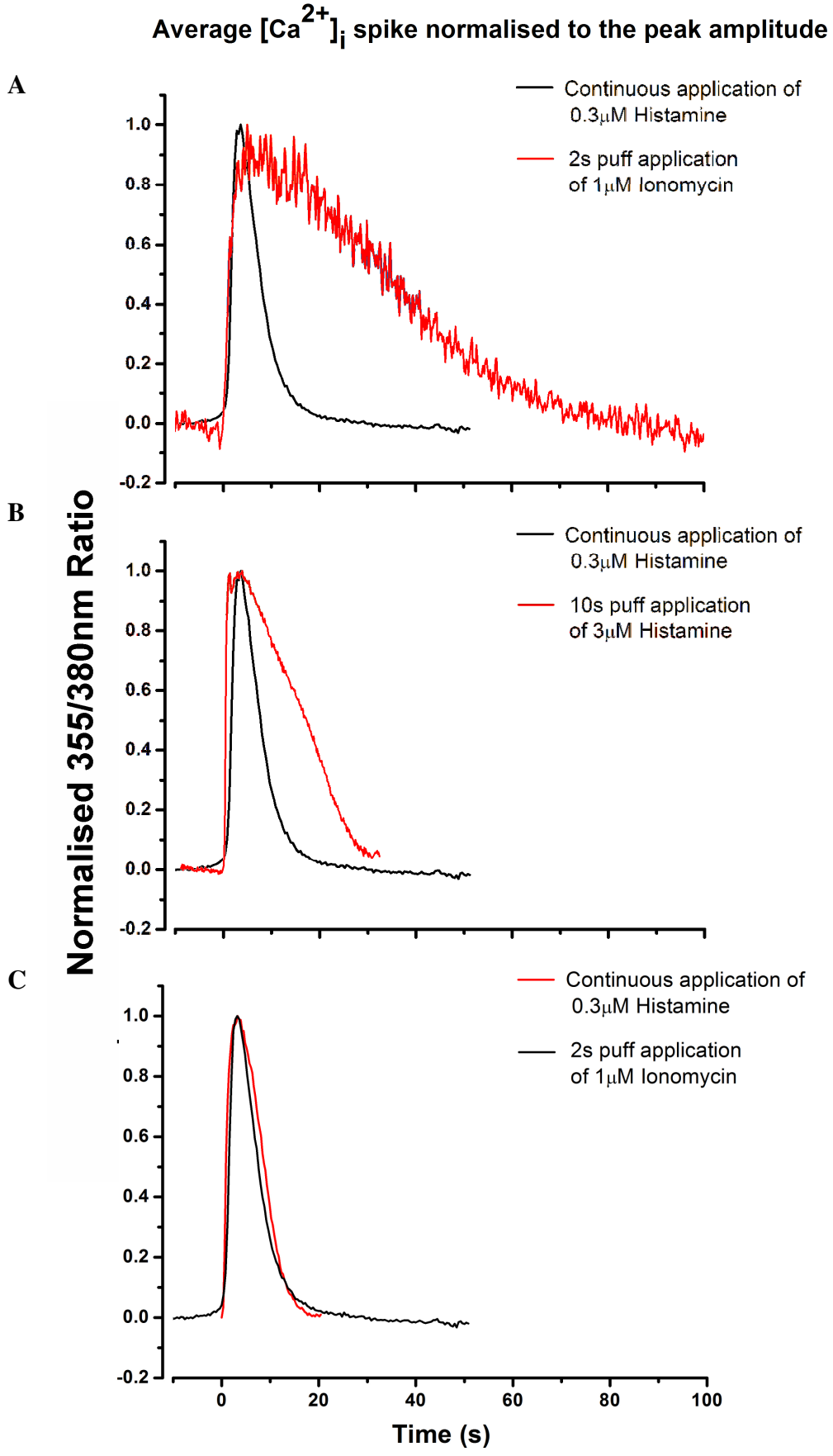
Average [Ca2+]i spike normalised to the peak amplitude
A
B
C
Continuous application of 0.3μM Histamine
2s puff application of 1μM Ionomycin
Continuous application of 0.3μM Histamine
10s puff application of 3μM Histamine
Continuous application of 0.3μM Histamine
2s puff application of 1μM Ionomycin
Normalised 355/380nm Ratio
Time (s)
1.0
0.8
0.6
0.4
0.2
0.0
-0.2
0
20
40
60
80
100

Figure 7.4 The time-course of Ca^{2+} spikes produced by continuous or puff application of ionomycin or histamine

*The black trace in **A, B** and **C** is the average time-course of 12 typical Ca^{2+} spikes from 6 un-transfected HUVEC perfused with 0.3μM histamine, normalised to the peak amplitude (reference spike). This is compared to the average Ca^{2+} spike produced by 2s puff application of 1μM ionomycin (**A**; n=4 Ca^{2+}spikes, 1 cell); by 10s puff application of 3μM histamine (**B**; n=4 Ca^{2+} spikes, 1 cell) and by 2s puff application of 3μM histamine on a single cell (**C**; n=5 Ca^{2+} spikes, 1 cell). The Ca^{2+} spikes were normalized to the peak fluorescence level and offset so that the $[Ca^{2+}]_i$ increase occured at t=0.*

Examples of 2s puff applications of 3μM histamine are shown in Figure 7.5. In this Figure $[Ca^{2+}]_i$ spikes produced during continuous application of histamine on un-transfected cells (spikes shown correspond to those produced after the first initial release of Ca^{2+} from the internal store) are compared with those produced by 2s periodic application of histamine by puffer pipette at 60, 120 and 180s intervals onto proregion-mEGFP expressing cells. This demonstrates that with the repetitive puff application method, Ca^{2+} transients can be produced at similar intervals to those produced during continuous hormone action. A feature in experiments where histamine was applied by puffer was a decrease in the amplitude of the second and subsequent Ca^{2+} spikes. This effect was independent of the histamine concentration used (Figure 7.5), and was seen in both proregion-mEGFP expressing and un-transfected cells (Figure 7.6), suggesting the effect is unrelated to possible perturbations in Ca^{2+} signalling due to expression of proregion-mEGFP by Nucleofection.

It is known that $[Ca^{2+}]_i$ spikes in cells perfused with agonists do change in amplitude; typically the first spike is larger than the second, however, subsequent spikes are often of similar amplitude [668]. This is shown in Figure 7.7 (black squares). Qualitatively, the behaviour of Ca^{2+} spikes generated by puff application of histamine was similar, although the amplitude of second and subsequent spikes was on average smaller than those produced during continuous perfusion of histamine (Figure 7.7).

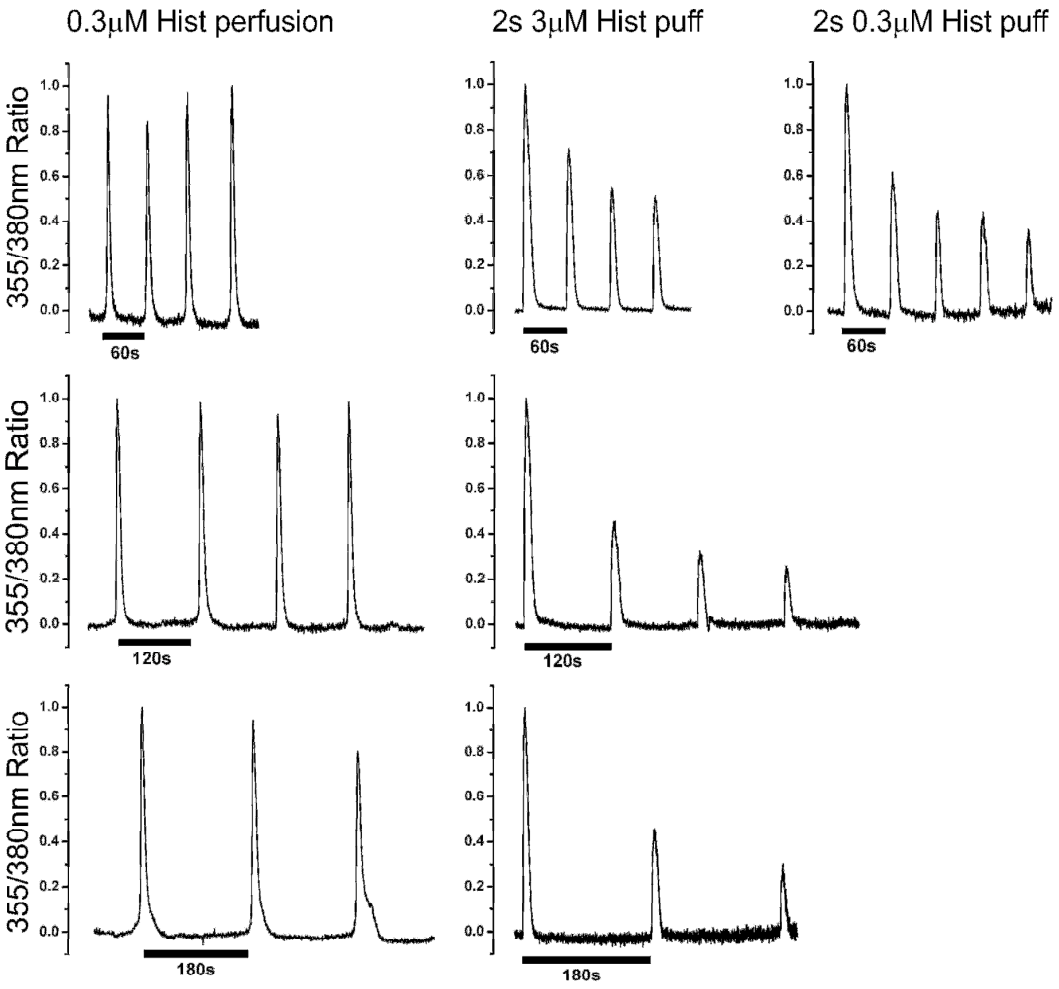

Figure 7.5 Simulating $[Ca^{2+}]_i$ spiking patterns by puff application of hormone.

Single cell representative examples of the normalised Fura-2 ratio changes produced by 0.3μM histamine perfused onto un-transfected HUVEC (left panels) and by 2s puff application of histamine (3μM for the middle panels and 0.3μM for the right panel) onto proregion-mEGFP expressing HUVEC at the defined intervals indicated. Ca^{2+} spikes shown for histamine perfusion (left panels) do not include the initial spike due to release of Ca^{2+} from the internal stores.

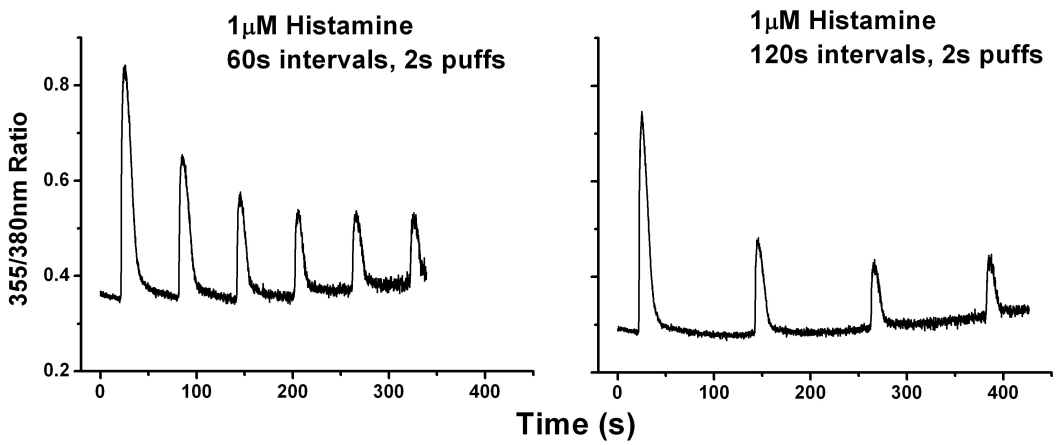

Figure 7.6 Controlled puff application on un-transfected HUVEC is also subject to desensitization

Two representative examples of Fura-2 ratio traces from un-transfected HUVEC stimulated with 1μM histamine at 2s puff applications at 60s (left panel) and 120s (right panel) intervals.

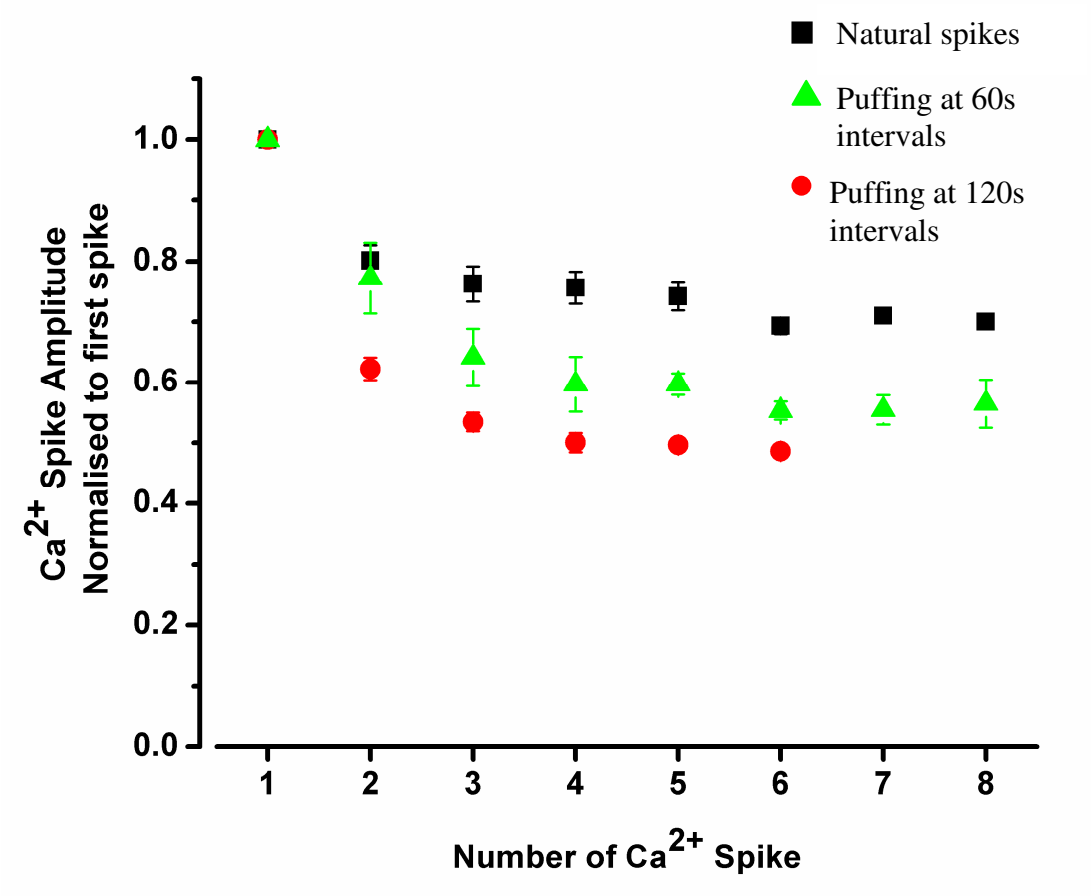

Figure 7.7 Controlled puff application causes a larger drop in the Ca^{2+} spike amplitude between the initial and subsequent spikes than seen during perfusion with histamine

The Fura-2 traces were normalised to the first spike and the peak amplitude of each spike is plotted for cells perfused with 0.3μM histamine (black square; n=9 cells for spike1 and 2, n=7 for spike3, n=6 for spike4, n=5 for spike5, n=3 for spike 6 and n=1 for spike7 and 8); stimulated with controlled puff application of 3μM histamine at 60s intervals (green triangle; n=15 for spike1-4, n=12 for spike 5, n=8 for spike 6, n=5 for spike 7 and n=4 for spike8) and at 120s intervals (red circles; n=13 for spike1-4, n=7 for spike 5 and n=4 for spike 6).

Having established that puff application could in some way mimic Ca^{2+} spikes produced by perfusion of histamine while allowing control over the interval between the spikes we next tried to determine if WPB exocytosis occurred during these artificial spikes. Figure 7.8 shows a representative example of the Fura-2 ratio change and the WPB exocytotic responses pooled from 12 cells stimulated with 3μM histamine at 2s puff applications with an interval of 60s (A) or 120s (B), typical of the intervals seen with continuous perfusion with low histamine concentrations (e.g. Figure 7.5). There was a consistent burst of secretion correlating with each Ca^{2+} spike, however on average the number of WPB fusion events decreased with successive periods of application. This is quantified for these experiments in panels Aiii and Biii. The delay between histamine arrival at the cell and the rise in $[Ca^{2+}]_i$ (*D1*) was relatively stable with repetitive applications of stimulus, as was the delay between the rise in $[Ca^{2+}]_i$ and exocytosis (*D2*), although there was a slight tendency for an increase in *D2* with each spike (panels Aiv and Biv); an effect more obvious for shorter intervals between spikes (60s).

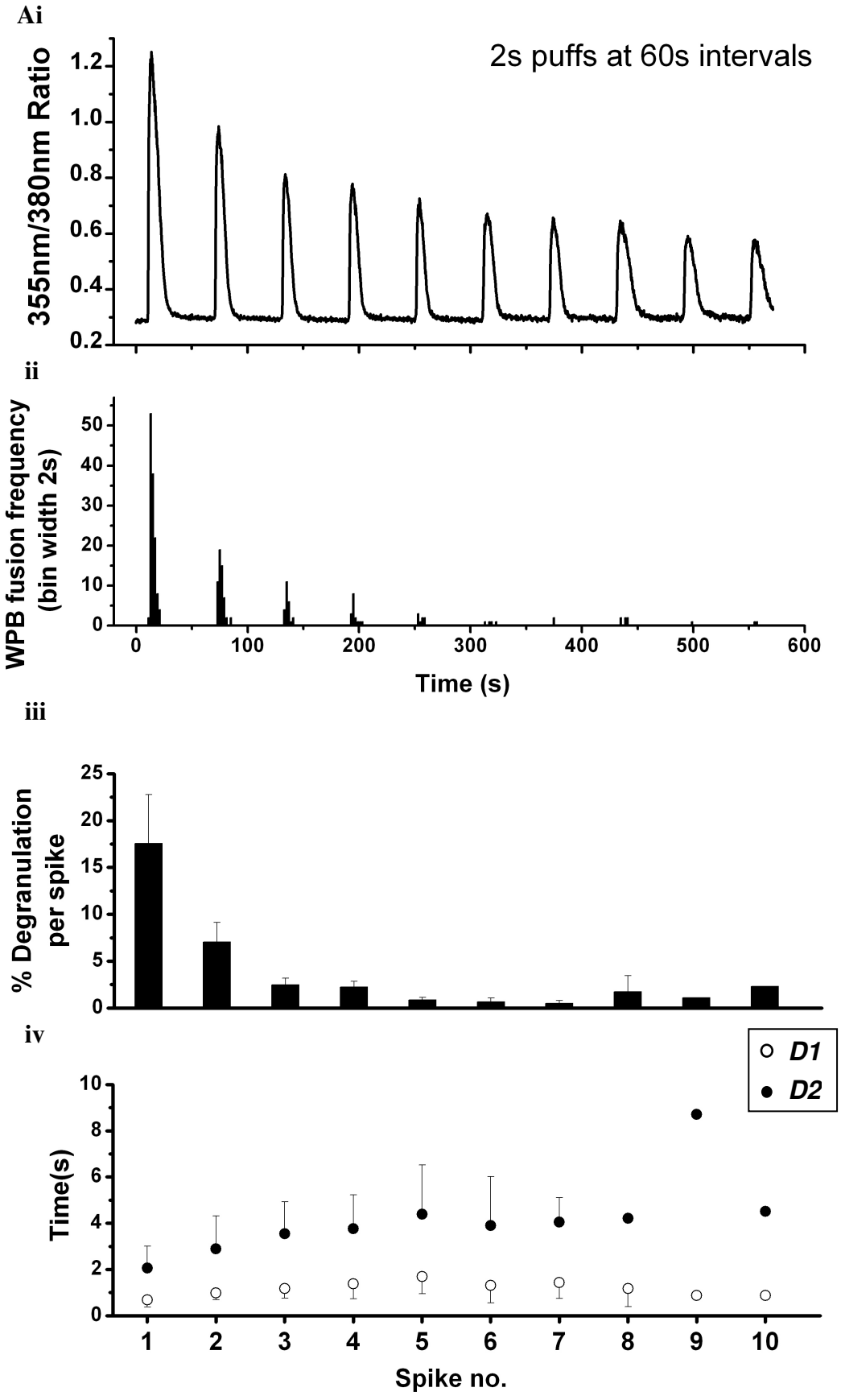
Ai
2s puffs at 60s intervals
355nm/380nm Ratio
1.2
1.0
0.8
0.6
0.4
0.2
ii
WPB fusion frequency
(bin width 2s)
50
40
30
20
10
0
0
100
200
300
400
500
600
Time (s)
iii
% Degranulation
per spike
25
20
15
10
5
0
iv
D1
D2
Time(s)
10
8
6
4
2
0
1
2
3
4
5
6
7
8
9
10
Spike no.

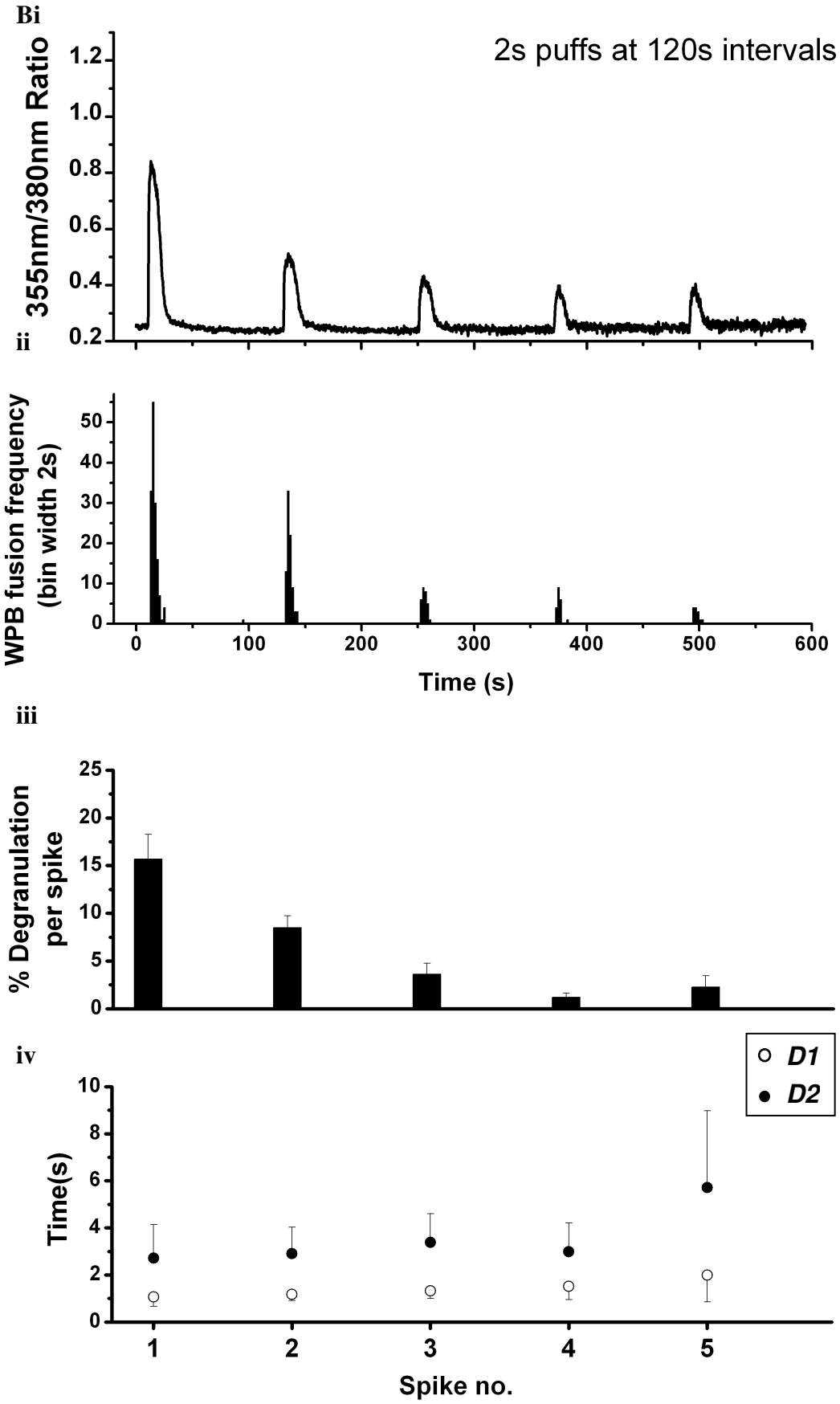
Bi
2s puffs at 120s intervals
355nm/380nm Ratio
1.2
1.0
0.8
0.6
0.4
0.2
ii
WPB fusion frequency
(bin width 2s)
50
40
30
20
10
0
0
100
200
300
400
500
600
Time (s)
iii
% Degranulation
per spike
25
20
15
10
5
0
iv
D1
D2
Time(s)
10
8
6
4
2
0
1
2
3
4
5
Spike no.

Figure 7.8 Pooled secretory responses to controlled puff application of 3μM histamine onto proregion-mEGFP nucleofected HUVEC

Panel **I** *of **A** and **B** show a representative example of the Fura-2 ratio changes induced by puffing 3μM histamine onto proregion-mEGFP nucleofected HUVEC for 2s at 60s intervals (**A**) and 120s intervals (**B**). Panel **II** in **A** and **B** show the first latency distributions of WPB exocytosis in histograms (bin width 2s) from 12 cells in each case. The pooled secretory events were offset so that D2 was maintained for the representative Ca^{2+} response in each case. Panel **III** in **A** and **B** summary the pooled percentage of WPB degranulation at each Ca^{2+} spike calculated from the initial total number of granules for each cell (mean±se; n between 1-12 cells). Panel **IV** in **A** and **B** summary the delays between histamine arrival at the cell and the rise in $[Ca^{2+}]_i$ (D1; open circles) and between the rise in $[Ca^{2+}]_i$ and exocytosis (D2; closed circles) for each spike (mean ±sd; n between 1-12 cells for each value for D1 and D2 in **A** and **B**).*

Although the numbers of WPBs that fused during each Ca^{2+} spike decreased, on average, with increasing spike number, it was noted that in 4 out of 12 cells studied with an inter spike interval of 60s, the numbers of WPBs that fused during the second application of histamine increased, despite the amplitude of the second spike being smaller than the first. Figure 7.9 shows the fusion events observed in the 4 experiments with a representative Ca^{2+} record as reference for the position of the Ca^{2+} spikes produced. The delay from $[Ca^{2+}]_i$ rise to exocytosis (*D2*) decreased in the second spike in 2 examples and remained the same in 1 example out of these 4. Also 3 out of 12 cells studied with a 120s inter spike interval were noted with the same WPB secretion kinetics (not shown).

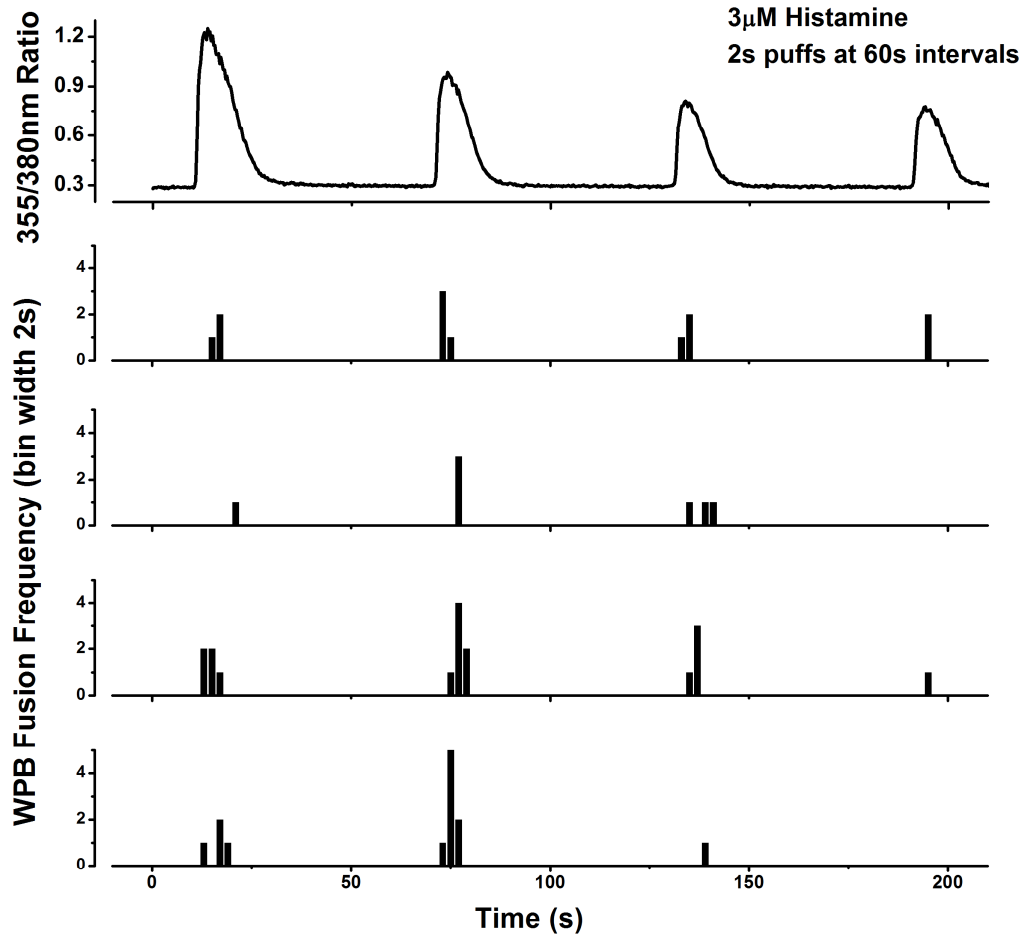

Figure 7.9 Individual single cell examples that responded to controlled puff application of histamine with a larger exocytotic response during the second Ca^{2+} spike than the first

The first panel shows a representative example of the Fura-2 ratio evoked by 2s controlled puffs of 3μM histamine at 60s intervals. The panels beneath show the first latency distribution of the WPB exocytotic response of 4 individual cells.

7.5 Ca^{2+} oscillations and WPB exocytosis in proregion-mEGFP expressing HUVEC during continuous exposure to histamine

There was considerable cell to cell variability in the $[Ca^{2+}]_i$ responses produced during continuous exposure to histamine. Despite this an attempt was made to determine if WPB exocytosis occurs during Ca^{2+} spikes. It was hoped that by analysing a sufficient number of cells it might be possible to correlate the kinetics of WPB exocytosis with Ca^{2+} spike frequency. This proved difficult because it turned out that proregion-mEGFP expressing cells were less likely to show Ca^{2+} oscillation when perfused with low histamine concentrations, than non-expressing cells. In addition, in the proregion-mEGFP expressing cells that did respond with $[Ca^{2+}]_i$ oscillations the shape of the Ca^{2+} spikes appeared perturbed. Figure 7.10 shows examples of single Fura-2 loaded cells perfused with increasing concentrations of histamine and illustrates the patterns of Ca^{2+} spikes in a non-expressing cell with that of cells expressing proregion-mEGFP. The Ca^{2+} spikes in the expressing cells appeared slower to rise, smaller in amplitude, and longer lasting than the spikes in non-expressing cells. The mean time-course of Ca^{2+} spikes, obtained from averaging Ca^{2+} spikes from proregion-mEGFP expressing cells is shown in Figure 7.11.

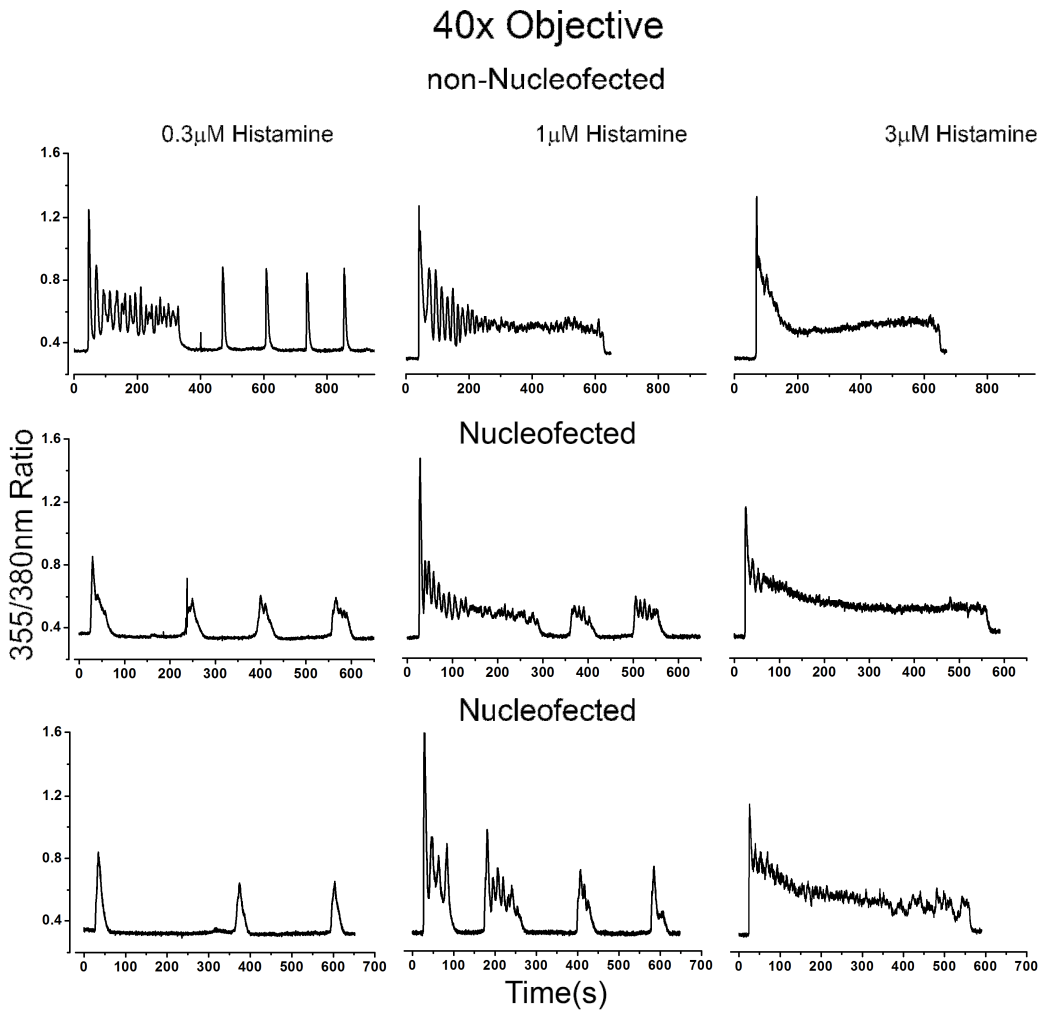

Figure 7.10 Nucleofected HUVEC respond with perturbed $[Ca^{2+}]_i$ oscillations when perfused with increasing histamine concentrations

Fura-2 loaded HUVEC were perfused with increasing concentrations of histamine; 0.3μM (left panels), 1μM (middle panels) and 3μM (right panels) and imaged using a 40 times objective. In each case the stimulus is applied 10-20s after the onset of the recordings and removed 10-20 seconds before the end of the recordings. The top panels represent an example of a single non-nucleofected HUVEC whereas the two below panels represent examples of two proregion-mEGFP-expressing HUVEC. The cells were washed with physiological saline between stimulations to bring the $[Ca^{2+}]_i$ levels back to pre-stimulated levels.

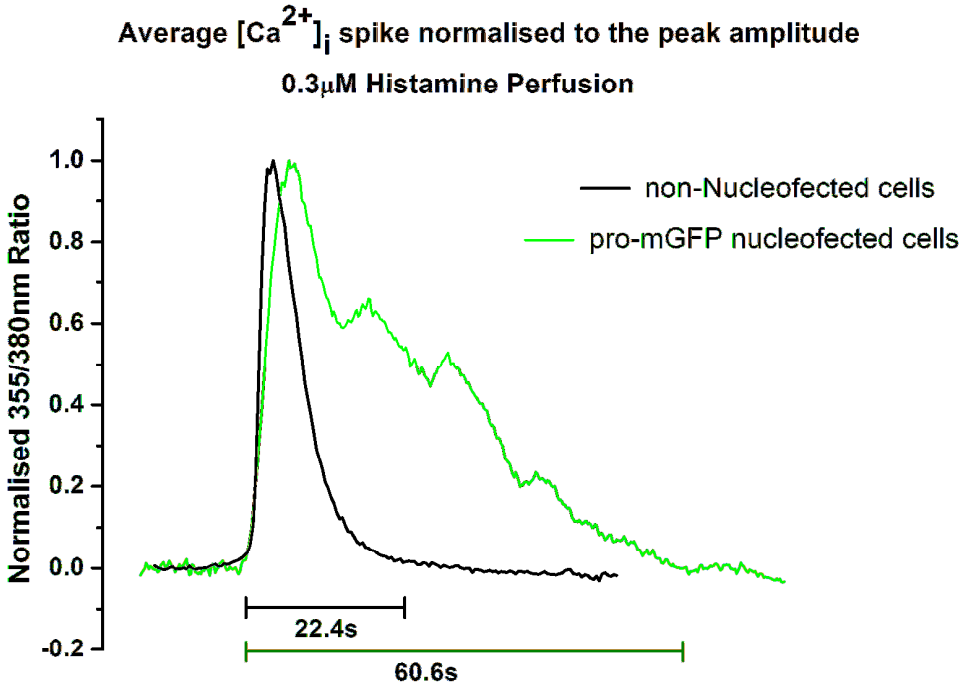

Figure 7.11 $[Ca^{2+}]_i$ spikes of proregion-mEGFP nucleofected cells were of longer duration and have a slower rate of rise than non-nucleofected cells

Averaged Fura-2 ratio Ca^{2+} spikes normalised to the peak amplitude and offset so that the Ca^{2+} rise starts at t=0; for non-Nucleofected cells (black trace; n=12 typical spikes from 6 cells) and for proregion-mEGFP nucleofected cells (green trace; n=7 typical spikes from 5 cells) perfused with 0.3μM histamine. The mean duration of the spikes was 22.4s for the non-Nucleofected cells and 60.6s for the expressing cells.

Why might expression of proregion-mEGFP affect the ability to generate Ca^{2+} spikes and the shape of Ca^{2+} spikes? It could be that the procedure of Nucleofection itself (irrespective of whether a protein is expressed or not) somehow disrupts the processes that determine the size and shape of Ca^{2+} spikes as well as their generation and regulation. To test this HUVEC were nucleofected without plasmid DNA (sham Nucleofection) and 24 hours later cells were perfused with low concentrations of histamine and the ability to produce Ca^{2+} spikes and the shape of the $[Ca^{2+}]_i$ spikes during oscillations was compared to un-transfected cells. The $[Ca^{2+}]_i$ oscillations observed in either case were very similar (Figure 7.12A; upper panel), and the shape, amplitude and rate of rise were the same (Figure 7.12A; lower panel) suggesting that Nucleofection per se was not responsible for the changes seen when proregion-mEGFP was expressed.

This data suggests that protein over-expression is most likely responsible for this effect, although it was not clear if this was a general phenomenon of protein over-expression or an effect specific for the expression of proteins that enter the lumen of the secretory pathway (proregion-mEGFP). To test whether protein over-expression *per se* was responsible for the effects on $[Ca^{2+}]_i$ spikes, HUVEC were nucleofected with cytosolic-GFP (pEGFP-N1) (Figure 7.13), a construct that does not enter the secretory pathway. Cells expressing cytosolic GFP were able to generate $[Ca^{2+}]_i$ oscillations (Figure 7.12B; upper panel) and the shape of the Ca^{2+} spikes was similar to those seen in sham or non-Nucleofected cells (Figure 7.12B; lower panel).

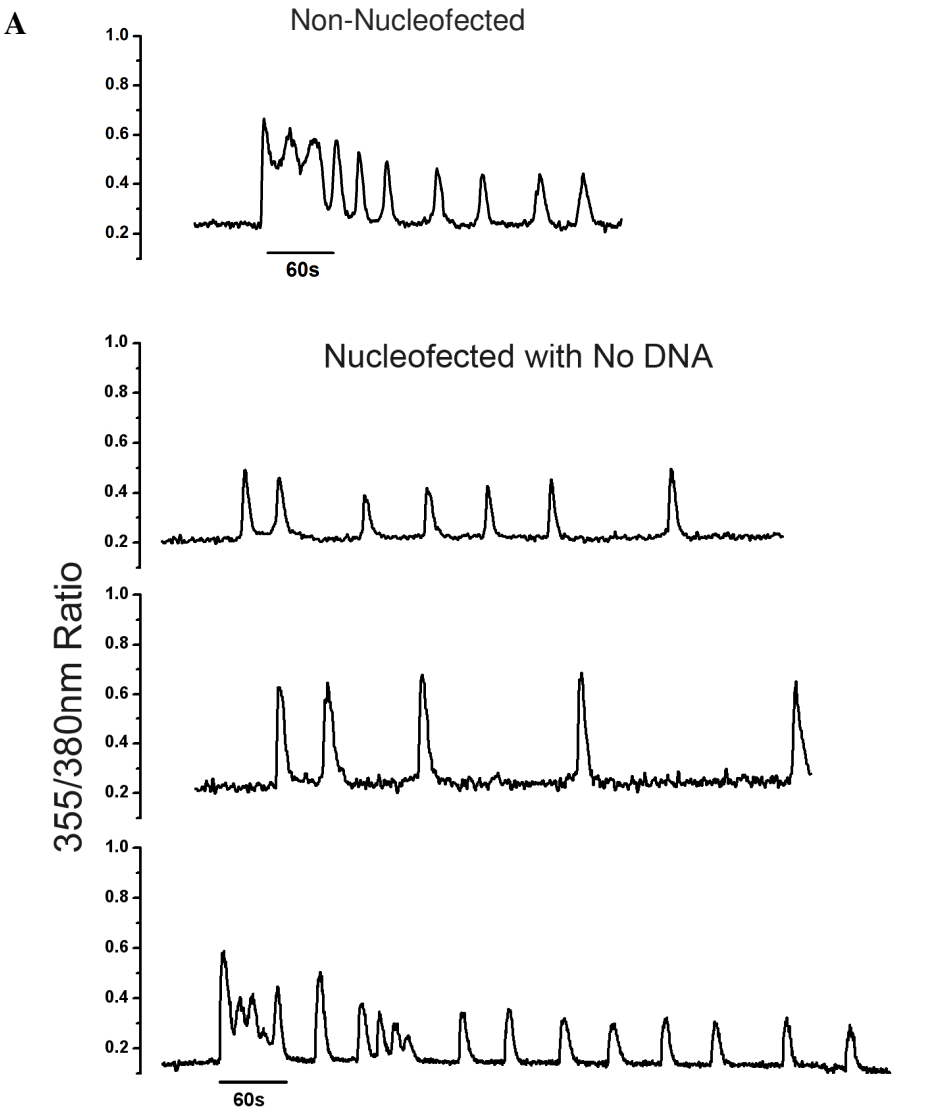
A
Non-Nucleofected
Nucleofected with No DNA
355/380nm Ratio
1.0
0.8
0.6
0.4
0.2
60s

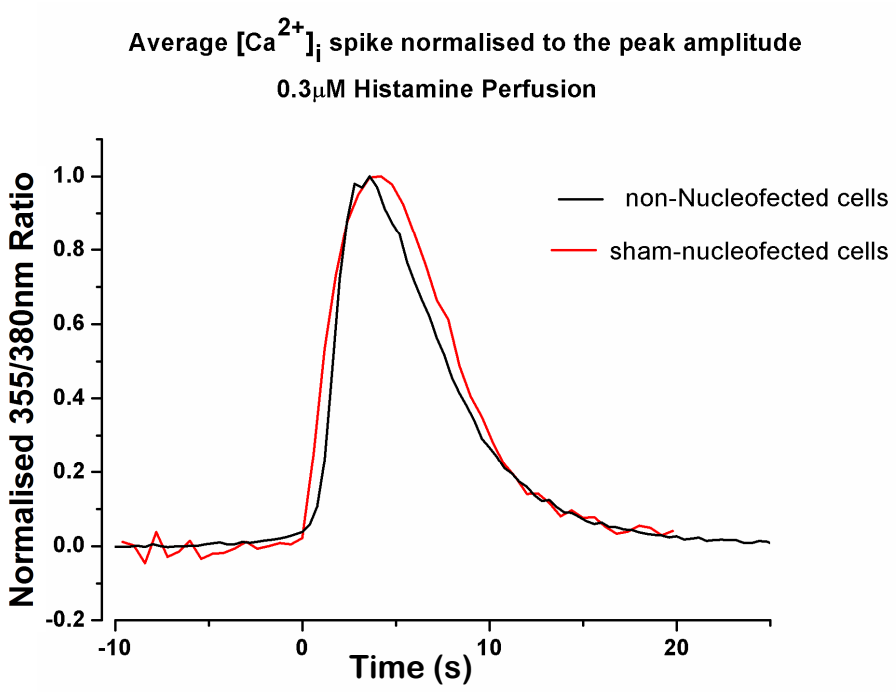
Average [Ca2+]i spike normalised to the peak amplitude
0.3μM Histamine Perfusion
Normalised 355/380nm Ratio
1.0
0.8
0.6
0.4
0.2
0.0
-0.2
-10
0
10
20
Time (s)
non-Nucleofected cells
sham-nucleofected cells

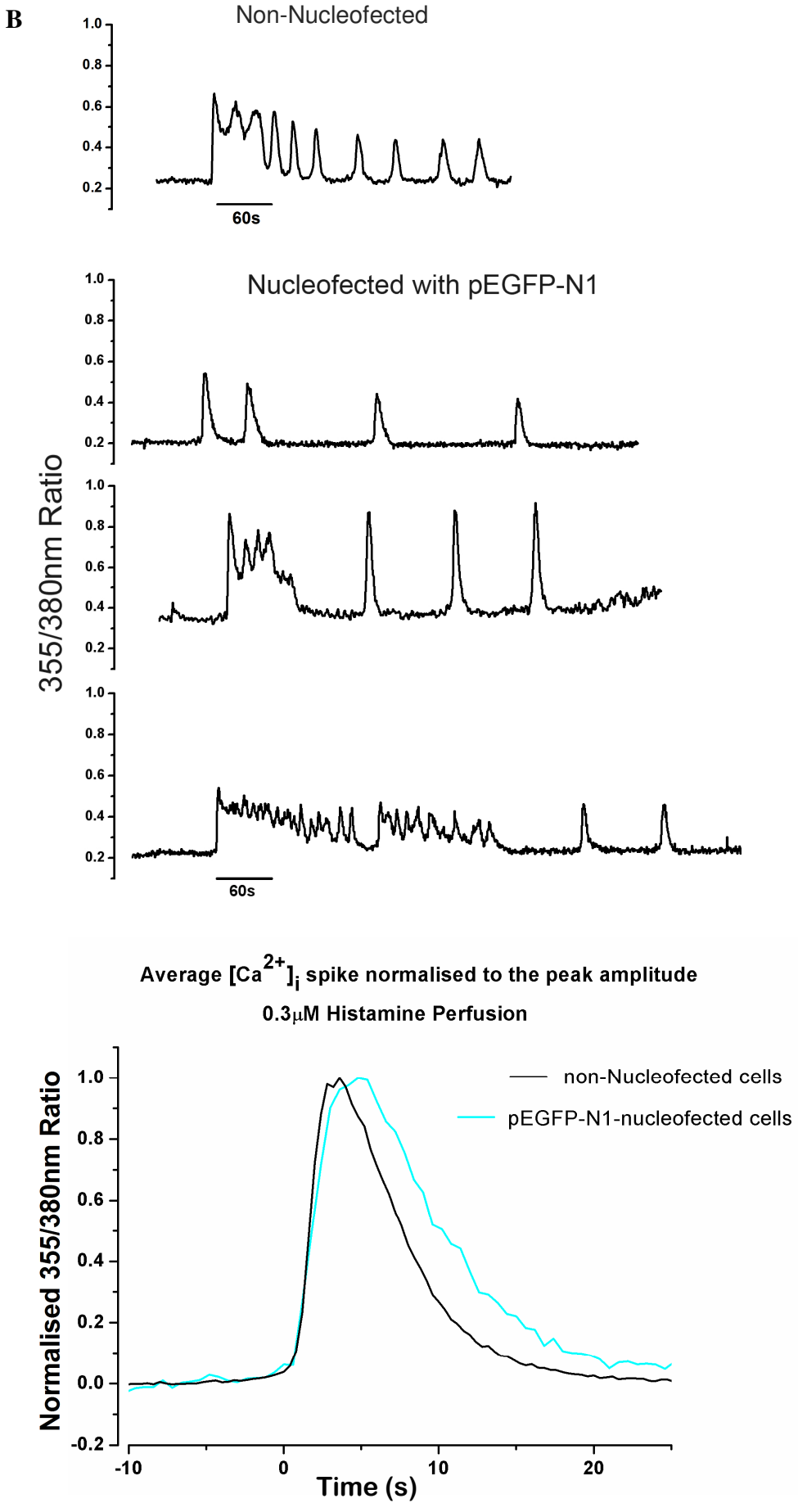
B
Non-Nucleofected
Nucleofected with pEGFP-N1
355/380nm Ratio
60s
60s
Average [Ca2+]i spike normalised to the peak amplitude
0.3μM Histamine Perfusion
non-Nucleofected cells
pEGFP-N1-nucleofected cells
Normalised 355/380nm Ratio
Time (s)

Figure 7.12 Sham nucleofection and pEGFP-N1 nucleofection do not perturb the shape of the Ca^{2+} spikes

*The upper panel in **A** and **B** shows the Fura-2 ratio traces of single cell examples perfused with 0.3μM histamine for sham-nucleofected (**A**) or nucleofected with pEGFP-N1 (**B**) cells compared to un-transfected cells (top trace). The lower panel in **A** and **B** shows the averaged Fura-2 ratio of Ca^{2+} spikes normalised to the peak amplitude and offset so that the Ca^{2+} rise starts at t=0 for non-nucleofected cells in **A** and **B** (black trace; n=12 spikes from 6 cells), sham nucleofected cells in **A** (red trace; n=21 spikes from 6 cells) and pEGFP-N1 nucleofected cells in **B** (cyan trace; n=18 spikes from 11 cells) perfused with 0.3μM histamine.*

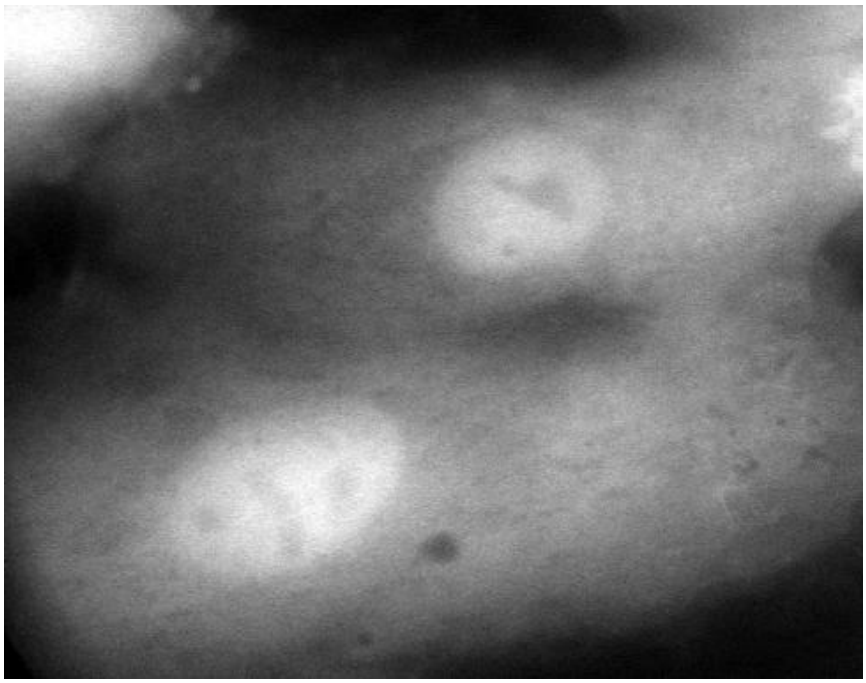

Figure 7.13 HUVEC expressing pEGFP-N1 construct

HUVEC expressing pEGFP-N1 24hours post-nucleofection imaged with a 100x objective

Together this data suggests that over expression of protein specifically within the lumen of the secretory pathway is most likely the cause of the changes in Ca^{2+} spiking and the shape of Ca^{2+} spikes in proregion-mEGFP nucleofected cells in response to low histamine concentrations. The ER, in addition to being the first compartment into which soluble proteins destined for secretion enter, is also the main Ca^{2+} store within the cell, the compartment from which Ca^{2+} spikes arise [214, 215]. A large increase in protein expression within this compartment during expression of WPB targeted mEGFP constructs may well perturb the intra-ER environment leading to changes in Ca^{2+} storage or the processes that generate or regulate $[Ca^{2+}]_i$ spikes (see introduction 1.6.2).

7.6 Ca^{2+} oscillations in Cycloheximide (CHX) treated proregion-mEGFP expressing HUVEC

In an attempt to restore Ca^{2+} spike shape and amplitude in proregion-mEGFP expressing cells, experiments were designed to try and reduce the potential ER stress due to high levels of protein synthesis. Initial efforts were made to circumvent this effect by choosing cells for experiments that had minimal ER fluorescent signal; for example at 72hours post-Nucleofection, a time-point when expression of the plasmid DNA was declining. These cells however, also showed altered kinetics of the Ca^{2+} signalling (not shown). We next tried to reduce protein load on the ER using a reversible inhibitor of protein synthesis, Cycloheximide (CHX). The strategy was to culture cells Nucleofected with proregion-mEGFP for 48hours to allow WPB formation and accumulation, after which the cells were exposed to a short period of treatment with Cycloheximide (CHX). Because WPBs are long-lived organelles it was hoped that a short period of protein synthesis inhibition would not significantly affect the numbers of

fluorescent WPBs, but might permit the ER to recover from the stress of over-expression of the plasmid construct allowing normal Ca^{2+} signalling to resume. In order to minimise the effect of inhibition of protein synthesis on cellular processes, including exocytosis, we aimed to treat the cells with CHX for as short a time as possible (a few hours, see below). However due to the reversible action of CHX, it was kept in solution for the duration of the experiments.

To check that CHX treatment blocked synthesis of the EGFP-constructs in our cells, we monitored the loss of non-WPBs in cells expressing t-PA-EGFP. Non-WPBs are made continuously but not stored in these cells, so a block in the synthesis of the EGFP construct should result in a total (ER and granule) loss of EGFP fluorescence from the cells. We first tried 3-4hour periods of treatment with 10μM CHX. HUVEC expressing t-PA-EGFP were treated with CHX 4hours post-Nucleofection for a further 4hour period and then imaged. In sham (no-CHX) treated cells a strong ER signal and extensive t-PA-EGFP positive puncta were observed while in the CHX treated cells no granules could be seen and the ER EGFP signal was absent (Figure 7.14). This data indicated an effective block of synthesis of t-PA-EGFP at the CHX concentration and treatment period used.

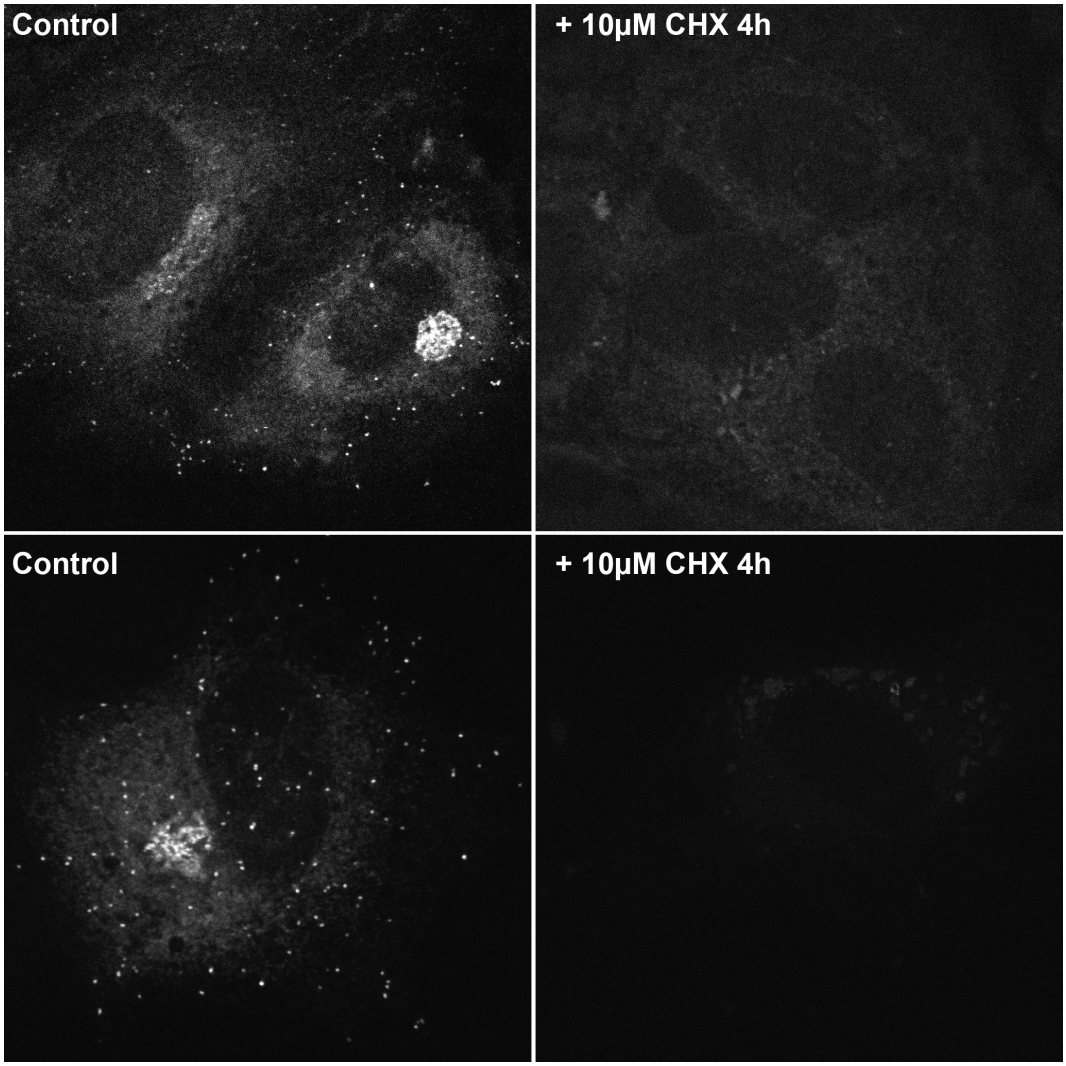

Figure 7.14 Treatment of t-PA-EGFP expressing HUVEC with 10µM CHX for 4hours inhibited t-PA-EGFP protein synthesis

HUVEC were Nucleofected with t-PA-EGFP and 4hours post Nucleofection incubated with or without 10µM CHX for further 4hours and then fixed and imaged.

We next determined if this period of treatment altered Ca^{2+} spiking or the shape of the Ca^{2+} spikes in non-expressing cells. Under these conditions, CHX did not prevent Ca^{2+} spikes evoked by perfusion of histamine and the shape of the Ca^{2+} spikes was similar to un-transfected non-CHX treated cells (Figure 7.15). We next checked proregion-mEGFP expressing cells treated with CHX; here the shape and time course of the averaged Ca^{2+} spike evoked by perfusion with histamine was restored close to that of control (non-Nucleofected) cells (Figure 7.16).

One potential problem with this approach is that inhibition of protein synthesis could have untoward effects on Ca^{2+}-driven processes, such as WPB exocytosis itself, by, for example, a reduction in the levels of some fast turning protein involved in transport, docking, Ca^{2+}-sensing or fusion of the organelle. To test if this were the case, the kinetics of fluorescent WPB exocytosis of proregion-mEGFP expressing HUVEC treated with CHX for 3-4hours were determined and compared to untreated cells, stimulated with a medium (1μM) or high (100μM) histamine concentration. Figure 7.17 summaries the delay from $[Ca^{2+}]_i$ rise to exocytosis (*D2*), the maximal rates of exocytosis and extent of degranulation under these conditions and shows that 3-4hour treatment with CHX had no significant effect on the initial kinetics of histamine-evoked WPB exocytosis.

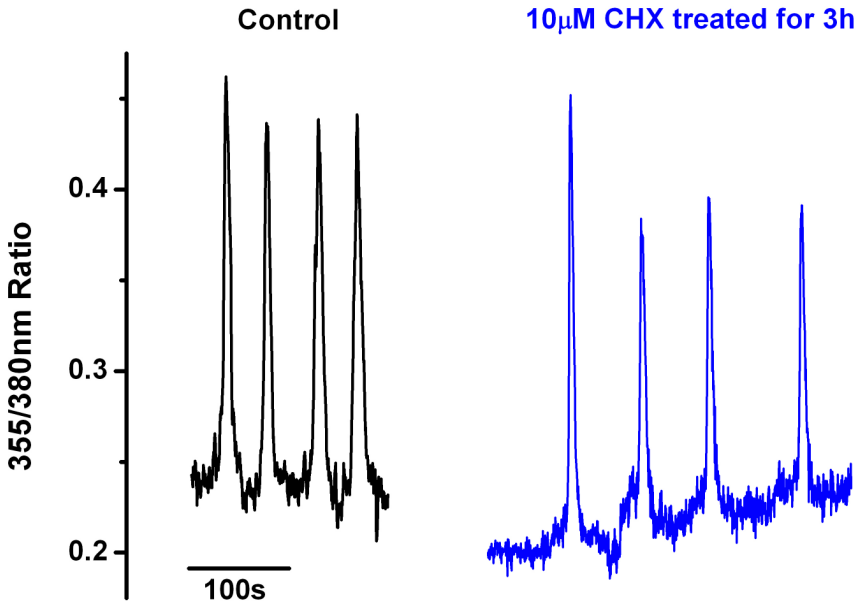

Figure 7.15 $[Ca^{2+}]_i$ responses between non-nucleofected untreated and CHX treated cells were similar

Non- nucleofected single HUVEC were perfused with 0.3μM histamine to observe Ca^{2+} signals. CHX un-treated cells (black) were compared to 10μM CHX treated cells (blue) for 3hours. The CHX was present in the physiological saline for the whole duration of the experiment.

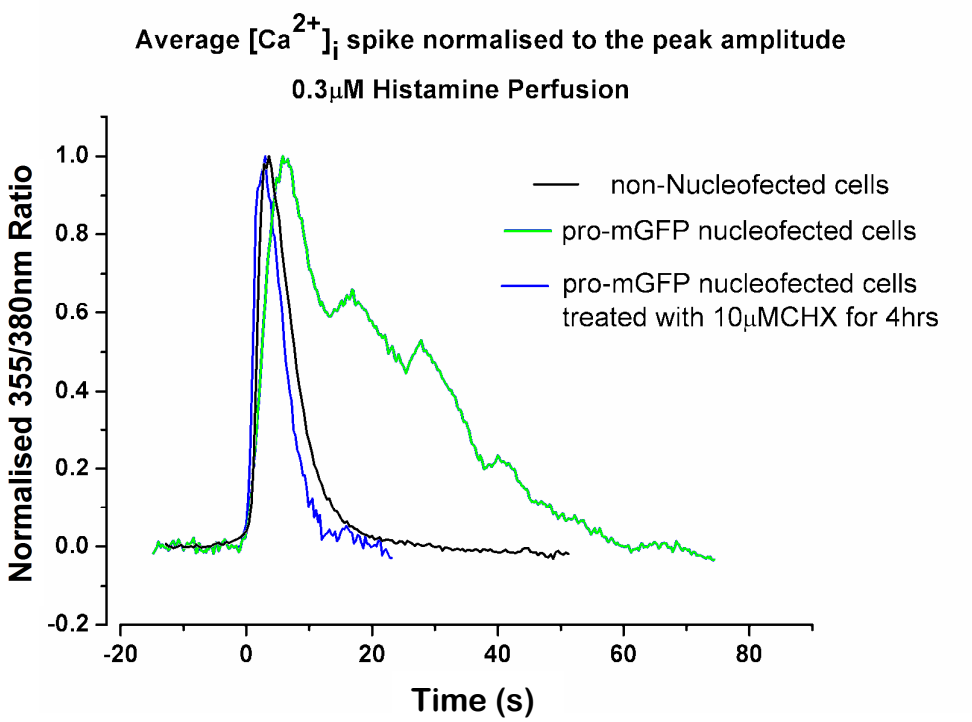

Figure 7.16 $[Ca^{2+}]_i$ spike duration in CHX treated cells is similar to control

The averaged $[Ca^{2+}]_i$ spike induced by perfusion of 0.3μM histamine normalised to the peak amplitude of non-nucleofected HUVEC (black trace; 12 spikes; 6 cells); proregion-mEGFP nucleofected HUVEC (green trace; 7 spikes; 5 cells) and proregion-mEGFP nucleofected HUVEC treated with 10μM CHX for 4hours (blue trace; 5 spikes; 4 cells).

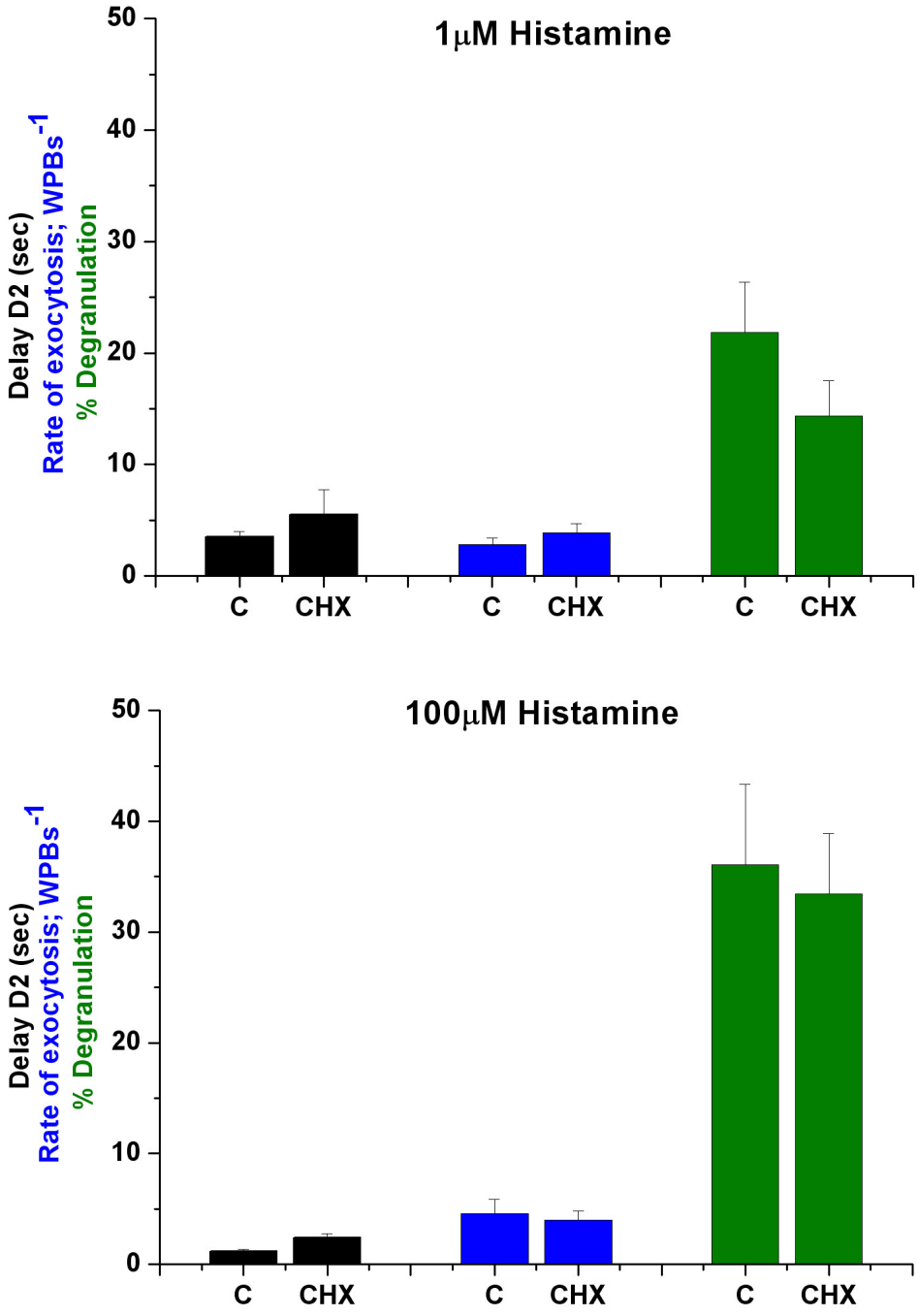

Figure 7.17 Kinetics of WPB exocytosis in control and CHX treated HUVEC

Comparison of the delay (D2) between $[Ca^{2+}]_i$ rise and the onset of WPB exocytosis (black bars); maximal rates of WPB exocytosis (blue bars) and percentage of degranulation (green bars) between control (C) and CHX treated HUVEC (10μM for 3-4 hours) stimulated with 1μM (top) or 100μM (bottom) histamine.

Having established conditions under which cells expressing proregion-mEGFP produced Ca^{2+} -spiking patterns similar to those seen in non-transfected cells we began to look at the relationship between the pattern of Ca^{2+} spikes and WPB exocytosis. Due to time limitations I was not able to study this relationship in detail, however, examples of $[Ca^{2+}]_i$ and WPB fusion in response to continuous perfusion with 0.3μM histamine in single CHX treated proregion-mEGFP expressing HUVEC are shown in Figure 7.18. These examples suggest that exocytosis does occur during Ca^{2+} spikes; however, not enough data was obtained to provide any conclusions about the role of Ca^{2+} spikes and the frequency and kinetics of WPB exocytosis.

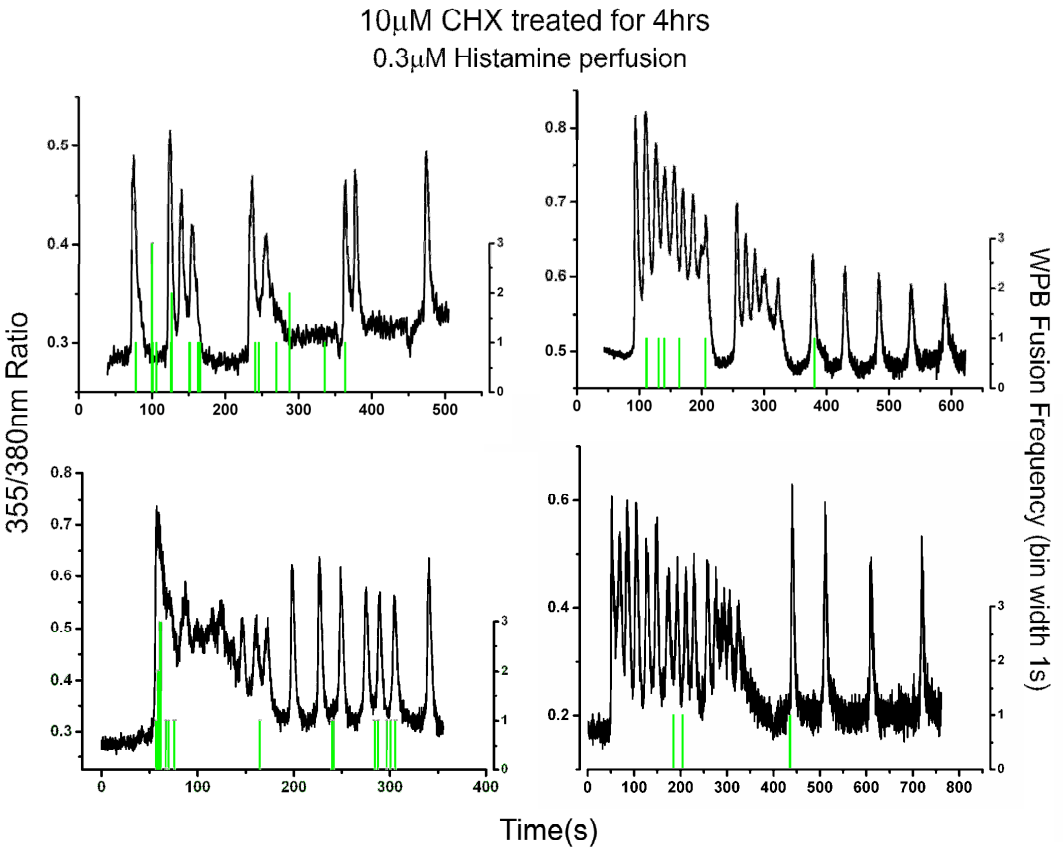

Figure 7.18 Examples of Ca^{2+} oscillations and WPB exocytosis from CHX treated single HUVEC

Fura-2 ratio traces and histograms of WPB first latency distributions (bin width 1s) of single HUVEC expressing proregion-mEGFP treated with 10μM CHX for 4hours prior to perfusion with 0.3μM histamine. CHX was present in the physiological saline at all times. Histamine perfusion was activated 20-50s after the onset of recordings and inactivated 10-20s before the termination of recordings in each case.

7.7 Discussion

7.7.1 $[Ca^{2+}]_i$ oscillations in non-nucleofected HUVEC

Consistent with previous studies we showed that the second phase of the $[Ca^{2+}]_i$ response in HUVEC was dependent on extracellular Ca^{2+} [100, 105, 152, 183] and often comprised either of a sustained plateau or $[Ca^{2+}]_i$ oscillations, particularly at low to medium histamine concentrations (Figure 7.1). The amplitude of the Ca^{2+} spikes was variable from cell to cell, but typically, they were 70-80% of the initial spike amplitude within any individual cell (Figure 7.7), similar to that previously calculated using low affinity Ca^{2+} indicators (Furaptra) in EC of the rat aorta [668]. The frequency of Ca^{2+} spikes increased with increasing hormone concentration, until at high concentrations they merged into a sustained elevated plateau, sometimes superimposed with fast oscillations. A correlation between agonist concentration and frequency has also been reported in epithelial cells [294] and hepatocytes [227, 719], suggesting a role for frequency encoded signalling in cell responses including exocytosis. Such a role may be potentially carried out by Ca^{2+}-modulated enzymes such as CaMKII [303, 720, 721] and PKC [266, 296] whose activity is shown to be determined by Ca^{2+} oscillation frequency and amplitude. PKC phosphorylation provides a negative feedback for agonist-induced Ca^{2+} rises [99, 116] or oscillations [215, 297] in EC. Moreover agonist-induced activation of PKC is thought to regulate WPB release by phosphorylating proteins of the fusion machinery [421, 722]. Thus CaMKII and PKC may be involved in decoding frequency modulated $[Ca^{2+}]_i$ signals to regulate cellular processes regulated by Ca^{2+} such as exocytosis.

There was a marked heterogeneity in the pattern of $[Ca^{2+}]_i$ oscillations between individual cells as previously noted [152, 723]. None-the-less individual cells can display consistent and reproducible $[Ca^{2+}]_i$ responses to the same stimulus [719, 724]. This suggests that each cell may have a unique "Ca^{2+} signalling fingerprint" [724]. Factors contributing to this cellular identity may include the content of agonist receptors (HR_1) [139] or IP_3R [725]; the extent of cell-specific $[Ca^{2+}]_i$ buffering by cytosolic Ca^{2+}-binding proteins [726, 727], mitochondria [534] or ER [313, 728]; the rate of $[Ca^{2+}]_i$ removal mechanisms by pumps including the Na^+/Ca^{2+} exchanger and the Ca^{2+}-ATPase on the plasma membrane [304, 312]; the rate of IP_3R recovery from inhibition by local IP_3 and Ca^{2+} levels [267, 715] and finally the rate of Ca^{2+} ER refilling by SERCA [307]. All these mechanisms constitute the balance between release of Ca^{2+} into the cytosol and clearance of Ca^{2+} from the cytosol thought to shape the $[Ca^{2+}]_i$ signalling of individual cells.

In these experiments $[Ca^{2+}]_i$ oscillations in confluent cultured HUVEC were typically asynchronous between cells, unless cells were in contact with each other, as previously shown in primary cultures of human EC [152]. Synchronized oscillatory activity has been observed in cultured confluent monolayers of endothelial cells stimulated with bradykinin [266, 729] or mechanical stimulation [278]. It is thought that synchronization of Ca^{2+} responses occurs due to intercellular coupling between confluent cells and depends on culture conditions [266]. It is possible that synchronous waves of oscillations across the endothelium *in vivo* would co-ordinate the cellular functions regulated by Ca^{2+} (see review [730]).

7.7.2 Simulated Ca^{2+} spiking and WPB exocytosis

Biochemical studies have shown that removal of extracellular Ca^{2+} reduces vWF secretion [84]. Here, experiments in which extracellular Ca^{2+} was removed confirmed that the Ca^{2+}-dependent component is responsible for a significant fraction of the WPB exocytotic response (up to 60%), although the initial kinetics of fusion were determined almost solely by the initial pulse of Ca^{2+} from the internal stores. This observation led us to investigate more closely the second phase of the Ca^{2+} response, specifically Ca^{2+} oscillations, and WPB exocytosis during this phase.

The heterogeneity in $[Ca^{2+}]_i$ responses between individual HUVEC posed a problem for easy analysis of the relation between $[Ca^{2+}]_i$ spike frequency and exocytosis; no two cells produce exactly the same frequency of Ca^{2+} oscillations. One possible solution to this problem was to impose upon the cell patterns of Ca^{2+} spiking with well defined frequencies. To do this a method of controlled repetitive application of a stimulus at defined intervals was developed. Initially ionomycin was used as this agonist bypasses receptors and signalling cascades by forming lipophilic complexes with Ca^{2+} that act directly on the ER to export Ca^{2+} in the cytosol [202, 203, 205]. In endothelial cells ionomycin is reported not to activate PLC and hence IP_3 and DAG production [206]. Thus by bypassing the receptor transduction pathways it was hoped that the effect of 'Ca^{2+} spikes' alone on WPB exocytosis could be investigated with fewer complications due to activation of other possible signalling cascades (DAG-PKC pathway etc). It was hoped that brief repetitive applications of ionomycin would elicit $[Ca^{2+}]_i$ spikes of similar amplitude and with similar time-course to those produced during responses to hormone perfusion. However, the $[Ca^{2+}]_i$ spikes produced were slow to recover

back to pre-stimulated levels and did not mimic the time-course of $[Ca^{2+}]_i$ spikes produced by hormone action. The slower decay phase for ionomycin-evoked $[Ca^{2+}]_i$ responses is possibly two-fold; first although ionomycin can partition into and out of lipid membranes the kinetics of this process may be slow compared to the time-scale of the Ca^{2+} spike, resulting in prolonged periods of Ca^{2+} translocation after termination of the puff application. Second, ionomycin acts directly on the internal stores, depleting them from Ca^{2+} and this strongly activates capacitative Ca^{2+} entry into the cell which might result in a tendency to sustain the $[Ca^{2+}]_i$ increase [206]. Because of this practical problem with ionomycin this secretagogue was abandoned and histamine was used instead.

Cells exposed to repetitive brief applications of histamine showed brief $[Ca^{2+}]_i$ spikes. By adjusting the duration of exposure to histamine the kinetics of these brief $[Ca^{2+}]_i$ spikes were made similar to those seen during continuous perfusion with histamine. A feature of these spikes was a decrease in amplitude with successive puff applications. Moreover the delay from agonist application to the onset of the $[Ca^{2+}]_i$ rise (*D1*) increased slightly after the initial spike both for short and long application intervals. Possible reasons for this phenomenon include desensitization of the HR_1 histamine receptor. This has been observed during prolonged (hours) or repetitive exposure to high histamine concentrations [147-151, 695, 731], however, low histamine concentrations can elicit $[Ca^{2+}]_i$ oscillations with a steady spike amplitude for long periods of time (30min) [152], well within the time-course of these experiments (10min). Perhaps the periodic nature of the application of histamine promoted HR_1 desensitization more readily compared to what happens during continuous exposure to histamine. Despite the tendency for a progressive decrease in spike amplitude the general pattern

produced by puff application was not entirely dissimilar to that seen with hormone action.

During the first puff application of histamine cells underwent a brief pulse of exocytosis that terminated abruptly as the Ca^{2+} declined. This was similar to what was seen in the absence of extracellular Ca^{2+} (Figure 7.3). The percentage of WPBs that underwent degranulation was ~15-20% of the initial total number of fluorescent WPBs counted in the cell. During second and subsequent $[Ca^{2+}]_i$ spikes, the proportion of WPBs that were released decreased (measured as the % of the total number of WPBs at the start), both during short (60s) and long (120s) intervals of stimulations (Figure 7.8iii). The mean percentage of WPBs that underwent degranulation over the duration of the experiments was~36.5% for the 60s intervals (8-10 puff applications) and 31.3% for the 120s intervals (4-5 puff applications), both well within the capacity of the cell to release, as shown in chapter 4 (ionomycin stimulation gave 66.5% degranulation and 100μM histamine 47.8%). This data suggests the cells were not depleted of the releasable pool of WPBs, but rather the decrease in the extent of exocytosis is due to some other phenomena. The most likely explanation is the decrease in spike amplitude with increasing number of applications. In chapter 4 it was shown that there is a threshold for Ca^{2+}-evoked WPB exocytosis and that WPB exocytosis increased in a concentration dependent fashion as the size of the Ca^{2+} response increased (although we decided that a formal correlation of the rates of rise or amplitude of the Fura-2 ratio with WPB exocytosis was likely to be prone to errors due to Fura-2 saturation (Figure 4.5). A way to confirm whether indeed the single cells did not run out of the releasable pool of granules during the course of the experiment (up to 10 puff applications), would be to stimulate the cells with Ionomycin at the end

of the hormone stimulations. The strong secretagogue would stimulate the release of all the remaining granules of the releasable pool and this would indicate the capacity of the cell under study to release.

We observe however, that in some cells (4/12 cells studied with 60s intervals and 3/12 with 120s intervals) there was an increase in fusion frequency during the second application of histamine despite a decrease in the Ca^{2+} spike amplitude. This suggests the initial Ca^{2+} spike may have primed or led to recruitment of granules to the cell membrane ready for release in the event of a second Ca^{2+} spike. Indeed the delays from the $[Ca^{2+}]_i$ rise to exocytosis decreased for the second spike in 2 out of the 4 examples and remained the same in 1 example, suggesting that granule priming may have taken place to decrease the time taken for fusion from the Ca^{2+} rise. Evidence for Ca^{2+}-dependent priming of secretory granules in HUVEC have come from capacitance recordings [88]. Further studies are needed to examine this in more detail.

These experiments show that WPB exocytosis can occur during repetitive transient pulses of Ca^{2+}, and that the fusion events are tightly confined to the transient increase in Ca^{2+}. Further experiments are required to determine the kinetics of WPB exocytosis as a function of spike frequency and amplitude, perhaps using low affinity Ca^{2+} indicators capable of monitoring more reliably the kinetics and amplitude of large fast rising Ca^{2+} transients that occur in these cells.

7.7.3 Ca^{2+} spiking in proregion-mEGFP expressing HUVEC

In proregion-mEGFP nucleofected HUVEC the Ca^{2+} spiking behaviour was less frequently observed. The cells that responded with $[Ca^{2+}]_i$ spikes had lower amplitudes, longer durations and slower rise times than non-nucleofected HUVEC

(Figures 7.11). This effect appears to be due to the specific over-expression of a protein in the lumen of the secretory pathway. What might be the mechanism for this interference? It is possible that the over-expressed protein binds to free Ca^{2+} in the ER, competing with endogenous buffers to alter the diffusion rate of Ca^{2+}, the amount of Ca^{2+} and the availability for release. Alternatively the excess expressed protein may induce a mild stress response [732, 733] resulting in the expression of chaperone and other proteins that could alter Ca^{2+} handling and regulation of the IP_3R [734, 735]. To elucidate the precise mechanism for this effect requires further studies.

To overcome this problem I initially tried to take advantage of the fact that we used transient expression of the secreted proteins in these studies. By using cells 72hours post transfection, when the levels of expression were falling, we hoped that the ER stress due to protein over expression would be reduced. This was judged by the amount of ER-mEGFP fluorescence which was reduced at 72hours and the cells appeared with just granule staining. However we encountered the same problems in these cells.

Brief CHX treatment was used to reduce ER stress without interfering significantly with Ca^{2+}-driven exocytosis of WPBs. A 3-4hour pre-treatment with CHX did not alter the initial kinetics of histamine-evoked WPB exocytosis suggesting that the machinery for fusion is not turned over (degraded and re-synthesised) on this time scale. Under these conditions the kinetics of Ca^{2+} spikes were restored close to that in non-Nucleofected cells indicating that the processes underlying this phenomena are readily reversible with a reduction in ER load.

In the limited number of experiments carried out in CHX treated HUVEC expressing proregion-mEGFP it was apparent that WPB exocytosis could occur

during $[Ca^{2+}]_i$ spikes, although not all Ca^{2+} spikes evoked exocytosis. Indeed very few WPBs appear to fuse during these brief Ca^{2+} spikes (Figure 7.18). This suggests that Ca^{2+} spiking may indeed provide a mechanism to limit WPB exocytosis while allowing, perhaps, other Ca^{2+}-dependent processes to operate (e.g. NO production, PGI_2 synthesis etc). Further studies are required to establish if a relation exists between the amplitude and more specifically the frequency of $[Ca^{2+}]_i$ oscillations and the secretion of WPBs. The use of CHX to help restore 'normal Ca^{2+} signalling' in cells expressing fluorescent fusion proteins in the lumen of the secretory pathway may provide a potential system for further detailed studies on single cells, perhaps in combination with controlled Ca^{2+} spikes produced either by agonist application as described above or from flash photolysis of intracellular caged Ca^{2+} in whole cell patch clamped HUVEC [88, 103].

8 Summary and Conclusions

Optical studies of fluorescent secretory granules in single HUVEC described in this thesis provide a direct and time-resolved analysis of the properties and exocytosis of secretory granules in endothelial cells. In combination with Ca^{2+} sensitive dyes the relationship between $[Ca^{2+}]_i$ signalling and secretory granule exocytosis was examined with subsecond time resolution. Two distinct granules in EC were investigated; the WPB and the non-WPB. Data presented in this thesis summarises the differences in cargo, intragranule pH, sensitivity of exocytosis to $[Ca^{2+}]_i$ and time-course of stimulated exocytosis between the WPB and non-WPB organelles, not previously shown. The last two chapters of this thesis deal with the role of mitochondria in Ca^{2+} signaling in EC and the potential regulation of secretion by Ca^{2+} oscillations, however data in those chapters is still preliminary; nevertheless the work established experimental conditions that show the potential for future work as described below.

A major aim of these studies was to characterise the properties and exocytosis of the WPB and the non-WPB granules. The pH sensitive properties of EGFP were utilised for this purpose. Using EGFP as an organelle-targeted pH indicator, the pH in the lumen of the WPB and the non-WPB organelle were determined in chapter 3, revealing significant differences between these two organelles. The WPB showed a time-dependent acidification to ~pH5.5, consistent with true storage organelles in other secretory systems [343, 344, 636]. No such time-dependent acidification was seen for the non-WPB. Unlike the WPB, the non-WPB appears to be a transient organelle that is not stored in the cell. The half-life has been estimated to be ~15min (T Carter; unpublished data); thus following formation at the TGN, these organelles may not have sufficient time to fully acidify before they undergo unstimulated exocytosis. This chapter

also confirms that EGFP targeted to secretory granules is a valuable tool in exocytosis due to its pH sensitive properties. The higher intra-granule pH in the non-WPB leads to smaller increases in EGFP fluorescence upon fusion than the WPB, however these were still sufficiently detectable to allow for kinetic studies.

Results chapters 4 and 5 describe the kinetics of exocytosis of the WPB and the non-WPB respectively. Here, taking advantage of the pH-dependent increase in EGFP fluorescence upon vesicle fusion, direct information about the dose-dependence of delays, rates and extent of the WPB and non-WPB exocytosis for histamine and thrombin and the pharmacological agent ionomycin were obtained. Ionomycin was the strongest secretagogue as it bypasses cell signalling cascades to elevate $[Ca^{2+}]_i$ to high levels whereas histamine was shown to be more potent than thrombin in elevating intracellular Ca^{2+} and evoking exocytosis in the cells used in this study. The reason for the different potency between histamine and thrombin summarised in figure 4.15, is not well understood, however it could be partly due to differences in receptor activation as illustrated in figure 1.2. The data provides additional evidence that a threshold for Ca^{2+}-evoked WPB exocytosis exists, however the identity of Ca^{2+} sensors involved in regulating WPB exocytosis have not yet been characterised. The long delays from the $[Ca^{2+}]_i$ rise to granule exocytosis demonstrate the existence of a slow process (or processes) in Ca^{2+}-driven WPB exocytosis. This could involve trafficking, tethering and docking of the granules to the plasma membrane prior to fusion. Experiments to address the role of the cytoskeleton in Ca^{2+}-driven WPB exocytosis might include selectively inhibiting components of the cytoskeleton involved in trafficking (microtubules) and tethering (actin filaments) of the granules and comparing how the delays and overall extent of WPB exocytosis change. Data in figure 7.9

suggests the existence of granules that are readily releasable or less readily releasable, similar to that seen in neuroendocrine granules [391-395]. It is hypothesised that granules that are already near or tethered to the plasma membrane, perhaps immobilised by the actin cytoskeleton [57, 390], are the first granules available for rapid release upon a stimulus. Granules further away from the plasma membrane need to be trafficked to the site of fusion prior to their exocytosis introducing a longer delay. Possible experiments to study this may be to disrupt the microtubule network and look to see if the slow component of events in the first latency distribution is lost.

The kinetics of the non-WPB exocytosis differ from the WPB and suggested a higher sensitivity to $[Ca^{2+}]_i$. These differences provide further evidence that the two secretory granules are distinct organelles and suggest the two population of granules may express different Ca^{2+} sensors on their membranes. Although information on the time-course of exocytosis of the two organelles was determined the molecular mechanisms underlying the exocytotic process are not clear. As already discussed the granules could undergo fusion either via the classical SNARE pathway or via the exocyst (figure 1.4). Future experiments that could identify whether the granules accomplish fusion pore formation through assembly of the SNARE complex would be by treating the cells with botulinum toxins, selective blockers of the SNARE proteins [736, 737]. If botulinum toxin treatment inhibits or decreases agonist-evoked granule exocytosis it would suggest WPBs or non-WPB depend on the SNARE complex formation for exocytosis.

Chapter 6 attempted to address whether mitochondrial Ca^{2+} uptake in EC contributes to intracellular Ca^{2+} hoemeostasis and fine-tunes the kinetics of WPB exocytosis. The approach taken to address this question was to collapse the mitochondrial membrane potential by treating EC with the mitochondrial uncoupler FCCP (in combination with oligomycin to prevent consumption of cellular ATP). The conditions were established for imaging $[Ca^{2+}]_{i,}$ $[Ca^{2+}]_m$ and secretion simultaneously and for blocking mitochondrial Ca^{2+} uptake. Initial data from optical studies demonstrated that inhibition of mitochondrial Ca^{2+} uptake decreased both the amplitude of the histamine-evoked Ca^{2+} transient and the extent of WPB exocytosis. The decrease in the Ca^{2+} transient is likely to underlie the reduction in the extent of WPB exocytosis; however the mechanism that results in the decreased Ca^{2+} transient is not clear. Mitochondria are reported to modulate both IP_3R activity at the ER level and extracellular Ca^{2+} entry at the subplasmalemmal level through their Ca^{2+} buffering capacity (see 1.10.4). The source of Ca^{2+} that is modulated by mitochondria is important in defining the pattern of Ca^{2+} signalling that results from hormone action. In order to understand how mitochondrial Ca^{2+} uptake affects Ca^{2+} homeostasis in our cells, it would be important to identify whether mitochondria are modulating Ca^{2+} levels at the ER level or the subplasmalemmal level. It is unlikely that the mitochondria are buffering Ca^{2+} entering the cell via CCE at the subplasmallemal level because, as seen in figure 7.2 and 7.3, in the absence of extracellular Ca^{2+} the initial $[Ca^{2+}]_i$ phase and WPB exocytosis is not affected. Such buffering effect may be most important during the prolonged phase of the Ca^{2+} response, not studied here. In order to investigate whether the $[Ca^{2+}]_i$ decrease induced by mitochondrial depolarisation is due to mitochondria buffering at the IP_3R level, future work can

examine the response of FCCP treated cells to flash photolysis of caged-IP_3. Release of caged IP_3 activates the IP_3R directly to discharge Ca^{2+} from the ER. If Ca^{2+} signalling was found to differ between control cells and cells treated with FCCP, this would indicate a role for mitochondria in buffering Ca^{2+} at the IP_3R level thus affecting the IP_3R opening probability and Ca^{2+} release from the ER.

Chapter 7 looked at exocytosis during the prolonged phase of the Ca^{2+} response. Evidence for Ca^{2+} oscillations in non-excitable cells and their potential significance in regulating cellular processes, led us to investigate their role in regulating Ca^{2+}-driven exocytosis of WPB in EC. The approach taken was to simultaneously correlate naturally occurring hormone-evoked Ca^{2+} oscillations with WPB exocytosis of proregion-EGFP expressing HUVEC. In some experiments Ca^{2+} spikes with uniform intervals were generated by brief application of hormone in order to study systematically the relationship between spike interval and exocytosis. Expression of fluorescent fusion proteins in the secretory pathway of HUVEC provides an excellent method for visualising secretory granules; allowing their trafficking and the early kinetics of Ca^{2+}-driven WPB exocytosis to be investigated, however, this approach is not without any problems. This methodology led to a perturbation of prolonged Ca^{2+} signalling, in particular Ca^{2+} spiking and Ca^{2+} spike shape in our cells. A simple approach was developed using short exposure of proregion EGFP expressing cells to the protein synthesis inhibitor CHX that to a large extent ameliorated this problem. Despite this, a systematic analysis of the relation between spike frequency and WPB exocytosis is likely to be difficult in single cells largely because no two cells behave alike, and because they have a finite pool of WPBs that do not turn over rapidly after agonist stimulation [738]. This makes repeated experiments on the

same cells impossible. Protocols to generate well defined patterns of Ca^{2+} spikes of known interval may offer a way to investigate the relationship between spike frequency and the rate and extent of WPB exocytosis. The approach described in chapter 7 suggests that WPB fusion can occur during repetitive brief Ca^{2+} spikes however, the data is not yet complete enough for any solid conclusions to be drawn. A particular issue needing attention is the gradual reduction in the Ca^{2+} spike amplitudes during hormone puff application. Data in chapter 4 indicated that the amplitude of the Ca^{2+} signal is important in determining the extent of exocytosis. Thus the secretory responses seen may well represent a composite of spike frequency and spike amplitude making the interpretation of the role of the spike interval itself on WPB fusion difficult. A way to overcome this problem would be to treat intact cells with CHX which might rescue normal Ca^{2+} signalling in transfected cells exposed to repetitive hormone stimulations. An alternative approach to control $[Ca^{2+}]_i$ transients directly without affecting any signalling pathways would be by flash photolysis of caged Ca^{2+} in combination with a low affinity Ca^{2+} indicators such as Furaptra, as previously shown [88, 103].

In conclusion fluorescence microscopy can give us direct measurements of the kinetics of exocytosis of secretory granule populations in single HUVEC and this will ultimately help us understand the underlying mechanisms that regulate release of pro- and anti- coagulant molecules involved in regulating haemostasis and inflammation.

9 Acknowledgments

Firstly and foremost I would like to thank my supervisor Dr Tom Carter for his guidance and support throughout my PhD. His supervision and his patience both with technical difficulties and advice in the right progression were valuable for the completion of this work. I would also like to thank my second supervisor Dr Matthew Hannah whose criticism was helpful to set the project in the right direction and for his consistent advice in experimental design. I am thankful to both my supervisors for making my PhD pleasant in a relaxed atmosphere. This also involves the other members of the Carter and Hannah lab whose presence contributed to a comfortable environment. Specifically I would like to thank Dr Victor Babitch for teaching me molecular biology, Dr Lidsey Hewlet for her advice in biochemical techniques, Dr Nicolai Kiskin for resolving any mathematical or computer problem, Dr Ruben Biering for prompting me to ask questions, Dr Caroline Wheeler Jones for advice on general vascular biology, Bijal Patel for being a good listener and Nicola Hellen and Emma Cookson for being there during my writing up period.

Special thanks to my family, my father Michael Melis, my mother Helen Meli and my siblings Chrysostomos, Emilios and Joanna, for their moral support, understanding and the enjoyable holiday in Cyprus.

Further thanks to my flatmates Claire Pearson and Eve Hornsbey and all my friends for the good times.

10 Supplementary material

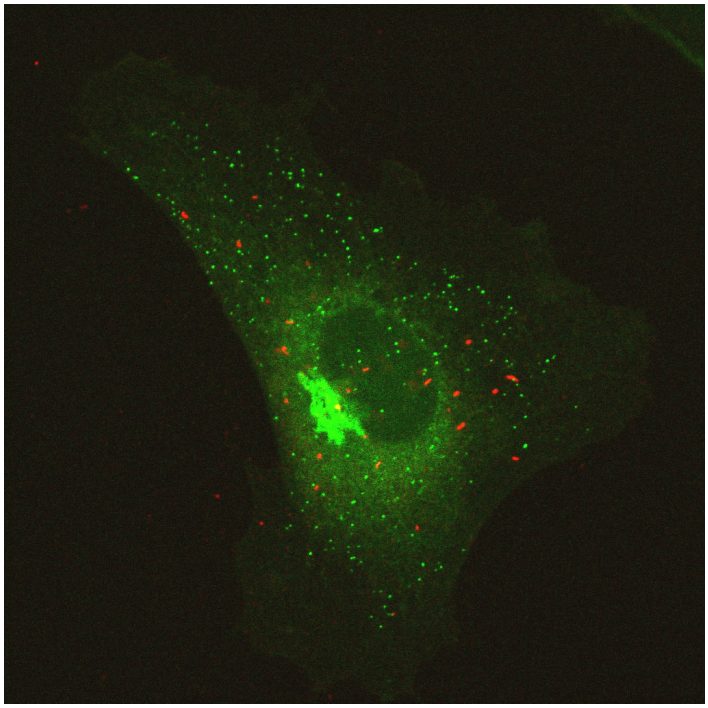

Figure I. Single HUVEC co-expressing EGFP-GRO-αand proregion-mRFP

Proregion-mRFP specifically labels the WPBs and EGFP-GRO-α specifically labels the non-WPB population of granules

11 ABBREVIATIONS

ATP	Adenosine Triphosphate
CaM	Calmodulin
cAMP	cyclic Adenosine Monophosphate
CHX	Cyclohexaminde
CRAC	Ca^{2+} release activated Ca^{2+}
DAG	Diacylglycerol
DsRed	Discosoma sp. Red
EC	Endothelial Cells
EGFP	Enhanced Green Fluorescent Protein
ELISA	Enzyme Linked ImmunoSorbent Assay
eNOS	endothelial Nitric Oxide Synthase
FCCP	Carbonyl cyanide-p-trifluoromethoxyphenylhydrazone
GFP	Green Fluorescent Protein
GPCR	G-protein coupled receptor
HR	Histamine Receptor
HUVEC	Human Umbilical Vein Endothelial Cells
IP_3	Inositol 1,4,5-Trisphosphate
IP_3R	Inositol 1,4,5-Trisphosphate Receptor
mGFP	monomeric Green Fluorescent Protein
mRFP	monomeric Red Fluorescent Protein
NCE	Na^+:Ca^{2+} Exchanger
NHE	Na^+:H^{2+} Exchanger
NO	Nitric Oxide
PAR	Proteinase Activated Receptor
PGI_2	Prostacyclin
PKA	Protein Kinase A
PKC	Protein Kinase C
PLC	Phospholipase C
PMCA	Plasma Membrane Ca^{2+}-ATPase
PS	Physiological Saline

ROS Reactive Oxygen Species

SERCA Sarco/Endoplasmic Reticulum Ca^{2+} ATPase

SNARE Soluble N-thylmaleimide-sensitive factor (NSF) Attachment protein Receptor

TGN Trans-Golgi Network

t-PA Tissue Plasminogen Activator

Trp Transient receptor potential

vWF von Willebrand Factor

WPB Weibel Palade Body

12REFERENCES

1. Erent, M., et al., *Rate, extent and concentration dependence of histamine-evoked Weibel-Palade body exocytosis determined from individual fusion events in human endothelial cells.* J Physiol, 2007. **583**(Pt 1): p. 195-212.
2. Cines, D.B., et al., *Endothelial cells in physiology and in the pathophysiology of vascular disorders.* Blood, 1998. **91**(10): p. 3527-61.
3. Fishman, A.P., *Endothelium: a distributed organ of diverse capabilities.* Ann N Y Acad Sci, 1982. **401**: p. 1-8.
4. PALADE G, E., *Fine structure of blood capillaries.* J. Appl. Physiol., 1953. **24**: p. 1424.
5. Gowans, J.L., *The recirculation of lymphocytes from blood to lymph in the rat.* J Physiol, 1959. **146**(1): p. 54-69.
6. Aird, W.C., *Phenotypic heterogeneity of the endothelium: I. Structure, function, and mechanisms.* Circ Res, 2007. **100**(2): p. 158-73.
7. Kumar, S., D.C. West, and A. Ager, *Heterogeneity in endothelial cells from large vessels and microvessels.* Differentiation, 1987. **36**(1): p. 57-70.
8. Dejana, E., *Endothelial adherens junctions: implications in the control of vascular permeability and angiogenesis.* J Clin Invest, 1996. **98**(9): p. 1949-53.
9. Mitra, D., et al., *Thrombotic thrombocytopenic purpura and sporadic hemolytic-uremic syndrome plasmas induce apoptosis in restricted lineages of human microvascular endothelial cells.* Blood, 1997. **89**(4): p. 1224-34.
10. Levin, E.G., L. Santell, and K.G. Osborn, *The expression of endothelial tissue plasminogen activator in vivo: a function defined by vessel size and anatomic location.* J Cell Sci, 1997. **110 (Pt 2)**: p. 139-48.
11. Jaffe, E.A., et al., *Culture of human endothelial cells derived from umbilical veins. Identification by morphologic and immunologic criteria.* J Clin Invest, 1973. **52**(11): p. 2745-56.
12. Gimbrone, M.A., Jr., R.S. Cotran, and J. Folkman, *Human vascular endothelial cells in culture. Growth and DNA synthesis.* J Cell Biol, 1974. **60**(3): p. 673-84.
13. Lewis, L.J., et al., *Replication of human endothelial cells in culture.* Science, 1973. **181**(98): p. 453-4.
14. Grant, D.S., et al., *Two different laminin domains mediate the differentiation of human endothelial cells into capillary-like structures in vitro.* Cell, 1989. **58**(5): p. 933-43.
15. Bachetti, T. and L. Morbidelli, *Endothelial cells in culture: a model for studying vascular functions.* Pharmacol Res, 2000. **42**(1): p. 9-19.
16. van Hinsbergh, V.W., *The endothelium: vascular control of haemostasis.* Eur J Obstet Gynecol Reprod Biol, 2001. **95**(2): p. 198-201.
17. Yao, X., et al., *A protein kinase G-sensitive channel mediates flow-induced Ca(2+) entry into vascular endothelial cells.* FASEB J, 2000. **14**(7): p. 932-8.

18. Maliba, R., et al., *Angiopoietins-1 and -2 are both capable of mediating endothelial PAF synthesis: intracellular signalling pathways.* Cell Signal, 2006. **18**(11): p. 1947-57.
19. Vane, J.R. and R.M. Botting, *Formation by the endothelium of prostacyclin, nitric oxide and endothelin.* J Lipid Mediat, 1993. **6**(1-3): p. 395-404.
20. Goerge, T., et al., *Secretion pores in human endothelial cells during acute hypoxia.* J Membr Biol, 2002. **187**(3): p. 203-11.
21. Prasad, A.R., et al., *Flow-related responses of intracellular inositol phosphate levels in cultured aortic endothelial cells.* Circ Res, 1993. **72**(4): p. 827-36.
22. Mann, K.G., *Thrombosis: theoretical considerations.* Am J Clin Nutr, 1997. **65**(5 Suppl): p. 1657S-1664S.
23. Weibel, E.R. and G.E. Palade, *New Cytoplasmic Components in Arterial Endothelia.* J Cell Biol, 1964. **23**: p. 101-12.
24. Wagner, D.D., *Cell biology of von Willebrand factor.* Annu Rev Cell Biol, 1990. **6**: p. 217-46.
25. Wagner, D.D., J.B. Olmsted, and V.J. Marder, *Immunolocalization of von Willebrand protein in Weibel-Palade bodies of human endothelial cells.* J Cell Biol, 1982. **95**(1): p. 355-60.
26. Huang, R.H., et al., *Assembly of Weibel-Palade body-like tubules from N-terminal domains of von Willebrand factor.* Proc Natl Acad Sci U S A, 2008. **105**(2): p. 482-7.
27. Zenner, H.L., et al., *High-pressure freezing provides insights into Weibel-Palade body biogenesis.* J Cell Sci, 2007. **120**(Pt 12): p. 2117-25.
28. Ewenstein, B.M., et al., *Composition of the von Willebrand factor storage organelle (Weibel-Palade body) isolated from cultured human umbilical vein endothelial cells.* J Cell Biol, 1987. **104**(5): p. 1423-33.
29. Michaux, G., et al., *The physiological function of von Willebrand's factor depends on its tubular storage in endothelial Weibel-Palade bodies.* Dev Cell, 2006. **10**(2): p. 223-32.
30. Andre, P., et al., *Platelets adhere to and translocate on von Willebrand factor presented by endothelium in stimulated veins.* Blood, 2000. **96**(10): p. 3322-8.
31. Dong, J.F., et al., *ADAMTS-13 rapidly cleaves newly secreted ultralarge von Willebrand factor multimers on the endothelial surface under flowing conditions.* Blood, 2002. **100**(12): p. 4033-9.
32. Sadler, J.E., *Biochemistry and genetics of von Willebrand factor.* Annu Rev Biochem, 1998. **67**: p. 395-424.
33. Siedlecki, C.A., et al., *Shear-dependent changes in the three-dimensional structure of human von Willebrand factor.* Blood, 1996. **88**(8): p. 2939-50.
34. Vischer, U.M. and D.D. Wagner, *von Willebrand factor proteolytic processing and multimerization precede the formation of Weibel-Palade bodies.* Blood, 1994. **83**(12): p. 3536-44.
35. Hannah, M.J., et al., *Differential kinetics of cell surface loss of von Willebrand factor and its propolypeptide after secretion from Weibel-Palade bodies in living human endothelial cells.* J Biol Chem, 2005. **280**(24): p. 22827-30.

36. Kalafatis, M., et al., *Localization of a collagen-interactive domain of human von Willebrand factor between amino acid residues Gly 911 and Glu 1,365.* Blood, 1987. **70**(5): p. 1577-83.
37. Perrault, C., et al., *Relative importance of the glycoprotein Ib-binding domain and the RGD sequence of von Willebrand factor for its interaction with endothelial cells.* Blood, 1997. **90**(6): p. 2335-44.
38. Denis, C., et al., *Solid-phase von Willebrand factor contains a conformationally active RGD motif that mediates endothelial cell adhesion through the alpha v beta 3 receptor.* Blood, 1993. **82**(12): p. 3622-30.
39. Huang, J., et al., *Integrin {alpha}v{beta}3 on human endothelial cells binds von Willebrand factor strings under fluid shear stress.* Blood, 2008.
40. Isobe, T., et al., *Propolypeptide of von Willebrand factor is a novel ligand for very late antigen-4 integrin.* J Biol Chem, 1997. **272**(13): p. 8447-53.
41. Romani de Wit, T., et al., *Von Willebrand factor targets IL-8 to Weibel-Palade bodies in an endothelial cell line.* Exp Cell Res, 2003. **286**(1): p. 67-74.
42. Takagi, J., et al., *Inhibition of platelet-collagen interaction by propolypeptide of von Willebrand factor.* J Biol Chem, 1989. **264**(11): p. 6017-20.
43. Dejana, E., et al., *Von Willebrand factor promotes endothelial cell adhesion via an Arg-Gly-Asp-dependent mechanism.* J Cell Biol, 1989. **109**(1): p. 367-75.
44. McEver, R.P., et al., *GMP-140, a platelet alpha-granule membrane protein, is also synthesized by vascular endothelial cells and is localized in Weibel-Palade bodies.* J Clin Invest, 1989. **84**(1): p. 92-9.
45. Bonfanti, R., et al., *PADGEM (GMP140) is a component of Weibel-Palade bodies of human endothelial cells.* Blood, 1989. **73**(5): p. 1109-12.
46. Hamburger, S.A. and R.P. McEver, *GMP-140 mediates adhesion of stimulated platelets to neutrophils.* Blood, 1990. **75**(3): p. 550-4.
47. Mayadas, T.N., et al., *Leukocyte rolling and extravasation are severely compromised in P selectin-deficient mice.* Cell, 1993. **74**(3): p. 541-54.
48. Chidgey, M.A., *Protein targeting to dense-core secretory granules.* Bioessays, 1993. **15**(5): p. 317-21.
49. Hattori, R., et al., *Stimulated secretion of endothelial von Willebrand factor is accompanied by rapid redistribution to the cell surface of the intracellular granule membrane protein GMP-140.* J Biol Chem, 1989. **264**(14): p. 7768-71.
50. Subramaniam, M., J.A. Koedam, and D.D. Wagner, *Divergent fates of P- and E-selectins after their expression on the plasma membrane.* Mol Biol Cell, 1993. **4**(8): p. 791-801.
51. Cleator, J.H., et al., *Differential regulation of endothelial exocytosis of P-selectin and von Willebrand factor by protease-activated receptors and cAMP.* Blood, 2006. **107**(7): p. 2736-44.
52. Hop, C., et al., *Assembly of multimeric von Willebrand factor directs sorting of P-selectin.* Arterioscler Thromb Vasc Biol, 2000. **20**(7): p. 1763-8.
53. Pfeffer, S.R., *Rab GTPases: specifying and deciphering organelle identity and function.* Trends Cell Biol, 2001. **11**(12): p. 487-91.

54. Hannah, M.J., et al., *Weibel-Palade bodies recruit Rab27 by a content-driven, maturation-dependent mechanism that is independent of cell type.* J Cell Sci, 2003. **116**(Pt 19): p. 3939-48.
55. Knop, M., et al., *Rab3D and annexin A2 play a role in regulated secretion of vWF, but not tPA, from endothelial cells.* Embo J, 2004. **23**(15): p. 2982-92.
56. de Leeuw, H.P., et al., *Small GTP-binding protein RalA associates with Weibel-Palade bodies in endothelial cells.* Thromb Haemost, 1999. **82**(3): p. 1177-81.
57. Nightingale, T.D., et al., *Rab27a and MyRIP regulate the amount and multimeric state of VWF released from endothelial cells.* Blood, 2009.
58. Vischer, U.M. and D.D. Wagner, *CD63 is a component of Weibel-Palade bodies of human endothelial cells.* Blood, 1993. **82**(4): p. 1184-91.
59. Arribas, M. and D.F. Cutler, *Weibel-Palade body membrane proteins exhibit differential trafficking after exocytosis in endothelial cells.* Traffic, 2000. **1**(10): p. 783-93.
60. Stinchcombe, J.C. and G.M. Griffiths, *Regulated secretion from hemopoietic cells.* J Cell Biol, 1999. **147**(1): p. 1-6.
61. Andrews, N.W., *Regulated secretion of conventional lysosomes.* Trends Cell Biol, 2000. **10**(8): p. 316-21.
62. Rodriguez, A., et al., *Lysosomes behave as Ca2+-regulated exocytic vesicles in fibroblasts and epithelial cells.* J Cell Biol, 1997. **137**(1): p. 93-104.
63. Marks, M.S. and M.C. Seabra, *The melanosome: membrane dynamics in black and white.* Nat Rev Mol Cell Biol, 2001. **2**(10): p. 738-48.
64. Metcalf, D.J., et al., *Formation and function of Weibel-Palade bodies.* J Cell Sci, 2008. **121**(Pt 1): p. 19-27.
65. Utgaard, J.O., et al., *Rapid secretion of prestored interleukin 8 from Weibel-Palade bodies of microvascular endothelial cells.* J Exp Med, 1998. **188**(9): p. 1751-6.
66. Wolff, B., et al., *Endothelial cell "memory" of inflammatory stimulation: human venular endothelial cells store interleukin 8 in Weibel-Palade bodies.* J Exp Med, 1998. **188**(9): p. 1757-62.
67. Oynebraten, I., et al., *Rapid chemokine secretion from endothelial cells originates from 2 distinct compartments.* Blood, 2004. **104**(2): p. 314-20.
68. Rondaij, M.G., et al., *Dynamics and plasticity of Weibel-Palade bodies in endothelial cells.* Arterioscler Thromb Vasc Biol, 2006. **26**(5): p. 1002-7.
69. Russell, F.D., J.N. Skepper, and A.P. Davenport, *Endothelin peptide and converting enzymes in human endothelium.* J Cardiovasc Pharmacol, 1998. **31 Suppl 1**: p. S19-21.
70. Rosnoblet, C., et al., *Storage of tissue-type plasminogen activator in Weibel-Palade bodies of human endothelial cells.* Arterioscler Thromb Vasc Biol, 1999. **19**(7): p. 1796-803.
71. Fiedler, U., et al., *The Tie-2 ligand angiopoietin-2 is stored in and rapidly released upon stimulation from endothelial cell Weibel-Palade bodies.* Blood, 2004. **103**(11): p. 4150-6.
72. Fiedler, U., et al., *Angiopoietin-2 sensitizes endothelial cells to TNF-alpha and has a crucial role in the induction of inflammation.* Nat Med, 2006. **12**(2): p. 235-9.

73. Zauli, G., et al., *Osteoprotegerin increases leukocyte adhesion to endothelial cells both in vitro and in vivo.* Blood, 2007. **110**(2): p. 536-43.
74. Zannettino, A.C., et al., *Osteoprotegerin (OPG) is localized to the Weibel-Palade bodies of human vascular endothelial cells and is physically associated with von Willebrand factor.* J Cell Physiol, 2005. **204**(2): p. 714-23.
75. Rosenberg, J.B., et al., *Intracellular trafficking of factor VIII to von Willebrand factor storage granules.* J Clin Invest, 1998. **101**(3): p. 613-24.
76. Kooistra, T., et al., *Regulation of endothelial cell t-PA synthesis and release.* Int J Hematol, 1994. **59**(4): p. 233-55.
77. Aspelin, T., et al., *Cardiac fibrinolytic capacity is markedly increased after brief periods of local myocardial ischemia, but declines following successive periods in anesthetized pigs.* J Thromb Haemost, 2005. **3**(9): p. 1947-54.
78. Chandler, W.L., et al., *A kinetic model of the circulatory regulation of tissue plasminogen activator during exercise, epinephrine infusion, and endurance training.* Blood, 1993. **81**(12): p. 3293-302.
79. Datta, Y.H., et al., *Targeting of a heterologous protein to a regulated secretion pathway in cultured endothelial cells.* Blood, 1999. **94**(8): p. 2696-703.
80. Huber, D., et al., *Tissue-type plasminogen activator (t-PA) is stored in Weibel-Palade bodies in human endothelial cells both in vitro and in vivo.* Blood, 2002. **99**(10): p. 3637-45.
81. Rosnoblet, C., et al., *Regulated von Willebrand factor (vWf) secretion is restored by pro-vWf expression in a transfectable endothelial cell line.* Biochim Biophys Acta, 2000. **1495**(1): p. 112-9.
82. van den Eijnden-Schrauwen, Y., et al., *Studies on the acute release of tissue-type plasminogen activator from human endothelial cells in vitro and in rats in vivo: evidence for a dynamic storage pool.* Blood, 1995. **85**(12): p. 3510-7.
83. Knop, M. and V. Gerke, *Ca2+ -regulated secretion of tissue-type plasminogen activator and von Willebrand factor in human endothelial cells.* Biochim Biophys Acta, 2002. **1600**(1-2): p. 162-7.
84. van den Eijnden-Schrauwen, Y., et al., *Involvement of calcium and G proteins in the acute release of tissue-type plasminogen activator and von Willebrand factor from cultured human endothelial cells.* Arterioscler Thromb Vasc Biol, 1997. **17**(10): p. 2177-87.
85. Hegeman, R.J., Y. van den Eijnden-Schrauwen, and J.J. Emeis, *Adenosine 3':5'-cyclic monophosphate induces regulated secretion of tissue-type plasminogen activator and von Willebrand factor from cultured human endothelial cells.* Thromb Haemost, 1998. **79**(4): p. 853-8.
86. Wall, U., et al., *Evidence of a local mechanism for desmopressin-induced tissue-type plasminogen activator release in human forearm.* Blood, 1998. **91**(2): p. 529-37.
87. Emeis, J.J., et al., *An endothelial storage granule for tissue-type plasminogen activator.* J Cell Biol, 1997. **139**(1): p. 245-56.
88. Zupancic, G., et al., *Differential exocytosis from human endothelial cells evoked by high intracellular Ca(2+) concentration.* J Physiol, 2002. **544**(Pt 3): p. 741-55.

89. Suzuki, Y., et al., *Unique secretory dynamics of tissue plasminogen activator and its modulation by plasminogen activator inhibitor-1 in vascular endothelial cells.* Blood, 2008.
90. Stern, D., et al., *Participation of endothelial cells in the protein C-protein S anticoagulant pathway: the synthesis and release of protein S.* J Cell Biol, 1986. **102**(5): p. 1971-8.
91. Brett, J.G., et al., *Norepinephrine down-regulates the activity of protein S on endothelial cells.* J Cell Biol, 1988. **106**(6): p. 2109-18.
92. Oynebraten, I., et al., *Characterization of a novel chemokine-containing storage granule in endothelial cells: evidence for preferential exocytosis mediated by protein kinase A and diacylglycerol.* J Immunol, 2005. **175**(8): p. 5358-69.
93. Rickles, F.R., et al., *The effects of epinephrine infusion in patients with von Willebrand's disease.* J Clin Invest, 1976. **57**(6): p. 1618-25.
94. Ishida, T., et al., *Fluid shear stress-mediated signal transduction: how do endothelial cells transduce mechanical force into biological responses?* Ann N Y Acad Sci, 1997. **811**: p. 12-23; discussion 23-4.
95. Loesberg, C., et al., *The effect of calcium on the secretion of factor VIII-related antigen by cultured human endothelial cells.* Biochim Biophys Acta, 1983. **763**(2): p. 160-8.
96. Reinders, J.H., et al., *Isolation of a storage and secretory organelle containing Von Willebrand protein from cultured human endothelial cells.* Biochim Biophys Acta, 1984. **804**(3): p. 361-9.
97. Hamilton, K.K. and P.J. Sims, *Changes in cytosolic Ca2+ associated with von Willebrand factor release in human endothelial cells exposed to histamine. Study of microcarrier cell monolayers using the fluorescent probe indo-1.* J Clin Invest, 1987. **79**(2): p. 600-8.
98. Paltauf-Doburzynska, J., et al., *Histamine-induced Ca2+ oscillations in a human endothelial cell line depend on transmembrane ion flux, ryanodine receptors and endoplasmic reticulum Ca2+-ATPase.* J Physiol, 2000. **524 Pt 3**: p. 701-13.
99. Brock, T.A. and E.A. Capasso, *Thrombin and histamine activate phospholipase C in human endothelial cells via a phorbol ester-sensitive pathway.* J Cell Physiol, 1988. **136**(1): p. 54-62.
100. Hallam, T.J. and J.D. Pearson, *Exogenous ATP raises cytoplasmic free calcium in fura-2 loaded piglet aortic endothelial cells.* FEBS Lett, 1986. **207**(1): p. 95-9.
101. Vischer, U.M. and C.B. Wollheim, *Purine nucleotides induce regulated secretion of von Willebrand factor: involvement of cytosolic Ca2+ and cyclic adenosine monophosphate-dependent signaling in endothelial exocytosis.* Blood, 1998. **91**(1): p. 118-27.
102. Matsushita, K., et al., *Vascular endothelial growth factor regulation of Weibel-Palade-body exocytosis.* Blood, 2005. **105**(1): p. 207-14.
103. Carter, T.D., et al., *Membrane capacitance changes induced by thrombin and calcium in single endothelial cells cultured from human umbilical vein.* J Physiol, 1998. **513 (Pt 3)**: p. 845-55.
104. Levine, J.D., et al., *Thrombin-mediated release of factor VIII antigen from human umbilical vein endothelial cells in culture.* Blood, 1982. **60**(2): p. 531-4.

105. Hallam, T.J., J.D. Pearson, and L.A. Needham, *Thrombin-stimulated elevation of human endothelial-cell cytoplasmic free calcium concentration causes prostacyclin production.* Biochem J, 1988. **251**(1): p. 243-9.
106. Schluter, T. and R. Bohnensack, *Serotonin-induced secretion of von Willebrand factor from human umbilical vein endothelial cells via the cyclic AMP-signaling systems independent of increased cytoplasmic calcium concentration.* Biochem Pharmacol, 1999. **57**(10): p. 1191-7.
107. Kaufmann, J.E., et al., *Vasopressin-induced von Willebrand factor secretion from endothelial cells involves V2 receptors and cAMP.* J Clin Invest, 2000. **106**(1): p. 107-16.
108. Vischer, U.M. and C.B. Wollheim, *Epinephrine induces von Willebrand factor release from cultured endothelial cells: involvement of cyclic AMP-dependent signalling in exocytosis.* Thromb Haemost, 1997. **77**(6): p. 1182-8.
109. Akdis, C.A. and K. Blaser, *Histamine in the immune regulation of allergic inflammation.* J Allergy Clin Immunol, 2003. **112**(1): p. 15-22.
110. Berridge, M.J. and R.F. Irvine, *Inositol trisphosphate, a novel second messenger in cellular signal transduction.* Nature, 1984. **312**(5992): p. 315-21.
111. Berridge, M.J. and R.F. Irvine, *Inositol phosphates and cell signalling.* Nature, 1989. **341**(6239): p. 197-205.
112. Nishizuka, Y., *Turnover of inositol phospholipids and signal transduction.* Science, 1984. **225**(4668): p. 1365-70.
113. Bansal, V.S. and P.W. Majerus, *Phosphatidylinositol-derived precursors and signals.* Annu Rev Cell Biol, 1990. **6**: p. 41-67.
114. Ron, D. and M.G. Kazanietz, *New insights into the regulation of protein kinase C and novel phorbol ester receptors.* FASEB J, 1999. **13**(13): p. 1658-76.
115. Birch, K.A., et al., *Calcium/calmodulin transduces thrombin-stimulated secretion: studies in intact and minimally permeabilized human umbilical vein endothelial cells.* J Cell Biol, 1992. **118**(6): p. 1501-10.
116. Carter, T.D., T.J. Hallam, and J.D. Pearson, *Protein kinase C activation alters the sensitivity of agonist-stimulated endothelial-cell prostacyclin production to intracellular Ca2+.* Biochem J, 1989. **262**(2): p. 431-7.
117. Carew, M.A., E.M. Paleolog, and J.D. Pearson, *The roles of protein kinase C and intracellular Ca2+ in the secretion of von Willebrand factor from human vascular endothelial cells.* Biochem J, 1992. **286 (Pt 2)**: p. 631-5.
118. Ferris, C.D., et al., *Purified inositol 1,4,5-trisphosphate receptor mediates calcium flux in reconstituted lipid vesicles.* Nature, 1989. **342**(6245): p. 87-9.
119. Supattapone, S., et al., *Cyclic AMP-dependent phosphorylation of a brain inositol trisphosphate receptor decreases its release of calcium.* Proc Natl Acad Sci U S A, 1988. **85**(22): p. 8747-50.
120. Ross, C.A., et al., *Three additional inositol 1,4,5-trisphosphate receptors: molecular cloning and differential localization in brain and peripheral tissues.* Proc Natl Acad Sci U S A, 1992. **89**(10): p. 4265-9.
121. Vermassen, E., J.B. Parys, and J.P. Mauger, *Subcellular distribution of the inositol 1,4,5-trisphosphate receptors: functional relevance and molecular determinants.* Biol Cell, 2004. **96**(1): p. 3-17.

122. Bezprozvanny, I. and B.E. Ehrlich, *The inositol 1,4,5-trisphosphate (InsP3) receptor.* J Membr Biol, 1995. **145**(3): p. 205-16.
123. Tran, Q.K., K. Ohashi, and H. Watanabe, *Calcium signalling in endothelial cells.* Cardiovasc Res, 2000. **48**(1): p. 13-22.
124. Rondaij, M.G., et al., *Guanine exchange factor RalGDS mediates exocytosis of Weibel-Palade bodies from endothelial cells.* Blood, 2008. **112**(1): p. 56-63.
125. Haruta, T., et al., *Ca2+-dependent interaction of the growth-associated protein GAP-43 with the synaptic core complex.* Biochem J, 1997. **325 (Pt 2)**: p. 455-63.
126. Chamberlain, L.H., et al., *Distinct effects of alpha-SNAP, 14-3-3 proteins, and calmodulin on priming and triggering of regulated exocytosis.* J Cell Biol, 1995. **130**(5): p. 1063-70.
127. Vischer, U.M., H. Barth, and C.B. Wollheim, *Regulated von Willebrand factor secretion is associated with agonist-specific patterns of cytoskeletal remodeling in cultured endothelial cells.* Arterioscler Thromb Vasc Biol, 2000. **20**(3): p. 883-91.
128. Romani de Wit, T., et al., *Real-time imaging of the dynamics and secretory behavior of Weibel-Palade bodies.* Arterioscler Thromb Vasc Biol, 2003. **23**(5): p. 755-61.
129. Mannucci, P.M., et al., *1-Deamino-8-d-arginine vasopressin: a new pharmacological approach to the management of haemophilia and von Willebrands' diseases.* Lancet, 1977. **1**(8017): p. 869-72.
130. Endo, Y., *Simultaneous induction of histidine and ornithine decarboxylases and changes in their product amines following the injection of Escherichia coli lipopolysaccharide into mice.* Biochem Pharmacol, 1982. **31**(8): p. 1643-7.
131. Miyazawa, N., et al., *Role of histamine H1 and H2 receptor antagonists in the prevention of intimal thickening.* Eur J Pharmacol, 1998. **362**(1): p. 53-9.
132. Jutel, M., et al., *Immune regulation by histamine.* Curr Opin Immunol, 2002. **14**(6): p. 735-40.
133. Tanimoto, A., et al., *Histamine increases the expression of LOX-1 via H2 receptor in human monocytic THP-1 cells.* FEBS Lett, 2001. **508**(3): p. 345-9.
134. Riley, J.F. and G.B. West, *The presence of histamine in tissue mast cells.* J Physiol, 1953. **120**(4): p. 528-37.
135. Graham, H.T., et al., *Distribution of histamine among leukocytes and platelets.* Blood, 1955. **10**(5): p. 467-81.
136. Ishizaka, T. and D.H. Conrad, *Binding characteristics of human IgE receptors and initial triggering events in human mast cells for histamine release.* Monogr Allergy, 1983. **18**: p. 14-24.
137. Atkinson, J.B., et al., *The association of mast cells and atherosclerosis: a morphologic study of early atherosclerotic lesions in young people.* Hum Pathol, 1994. **25**(2): p. 154-9.
138. Jutel, M., K. Blaser, and C.A. Akdis, *The role of histamine in regulation of immune responses.* Chem Immunol Allergy, 2006. **91**: p. 174-87.
139. Hill, S.J., *Distribution, properties, and functional characteristics of three classes of histamine receptor.* Pharmacol Rev, 1990. **42**(1): p. 45-83.

140. Heltianu, C., M. Simionescu, and N. Simionescu, *Histamine receptors of the microvascular endothelium revealed in situ with a histamine-ferritin conjugate: characteristic high-affinity binding sites in venules.* J Cell Biol, 1982. **93**(2): p. 357-64.
141. Schaefer, U., et al., *Histamine induced homologous and heterologous regulation of histamine receptor subtype mRNA expression in cultured endothelial cells.* Shock, 1999. **12**(4): p. 309-15.
142. Schwartz, T.W. and M.M. Rosenkilde, *Is there a 'lock' for all agonist 'keys' in 7TM receptors?* Trends Pharmacol Sci, 1996. **17**(6): p. 213-6.
143. Ohta, K., et al., *Site-directed mutagenesis of the histamine H1 receptor: roles of aspartic acid107, asparagine198 and threonine194.* Biochem Biophys Res Commun, 1994. **203**(2): p. 1096-101.
144. Hill, S.J., J.M. Young, and D.H. Marrian, *Specific binding of 3H-mepyramine to histamine H1 receptors in intestinal smooth muscle.* Nature, 1977. **270**(5635): p. 361-3.
145. Huganir, R.L. and P. Greengard, *Regulation of neurotransmitter receptor desensitization by protein phosphorylation.* Neuron, 1990. **5**(5): p. 555-67.
146. Barsoum, G.S. and J.H. Gaddum, *The pharmacological estimation of adenosine and histamine in blood.* J Physiol, 1935. **85**(1): p. 1-14.
147. Smit, M.J., et al., *Short-term desensitization of the histamine H1 receptor in human HeLa cells: involvement of protein kinase C dependent and independent pathways.* Br J Pharmacol, 1992. **107**(2): p. 448-55.
148. Brown, R.D., P. Prendiville, and C. Cain, *Alpha 1-adrenergic and H1-histamine receptor control of intracellular Ca2+ in a muscle cell line: the influence of prior agonist exposure on receptor responsiveness.* Mol Pharmacol, 1986. **29**(6): p. 531-9.
149. Nakahata, N. and T.K. Harden, *Regulation of inositol trisphosphate accumulation by muscarinic cholinergic and H1-histamine receptors on human astrocytoma cells. Differential induction of desensitization by agonists.* Biochem J, 1987. **241**(2): p. 337-44.
150. Kenakin, T.P. and D.A. Cook, *The effect of desensitization on the antagonism of the histamine response by phenoxybenzamine.* Mol Pharmacol, 1980. **17**(3): p. 309-13.
151. Hishinuma, S. and M.K. Uchida, *Short-term desensitization of guinea-pig taenia caecum induced by carbachol occurs at intracellular Ca stores and that by histamine at H1-receptors.* Br J Pharmacol, 1988. **94**(3): p. 882-9.
152. Jacob, R., et al., *Repetitive spikes in cytoplasmic calcium evoked by histamine in human endothelial cells.* Nature, 1988. **335**(6185): p. 40-5.
153. Hide, M., et al., *Histamine H1-receptor in endothelial and smooth muscle cells of guinea-pig aorta.* Eur J Pharmacol, 1988. **148**(2): p. 161-9.
154. Bull, H.A., et al., *Characterization of histamine receptor sub-types regulating prostacyclin release from human endothelial cells.* Br J Pharmacol, 1992. **107**(2): p. 276-81.
155. Takagishi, T., et al., *Expression of the histamine H1 receptor gene in relation to atherosclerosis.* Am J Pathol, 1995. **146**(4): p. 981-8.
156. Iriyoshi, N., et al., *Increased expression of histamine H1 receptor mRNA in allergic rhinitis.* Clin Exp Allergy, 1996. **26**(4): p. 379-85.
157. Lo, W.W. and T.P. Fan, *Histamine stimulates inositol phosphate accumulation via the H1-receptor in cultured human endothelial cells.* Biochem Biophys Res Commun, 1987. **148**(1): p. 47-53.

158. Dale, H.H. and P.P. Laidlaw, *The physiological action of beta-iminazolylethylamine.* J Physiol, 1910. **41**(5): p. 318-44.
159. Majno, G. and G.E. Palade, *Studies on inflammation. 1. The effect of histamine and serotonin on vascular permeability: an electron microscopic study.* J Biophys Biochem Cytol, 1961. **11**: p. 571-605.
160. Becker, C.G. and R.L. Nachman, *Contractile proteins of endothelial cells, platelets and smooth muscle.* Am J Pathol, 1973. **71**(1): p. 1-22.
161. Baenziger, N.L., L.E. Force, and P.R. Becherer, *Histamine stimulate prostacyclin synthesis in cultured human umbilical vein endothelial cells.* Biochem Biophys Res Commun, 1980. **92**(4): p. 1435-40.
162. Schwartz, J.C., H. Pollard, and T.T. Quach, *Histamine as a neurotransmitter in mammalian brain: neurochemical evidence.* J Neurochem, 1980. **35**(1): p. 26-33.
163. Noble, E.P., et al., *H1-histaminergic activation of catecholamine release by chromaffin cells.* Biochem Pharmacol, 1988. **37**(2): p. 221-8.
164. Esmon, C.T., et al., *The action of thrombin on blood clotting factor V: conversion of factor V to a prothrombin-binding protein.* Biochim Biophys Acta, 1973. **310**(1): p. 289-94.
165. Colman, R.W. and R.M. Weinberg, *Factor V.* Methods Enzymol, 1976. **45**: p. 107-22.
166. Kandall, C.L., R. Rosenberg, and R.W. Colman, *Molecular changes associated with proteolysis of bovine factor V by thrombin.* Eur J Biochem, 1975. **58**(1): p. 203-11.
167. Ware, A.G., M.M. Guest, and W.H. Seegers, *Plasma Accelerator Factor and Purified Prothrombin Activation.* Science, 1947. **106**(2741): p. 41-42.
168. Prentice, C.R., O.D. Ratnoff, and R.T. Breckenridge, *Experiments on the nature of the prothrombin-converting principle: alteration of proaccelerin by thrombin.* Br J Haematol, 1967. **13**(6): p. 898-914.
169. Kisiel, W., L.H. Ericsson, and E.W. Davie, *Proteolytic activation of protein C from bovine plasma.* Biochemistry, 1976. **15**(22): p. 4893-900.
170. Altieri, D.C., *Proteases and protease receptors in modulation of leukocyte effector functions.* J Leukoc Biol, 1995. **58**(2): p. 120-7.
171. Molloy, C.J., et al., *Thrombin receptor activation elicits rapid protein tyrosine phosphorylation and stimulation of the raf-1/MAP kinase pathway preceding delayed mitogenesis in cultured rat aortic smooth muscle cells: evidence for an obligate autocrine mechanism promoting cell proliferation induced by G-protein-coupled receptor agonist.* J Clin Invest, 1996. **97**(5): p. 1173-83.
172. Sower, L.E., et al., *Thrombin induces IL-6 production in fibroblasts and epithelial cells. Evidence for the involvement of the seven-transmembrane domain (STD) receptor for alpha-thrombin.* J Immunol, 1995. **155**(2): p. 895-901.
173. Glusa, E., M. Paintz, and E. Bretschneider, *Relaxant and contractile responses of porcine pulmonary arteries to thrombin and thrombin receptor activating peptides.* Semin Thromb Hemost, 1996. **22**(3): p. 261-5.
174. Macfarlane, S.R., et al., *Proteinase-activated receptors.* Pharmacol Rev, 2001. **53**(2): p. 245-82.

175. Trejo, J., *Protease-activated receptors: new concepts in regulation of G protein-coupled receptor signaling and trafficking.* J Pharmacol Exp Ther, 2003. **307**(2): p. 437-42.
176. Bohm, S.K., et al., *Proteinase-Activated Receptors: New Functions for Old Enzymes.* News Physiol Sci, 1998. **13**: p. 231-240.
177. Vu, T.K., et al., *Molecular cloning of a functional thrombin receptor reveals a novel proteolytic mechanism of receptor activation.* Cell, 1991. **64**(6): p. 1057-68.
178. Klarenbach, S.W., et al., *Differential actions of PAR2 and PAR1 in stimulating human endothelial cell exocytosis and permeability: the role of Rho-GTPases.* Circ Res, 2003. **92**(3): p. 272-8.
179. Hirano, K. and H. Kanaide, *Role of protease-activated receptors in the vascular system.* J Atheroscler Thromb, 2003. **10**(4): p. 211-25.
180. Steinberg, S.F., *The cardiovascular actions of protease-activated receptors.* Mol Pharmacol, 2005. **67**(1): p. 2-11.
181. Ellis, C.A., et al., *Time course of recovery of endothelial cell surface thrombin receptor (PAR-1) expression.* Am J Physiol, 1999. **276**(1 Pt 1): p. C38-45.
182. Coughlin, S.R., *How the protease thrombin talks to cells.* Proc Natl Acad Sci U S A, 1999. **96**(20): p. 11023-7.
183. Birch, K.A., et al., *Prolonged peak elevations in cytoplasmic free calcium ions, derived from intracellular stores, correlate with the extent of thrombin-stimulated exocytosis in single human umbilical vein endothelial cells.* J Cell Physiol, 1994. **160**(3): p. 545-54.
184. Hirano, K., *The roles of proteinase-activated receptors in the vascular physiology and pathophysiology.* Arterioscler Thromb Vasc Biol, 2007. **27**(1): p. 27-36.
185. Lum, H. and A.B. Malik, *Regulation of vascular endothelial barrier function.* Am J Physiol, 1994. **267**(3 Pt 1): p. L223-41.
186. Vogel, S.M., et al., *Abrogation of thrombin-induced increase in pulmonary microvascular permeability in PAR-1 knockout mice.* Physiol Genomics, 2000. **4**(2): p. 137-145.
187. Laposata, M., D.K. Dovnarsky, and H.S. Shin, *Thrombin-induced gap formation in confluent endothelial cell monolayers in vitro.* Blood, 1983. **62**(3): p. 549-56.
188. Rabiet, M.J., et al., *Thrombin-induced increase in endothelial permeability is associated with changes in cell-to-cell junction organization.* Arterioscler Thromb Vasc Biol, 1996. **16**(3): p. 488-96.
189. Sacks, R.S., et al., *Thrombin-mediated increases in cytosolic [Ca2+] involve different mechanisms in human pulmonary artery smooth muscle and endothelial cells.* Am J Physiol Lung Cell Mol Physiol, 2008. **295**(6): p. L1048-55.
190. Horgan, M.J., J.W. Fenton, 2nd, and A.B. Malik, *Alpha-thrombin-induced pulmonary vasoconstriction.* J Appl Physiol, 1987. **63**(5): p. 1993-2000.
191. Garcia, J.G., H.W. Davis, and C.E. Patterson, *Regulation of endothelial cell gap formation and barrier dysfunction: role of myosin light chain phosphorylation.* J Cell Physiol, 1995. **163**(3): p. 510-22.
192. Hoth, M. and R. Penner, *Calcium release-activated calcium current in rat mast cells.* J Physiol, 1993. **465**: p. 359-86.

193. Graier, W.F., et al., *Submaximal stimulation of porcine endothelial cells causes focal Ca2+ elevation beneath the cell membrane.* J Physiol, 1998. **506 (Pt 1)**: p. 109-25.
194. Hilgenfeld, R. and W. Saenger, *Structural chemistry of natural and synthetic ionophores and their complexes with cations.* Top Curr Chem, 1982. **101**: p. 1-82.
195. Liu, W.C., et al., *Ionomycin, a new polyether antibiotic.* J Antibiot (Tokyo), 1978. **31**(9): p. 815-9.
196. Bennett, J.P., S. Cockcroft, and B.D. Gomperts, *Ionomycin stimulates mast cell histamine secretion by forming a lipid-soluble calcium complex.* Nature, 1979. **282**(5741): p. 851-3.
197. Stiles, M.K., et al., *The formation constants of ionomycin with divalent cations in 80% methanol/water.* J Biol Chem, 1991. **266**(13): p. 8336-42.
198. Kauffman, R.F., R.W. Taylor, and D.R. Pfeiffer, *Acid-base properties of ionophore A23187 in methanol-water solutions and bound to unilamellar vesicles of dimyristoylphosphatidylcholine.* Biochemistry, 1982. **21**(10): p. 2426-35.
199. Taylor, R.W., C.J. Chapman, and D.R. Pfeiffer, *Effect of membrane association on the stability of complexes between ionophore A23187 and monovalent cations.* Biochemistry, 1985. **24**(18): p. 4852-9.
200. Chapman, C.J., et al., *Equilibria between ionophore A23187 and divalent cations: stability of 1:1 complexes in solutions of 80% methanol/water.* Biochemistry, 1987. **26**(16): p. 5009-18.
201. Liu, C. and T.E. Hermann, *Characterization of ionomycin as a calcium ionophore.* J Biol Chem, 1978. **253**(17): p. 5892-4.
202. Beeler, T.J., I. Jona, and A. Martonosi, *The effect of ionomycin on calcium fluxes in sarcoplasmic reticulum vesicles and liposomes.* J Biol Chem, 1979. **254**(14): p. 6229-31.
203. Kauffman, R.F., R.W. Taylor, and D.R. Pfeiffer, *Cation transport and specificity of ionomycin. Comparison with ionophore A23187 in rat liver mitochondria.* J Biol Chem, 1980. **255**(7): p. 2735-9.
204. Fasolato, C. and T. Pozzan, *Effect of membrane potential on divalent cation transport catalyzed by the "electroneutral" ionophores A23187 and ionomycin.* J Biol Chem, 1989. **264**(33): p. 19630-6.
205. Erdahl, W.L., et al., *Ca2+ transport properties of ionophores A23187, ionomycin, and 4-BrA23187 in a well defined model system.* Biophys J, 1994. **66**(5): p. 1678-93.
206. Morgan, A.J. and R. Jacob, *Ionomycin enhances Ca2+ influx by stimulating store-regulated cation entry and not by a direct action at the plasma membrane.* Biochem J, 1994. **300 (Pt 3)**: p. 665-72.
207. Carafoli, E., *Calcium signaling: a tale for all seasons.* Proc Natl Acad Sci U S A, 2002. **99**(3): p. 1115-22.
208. Nicotera, P., G. Bellomo, and S. Orrenius, *Calcium-mediated mechanisms in chemically induced cell death.* Annu Rev Pharmacol Toxicol, 1992. **32**: p. 449-70.
209. Wood, P.G. and J.I. Gillespie, *Evidence for mitochondrial Ca(2+)-induced Ca2+ release in permeabilised endothelial cells.* Biochem Biophys Res Commun, 1998. **246**(2): p. 543-8.

210. Hebert, D.N. and M. Molinari, *In and out of the ER: protein folding, quality control, degradation, and related human diseases.* Physiol Rev, 2007. **87**(4): p. 1377-408.
211. Sambrook, J.F., *The involvement of calcium in transport of secretory proteins from the endoplasmic reticulum.* Cell, 1990. **61**(2): p. 197-9.
212. Michalak, M., et al., *Calreticulin, a multi-process calcium-buffering chaperone of the endoplasmic reticulum.* Biochem J, 2009. **417**(3): p. 651-66.
213. Lievremont, J.P., et al., *BiP, a major chaperone protein of the endoplasmic reticulum lumen, plays a direct and important role in the storage of the rapidly exchanging pool of Ca2+.* J Biol Chem, 1997. **272**(49): p. 30873-9.
214. Berridge, M.J., *Inositol trisphosphate and calcium signalling.* Nature, 1993. **361**(6410): p. 315-25.
215. Carter, T.D., R.G. Bogle, and T. Bjaaland, *Spiking of intracellular calcium ion concentration in single cultured pig aortic endothelial cells stimulated with ATP or bradykinin.* Biochem J, 1991. **278 (Pt 3)**: p. 697-704.
216. Laskey, R.E., et al., *Membrane potential and Na(+)-K+ pump activity modulate resting and bradykinin-stimulated changes in cytosolic free calcium in cultured endothelial cells from bovine atria.* J Biol Chem, 1990. **265**(5): p. 2613-9.
217. Berridge, M.J., P.H. Cobbold, and K.S. Cuthbertson, *Spatial and temporal aspects of cell signalling.* Philos Trans R Soc Lond B Biol Sci, 1988. **320**(1199): p. 325-43.
218. Sage, S.O., et al., *Receptor-mediated calcium entry in fura-2-loaded human platelets stimulated with ADP and thrombin. Dual-wavelengths studies with Mn2+.* Biochem J, 1989. **258**(3): p. 923-6.
219. Hallam, T.J., R. Jacob, and J.E. Merritt, *Evidence that agonists stimulate bivalent-cation influx into human endothelial cells.* Biochem J, 1988. **255**(1): p. 179-84.
220. Putney, J.W., Jr., *Capacitative calcium entry revisited.* Cell Calcium, 1990. **11**(10): p. 611-24.
221. Putney, J.W., Jr., *A model for receptor-regulated calcium entry.* Cell Calcium, 1986. **7**(1): p. 1-12.
222. Huser, J., et al., *Focal agonist stimulation results in spatially restricted Ca2+ release and capacitative Ca2+ entry in bovine vascular endothelial cells.* J Physiol, 1999. **514 (Pt 1)**: p. 101-9.
223. Dolor, R.J., et al., *Regulation of extracellular calcium entry in endothelial cells: role of intracellular calcium pool.* Am J Physiol, 1992. **262**(1 Pt 1): p. C171-81.
224. Schilling, W.P., O.A. Cabello, and L. Rajan, *Depletion of the inositol 1,4,5-trisphosphate-sensitive intracellular Ca2+ store in vascular endothelial cells activates the agonist-sensitive Ca(2+)-influx pathway.* Biochem J, 1992. **284 (Pt 2)**: p. 521-30.
225. Montero, M., J. Alvarez, and J. Garcia-Sancho, *Control of plasma-membrane Ca2+ entry by the intracellular Ca2+ stores. Kinetic evidence for a short-lived mediator.* Biochem J, 1992. **288 (Pt 2)**: p. 519-25.
226. Foskett, J.K. and D.C. Wong, *[Ca2+]i inhibition of Ca2+ release-activated Ca2+ influx underlies agonist- and thapsigargin-induced*

[Ca2+]i oscillations in salivary acinar cells. J Biol Chem, 1994. **269**(50): p. 31525-32.
227. Woods, N.M., K.S. Cuthbertson, and P.H. Cobbold, *Repetitive transient rises in cytoplasmic free calcium in hormone-stimulated hepatocytes.* Nature, 1986. **319**(6054): p. 600-2.
228. Hoth, M. and R. Penner, *Depletion of intracellular calcium stores activates a calcium current in mast cells.* Nature, 1992. **355**(6358): p. 353-6.
229. Parekh, A.B., *Store-operated Ca2+ entry: dynamic interplay between endoplasmic reticulum, mitochondria and plasma membrane.* J Physiol, 2003. **547**(Pt 2): p. 333-48.
230. Zweifach, A. and R.S. Lewis, *Rapid inactivation of depletion-activated calcium current (ICRAC) due to local calcium feedback.* J Gen Physiol, 1995. **105**(2): p. 209-26.
231. Zweifach, A. and R.S. Lewis, *Slow calcium-dependent inactivation of depletion-activated calcium current. Store-dependent and -independent mechanisms.* J Biol Chem, 1995. **270**(24): p. 14445-51.
232. Gericke, M., G. Droogmans, and B. Nilius, *Thapsigargin discharges intracellular calcium stores and induces transmembrane currents in human endothelial cells.* Pflugers Arch, 1993. **422**(6): p. 552-7.
233. Oike, M., et al., *Calcium entry activated by store depletion in human umbilical vein endothelial cells.* Cell Calcium, 1994. **16**(5): p. 367-76.
234. Hardie, R.C. and B. Minke, *Novel Ca2+ channels underlying transduction in Drosophila photoreceptors: implications for phosphoinositide-mediated Ca2+ mobilization.* Trends Neurosci, 1993. **16**(9): p. 371-6.
235. Cosens, D.J. and A. Manning, *Abnormal electroretinogram from a Drosophila mutant.* Nature, 1969. **224**(5216): p. 285-7.
236. Montell, C. and G.M. Rubin, *Molecular characterization of the Drosophila trp locus: a putative integral membrane protein required for phototransduction.* Neuron, 1989. **2**(4): p. 1313-23.
237. Zhu, X. and L. Birnbaumer, *Calcium Channels Formed by Mammalian Trp Homologues.* News Physiol Sci, 1998. **13**: p. 211-217.
238. Zhu, X., et al., *trp, a novel mammalian gene family essential for agonist-activated capacitative Ca2+ entry.* Cell, 1996. **85**(5): p. 661-71.
239. Yao, X. and C.J. Garland, *Recent developments in vascular endothelial cell transient receptor potential channels.* Circ Res, 2005. **97**(9): p. 853-63.
240. Nilius, B. and G. Droogmans, *Ion channels and their functional role in vascular endothelium.* Physiol Rev, 2001. **81**(4): p. 1415-59.
241. Kwan, H.Y., Y. Huang, and X. Yao, *TRP channels in endothelial function and dysfunction.* Biochim Biophys Acta, 2007. **1772**(8): p. 907-14.
242. Mehta, D., et al., *RhoA interaction with inositol 1,4,5-trisphosphate receptor and transient receptor potential channel-1 regulates Ca2+ entry. Role in signaling increased endothelial permeability.* J Biol Chem, 2003. **278**(35): p. 33492-500.
243. Ahmmed, G.U., et al., *Protein kinase Calpha phosphorylates the TRPC1 channel and regulates store-operated Ca2+ entry in endothelial cells.* J Biol Chem, 2004. **279**(20): p. 20941-9.

244. Cioffi, D.L., et al., *Activation of the endothelial store-operated ISOC Ca2+ channel requires interaction of protein 4.1 with TRPC4.* Circ Res, 2005. **97**(11): p. 1164-72.
245. Kamouchi, M., et al., *Nonselective cation channels in endothelial cells derived from human umbilical vein.* J Membr Biol, 1999. **169**(1): p. 29-38.
246. Parekh, A.B. and R. Penner, *Store depletion and calcium influx.* Physiol Rev, 1997. **77**(4): p. 901-30.
247. Putney, J.W., Jr. and R.R. McKay, *Capacitative calcium entry channels.* Bioessays, 1999. **21**(1): p. 38-46.
248. Parekh, A.B., H. Terlau, and W. Stuhmer, *Depletion of InsP3 stores activates a Ca2+ and K+ current by means of a phosphatase and a diffusible messenger.* Nature, 1993. **364**(6440): p. 814-8.
249. Csutora, P., et al., *Calcium influx factor is synthesized by yeast and mammalian cells depleted of organellar calcium stores.* Proc Natl Acad Sci U S A, 1999. **96**(1): p. 121-6.
250. Randriamampita, C. and R.Y. Tsien, *Emptying of intracellular Ca2+ stores releases a novel small messenger that stimulates Ca2+ influx.* Nature, 1993. **364**(6440): p. 809-14.
251. Watanabe, H., et al., *Anandamide and arachidonic acid use epoxyeicosatrienoic acids to activate TRPV4 channels.* Nature, 2003. **424**(6947): p. 434-8.
252. Hoebel, B.G., G.M. Kostner, and W.F. Graier, *Activation of microsomal cytochrome P450 mono-oxygenase by Ca2+ store depletion and its contribution to Ca2+ entry in porcine aortic endothelial cells.* Br J Pharmacol, 1997. **121**(8): p. 1579-88.
253. Graier, W.F., S. Simecek, and M. Sturek, *Cytochrome P450 mono-oxygenase-regulated signalling of Ca2+ entry in human and bovine endothelial cells.* J Physiol, 1995. **482 (Pt 2)**: p. 259-74.
254. Xie, Q., et al., *Calcium influx factor from cytochrome P-450 metabolism and secretion-like coupling mechanisms for capacitative calcium entry in corneal endothelial cells.* J Biol Chem, 2002. **277**(19): p. 16559-66.
255. Mombouli, J.V., et al., *Potentiation of Ca2+ signaling in endothelial cells by 11,12-epoxyeicosatrienoic acid.* J Cardiovasc Pharmacol, 1999. **33**(5): p. 779-84.
256. Fasolato, C., M. Hoth, and R. Penner, *A GTP-dependent step in the activation mechanism of capacitative calcium influx.* J Biol Chem, 1993. **268**(28): p. 20737-40.
257. Yao, Y., et al., *Activation of store-operated Ca2+ current in Xenopus oocytes requires SNAP-25 but not a diffusible messenger.* Cell, 1999. **98**(4): p. 475-85.
258. Irvine, R.F., *'Quantal' Ca2+ release and the control of Ca2+ entry by inositol phosphates--a possible mechanism.* FEBS Lett, 1990. **263**(1): p. 5-9.
259. Cabello, O.A. and W.P. Schilling, *Vectorial Ca2+ flux from the extracellular space to the endoplasmic reticulum via a restricted cytoplasmic compartment regulates inositol 1,4,5-trisphosphate-stimulated Ca2+ release from internal stores in vascular endothelial cells.* Biochem J, 1993. **295 (Pt 2)**: p. 357-66.
260. Roos, J., et al., *STIM1, an essential and conserved component of store-operated Ca2+ channel function.* J Cell Biol, 2005. **169**(3): p. 435-45.

261. Liou, J., et al., *STIM is a Ca2+ sensor essential for Ca2+-store-depletion-triggered Ca2+ influx.* Curr Biol, 2005. **15**(13): p. 1235-41.
262. Feske, S., et al., *A mutation in Orai1 causes immune deficiency by abrogating CRAC channel function.* Nature, 2006. **441**(7090): p. 179-85.
263. Putney, J.W., Jr., *Recent breakthroughs in the molecular mechanism of capacitative calcium entry (with thoughts on how we got here).* Cell Calcium, 2007. **42**(2): p. 103-10.
264. Abdullaev, I.F., et al., *Stim1 and Orai1 mediate CRAC currents and store-operated calcium entry important for endothelial cell proliferation.* Circ Res, 2008. **103**(11): p. 1289-99.
265. Rink, T.J. and T.J. Hallam, *Calcium signalling in non-excitable cells: notes on oscillations and store refilling.* Cell Calcium, 1989. **10**(5): p. 385-95.
266. Sage, S.O., D.J. Adams, and C. van Breemen, *Synchronized oscillations in cytoplasmic free calcium concentration in confluent bradykinin-stimulated bovine pulmonary artery endothelial cell monolayers.* J Biol Chem, 1989. **264**(1): p. 6-9.
267. Carter, T.D. and D. Ogden, *Kinetics of Ca2+ release by InsP3 in pig single aortic endothelial cells: evidence for an inhibitory role of cytosolic Ca2+ in regulating hormonally evoked Ca2+ spikes.* J Physiol, 1997. **504 (Pt 1)**: p. 17-33.
268. Marshall, I.C. and C.W. Taylor, *Biphasic effects of cytosolic Ca2+ on Ins(1,4,5)P3-stimulated Ca2+ mobilization in hepatocytes.* J Biol Chem, 1993. **268**(18): p. 13214-20.
269. Bezprozvanny, I., J. Watras, and B.E. Ehrlich, *Bell-shaped calcium-response curves of Ins(1,4,5)P3- and calcium-gated channels from endoplasmic reticulum of cerebellum.* Nature, 1991. **351**(6329): p. 751-4.
270. Iino, M. and M. Endo, *Calcium-dependent immediate feedback control of inositol 1,4,5-triphosphate-induced Ca2+ release.* Nature, 1992. **360**(6399): p. 76-8.
271. Finch, E.A., T.J. Turner, and S.M. Goldin, *Calcium as a coagonist of inositol 1,4,5-trisphosphate-induced calcium release.* Science, 1991. **252**(5004): p. 443-6.
272. Goto, Y., M. Miura, and T. Iijima, *Extrusion mechanisms of intracellular Ca2+ in human aortic endothelial cells.* Eur J Pharmacol, 1996. **314**(1-2): p. 185-92.
273. Kaftan, E.J., B.E. Ehrlich, and J. Watras, *Inositol 1,4,5-trisphosphate (InsP3) and calcium interact to increase the dynamic range of InsP3 receptor-dependent calcium signaling.* J Gen Physiol, 1997. **110**(5): p. 529-38.
274. Kasai, H., Y.X. Li, and Y. Miyashita, *Subcellular distribution of Ca2+ release channels underlying Ca2+ waves and oscillations in exocrine pancreas.* Cell, 1993. **74**(4): p. 669-77.
275. Iino, M., et al., *Critical intracellular Ca2+ concentration for all-or-none Ca2+ spiking in single smooth muscle cells.* Embo J, 1993. **12**(13): p. 5287-91.
276. Rooney, T.A., E.J. Sass, and A.P. Thomas, *Agonist-induced cytosolic calcium oscillations originate from a specific locus in single hepatocytes.* J Biol Chem, 1990. **265**(18): p. 10792-6.

277. Dupont, G. and A. Goldbeter, *Properties of intracellular Ca2+ waves generated by a model based on Ca(2+)-induced Ca2+ release.* Biophys J, 1994. **67**(6): p. 2191-204.
278. Moerenhout, M., J. Vereecke, and B. Himpens, *Mechanism of intracellular Ca(2+)-wave propagation elicited by mechanical stimulation in cultured endothelial CPAE cells.* Cell Calcium, 2001. **29**(2): p. 117-23.
279. Douglas, W.W., *Stimulus-secretion coupling: the concept and clues from chromaffin and other cells.* Br J Pharmacol, 1968. **34**(3): p. 451-74.
280. Tse, F.W., et al., *Local Ca2+ release from internal stores controls exocytosis in pituitary gonadotrophs.* Neuron, 1997. **18**(1): p. 121-32.
281. Finnegan, J.M. and R.M. Wightman, *Correlation of real-time catecholamine release and cytosolic Ca2+ at single bovine chromaffin cells.* J Biol Chem, 1995. **270**(10): p. 5353-9.
282. Malgaroli, A. and J. Meldolesi, *[Ca2+]i oscillations from internal stores sustain exocytic secretion from the chromaffin cells of the rat.* FEBS Lett, 1991. **283**(2): p. 169-72.
283. Tengholm, A. and E. Gylfe, *Oscillatory control of insulin secretion.* Mol Cell Endocrinol, 2008.
284. Foskett, J.K. and J.E. Melvin, *Activation of salivary secretion: coupling of cell volume and [Ca2+]i in single cells.* Science, 1989. **244**(4912): p. 1582-5.
285. Cuthbertson, K.S. and P.H. Cobbold, *Phorbol ester and sperm activate mouse oocytes by inducing sustained oscillations in cell Ca2+.* Nature, 1985. **316**(6028): p. 541-2.
286. Millard, P.J., et al., *Immunoglobulin E receptor cross-linking induces oscillations in intracellular free ionized calcium in individual tumor mast cells.* J Biol Chem, 1989. **264**(33): p. 19730-9.
287. Marks, P.W. and F.R. Maxfield, *Transient increases in cytosolic free calcium appear to be required for the migration of adherent human neutrophils.* J Cell Biol, 1990. **110**(1): p. 43-52.
288. Weissberg, P.L., P.J. Little, and A. Bobik, *Spontaneous oscillations in cytoplasmic calcium concentration in vascular smooth muscle.* Am J Physiol, 1989. **256**(5 Pt 1): p. C951-7.
289. Neylon, C.B. and R.F. Irvine, *Synchronized repetitive spikes in cytoplasmic calcium in confluent monolayers of human umbilical vein endothelial cells.* FEBS Lett, 1990. **275**(1-2): p. 173-6.
290. Woods, N.M., K.S. Cuthbertson, and P.H. Cobbold, *Agonist-induced oscillations in cytoplasmic free calcium concentration in single rat hepatocytes.* Cell Calcium, 1987. **8**(1): p. 79-100.
291. Lisman, J., H. Schulman, and H. Cline, *The molecular basis of CaMKII function in synaptic and behavioural memory.* Nat Rev Neurosci, 2002. **3**(3): p. 175-90.
292. Dolmetsch, R.E., K. Xu, and R.S. Lewis, *Calcium oscillations increase the efficiency and specificity of gene expression.* Nature, 1998. **392**(6679): p. 933-6.
293. Kasai, H. and G.J. Augustine, *Cytosolic Ca2+ gradients triggering unidirectional fluid secretion from exocrine pancreas.* Nature, 1990. **348**(6303): p. 735-8.

294. Jung, S.R., et al., *Pattern of Ca2+ increase determines the type of secretory mechanism activated in dog pancreatic duct epithelial cells.* J Physiol, 2006. **576**(Pt 1): p. 163-78.
295. Goldbeter, A., G. Dupont, and M.J. Berridge, *Minimal model for signal-induced Ca2+ oscillations and for their frequency encoding through protein phosphorylation.* Proc Natl Acad Sci U S A, 1990. **87**(4): p. 1461-5.
296. Oancea, E. and T. Meyer, *Protein kinase C as a molecular machine for decoding calcium and diacylglycerol signals.* Cell, 1998. **95**(3): p. 307-18.
297. Montero, M., et al., *Modulation of histamine-induced Ca2+ release by protein kinase C. Effects on cytosolic and mitochondrial [Ca2+] peaks.* J Biol Chem, 2003. **278**(50): p. 49972-9.
298. Ferris, C.D., et al., *Inositol trisphosphate receptor: phosphorylation by protein kinase C and calcium calmodulin-dependent protein kinases in reconstituted lipid vesicles.* Proc Natl Acad Sci U S A, 1991. **88**(6): p. 2232-5.
299. Giovannucci, D.R., et al., *Targeted phosphorylation of inositol 1,4,5-trisphosphate receptors selectively inhibits localized Ca2+ release and shapes oscillatory Ca2+ signals.* J Biol Chem, 2000. **275**(43): p. 33704-11.
300. Bruce, J.I., et al., *Phosphorylation of inositol 1,4,5-trisphosphate receptors in parotid acinar cells. A mechanism for the synergistic effects of cAMP on Ca2+ signaling.* J Biol Chem, 2002. **277**(2): p. 1340-8.
301. Hajnoczky, G., et al., *Multiple mechanisms by which protein kinase A potentiates inositol 1,4,5-trisphosphate-induced Ca2+ mobilization in permeabilized hepatocytes.* Biochem J, 1993. **293 (Pt 2)**: p. 413-22.
302. Komalavilas, P. and T.M. Lincoln, *Phosphorylation of the inositol 1,4,5-trisphosphate receptor. Cyclic GMP-dependent protein kinase mediates cAMP and cGMP dependent phosphorylation in the intact rat aorta.* J Biol Chem, 1996. **271**(36): p. 21933-8.
303. De Koninck, P. and H. Schulman, *Sensitivity of CaM kinase II to the frequency of Ca2+ oscillations.* Science, 1998. **279**(5348): p. 227-30.
304. Sedova, M. and L.A. Blatter, *Dynamic regulation of [Ca2+]i by plasma membrane Ca(2+)-ATPase and Na+/Ca2+ exchange during capacitative Ca2+ entry in bovine vascular endothelial cells.* Cell Calcium, 1999. **25**(5): p. 333-43.
305. Hansen, B.A., D.C. Batlle, and M.E. O'Donnell, *Sodium-calcium exchange in bovine aortic endothelial cells.* Ann N Y Acad Sci, 1991. **639**: p. 566-9.
306. Sage, S.O., C. van Breemen, and M.B. Cannell, *Sodium-calcium exchange in cultured bovine pulmonary artery endothelial cells.* J Physiol, 1991. **440**: p. 569-80.
307. Morgan, A.J. and R. Jacob, *Differential modulation of the phases of a Ca2+ spike by the store Ca2+-ATPase in human umbilical vein endothelial cells.* J Physiol, 1998. **513 (Pt 1)**: p. 83-101.
308. Berridge, M.J., M.D. Bootman, and H.L. Roderick, *Calcium signalling: dynamics, homeostasis and remodelling.* Nat Rev Mol Cell Biol, 2003. **4**(7): p. 517-29.
309. Blaustein, M.P. and W.J. Lederer, *Sodium/calcium exchange: its physiological implications.* Physiol Rev, 1999. **79**(3): p. 763-854.

310. Mountian, I., et al., *Expression patterns of sarco/endoplasmic reticulum Ca(2+)-ATPase and inositol 1,4,5-trisphosphate receptor isoforms in vascular endothelial cells.* Cell Calcium, 1999. **25**(5): p. 371-80.
311. Gunter, T.E. and D.R. Pfeiffer, *Mechanisms by which mitochondria transport calcium.* Am J Physiol, 1990. **258**(5 Pt 1): p. C755-86.
312. Domotor, E., N.J. Abbott, and V. Adam-Vizi, *Na+-Ca2+ exchange and its implications for calcium homeostasis in primary cultured rat brain microvascular endothelial cells.* J Physiol, 1999. **515 (Pt 1)**: p. 147-55.
313. Mogami, H., A.V. Tepikin, and O.H. Petersen, *Termination of cytosolic Ca2+ signals: Ca2+ reuptake into intracellular stores is regulated by the free Ca2+ concentration in the store lumen.* Embo J, 1998. **17**(2): p. 435-42.
314. Moccia, F., et al., *Ca2+ uptake by the endoplasmic reticulum Ca2+-ATPase in rat microvascular endothelial cells.* Biochem J, 2002. **364**(Pt 1): p. 235-44.
315. Michaux, G. and D.F. Cutler, *How to roll an endothelial cigar: the biogenesis of Weibel-Palade bodies.* Traffic, 2004. **5**(2): p. 69-78.
316. Wagner, D.D., et al., *Induction of specific storage organelles by von Willebrand factor propolypeptide.* Cell, 1991. **64**(2): p. 403-13.
317. Voorberg, J., et al., *Biogenesis of von Willebrand factor-containing organelles in heterologous transfected CV-1 cells.* Embo J, 1993. **12**(2): p. 749-58.
318. Denis, C., et al., *A mouse model of severe von Willebrand disease: defects in hemostasis and thrombosis.* Proc Natl Acad Sci U S A, 1998. **95**(16): p. 9524-9.
319. Sadler, J.E., et al., *Cloning and characterization of two cDNAs coding for human von Willebrand factor.* Proc Natl Acad Sci U S A, 1985. **82**(19): p. 6394-8.
320. Ginsburg, D., et al., *Human von Willebrand factor (vWF): isolation of complementary DNA (cDNA) clones and chromosomal localization.* Science, 1985. **228**(4706): p. 1401-6.
321. Titani, K., et al., *Amino acid sequence of human von Willebrand factor.* Biochemistry, 1986. **25**(11): p. 3171-84.
322. Collins, C.J., et al., *Molecular cloning of the human gene for von Willebrand factor and identification of the transcription initiation site.* Proc Natl Acad Sci U S A, 1987. **84**(13): p. 4393-7.
323. Verweij, C.L., et al., *Full-length von Willebrand factor (vWF) cDNA encodes a highly repetitive protein considerably larger than the mature vWF subunit.* Embo J, 1986. **5**(8): p. 1839-47.
324. Blobel, G. and V.R. Potter, *Studies on free and membrane-bound ribosomes in rat liver. I. Distribution as related to total cellular RNA.* J Mol Biol, 1967. **26**(2): p. 279-92.
325. Lippincott-Schwartz, J., T.H. Roberts, and K. Hirschberg, *Secretory protein trafficking and organelle dynamics in living cells.* Annu Rev Cell Dev Biol, 2000. **16**: p. 557-89.
326. Sabatini, D.D., Y. Tashiro, and G.E. Palade, *On the attachment of ribosomes to microsomal membranes.* J Mol Biol, 1966. **19**(2): p. 503-24.
327. Walter, P. and A.E. Johnson, *Signal sequence recognition and protein targeting to the endoplasmic reticulum membrane.* Annu Rev Cell Biol, 1994. **10**: p. 87-119.

328. Redman, C.M. and D.D. Sabatini, *Vectorial discharge of peptides released by puromycin from attached ribosomes.* Proc Natl Acad Sci U S A, 1966. **56**(2): p. 608-15.
329. Anelli, T. and R. Sitia, *Protein quality control in the early secretory pathway.* Embo J, 2008. **27**(2): p. 315-27.
330. Wagner, D.D. and V.J. Marder, *Biosynthesis of von Willebrand protein by human endothelial cells. Identification of a large precursor polypeptide chain.* J Biol Chem, 1983. **258**(4): p. 2065-7.
331. Wagner, D.D. and V.J. Marder, *Biosynthesis of von Willebrand protein by human endothelial cells: processing steps and their intracellular localization.* J Cell Biol, 1984. **99**(6): p. 2123-30.
332. Fretto, L.J., et al., *Substructure of human von Willebrand factor. Proteolysis by V8 and characterization of two functional domains.* J Biol Chem, 1986. **261**(33): p. 15679-89.
333. Fowler, W.E., et al., *Substructure of human von Willebrand factor.* J Clin Invest, 1985. **76**(4): p. 1491-500.
334. Wagner, D.D., T. Mayadas, and V.J. Marder, *Initial glycosylation and acidic pH in the Golgi apparatus are required for multimerization of von Willebrand factor.* J Cell Biol, 1986. **102**(4): p. 1320-4.
335. Voorberg, J., et al., *Assembly and routing of von Willebrand factor variants: the requirements for disulfide-linked dimerization reside within the carboxy-terminal 151 amino acids.* J Cell Biol, 1991. **113**(1): p. 195-205.
336. Serafini, T., et al., *ADP-ribosylation factor is a subunit of the coat of Golgi-derived COP-coated vesicles: a novel role for a GTP-binding protein.* Cell, 1991. **67**(2): p. 239-53.
337. Griffiths, G. and K. Simons, *The trans Golgi network: sorting at the exit site of the Golgi complex.* Science, 1986. **234**(4775): p. 438-43.
338. Moore, H.P. and R.B. Kelly, *Secretory protein targeting in a pituitary cell line: differential transport of foreign secretory proteins to distinct secretory pathways.* J Cell Biol, 1985. **101**(5 Pt 1): p. 1773-81.
339. Orci, L., et al., *The trans-most cisternae of the Golgi complex: a compartment for sorting of secretory and plasma membrane proteins.* Cell, 1987. **51**(6): p. 1039-51.
340. Tooze, S.A. and W.B. Huttner, *Cell-free protein sorting to the regulated and constitutive secretory pathways.* Cell, 1990. **60**(5): p. 837-47.
341. Novikoff, A.B., E. Essner, and N. Quintana, *Golgi Apparatus and Lysosomes.* Fed Proc, 1964. **23**: p. 1010-22.
342. Griffiths, G., et al., *The dynamic nature of the Golgi complex.* J Cell Biol, 1989. **108**(2): p. 277-97.
343. Jamieson, J.D. and G.E. Palade, *Synthesis, intracellular transport, and discharge of secretory proteins in stimulated pancreatic exocrine cells.* J Cell Biol, 1971. **50**(1): p. 135-58.
344. Wu, M.M., et al., *Mechanisms of pH regulation in the regulated secretory pathway.* J Biol Chem, 2001. **276**(35): p. 33027-35.
345. Llopis, J., et al., *Measurement of cytosolic, mitochondrial, and Golgi pH in single living cells with green fluorescent proteins.* Proc Natl Acad Sci U S A, 1998. **95**(12): p. 6803-8.

346. Paroutis, P., N. Touret, and S. Grinstein, *The pH of the secretory pathway: measurement, determinants, and regulation.* Physiology (Bethesda), 2004. **19**: p. 207-15.
347. Moore, H.P., et al., *Biosynthesis and secretion of pituitary hormones: dynamics and regulation.* Arch Physiol Biochem, 2002. **110**(1-2): p. 16-25.
348. Carew, J.A., P.J. Browning, and D.C. Lynch, *Sulfation of von Willebrand factor.* Blood, 1990. **76**(12): p. 2530-9.
349. Denault, J.B., et al., *Processing of proendothelin-1 by human furin convertase.* FEBS Lett, 1995. **362**(3): p. 276-80.
350. Sporn, L.A., V.J. Marder, and D.D. Wagner, *Inducible secretion of large, biologically potent von Willebrand factor multimers.* Cell, 1986. **46**(2): p. 185-90.
351. Wagner, D.D., et al., *Divergent fates of von Willebrand factor and its propolypeptide (von Willebrand antigen II) after secretion from endothelial cells.* Proc Natl Acad Sci U S A, 1987. **84**(7): p. 1955-9.
352. Verweij, C.L., M. Hart, and H. Pannekoek, *Expression of variant von Willebrand factor (vWF) cDNA in heterologous cells: requirement of the pro-polypeptide in vWF multimer formation.* Embo J, 1987. **6**(10): p. 2885-90.
353. Wise, R.J., et al., *The propeptide of von Willebrand factor independently mediates the assembly of von Willebrand multimers.* Cell, 1988. **52**(2): p. 229-36.
354. Mayadas, T.N. and D.D. Wagner, *In vitro multimerization of von Willebrand factor is triggered by low pH. Importance of the propolypeptide and free sulfhydryls.* J Biol Chem, 1989. **264**(23): p. 13497-503.
355. Mayadas, T.N. and D.D. Wagner, *Vicinal cysteines in the prosequence play a role in von Willebrand factor multimer assembly.* Proc Natl Acad Sci U S A, 1992. **89**(8): p. 3531-5.
356. Lui-Roberts, W.W., et al., *An AP-1/clathrin coat plays a novel and essential role in forming the Weibel-Palade bodies of endothelial cells.* J Cell Biol, 2005. **170**(4): p. 627-36.
357. Pennica, D., et al., *Cloning and expression of human tissue-type plasminogen activator cDNA in E. coli.* Nature, 1983. **301**(5897): p. 214-21.
358. Pohl, G., et al., *Tissue plasminogen activator: peptide analyses confirm an indirectly derived amino acid sequence, identify the active site serine residue, establish glycosylation sites, and localize variant differences.* Biochemistry, 1984. **23**(16): p. 3701-7.
359. Burgess, T.L. and R.B. Kelly, *Constitutive and regulated secretion of proteins.* Annu Rev Cell Biol, 1987. **3**: p. 243-93.
360. Griffiths, G., et al., *Exit of newly synthesized membrane proteins from the trans cisterna of the Golgi complex to the plasma membrane.* J Cell Biol, 1985. **101**(3): p. 949-64.
361. Baron, C.L. and V. Malhotra, *Role of diacylglycerol in PKD recruitment to the TGN and protein transport to the plasma membrane.* Science, 2002. **295**(5553): p. 325-8.
362. Bard, F. and V. Malhotra, *The formation of TGN-to-plasma-membrane transport carriers.* Annu Rev Cell Dev Biol, 2006. **22**: p. 439-55.

363. Brignoni, M., et al., *Cyclic AMP modulates the rate of 'constitutive' exocytosis of apical membrane proteins in Madin-Darby canine kidney cells.* J Cell Sci, 1995. **108 (Pt 5)**: p. 1931-43.
364. Buys, S.S., E.A. Keogh, and J. Kaplan, *Fusion of intracellular membrane pools with cell surfaces of macrophages stimulated by phorbol esters and calcium ionophores.* Cell, 1984. **38**(2): p. 569-76.
365. Beckers, C.J. and W.E. Balch, *Calcium and GTP: essential components in vesicular trafficking between the endoplasmic reticulum and Golgi apparatus.* J Cell Biol, 1989. **108**(4): p. 1245-56.
366. Chang, S., et al., *Constitutive secretion of exogenous neurotransmitter by nonneuronal cells: implications for neuronal secretion.* Biophys J, 1998. **75**(3): p. 1354-64.
367. Page, E., et al., *Inhibition of atrial peptide secretion at different stages of the secretory process: Ca2+ dependence.* Am J Physiol, 1991. **261**(6 Pt 1): p. C1162-72.
368. Verchere, C.B., et al., *The constitutive secretory pathway is a major route for islet amyloid polypeptide secretion in neonatal but not adult rat islet cells.* Diabetes, 2000. **49**(9): p. 1477-84.
369. De Lisle, R.C. and R. Bansal, *Brefeldin A inhibits the constitutive-like secretion of a sulfated protein in pancreatic acinar cells.* Eur J Cell Biol, 1996. **71**(1): p. 62-71.
370. Baumgartner, R.A., V.A. Deramo, and M.A. Beaven, *Constitutive and inducible mechanisms for synthesis and release of cytokines in immune cell lines.* J Immunol, 1996. **157**(9): p. 4087-93.
371. Giblin, J.P., L.J. Hewlett, and M.J. Hannah, *Basal secretion of von Willebrand factor from human endothelial cells.* Blood, 2008. **112**(4): p. 957-64.
372. Saraste, J., G.E. Palade, and M.G. Farquhar, *Temperature-sensitive steps in the transport of secretory proteins through the Golgi complex in exocrine pancreatic cells.* Proc Natl Acad Sci U S A, 1986. **83**(17): p. 6425-9.
373. Hirschberg, K., et al., *Kinetic analysis of secretory protein traffic and characterization of golgi to plasma membrane transport intermediates in living cells.* J Cell Biol, 1998. **143**(6): p. 1485-503.
374. Miller, S.G. and H.P. Moore, *Reconstitution of constitutive secretion using semi-intact cells: regulation by GTP but not calcium.* J Cell Biol, 1991. **112**(1): p. 39-54.
375. Santell, L., K.R. Marotti, and E.G. Levin, *Targeting of tissue plasminogen activator into the regulated secretory pathway of neuroendocrine cells.* Brain Res, 1999. **816**(1): p. 258-65.
376. Brion, C., S.G. Miller, and H.P. Moore, *Regulated and constitutive secretion. Differential effects of protein synthesis arrest on transport of glycosaminoglycan chains to the two secretory pathways.* J Biol Chem, 1992. **267**(3): p. 1477-83.
377. Matsuuchi, L. and R.B. Kelly, *Constitutive and basal secretion from the endocrine cell line, AtT-20.* J Cell Biol, 1991. **112**(5): p. 843-52.
378. Bergen, L.G., R. Kuriyama, and G.G. Borisy, *Polarity of microtubules nucleated by centrosomes and chromosomes of Chinese hamster ovary cells in vitro.* J Cell Biol, 1980. **84**(1): p. 151-9.

379. Kupfer, A., S.J. Singer, and G. Dennert, *On the mechanism of unidirectional killing in mixtures of two cytotoxic T lymphocytes. Unidirectional polarization of cytoplasmic organelles and the membrane-associated cytoskeleton in the effector cell.* J Exp Med, 1986. **163**(3): p. 489-98.
380. Vale, R.D., T.S. Reese, and M.P. Sheetz, *Identification of a novel force-generating protein, kinesin, involved in microtubule-based motility.* Cell, 1985. **42**(1): p. 39-50.
381. Orci, L., et al., *Monolayer cell culture of neonatal rat pancreas: an ultrastructural and biochemical study of functioning endocrine cells.* J Ultrastruct Res, 1973. **43**(3): p. 270-97.
382. Freed, J.J. and M.M. Lebowitz, *The association of a class of saltatory movements with microtubules in cultured cells.* J Cell Biol, 1970. **45**(2): p. 334-54.
383. Sinha, S. and D.D. Wagner, *Intact microtubules are necessary for complete processing, storage and regulated secretion of von Willebrand factor by endothelial cells.* Eur J Cell Biol, 1987. **43**(3): p. 377-83.
384. Goode, B.L., D.G. Drubin, and G. Barnes, *Functional cooperation between the microtubule and actin cytoskeletons.* Curr Opin Cell Biol, 2000. **12**(1): p. 63-71.
385. Rogers, S.L. and V.I. Gelfand, *Membrane trafficking, organelle transport, and the cytoskeleton.* Curr Opin Cell Biol, 2000. **12**(1): p. 57-62.
386. Valentijn, K.M., F.D. Gumkowski, and J.D. Jamieson, *The subapical actin cytoskeleton regulates secretion and membrane retrieval in pancreatic acinar cells.* J Cell Sci, 1999. **112 (Pt 1)**: p. 81-96.
387. Orci, L., K.H. Gabbay, and W.J. Malaisse, *Pancreatic beta-cell web: its possible role in insulin secretion.* Science, 1972. **175**(26): p. 1128-30.
388. Burgoyne, R.D., M.J. Geisow, and J. Barron, *Dissection of stages in exocytosis in the adrenal chromaffin cell with use of trifluoperazine.* Proc R Soc Lond B Biol Sci, 1982. **216**(1202): p. 111-5.
389. Vitale, M.L., E.P. Seward, and J.M. Trifaro, *Chromaffin cell cortical actin network dynamics control the size of the release-ready vesicle pool and the initial rate of exocytosis.* Neuron, 1995. **14**(2): p. 353-63.
390. Manneville, J.B., et al., *Interaction of the actin cytoskeleton with microtubules regulates secretory organelle movement near the plasma membrane in human endothelial cells.* J Cell Sci, 2003. **116**(Pt 19): p. 3927-38.
391. Birks, R.I. and F.C. Macintosh, *Acetylcholine metabolism at nerve-endings.* Br Med Bull, 1957. **13**(3): p. 157-61.
392. Elmqvist, D. and D.M. Quastel, *A quantitative study of end-plate potentials in isolated human muscle.* J Physiol, 1965. **178**(3): p. 505-29.
393. Heinemann, C., et al., *A two-step model of secretion control in neuroendocrine cells.* Pflugers Arch, 1993. **424**(2): p. 105-12.
394. Smith, C., et al., *Cytosolic Ca2+ acts by two separate pathways to modulate the supply of release-competent vesicles in chromaffin cells.* Neuron, 1998. **20**(6): p. 1243-53.
395. Voets, T., E. Neher, and T. Moser, *Mechanisms underlying phasic and sustained secretion in chromaffin cells from mouse adrenal slices.* Neuron, 1999. **23**(3): p. 607-15.

396. Bennett, M.K., N. Calakos, and R.H. Scheller, *Syntaxin: a synaptic protein implicated in docking of synaptic vesicles at presynaptic active zones.* Science, 1992. **257**(5067): p. 255-9.
397. Steyer, J.A., H. Horstmann, and W. Almers, *Transport, docking and exocytosis of single secretory granules in live chromaffin cells.* Nature, 1997. **388**(6641): p. 474-8.
398. Rizzoli, S.O. and W.J. Betz, *The structural organization of the readily releasable pool of synaptic vesicles.* Science, 2004. **303**(5666): p. 2037-9.
399. Voets, T., et al., *Intracellular calcium dependence of large dense-core vesicle exocytosis in the absence of synaptotagmin I.* Proc Natl Acad Sci U S A, 2001. **98**(20): p. 11680-5.
400. Trimble, W.S., D.M. Cowan, and R.H. Scheller, *VAMP-1: a synaptic vesicle-associated integral membrane protein.* Proc Natl Acad Sci U S A, 1988. **85**(12): p. 4538-42.
401. Oyler, G.A., et al., *The identification of a novel synaptosomal-associated protein, SNAP-25, differentially expressed by neuronal subpopulations.* J Cell Biol, 1989. **109**(6 Pt 1): p. 3039-52.
402. Sollner, T., et al., *A protein assembly-disassembly pathway in vitro that may correspond to sequential steps of synaptic vesicle docking, activation, and fusion.* Cell, 1993. **75**(3): p. 409-18.
403. Yerrapureddy, A., et al., *Intracellular interaction between syntaxin and Munc 18-1 revealed by fluorescence resonance energy transfer.* Mol Membr Biol, 2005. **22**(5): p. 401-10.
404. Rizo, J. and T.C. Sudhof, *Snares and Munc18 in synaptic vesicle fusion.* Nat Rev Neurosci, 2002. **3**(8): p. 641-53.
405. Craig, T.J., G.J. Evans, and A. Morgan, *Physiological regulation of Munc18/nSec1 phosphorylation on serine-313.* J Neurochem, 2003. **86**(6): p. 1450-7.
406. Sutton, R.B., et al., *Crystal structure of a SNARE complex involved in synaptic exocytosis at 2.4 A resolution.* Nature, 1998. **395**(6700): p. 347-53.
407. Lynch, K.L., et al., *Synaptotagmin C2A loop 2 mediates Ca2+-dependent SNARE interactions essential for Ca2+-triggered vesicle exocytosis.* Mol Biol Cell, 2007. **18**(12): p. 4957-68.
408. Creutz, C.E., *The annexins and exocytosis.* Science, 1992. **258**(5084): p. 924-31.
409. Donnelly, S.R. and S.E. Moss, *Annexins in the secretory pathway.* Cell Mol Life Sci, 1997. **53**(6): p. 533-8.
410. Rizo, J., X. Chen, and D. Arac, *Unraveling the mechanisms of synaptotagmin and SNARE function in neurotransmitter release.* Trends Cell Biol, 2006. **16**(7): p. 339-50.
411. Nilius, B., et al., *Annexin II modulates volume-activated chloride currents in vascular endothelial cells.* J Biol Chem, 1996. **271**(48): p. 30631-6.
412. Konig, J., et al., *The annexin II-p11 complex is involved in regulated exocytosis in bovine pulmonary artery endothelial cells.* J Biol Chem, 1998. **273**(31): p. 19679-84.
413. Chasserot-Golaz, S., et al., *Annexin 2 promotes the formation of lipid microdomains required for calcium-regulated exocytosis of dense-core vesicles.* Mol Biol Cell, 2005. **16**(3): p. 1108-19.

414. Wang, L., G. Li, and S. Sugita, *RalA-exocyst interaction mediates GTP-dependent exocytosis.* J Biol Chem, 2004. **279**(19): p. 19875-81.
415. Li, G., et al., *RalA and RalB function as the critical GTP sensors for GTP-dependent exocytosis.* J Neurosci, 2007. **27**(1): p. 190-202.
416. Lipschutz, J.H. and K.E. Mostov, *Exocytosis: the many masters of the exocyst.* Curr Biol, 2002. **12**(6): p. R212-4.
417. Moskalenko, S., et al., *The exocyst is a Ral effector complex.* Nat Cell Biol, 2002. **4**(1): p. 66-72.
418. Vitale, N., et al., *The Small GTPase RalA controls exocytosis of large dense core secretory granules by interacting with ARF6-dependent phospholipase D1.* J Biol Chem, 2005. **280**(33): p. 29921-8.
419. Goehring, A.S., et al., *MyRIP anchors protein kinase A to the exocyst complex.* J Biol Chem, 2007. **282**(45): p. 33155-67.
420. de Leeuw, H.P., et al., *Small GTP-binding protein Ral modulates regulated exocytosis of von Willebrand factor by endothelial cells.* Arterioscler Thromb Vasc Biol, 2001. **21**(6): p. 899-904.
421. Fu, J., et al., *Protease-activated receptor-1 activation of endothelial cells induces protein kinase Calpha-dependent phosphorylation of syntaxin 4 and Munc18c: role in signaling p-selectin expression.* J Biol Chem, 2005. **280**(5): p. 3178-84.
422. Matsushita, K., et al., *Nitric oxide regulates exocytosis by S-nitrosylation of N-ethylmaleimide-sensitive factor.* Cell, 2003. **115**(2): p. 139-50.
423. Matsushita, K., C.N. Morrell, and C.J. Lowenstein, *A novel class of fusion polypeptides inhibits exocytosis.* Mol Pharmacol, 2005. **67**(4): p. 1137-44.
424. Blagoveshchenskaya, A.D., et al., *Selective and signal-dependent recruitment of membrane proteins to secretory granules formed by heterologously expressed von Willebrand factor.* Mol Biol Cell, 2002. **13**(5): p. 1582-93.
425. Rondaij, M.G., et al., *Small GTP-binding protein Ral is involved in cAMP-mediated release of von Willebrand factor from endothelial cells.* Arterioscler Thromb Vasc Biol, 2004. **24**(7): p. 1315-20.
426. Rothman, J.E. and F.T. Wieland, *Protein sorting by transport vesicles.* Science, 1996. **272**(5259): p. 227-34.
427. Holt, M., et al., *Synaptic vesicles are constitutively active fusion machines that function independently of Ca2+.* Curr Biol, 2008. **18**(10): p. 715-22.
428. Burgoyne, R.D. and A. Morgan, *Secretory granule exocytosis.* Physiol Rev, 2003. **83**(2): p. 581-632.
429. Fesce, R., et al., *Neurotransmitter release: fusion or 'kiss-and-run'?* Trends Cell Biol, 1994. **4**(1): p. 1-4.
430. Ceccarelli, B., W.P. Hurlbut, and A. Mauro, *Turnover of transmitter and synaptic vesicles at the frog neuromuscular junction.* J Cell Biol, 1973. **57**(2): p. 499-524.
431. Breckenridge, L.J. and W. Almers, *Currents through the fusion pore that forms during exocytosis of a secretory vesicle.* Nature, 1987. **328**(6133): p. 814-7.
432. Albillos, A., et al., *The exocytotic event in chromaffin cells revealed by patch amperometry.* Nature, 1997. **389**(6650): p. 509-12.
433. Scepek, S., J.R. Coorssen, and M. Lindau, *Fusion pore expansion in horse eosinophils is modulated by Ca2+ and protein kinase C via distinct mechanisms.* EMBO J, 1998. **17**(15): p. 4340-5.

434. Lollike, K., N. Borregaard, and M. Lindau, *The exocytotic fusion pore of small granules has a conductance similar to an ion channel.* J Cell Biol, 1995. **129**(1): p. 99-104.
435. Babich, V., et al., *Selective release of molecules from Weibel-Palade bodies during a lingering kiss.* Blood, 2008. **111**(11): p. 5282-90.
436. Rothman, J.E., *Mechanisms of intracellular protein transport.* Nature, 1994. **372**(6501): p. 55-63.
437. Pryer, N.K., L.J. Wuestehube, and R. Schekman, *Vesicle-mediated protein sorting.* Annu Rev Biochem, 1992. **61**: p. 471-516.
438. Holroyd, P., et al., *Imaging direct, dynamin-dependent recapture of fusing secretory granules on plasma membrane lawns from PC12 cells.* Proc Natl Acad Sci U S A, 2002. **99**(26): p. 16806-11.
439. MacDonald, P.E., et al., *Release of small transmitters through kiss-and-run fusion pores in rat pancreatic beta cells.* Cell Metab, 2006. **4**(4): p. 283-90.
440. Zimmerman, T.S., O.D. Ratnoff, and A.E. Powell, *Immunologic differentiation of classic hemophilia (factor 8 deficiency) and von Willebrand's dissase, with observations on combined deficiencies of antihemophilic factor and proaccelerin (factor V) and on an acquired circulating anticoagulant against antihemophilic factor.* J Clin Invest, 1971. **50**(1): p. 244-54.
441. Ruggeri, Z.M. and T.S. Zimmerman, *von Willebrand factor and von Willebrand disease.* Blood, 1987. **70**(4): p. 895-904.
442. Jaffe, E.A., L.W. Hoyer, and R.L. Nachman, *Synthesis of von Willebrand factor by cultured human endothelial cells.* Proc Natl Acad Sci U S A, 1974. **71**(5): p. 1906-9.
443. McEver, R.P. and M.N. Martin, *A monoclonal antibody to a membrane glycoprotein binds only to activated platelets.* J Biol Chem, 1984. **259**(15): p. 9799-804.
444. Sporn, L.A., et al., *Biosynthesis of von Willebrand protein by human megakaryocytes.* J Clin Invest, 1985. **76**(3): p. 1102-6.
445. Nachman, R., R. Levine, and E.A. Jaffe, *Synthesis of factor VIII antigen by cultured guinea pig megakaryocytes.* J Clin Invest, 1977. **60**(4): p. 914-21.
446. Ruggeri, Z.M., *Von Willebrand factor.* Curr Opin Hematol, 2003. **10**(2): p. 142-9.
447. Kieffer, N. and D.R. Phillips, *Platelet membrane glycoproteins: functions in cellular interactions.* Annu Rev Cell Biol, 1990. **6**: p. 329-57.
448. Sporn, L.A., V.J. Marder, and D.D. Wagner, *von Willebrand factor released from Weibel-Palade bodies binds more avidly to extracellular matrix than that secreted constitutively.* Blood, 1987. **69**(5): p. 1531-4.
449. Ofosu, F.A., J. Freedman, and J.W. Semple, *Plasma-derived biological medicines used to promote haemostasis.* Thromb Haemost, 2008. **99**(5): p. 851-62.
450. Franchini, M., *Surgical prophylaxis in von Willebrand's disease: a difficult balance to manage.* Blood Transfus, 2008. **6 Suppl 2**: p. s33-8.
451. Gill, J.C., *Treatment of urgent bleeding in von Willebrand disease.* Thromb Res, 2007. **120 Suppl 1**: p. S21-5.
452. Andrews, R.K., et al., *Glycoprotein Ib-IX-V.* Int J Biochem Cell Biol, 2003. **35**(8): p. 1170-4.

453. Tschopp, T.B., H.J. Weiss, and H.R. Baumgartner, *Decreased adhesion of platelets to subendothelium in von Willebrand's disease.* J Lab Clin Med, 1974. **83**(2): p. 296-300.
454. Houdijk, W.P., et al., *Subendothelial proteins and platelet adhesion. von Willebrand factor and fibronectin, not thrombospondin, are involved in platelet adhesion to extracellular matrix of human vascular endothelial cells.* Arteriosclerosis, 1986. **6**(1): p. 24-33.
455. Loscalzo, J., A. Inbal, and R.I. Handin, *von Willebrand protein facilitates platelet incorporation in polymerizing fibrin.* J Clin Invest, 1986. **78**(4): p. 1112-9.
456. Kroll, M.H., et al., *von Willebrand factor binding to platelet GpIb initiates signals for platelet activation.* J Clin Invest, 1991. **88**(5): p. 1568-73.
457. Razdan, K., J.D. Hellums, and M.H. Kroll, *Shear-stress-induced von Willebrand factor binding to platelets causes the activation of tyrosine kinase(s).* Biochem J, 1994. **302 (Pt 3)**: p. 681-6.
458. Phillips, D.R., et al., *The platelet membrane glycoprotein IIb-IIIa complex.* Blood, 1988. **71**(4): p. 831-43.
459. Kasirer-Friede, A., et al., *Lateral clustering of platelet GP Ib-IX complexes leads to up-regulation of the adhesive function of integrin alpha IIbbeta 3.* J Biol Chem, 2002. **277**(14): p. 11949-56.
460. Fressinaud, E., et al., *Platelet von Willebrand factor: evidence for its involvement in platelet adhesion to collagen.* Blood, 1987. **70**(4): p. 1214-7.
461. Savage, B., F. Almus-Jacobs, and Z.M. Ruggeri, *Specific synergy of multiple substrate-receptor interactions in platelet thrombus formation under flow.* Cell, 1998. **94**(5): p. 657-66.
462. Ofosu, F.A., *The blood platelet as a model for regulating blood coagulation on cell surfaces and its consequences.* Biochemistry (Mosc), 2002. **67**(1): p. 47-55.
463. De Marco, L., et al., *von Willebrand factor interaction with the glycoprotein IIb/IIa complex. Its role in platelet function as demonstrated in patients with congenital afibrinogenemia.* J Clin Invest, 1986. **77**(4): p. 1272-7.
464. Goto, S., et al., *Characterization of the unique mechanism mediating the shear-dependent binding of soluble von Willebrand factor to platelets.* J Biol Chem, 1995. **270**(40): p. 23352-61.
465. Ni, H., et al., *Persistence of platelet thrombus formation in arterioles of mice lacking both von Willebrand factor and fibrinogen.* J Clin Invest, 2000. **106**(3): p. 385-92.
466. De Marco, L., et al., *Interaction of asialo von Willebrand factor with glycoprotein Ib induces fibrinogen binding to the glycoprotein IIb/IIIa complex and mediates platelet aggregation.* J Clin Invest, 1985. **75**(4): p. 1198-203.
467. Tracy, P.B., M.E. Nesheim, and K.G. Mann, *Coordinate binding of factor Va and factor Xa to the unstimulated platelet.* J Biol Chem, 1981. **256**(2): p. 743-51.
468. Mann, K.G., *Thrombin formation.* Chest, 2003. **124**(3 Suppl): p. 4S-10S.
469. Weiss, H.J., Sussman, II, and L.W. Hoyer, *Stabilization of factor VIII in plasma by the von Willebrand factor. Studies on posttransfusion and*

dissociated factor VIII and in patients with von Willebrand's disease. J Clin Invest, 1977. **60**(2): p. 390-404.
470. Lenting, P.J., J.A. van Mourik, and K. Mertens, *The life cycle of coagulation factor VIII in view of its structure and function.* Blood, 1998. **92**(11): p. 3983-96.
471. Foster, P.A., et al., *A major factor VIII binding domain resides within the amino-terminal 272 amino acid residues of von Willebrand factor.* J Biol Chem, 1987. **262**(18): p. 8443-6.
472. Osterud, B. and S.I. Rapaport, *Activation of factor IX by the reaction product of tissue factor and factor VII: additional pathway for initiating blood coagulation.* Proc Natl Acad Sci U S A, 1977. **74**(12): p. 5260-4.
473. Berndt, M.C., et al., *Thrombin interactions with platelet membrane proteins.* Ann N Y Acad Sci, 1986. **485**: p. 374-86.
474. Lorand, L. and K. Konishi, *Activation of the Fibrin Stabilizing Factor of Plasma by Thrombin.* Arch Biochem Biophys, 1964. **105**: p. 58-67.
475. Laudano, A.P. and R.F. Doolittle, *Studies on synthetic peptides that bind to fibrinogen and prevent fibrin polymerization. Structural requirements, number of binding sites, and species differences.* Biochemistry, 1980. **19**(5): p. 1013-9.
476. Lindhout, T., J. Franssen, and G. Willems, *Kinetics of the inhibition of tissue factor-factor VIIa by tissue factor pathway inhibitor.* Thromb Haemost, 1995. **74**(3): p. 910-5.
477. Lupu, C., et al., *Thrombin induces the redistribution and acute release of tissue factor pathway inhibitor from specific granules within human endothelial cells in culture.* Arterioscler Thromb Vasc Biol, 1995. **15**(11): p. 2055-62.
478. Esmon, C.T. and W.G. Owen, *Identification of an endothelial cell cofactor for thrombin-catalyzed activation of protein C.* Proc Natl Acad Sci U S A, 1981. **78**(4): p. 2249-52.
479. Wun, T.C. and A. Capuano, *Initiation and regulation of fibrinolysis in human plasma at the plasminogen activator level.* Blood, 1987. **69**(5): p. 1354-62.
480. Ny, T., F. Elgh, and B. Lund, *The structure of the human tissue-type plasminogen activator gene: correlation of intron and exon structures to functional and structural domains.* Proc Natl Acad Sci U S A, 1984. **81**(17): p. 5355-9.
481. Juhan-Vague, I. and D. Collen, *On the role of coagulation and fibrinolysis in atherosclerosis.* Ann Epidemiol, 1992. **2**(4): p. 427-38.
482. Brommer, E.J., *The level of extrinsic plasminogen activator (t-PA) during clotting as a determinant of the rate of fibrinolysis; inefficiency of activators added afterwards.* Thromb Res, 1984. **34**(2): p. 109-15.
483. Hoylaerts, M., et al., *Kinetics of the activation of plasminogen by human tissue plasminogen activator. Role of fibrin.* J Biol Chem, 1982. **257**(6): p. 2912-9.
484. Harris, T.J., *Second-generation plasminogen activators.* Protein Eng, 1987. **1**(6): p. 449-58.
485. Levin, E.G., *Latent tissue plasminogen activator produced by human endothelial cells in culture: evidence for an enzyme-inhibitor complex.* Proc Natl Acad Sci U S A, 1983. **80**(22): p. 6804-8.

486. Urano, T., et al., *PAI-1 plays an important role in the expression of t-PA activity in the euglobulin clot lysis by controlling the concentration of free t-PA.* Thromb Haemost, 1991. **66**(4): p. 474-8.
487. Wagner, D.D., *New links between inflammation and thrombosis.* Arterioscler Thromb Vasc Biol, 2005. **25**(7): p. 1321-4.
488. Muller, W.A., et al., *PECAM-1 is required for transendothelial migration of leukocytes.* J Exp Med, 1993. **178**(2): p. 449-60.
489. Carlos, T., et al., *Human monocytes bind to two cytokine-induced adhesive ligands on cultured human endothelial cells: endothelial-leukocyte adhesion molecule-1 and vascular cell adhesion molecule-1.* Blood, 1991. **77**(10): p. 2266-71.
490. Meerschaert, J. and M.B. Furie, *The adhesion molecules used by monocytes for migration across endothelium include CD11a/CD18, CD11b/CD18, and VLA-4 on monocytes and ICAM-1, VCAM-1, and other ligands on endothelium.* J Immunol, 1995. **154**(8): p. 4099-112.
491. Weber, C. and T.A. Springer, *Interaction of very late antigen-4 with VCAM-1 supports transendothelial chemotaxis of monocytes by facilitating lateral migration.* J Immunol, 1998. **161**(12): p. 6825-34.
492. Wang, Q., X.N. Tang, and M.A. Yenari, *The inflammatory response in stroke.* J Neuroimmunol, 2006.
493. Into, T., et al., *Pathogen recognition by Toll-like receptor 2 activates Weibel-Palade body exocytosis in human aortic endothelial cells.* J Biol Chem, 2007. **282**(11): p. 8134-41.
494. Yamakuchi, M., et al., *Antibody to human leukocyte antigen triggers endothelial exocytosis.* Proc Natl Acad Sci U S A, 2007. **104**(4): p. 1301-6.
495. Smejkal, P., M. Matyskova, and M. Penka, *[Hemophilia].* Vnitr Lek, 2008. **54**(10): p. 992-9.
496. Rodriguez, N.I. and W.K. Hoots, *Advances in hemophilia: experimental aspects and therapy.* Pediatr Clin North Am, 2008. **55**(2): p. 357-76, viii.
497. Rodeghiero, F., G. Castaman, and E. Dini, *Epidemiological investigation of the prevalence of von Willebrand's disease.* Blood, 1987. **69**(2): p. 454-9.
498. Hovig, T. and H. Stormorken, *Ultrastructural studies on the platelet plug formation in bleeding time wounds from normal individuals and patients with von Willebrand's disease.* Acta Pathol Microbiol Scand Suppl, 1974. **Suppl 248**: p. 105-22.
499. Nichols, W.C. and D. Ginsburg, *von Willebrand disease.* Medicine (Baltimore), 1997. **76**(1): p. 1-20.
500. Badimon, L., et al., *von Willebrand factor and cardiovascular disease.* Thromb Haemost, 1993. **70**(1): p. 111-8.
501. Vischer, U.M., *von Willebrand factor, endothelial dysfunction, and cardiovascular disease.* J Thromb Haemost, 2006. **4**(6): p. 1186-93.
502. Methia, N., et al., *Localized reduction of atherosclerosis in von Willebrand factor-deficient mice.* Blood, 2001. **98**(5): p. 1424-8.
503. Johnson, R.C., et al., *Absence of P-selectin delays fatty streak formation in mice.* J Clin Invest, 1997. **99**(5): p. 1037-43.
504. Terraube, V., I. Marx, and C.V. Denis, *Role of von Willebrand factor in tumor metastasis.* Thromb Res, 2007. **120 Suppl 2**: p. S64-70.

505. Lijnen, H.R. and D. Collen, *Tissue-type plasminogen activator: mutants, variants, and adjunctive treatment.* Biotechnol Ther, 1989. **1**(3): p. 273-304.
506. Skulachev, V.P., *Mitochondrial filaments and clusters as intracellular power-transmitting cables.* Trends Biochem Sci, 2001. **26**(1): p. 23-9.
507. Sherratt, H.S., *Mitochondria: structure and function.* Rev Neurol (Paris), 1991. **147**(6-7): p. 417-30.
508. Rizzuto, R., P. Bernardi, and T. Pozzan, *Mitochondria as all-round players of the calcium game.* J Physiol, 2000. **529 Pt 1**: p. 37-47.
509. Mitchell, P. and J. Moyle, *Respiration-driven proton translocation in rat liver mitochondria.* Biochem J, 1967. **105**(3): p. 1147-1162.
510. Culic, O., M.L. Gruwel, and J. Schrader, *Energy turnover of vascular endothelial cells.* Am J Physiol, 1997. **273**(1 Pt 1): p. C205-13.
511. Spahr, R., et al., *Fatty acids are not an important fuel for coronary microvascular endothelial cells.* Mol Cell Biochem, 1989. **88**(1-2): p. 59-64.
512. Waypa, G.B. and P.T. Schumacker, *Hypoxic pulmonary vasoconstriction: redox events in oxygen sensing.* J Appl Physiol, 2005. **98**(1): p. 404-14.
513. Davidson, S.M. and M.R. Duchen, *Endothelial mitochondria: contributing to vascular function and disease.* Circ Res, 2007. **100**(8): p. 1128-41.
514. Quintero, M., et al., *Mitochondria as signaling organelles in the vascular endothelium.* Proc Natl Acad Sci U S A, 2006. **103**(14): p. 5379-84.
515. Bianchi, K., et al., *Calcium and mitochondria: mechanisms and functions of a troubled relationship.* Biochim Biophys Acta, 2004. **1742**(1-3): p. 119-31.
516. Frey, T.G., C.W. Renken, and G.A. Perkins, *Insight into mitochondrial structure and function from electron tomography.* Biochim Biophys Acta, 2002. **1555**(1-3): p. 196-203.
517. McCormack, J.G., A.P. Halestrap, and R.M. Denton, *Role of calcium ions in regulation of mammalian intramitochondrial metabolism.* Physiol Rev, 1990. **70**(2): p. 391-425.
518. Sesaki, H. and R.E. Jensen, *Division versus fusion: Dnm1p and Fzo1p antagonistically regulate mitochondrial shape.* J Cell Biol, 1999. **147**(4): p. 699-706.
519. Smirnova, E., et al., *Dynamin-related protein Drp1 is required for mitochondrial division in mammalian cells.* Mol Biol Cell, 2001. **12**(8): p. 2245-56.
520. Mozdy, A.D. and J.M. Shaw, *A fuzzy mitochondrial fusion apparatus comes into focus.* Nat Rev Mol Cell Biol, 2003. **4**(6): p. 468-78.
521. Duchen, M.R., A. Surin, and J. Jacobson, *Imaging mitochondrial function in intact cells.* Methods Enzymol, 2003. **361**: p. 353-89.
522. Vasington, F.D. and J.V. Murphy, *Ca ion uptake by rat kidney mitochondria and its dependence on respiration and phosphorylation.* J Biol Chem, 1962. **237**: p. 2670-7.
523. Deluca, H.F. and G.W. Engstrom, *Calcium uptake by rat kidney mitochondria.* Proc Natl Acad Sci U S A, 1961. **47**: p. 1744-50.
524. Lehninger, A.L., E. Carafoli, and C.S. Rossi, *Energy-linked ion movements in mitochondrial systems.* Adv Enzymol Relat Areas Mol Biol, 1967. **29**: p. 259-320.

525. Selwyn, M.J., A.P. Dawson, and S.J. Dunnett, *Calcium transport in mitochondria.* FEBS Lett, 1970. **10**(1): p. 1-5.
526. Puskin, J.S., et al., *Evidence for more than one Ca2+ transport mechanism in mitochondria.* Biochemistry, 1976. **15**(17): p. 3834-42.
527. Kirichok, Y., G. Krapivinsky, and D.E. Clapham, *The mitochondrial calcium uniporter is a highly selective ion channel.* Nature, 2004. **427**(6972): p. 360-4.
528. Rizzuto, R., et al., *Pathways for Ca2+ efflux in heart and liver mitochondria.* Biochem J, 1987. **246**(2): p. 271-7.
529. Kapus, A., et al., *Is the mitochondrial Ca2+ uniporter a voltage-modulated transport pathway?* FEBS Lett, 1991. **282**(1): p. 61-4.
530. Peng, Y.Y. and R.S. Zucker, *Release of LHRH is linearly related to the time integral of presynaptic Ca2+ elevation above a threshold level in bullfrog sympathetic ganglia.* Neuron, 1993. **10**(3): p. 465-73.
531. Nowycky, M.C., E.P. Seward, and N.I. Chernevskaya, *Excitation-secretion coupling in mammalian neurohypophysial nerve terminals.* Cell Mol Neurobiol, 1998. **18**(1): p. 65-80.
532. Rizzuto, R., et al., *Microdomains with high Ca2+ close to IP3-sensitive channels that are sensed by neighboring mitochondria.* Science, 1993. **262**(5134): p. 744-7.
533. Carafoli, E., *The calcium cycle of mitochondria.* FEBS Lett, 1979. **104**(1): p. 1-5.
534. Gunter, T.E., et al., *Mitochondrial calcium transport: physiological and pathological relevance.* Am J Physiol, 1994. **267**(2 Pt 1): p. C313-39.
535. Babcock, D.F., et al., *Mitochondrial participation in the intracellular Ca2+ network.* J Cell Biol, 1997. **136**(4): p. 833-44.
536. Crompton, M., M. Kunzi, and E. Carafoli, *The calcium-induced and sodium-induced effluxes of calcium from heart mitochondria. Evidence for a sodium-calcium carrier.* Eur J Biochem, 1977. **79**(2): p. 549-58.
537. Sedova, M. and L.A. Blatter, *Intracellular sodium modulates mitochondrial calcium signaling in vascular endothelial cells.* J Biol Chem, 2000. **275**(45): p. 35402-7.
538. Bernardi, P., *Mitochondrial transport of cations: channels, exchangers, and permeability transition.* Physiol Rev, 1999. **79**(4): p. 1127-55.
539. Wingrove, D.E. and T.E. Gunter, *Kinetics of mitochondrial calcium transport. II. A kinetic description of the sodium-dependent calcium efflux mechanism of liver mitochondria and inhibition by ruthenium red and by tetraphenylphosphonium.* J Biol Chem, 1986. **261**(32): p. 15166-71.
540. Jornot, L., et al., *Reactive oxygen metabolites increase mitochondrial calcium in endothelial cells: implication of the Ca2+/Na+ exchanger.* J Cell Sci, 1999. **112 (Pt 7)**: p. 1013-22.
541. Sparagna, G.C., et al., *Mitochondrial calcium uptake from physiological-type pulses of calcium. A description of the rapid uptake mode.* J Biol Chem, 1995. **270**(46): p. 27510-5.
542. Bernardi, P., et al., *Mitochondria and cell death. Mechanistic aspects and methodological issues.* Eur J Biochem, 1999. **264**(3): p. 687-701.
543. Duchen, M.R., *Mitochondria and Ca(2+)in cell physiology and pathophysiology.* Cell Calcium, 2000. **28**(5-6): p. 339-48.

544. Collins, T.J., et al., *Mitochondrial Ca(2+) uptake depends on the spatial and temporal profile of cytosolic Ca(2+) signals.* J Biol Chem, 2001. **276**(28): p. 26411-20.
545. Litsky, M.L. and D.R. Pfeiffer, *Regulation of the mitochondrial Ca2+ uniporter by external adenine nucleotides: the uniporter behaves like a gated channel which is regulated by nucleotides and divalent cations.* Biochemistry, 1997. **36**(23): p. 7071-80.
546. Pivovarova, N.B., et al., *Depolarization-induced mitochondrial Ca accumulation in sympathetic neurons: spatial and temporal characteristics.* J Neurosci, 1999. **19**(15): p. 6372-84.
547. Xu, T., et al., *Kinetic studies of Ca2+ binding and Ca2+ clearance in the cytosol of adrenal chromaffin cells.* Biophys J, 1997. **73**(1): p. 532-45.
548. Rizzuto, R., et al., *Close contacts with the endoplasmic reticulum as determinants of mitochondrial Ca2+ responses.* Science, 1998. **280**(5370): p. 1763-6.
549. Lawrie, A.M., et al., *A role for calcium influx in the regulation of mitochondrial calcium in endothelial cells.* J Biol Chem, 1996. **271**(18): p. 10753-9.
550. Rizzuto, R., et al., *Rapid changes of mitochondrial Ca2+ revealed by specifically targeted recombinant aequorin.* Nature, 1992. **358**(6384): p. 325-7.
551. Duchen, M.R., *Contributions of mitochondria to animal physiology: from homeostatic sensor to calcium signalling and cell death.* J Physiol, 1999. **516 (Pt 1)**: p. 1-17.
552. Kaftan, E.J., et al., *Mitochondria shape hormonally induced cytoplasmic calcium oscillations and modulate exocytosis.* J Biol Chem, 2000. **275**(33): p. 25465-70.
553. Boitier, E., R. Rea, and M.R. Duchen, *Mitochondria exert a negative feedback on the propagation of intracellular Ca2+ waves in rat cortical astrocytes.* J Cell Biol, 1999. **145**(4): p. 795-808.
554. Ricken, S., et al., *Simultaneous measurements of cytosolic and mitochondrial Ca2+ transients in HT29 cells.* J Biol Chem, 1998. **273**(52): p. 34961-9.
555. Drummond, R.M., et al., *Mitochondrial Ca2+ homeostasis during Ca2+ influx and Ca2+ release in gastric myocytes from Bufo marinus.* J Physiol, 2000. **522 Pt 3**: p. 375-90.
556. Park, Y.B., et al., *Ca2+ clearance mechanisms in isolated rat adrenal chromaffin cells.* J Physiol, 1996. **492 (Pt 2)**: p. 329-46.
557. Ales, E., et al., *Depolarization evokes different patterns of calcium signals and exocytosis in bovine and mouse chromaffin cells: the role of mitochondria.* Eur J Neurosci, 2005. **21**(1): p. 142-50.
558. Herrington, J., et al., *Dominant role of mitochondria in clearance of large Ca2+ loads from rat adrenal chromaffin cells.* Neuron, 1996. **16**(1): p. 219-28.
559. White, R.J. and I.J. Reynolds, *Mitochondria accumulate Ca2+ following intense glutamate stimulation of cultured rat forebrain neurones.* J Physiol, 1997. **498 (Pt 1)**: p. 31-47.
560. Werth, J.L. and S.A. Thayer, *Mitochondria buffer physiological calcium loads in cultured rat dorsal root ganglion neurons.* J Neurosci, 1994. **14**(1): p. 348-56.

561. Hehl, S., A. Golard, and B. Hille, *Involvement of mitochondria in intracellular calcium sequestration by rat gonadotropes.* Cell Calcium, 1996. **20**(6): p. 515-24.
562. Caputo, C. and P. Bolanos, *Effect of mitochondria poisoning by FCCP on Ca2+ signaling in mouse skeletal muscle fibers.* Pflugers Arch, 2008. **455**(4): p. 733-43.
563. Hajnoczky, G., R. Hager, and A.P. Thomas, *Mitochondria suppress local feedback activation of inositol 1,4, 5-trisphosphate receptors by Ca2+.* J Biol Chem, 1999. **274**(20): p. 14157-62.
564. Vay, L., et al., *Modulation of Ca(2+) release and Ca(2+) oscillations in HeLa cells and fibroblasts by mitochondrial Ca(2+) uniporter stimulation.* J Physiol, 2007. **580**(Pt 1): p. 39-49.
565. Colegrove, S.L., M.A. Albrecht, and D.D. Friel, *Dissection of mitochondrial Ca2+ uptake and release fluxes in situ after depolarization-evoked [Ca2+](i) elevations in sympathetic neurons.* J Gen Physiol, 2000. **115**(3): p. 351-70.
566. Jouaville, L.S., et al., *Synchronization of calcium waves by mitochondrial substrates in Xenopus laevis oocytes.* Nature, 1995. **377**(6548): p. 438-41.
567. Landolfi, B., et al., *Ca2+ homeostasis in the agonist-sensitive internal store: functional interactions between mitochondria and the ER measured In situ in intact cells.* J Cell Biol, 1998. **142**(5): p. 1235-43.
568. Hoth, M., C.M. Fanger, and R.S. Lewis, *Mitochondrial regulation of store-operated calcium signaling in T lymphocytes.* J Cell Biol, 1997. **137**(3): p. 633-48.
569. Gilabert, J.A. and A.B. Parekh, *Respiring mitochondria determine the pattern of activation and inactivation of the store-operated Ca(2+) current I(CRAC).* Embo J, 2000. **19**(23): p. 6401-7.
570. Glitsch, M.D., D. Bakowski, and A.B. Parekh, *Store-operated Ca2+ entry depends on mitochondrial Ca2+ uptake.* Embo J, 2002. **21**(24): p. 6744-54.
571. Malli, R., et al., *Mitochondria efficiently buffer subplasmalemmal Ca2+ elevation during agonist stimulation.* J Biol Chem, 2003. **278**(12): p. 10807-15.
572. Malli, R., et al., *The role of mitochondria for Ca2+ refilling of the endoplasmic reticulum.* J Biol Chem, 2005. **280**(13): p. 12114-22.
573. Malli, R., et al., *Sustained Ca2+ transfer across mitochondria is Essential for mitochondrial Ca2+ buffering, sore-operated Ca2+ entry, and Ca2+ store refilling.* J Biol Chem, 2003. **278**(45): p. 44769-79.
574. Parekh, A.B., *Slow feedback inhibition of calcium release-activated calcium current by calcium entry.* J Biol Chem, 1998. **273**(24): p. 14925-32.
575. Quesada, I., et al., *Glucose induces synchronous mitochondrial calcium oscillations in intact pancreatic islets.* Cell Calcium, 2008. **43**(1): p. 39-47.
576. Pralong, W.F., A. Spat, and C.B. Wollheim, *Dynamic pacing of cell metabolism by intracellular Ca2+ transients.* J Biol Chem, 1994. **269**(44): p. 27310-4.
577. Hajnoczky, G., et al., *Decoding of cytosolic calcium oscillations in the mitochondria.* Cell, 1995. **82**(3): p. 415-24.

578. Montero, M., et al., *Chromaffin-cell stimulation triggers fast millimolar mitochondrial Ca2+ transients that modulate secretion.* Nat Cell Biol, 2000. **2**(2): p. 57-61.
579. Jouaville, L.S., et al., *Regulation of mitochondrial ATP synthesis by calcium: evidence for a long-term metabolic priming.* Proc Natl Acad Sci U S A, 1999. **96**(24): p. 13807-12.
580. McCormack, J.G. and R.M. Denton, *Intracellular calcium ions and intramitochondrial Ca2+ in the regulation of energy metabolism in mammalian tissues.* Proc Nutr Soc, 1990. **49**(1): p. 57-75.
581. Maechler, P. and C.B. Wollheim, *Mitochondrial signals in glucose-stimulated insulin secretion in the beta cell.* J Physiol, 2000. **529 Pt 1**: p. 49-56.
582. Gil, A., et al., *The F-actin cytoskeleton modulates slow secretory components rather than readily releasable vesicle pools in bovine chromaffin cells.* Neuroscience, 2000. **98**(3): p. 605-14.
583. Giovannucci, D.R., M.D. Hlubek, and E.L. Stuenkel, *Mitochondria regulate the Ca(2+)-exocytosis relationship of bovine adrenal chromaffin cells.* J Neurosci, 1999. **19**(21): p. 9261-70.
584. Warashina, A., *Mode of mitochondrial Ca2+ clearance and its influence on secretory responses in stimulated chromaffin cells.* Cell Calcium, 2006. **39**(1): p. 35-46.
585. Keating, D.J., *Mitochondrial dysfunction, oxidative stress, regulation of exocytosis and their relevance to neurodegenerative diseases.* J Neurochem, 2008. **104**(2): p. 298-305.
586. Lin, M.T. and M.F. Beal, *Mitochondrial dysfunction and oxidative stress in neurodegenerative diseases.* Nature, 2006. **443**(7113): p. 787-95.
587. Brini, M., et al., *A calcium signaling defect in the pathogenesis of a mitochondrial DNA inherited oxidative phosphorylation deficiency.* Nat Med, 1999. **5**(8): p. 951-4.
588. Krieger, C. and M.R. Duchen, *Mitochondria, Ca2+ and neurodegenerative disease.* Eur J Pharmacol, 2002. **447**(2-3): p. 177-88.
589. Madamanchi, N.R. and M.S. Runge, *Mitochondrial dysfunction in atherosclerosis.* Circ Res, 2007. **100**(4): p. 460-73.
590. Campbell, R.E., et al., *A monomeric red fluorescent protein.* Proc Natl Acad Sci U S A, 2002. **99**(12): p. 7877-82.
591. Zacharias, D.A., et al., *Partitioning of lipid-modified monomeric GFPs into membrane microdomains of live cells.* Science, 2002. **296**(5569): p. 913-6.
592. Sambrook, J., Fritsch, EF., Maniatis, T., *Molecular cloning: A laboratory manual* 2ed. 1989: Cold Spring Harbor Laboratory Press. p.6.9.
593. Sambrook, J., Fritsch, EF., Maniatis, T., *Molecular cloning: A laboratory manual 1989*. 2 ed. 1989: Cold Spring Harbor Laboratory Press. p.1.63.
594. Sambrook, J., Fritsch, EF., Maniatis, T., *Molecular cloning: A laboratory manual* 2ed. 1989: Cold Spring Harbor Laboratory Press. p.1.74.
595. Sambrook, J., Fritsch, EF., Maniatis, T., *Molecular cloning: A laboratory manual*. 2 ed. 1989: Cold Spring Harbor Laboratory Press. p.1.25.
596. Mashanov, G.I., et al., *Visualizing single molecules inside living cells using total internal reflection fluorescence microscopy.* Methods, 2003. **29**(2): p. 142-52.

597. Mashanov, G.I., et al., *The spatial and temporal dynamics of pleckstrin homology domain binding at the plasma membrane measured by imaging single molecules in live mouse myoblasts.* J Biol Chem, 2004. **279**(15): p. 15274-80.
598. Trache, A. and G.A. Meininger, *Total internal reflection fluorescence (TIRF) microscopy.* Curr Protoc Microbiol, 2008. **Chapter 2**: p. Unit 2A 2 1-2A 2 22.
599. Roos, A. and W.F. Boron, *Intracellular pH.* Physiol Rev, 1981. **61**(2): p. 296-434.
600. Thomas, R.C., *Intracellular pH of snail neurones measured with a new pH-sensitive glass mirco-electrode.* J Physiol, 1974. **238**(1): p. 159-80.
601. Boron, W.F. and P. De Weer, *Intracellular pH transients in squid giant axons caused by CO2, NH3, and metabolic inhibitors.* J Gen Physiol, 1976. **67**(1): p. 91-112.
602. Grynkiewicz, G., M. Poenie, and R.Y. Tsien, *A new generation of Ca2+ indicators with greatly improved fluorescence properties.* J Biol Chem, 1985. **260**(6): p. 3440-50.
603. Rizzuto, R., M. Brini, and T. Pozzan, *Targeting recombinant aequorin to specific intracellular organelles.* Methods Cell Biol, 1994. **40**: p. 339-58.
604. Minta, A., J.P. Kao, and R.Y. Tsien, *Fluorescent indicators for cytosolic calcium based on rhodamine and fluorescein chromophores.* J Biol Chem, 1989. **264**(14): p. 8171-8.
605. Farkas, D.L., et al., *Simultaneous imaging of cell and mitochondrial membrane potentials.* Biophys J, 1989. **56**(6): p. 1053-69.
606. Ichimura, H., et al., *Mechano-oxidative coupling by mitochondria induces proinflammatory responses in lung venular capillaries.* J Clin Invest, 2003. **111**(5): p. 691-9.
607. Dedkova, E.N. and L.A. Blatter, *Modulation of mitochondrial Ca2+ by nitric oxide in cultured bovine vascular endothelial cells.* Am J Physiol Cell Physiol, 2005. **289**(4): p. C836-45.
608. Huser, J. and L.A. Blatter, *Fluctuations in mitochondrial membrane potential caused by repetitive gating of the permeability transition pore.* Biochem J, 1999. **343 Pt 2**: p. 311-7.
609. Shimomura, O., F.H. Johnson, and Y. Saiga, *Extraction, purification and properties of aequorin, a bioluminescent protein from the luminous hydromedusan, Aequorea.* J Cell Comp Physiol, 1962. **59**: p. 223-39.
610. Tsien, R.Y., *The green fluorescent protein.* Annu Rev Biochem, 1998. **67**: p. 509-44.
611. Prasher, D.C., et al., *Primary structure of the Aequorea victoria green-fluorescent protein.* Gene, 1992. **111**(2): p. 229-33.
612. Chalfie, M., *Green fluorescent protein.* Photochem Photobiol, 1995. **62**(4): p. 651-6.
613. Chalfie, M., et al., *Green fluorescent protein as a marker for gene expression.* Science, 1994. **263**(5148): p. 802-5.
614. Ormo, M., et al., *Crystal structure of the Aequorea victoria green fluorescent protein.* Science, 1996. **273**(5280): p. 1392-5.
615. Remington, S.J., *Fluorescent proteins: maturation, photochemistry and photophysics.* Curr Opin Struct Biol, 2006. **16**(6): p. 714-21.

616. Heim, R., D.C. Prasher, and R.Y. Tsien, *Wavelength mutations and posttranslational autoxidation of green fluorescent protein.* Proc Natl Acad Sci U S A, 1994. **91**(26): p. 12501-4.
617. Wachter, R.M., *Chromogenic cross-link formation in green fluorescent protein.* Acc Chem Res, 2007. **40**(2): p. 120-7.
618. Brejc, K., et al., *Structural basis for dual excitation and photoisomerization of the Aequorea victoria green fluorescent protein.* Proc Natl Acad Sci U S A, 1997. **94**(6): p. 2306-11.
619. Wachter, R.M., et al., *Crystallographic and energetic analysis of binding of selected anions to the yellow variants of green fluorescent protein.* J Mol Biol, 2000. **301**(1): p. 157-71.
620. Bokman, S.H. and W.W. Ward, *Renaturation of Aequorea gree-fluorescent protein.* Biochem Biophys Res Commun, 1981. **101**(4): p. 1372-80.
621. Niwa, H., et al., *Chemical nature of the light emitter of the Aequorea green fluorescent protein.* Proc Natl Acad Sci U S A, 1996. **93**(24): p. 13617-22.
622. Ward, W.W. and S.H. Bokman, *Reversible denaturation of Aequorea green-fluorescent protein: physical separation and characterization of the renatured protein.* Biochemistry, 1982. **21**(19): p. 4535-40.
623. Shaner, N.C., G.H. Patterson, and M.W. Davidson, *Advances in fluorescent protein technology.* J Cell Sci, 2007. **120**(Pt 24): p. 4247-60.
624. Chudakov, D.M., S. Lukyanov, and K.A. Lukyanov, *Fluorescent proteins as a toolkit for in vivo imaging.* Trends Biotechnol, 2005. **23**(12): p. 605-13.
625. Patterson, G.H., et al., *Use of the green fluorescent protein and its mutants in quantitative fluorescence microscopy.* Biophys J, 1997. **73**(5): p. 2782-90.
626. Yang, F., L.G. Moss, and G.N. Phillips, Jr., *The molecular structure of green fluorescent protein.* Nat Biotechnol, 1996. **14**(10): p. 1246-51.
627. Merritt, E.A. and M.E. Murphy, *Raster3D Version 2.0. A program for photorealistic molecular graphics.* Acta Crystallogr D Biol Crystallogr, 1994. **50**(Pt 6): p. 869-73.
628. Kneen, M., et al., *Green fluorescent protein as a noninvasive intracellular pH indicator.* Biophys J, 1998. **74**(3): p. 1591-9.
629. Naciri, M. and M. Al-Rubeai, *Non-invasive flow cytometric monitoring of pHi in cell culture processes using EGFP.* J Immunol Methods, 2006. **315**(1-2): p. 185-90.
630. Pace, C.S. and G. Sachs, *Glucose-induced proton uptake in secretory granules of beta-cells in monolayer culture.* Am J Physiol, 1982. **242**(5): p. C382-7.
631. Wachter, R.M., et al., *Structural basis of spectral shifts in the yellow-emission variants of green fluorescent protein.* Structure, 1998. **6**(10): p. 1267-77.
632. Chattoraj, M., et al., *Ultra-fast excited state dynamics in green fluorescent protein: multiple states and proton transfer.* Proc Natl Acad Sci U S A, 1996. **93**(16): p. 8362-7.
633. Mellman, I., R. Fuchs, and A. Helenius, *Acidification of the endocytic and exocytic pathways.* Annu Rev Biochem, 1986. **55**: p. 663-700.

634. Schoonderwoert, V.T. and G.J. Martens, *Proton pumping in the secretory pathway.* J Membr Biol, 2001. **182**(3): p. 159-69.
635. Denis, C.V., *Molecular and cellular biology of von Willebrand factor.* Int J Hematol, 2002. **75**(1): p. 3-8.
636. Orci, L., et al., *Conversion of proinsulin to insulin occurs coordinately with acidification of maturing secretory vesicles.* J Cell Biol, 1986. **103**(6 Pt 1): p. 2273-81.
637. Tompkins, L.S., et al., *Regulation of secretory granule pH in insulin-secreting cells.* Am J Physiol Cell Physiol, 2002. **283**(2): p. C429-37.
638. Han, W., et al., *Ca2+-induced deprotonation of peptide hormones inside secretory vesicles in preparation for release.* J Neurosci, 1999. **19**(3): p. 900-5.
639. Williams, R.M. and W.W. Webb, *Single granule pH cycling in antigen-induced mast cell secretion.* J Cell Sci, 2000. **113 Pt 21**: p. 3839-50.
640. Lang, T., et al., *Ca2+-triggered peptide secretion in single cells imaged with green fluorescent protein and evanescent-wave microscopy.* Neuron, 1997. **18**(6): p. 857-63.
641. Taraska, J.W., et al., *Secretory granules are recaptured largely intact after stimulated exocytosis in cultured endocrine cells.* Proc Natl Acad Sci U S A, 2003. **100**(4): p. 2070-5.
642. Tsuboi, T., et al., *Simultaneous evanescent wave imaging of insulin vesicle membrane and cargo during a single exocytotic event.* Curr Biol, 2000. **10**(20): p. 1307-10.
643. Ma, L., et al., *Direct imaging shows that insulin granule exocytosis occurs by complete vesicle fusion.* Proc Natl Acad Sci U S A, 2004. **101**(25): p. 9266-71.
644. Ohara-Imaizumi, M., et al., *Site of docking and fusion of insulin secretory granules in live MIN6 beta cells analyzed by TAT-conjugated anti-syntaxin 1 antibody and total internal reflection fluorescence microscopy.* J Biol Chem, 2004. **279**(9): p. 8403-8.
645. Holz, R.W. and D. Axelrod, *Secretory granule behaviour adjacent to the plasma membrane before and during exocytosis: total internal reflection fluorescence microscopy studies.* Acta Physiol (Oxf), 2008. **192**(2): p. 303-7.
646. Storck, J., et al., *Trypsin induced von Willebrand factor release from human endothelial cells in mediated by PAR-2 activation.* Thromb Res, 1996. **84**(6): p. 463-73.
647. Langer, F., et al., *Endothelial protease-activated receptor-2 induces tissue factor expression and von Willebrand factor release.* Br J Haematol, 1999. **105**(2): p. 542-50.
648. Busch, C., et al., *Binding of platelet factor 4 to cultured human umbilical vein endothelial cells.* Thromb Res, 1980. **19**(1-2): p. 129-37.
649. Schwartz, D., et al., *Role of the GRO family of chemokines in monocyte adhesion to MM-LDL-stimulated endothelium.* J Clin Invest, 1994. **94**(5): p. 1968-73.
650. Papadopoulou, C., et al., *The role of the chemokines MCP-1, GRO-alpha, IL-8 and their receptors in the adhesion of monocytic cells to human atherosclerotic plaques.* Cytokine, 2008. **43**(2): p. 181-6.

651. Hebert, C.A., R.V. Vitangcol, and J.B. Baker, *Scanning mutagenesis of interleukin-8 identifies a cluster of residues required for receptor binding.* J Biol Chem, 1991. **266**(28): p. 18989-94.
652. Schraufstatter, I.U., J. Chung, and M. Burger, *IL-8 activates endothelial cell CXCR1 and CXCR2 through Rho and Rac signaling pathways.* Am J Physiol Lung Cell Mol Physiol, 2001. **280**(6): p. L1094-103.
653. Weber, K.S., et al., *Differential immobilization and hierarchical involvement of chemokines in monocyte arrest and transmigration on inflamed endothelium in shear flow.* Eur J Immunol, 1999. **29**(2): p. 700-12.
654. Axelrod, D., N.L. Thompson, and T.P. Burghardt, *Total internal inflection fluorescent microscopy.* J Microsc, 1983. **129**(Pt 1): p. 19-28.
655. Pouli, A.E., et al., *Insulin targeting to the regulated secretory pathway after fusion with green fluorescent protein and firefly luciferase.* Biochem J, 1998. **331 (Pt 2)**: p. 669-75.
656. Kaether, C. and H.H. Gerdes, *Visualization of protein transport along the secretory pathway using green fluorescent protein.* FEBS Lett, 1995. **369**(2-3): p. 267-71.
657. Burke, N.V., et al., *Neuronal peptide release is limited by secretory granule mobility.* Neuron, 1997. **19**(5): p. 1095-102.
658. Poskanzer, K.E. and G.W. Davis, *Mobilization and fusion of a non-recycling pool of synaptic vesicles under conditions of endocytic blockade.* Neuropharmacology, 2004. **47**(5): p. 714-23.
659. Miesenbock, G., D.A. De Angelis, and J.E. Rothman, *Visualizing secretion and synaptic transmission with pH-sensitive green fluorescent proteins.* Nature, 1998. **394**(6689): p. 192-5.
660. Colomer, V., G.A. Kicska, and M.J. Rindler, *Secretory granule content proteins and the luminal domains of granule membrane proteins aggregate in vitro at mildly acidic pH.* J Biol Chem, 1996. **271**(1): p. 48-55.
661. Aspinwall, C.A., et al., *Effects of intravesicular H+ and extracellular H+ and Zn2+ on insulin secretion in pancreatic beta cells.* J Biol Chem, 1997. **272**(50): p. 31308-14.
662. Verdugo, P., *Goblet cells secretion and mucogenesis.* Annu Rev Physiol, 1990. **52**: p. 157-76.
663. Desseyn, J.L., et al., *Evolution of the large secreted gel-forming mucins.* Mol Biol Evol, 2000. **17**(8): p. 1175-84.
664. Verdugo, P., et al., *Molecular mechanism of product storage and release in mucin secretion. II. The role of extracellular Ca++.* Biorheology, 1987. **24**(6): p. 625-33.
665. Verdugo, P., et al., *Molecular mechanism of mucin secretion: I. The role of intragranular charge shielding.* J Dent Res, 1987. **66**(2): p. 506-8.
666. Kantardjieff, K.A. and B. Rupp, *Protein isoelectric point as a predictor for increased crystallization screening efficiency.* Bioinformatics, 2004. **20**(14): p. 2162-8.
667. Johns, L.M., et al., *Restriction of secretory granule motion near the plasma membrane of chromaffin cells.* J Cell Biol, 2001. **153**(1): p. 177-90.
668. Carter, T.D. and D. Ogden, *Acetylcholine-stimulated changes of membrane potential and intracellular Ca2+ concentration recorded in*

endothelial cells in situ in the isolated rat aorta. Pflugers Arch, 1994. **428**(5-6): p. 476-84.
669. Scrutton, M.C. and J.D. Pearson, *Ca2+-driven prostacylin synthesis and von Willebrand factor secretion in electropermeabilised endothelial cells.* British Journal of Pharmacology, 1989. **97**: p. 420P.
670. Khodakhah, K. and D. Ogden, *Fast activation and inactivation of inositol trisphosphate-evoked Ca2+ release in rat cerebellar Purkinje neurones.* J Physiol, 1995. **487 (Pt 2)**: p. 343-58.
671. Parker, I., Y. Yao, and V. Ilyin, *Fast kinetics of calcium liberation induced in Xenopus oocytes by photoreleased inositol trisphosphate.* Biophys J, 1996. **70**(1): p. 222-37.
672. Carter, T.D. and D. Ogden, *Kinetics of intracellular calcium release by inositol 1,4,5-trisphosphate and extracellular ATP in porcine cultured aortic endothelial cells.* Proc Biol Sci, 1992. **250**(1329): p. 235-41.
673. Kreft, M., et al., *Properties of Ca(2+)-dependent exocytosis in cultured astrocytes.* Glia, 2004. **46**(4): p. 437-45.
674. Ninomiya, Y., et al., *Ca2+-dependent exocytotic pathways in Chinese hamster ovary fibroblasts revealed by a caged-Ca2+ compound.* J Biol Chem, 1996. **271**(30): p. 17751-4.
675. Chow, R.H., L. von Ruden, and E. Neher, *Delay in vesicle fusion revealed by electrochemical monitoring of single secretory events in adrenal chromaffin cells.* Nature, 1992. **356**(6364): p. 60-3.
676. Heinemann, C., et al., *Kinetics of the secretory response in bovine chromaffin cells following flash photolysis of caged Ca2+.* Biophys J, 1994. **67**(6): p. 2546-57.
677. Thomas, P., J.G. Wong, and W. Almers, *Millisecond studies of secretion in single rat pituitary cells stimulated by flash photolysis of caged Ca2+.* Embo J, 1993. **12**(1): p. 303-6.
678. Hatakeyama, H., et al., *Two cAMP-dependent pathways differentially regulate exocytosis of large dense-core and small vesicles in mouse beta-cells.* J Physiol, 2007. **582**(Pt 3): p. 1087-98.
679. Ammala, C., et al., *Exocytosis elicited by action potentials and voltage-clamp calcium currents in individual mouse pancreatic B-cells.* J Physiol, 1993. **472**: p. 665-88.
680. Henkel, A.W. and W. Almers, *Fast steps in exocytosis and endocytosis studied by capacitance measurements in endocrine cells.* Curr Opin Neurobiol, 1996. **6**(3): p. 350-7.
681. Llinas, R., M. Sugimori, and R.B. Silver, *Microdomains of high calcium concentration in a presynaptic terminal.* Science, 1992. **256**(5057): p. 677-9.
682. Jaffe, E.A., et al., *Correlation between thrombin-induced prostacyclin production and inositol trisphosphate and cytosolic free calcium levels in cultured human endothelial cells.* J Biol Chem, 1987. **262**(18): p. 8557-65.
683. Geppert, M., et al., *Synaptotagmin I: a major Ca2+ sensor for transmitter release at a central synapse.* Cell, 1994. **79**(4): p. 717-27.
684. Fernandez-Chacon, R., et al., *Synaptotagmin I functions as a calcium regulator of release probability.* Nature, 2001. **410**(6824): p. 41-9.
685. Kreft, M., et al., *Synaptotagmin I increases the probability of vesicle fusion at low [Ca2+] in pituitary cells.* Am J Physiol Cell Physiol, 2003. **284**(2): p. C547-54.

686. Rupnik, M., et al., *Rapid regulated dense-core vesicle exocytosis requires the CAPS protein.* Proc Natl Acad Sci U S A, 2000. **97**(10): p. 5627-32.
687. Lorusso, A., et al., *Annexin2 coating the surface of enlargeosomes is needed for their regulated exocytosis.* Embo J, 2006. **25**(23): p. 5443-56.
688. Sudhof, T.C., *Synaptotagmins: why so many?* J Biol Chem, 2002. **277**(10): p. 7629-32.
689. van de Graaf, S.F., et al., *Functional expression of the epithelial Ca(2+) channels (TRPV5 and TRPV6) requires association of the S100A10-annexin 2 complex.* Embo J, 2003. **22**(7): p. 1478-87.
690. Schluter, O.M., et al., *Localization versus function of Rab3 proteins. Evidence for a common regulatory role in controlling fusion.* J Biol Chem, 2002. **277**(43): p. 40919-29.
691. Disse, J., et al., *Phospholipase D1 is specifically required for regulated secretion of von-Willebrand factor from endothelial cells.* Blood, 2008.
692. Mitchell, P. and J. Moyle, *Chemiosmotic hypothesis of oxidative phosphorylation.* Nature, 1967. **213**(5072): p. 137-9.
693. Babcock, D.F. and B. Hille, *Mitochondrial oversight of cellular Ca2+ signaling.* Curr Opin Neurobiol, 1998. **8**(3): p. 398-404.
694. Huijing, F. and E.C. Slater, *The use of oligomycin as an inhibitor of oxidative phosphorylation.* J Biochem, 1961. **49**: p. 493-501.
695. Jou, M.J., T.I. Peng, and S.S. Sheu, *Histamine induces oscillations of mitochondrial free Ca2+ concentration in single cultured rat brain astrocytes.* J Physiol, 1996. **497 (Pt 2)**: p. 299-308.
696. Rizzuto, R., et al., *Chimeric green fluorescent protein as a tool for visualizing subcellular organelles in living cells.* Curr Biol, 1995. **5**(6): p. 635-42.
697. Rizzuto, R., et al., *A gene specifying subunit VIII of human cytochrome c oxidase is localized to chromosome 11 and is expressed in both muscle and non-muscle tissues.* J Biol Chem, 1989. **264**(18): p. 10595-600.
698. Gunter, K.K. and T.E. Gunter, *Transport of calcium by mitochondria.* J Bioenerg Biomembr, 1994. **26**(5): p. 471-85.
699. Chalmers, S. and D.G. Nicholls, *The relationship between free and total calcium concentrations in the matrix of liver and brain mitochondria.* J Biol Chem, 2003. **278**(21): p. 19062-70.
700. Carafoli, E., C.S. Rossi, and A.L. Lehninger, *Uptake of Adenine Nucleotides by Respiring Mitochondria during Active Accumulation of Ca++ and Phosphate.* J Biol Chem, 1965. **240**: p. 2254-61.
701. Endow, S.A., *Kinesin motors as molecular machines.* Bioessays, 2003. **25**(12): p. 1212-9.
702. Bolanos, P., et al., *The use of CalciumOrange-5N as a specific marker of mitochondrial Ca2+ in mouse skeletal muscle fibers.* Pflugers Arch, 2008. **455**(4): p. 721-31.
703. Dufer, M., P. Krippeit-Drews, and G. Drews, *Inhibition of mitochondrial function affects cellular Ca2+ handling in pancreatic B-cells.* Pflugers Arch, 2002. **444**(1-2): p. 236-43.
704. Thayer, S.A. and R.J. Miller, *Regulation of the intracellular free calcium concentration in single rat dorsal root ganglion neurones in vitro.* J Physiol, 1990. **425**: p. 85-115.

705. White, R.J. and I.J. Reynolds, *Mitochondria and Na+/Ca2+ exchange buffer glutamate-induced calcium loads in cultured cortical neurons.* J Neurosci, 1995. **15**(2): p. 1318-28.
706. Parthasarathi, K., et al., *Mitochondrial reactive oxygen species regulate spatial profile of proinflammatory responses in lung venular capillaries.* J Immunol, 2002. **169**(12): p. 7078-86.
707. Petronilli, V., et al., *Physiological effectors modify voltage sensing by the cyclosporin A-sensitive permeability transition pore of mitochondria.* J Biol Chem, 1993. **268**(29): p. 21939-45.
708. Buckler, K.J. and R.D. Vaughan-Jones, *Effects of mitochondrial uncouplers on intracellular calcium, pH and membrane potential in rat carotid body type I cells.* J Physiol, 1998. **513 (Pt 3)**: p. 819-33.
709. Faber, S., et al., *Intracellular pH regulation in bovine aortic endothelial cells: evidence of both Na+/H+ exchange and Na+-dependent Cl-/HCO3- exchange.* Cell Physiol Biochem, 1998. **8**(4): p. 202-11.
710. Hunte, C., et al., *Structure of a Na+/H+ antiporter and insights into mechanism of action and regulation by pH.* Nature, 2005. **435**(7046): p. 1197-202.
711. Li, L. and C. van Breemen, *Na(+)-Ca2+ exchange in intact endothelium of rabbit cardiac valve.* Circ Res, 1995. **76**(3): p. 396-404.
712. Tretter, L., C. Chinopoulos, and V. Adam-Vizi, *Plasma membrane depolarization and disturbed Na+ homeostasis induced by the protonophore carbonyl cyanide-p-trifluoromethoxyphenyl-hydrazon in isolated nerve terminals.* Mol Pharmacol, 1998. **53**(4): p. 734-41.
713. Nilius, B., F. Viana, and G. Droogmans, *Ion channels in vascular endothelium.* Annu Rev Physiol, 1997. **59**: p. 145-70.
714. Rizzuto, R. and T. Pozzan, *Microdomains of intracellular Ca2+: molecular determinants and functional consequences.* Physiol Rev, 2006. **86**(1): p. 369-408.
715. Hajnoczky, G. and A.P. Thomas, *The inositol trisphosphate calcium channel is inactivated by inositol trisphosphate.* Nature, 1994. **370**(6489): p. 474-7.
716. Berridge, M.J. and A. Galione, *Cytosolic calcium oscillators.* Faseb J, 1988. **2**(15): p. 3074-82.
717. Collins, T.J., et al., *Inositol 1,4,5-trisphosphate-induced Ca2+ release is inhibited by mitochondrial depolarization.* Biochem J, 2000. **347**(Pt 2): p. 593-600.
718. Tse, A., et al., *Rhythmic exocytosis stimulated by GnRH-induced calcium oscillations in rat gonadotropes.* Science, 1993. **260**(5104): p. 82-4.
719. Rooney, T.A., E.J. Sass, and A.P. Thomas, *Characterization of cytosolic calcium oscillations induced by phenylephrine and vasopressin in single fura-2-loaded hepatocytes.* J Biol Chem, 1989. **264**(29): p. 17131-41.
720. Dupont, G. and A. Goldbeter, *CaM kinase II as frequency decoder of Ca2+ oscillations.* Bioessays, 1998. **20**(8): p. 607-10.
721. Eshete, F. and R.D. Fields, *Spike frequency decoding and autonomous activation of Ca2+-calmodulin-dependent protein kinase II in dorsal root ganglion neurons.* J Neurosci, 2001. **21**(17): p. 6694-705.
722. Lorenzi, O., et al., *Protein kinase C-delta mediates von Willebrand factor secretion from endothelial cells in response to vascular endothelial growth*

factor (VEGF) but not histamine. J Thromb Haemost, 2008. **6**(11): p. 1962-9.
723. Jacob, R., *Imaging cytoplasmic free calcium in histamine stimulated endothelial cells and in fMet-Leu-Phe stimulated neutrophils.* Cell Calcium, 1990. **11**(2-3): p. 241-9.
724. Prentki, M., et al., *Cell-specific patterns of oscillating free Ca2+ in carbamylcholine-stimulated insulinoma cells.* J Biol Chem, 1988. **263**(23): p. 11044-7.
725. Dupont, G. and L. Combettes, *Modelling the effect of specific inositol 1,4,5-trisphosphate receptor isoforms on cellular Ca2+ signals.* Biol Cell, 2006. **98**(3): p. 171-82.
726. Dargan, S.L. and I. Parker, *Buffer kinetics shape the spatiotemporal patterns of IP3-evoked Ca2+ signals.* J Physiol, 2003. **553**(Pt 3): p. 775-88.
727. Dargan, S.L., B. Schwaller, and I. Parker, *Spatiotemporal patterning of IP3-mediated Ca2+ signals in Xenopus oocytes by Ca2+-binding proteins.* J Physiol, 2004. **556**(Pt 2): p. 447-61.
728. Kang, Y.K. and M.K. Park, *Endoplasmic reticulum Ca2+ store: regulation of Ca2+ release and reuptake by intracellular and extracellular Ca2+ in pancreatic acinar cells.* Mol Cells, 2005. **19**(2): p. 268-78.
729. Laskey, R.E., et al., *Calcium entry-dependent oscillations of cytoplasmic calcium concentration in cultured endothelial cell monolayers.* Proc Natl Acad Sci U S A, 1992. **89**(5): p. 1690-4.
730. Jacob, R., *Calcium oscillations in endothelial cells.* Cell Calcium, 1991. **12**(2-3): p. 127-34.
731. McCreath, G., I.P. Hall, and S.J. Hill, *Agonist-induced desensitization of histamine H1 receptor-mediated inositol phospholipid hydrolysis in human umbilical vein endothelial cells.* Br J Pharmacol, 1994. **113**(3): p. 823-30.
732. Miura, H., et al., *A carbazole derivative protects cells against endoplasmic reticulum (ER) stress and glutathione depletion.* J Pharmacol Sci, 2008. **108**(2): p. 164-71.
733. Baker, H.L., et al., *A mathematical model predicts that calreticulin interacts with the endoplasmic reticulum Ca(2+)-ATPase.* Biophys J, 2002. **82**(2): p. 582-90.
734. Little, E., et al., *The glucose-regulated proteins (GRP78 and GRP94): functions, gene regulation, and applications.* Crit Rev Eukaryot Gene Expr, 1994. **4**(1): p. 1-18.
735. Kim, J., et al., *Overexpressed cyclophilin B suppresses apoptosis associated with ROS and Ca2+ homeostasis after ER stress.* J Cell Sci, 2008. **121**(Pt 21): p. 3636-48.
736. Blasi, J., et al., *Botulinum neurotoxin C1 blocks neurotransmitter release by means of cleaving HPC-1/syntaxin.* Embo J, 1993. **12**(12): p. 4821-8.
737. Blasi, J., et al., *Botulinum neurotoxin A selectively cleaves the synaptic protein SNAP-25.* Nature, 1993. **365**(6442): p. 160-3.
738. Mayadas, T., D.D. Wagner, and P.J. Simpson, *von Willebrand factor biosynthesis and partitioning between constitutive and regulated pathways of secretion after thrombin stimulation.* Blood, 1989. **73**(3): p. 706-11.